

**NASA CR-54243
AED R-2565**

**SUMMARY REPORT
on the
DEVELOPMENT OF THE SERT I SPACECRAFT**

**prepared for
NATIONAL AERONAUTICS AND SPACE ADMINISTRATION
CONTRACT NAS 8-2449**

February 1, 1966

**by the
RADIO CORPORATION OF AMERICA
ASTRO-ELECTRONICS DIVISION
PRINCETON, NEW JERSEY**

PREFACE

This summary report covers the development of the spacecraft system for the SERT program, which was carried out by the Astro-Electronics Division of RCA for the Lewis Research Center of the National Aeronautics and Space Administration under Contract NAS 8-2449. The report contains seven sections which describe the complete SERT system including the mechanical and electrical design of the spacecraft, the dynamics of the spin-stabilized spacecraft in flight, the ground support equipment, the testing program, and the reliability analyses performed during the program. Pertinent, detailed analyses and data are presented in appendixes at the end of the report.

TABLE OF CONTENTS

Section	Page
I INTRODUCTION	I-1
A. General	I-1
B. The SERT I Mission	I-2
C. The SERT I System	I-2
1. System Requirements	I-2
2. System Description	I-4
D. System Operation (Mission Profile)	I-13
E. System Development	I-18
II SPACECRAFT MECHANICAL DESIGN	II-1
A. General	II-1
B. Structure	II-1
1. General Discussion	II-1
2. Development of the Structure	II-6
3. Vibration Characteristics	II-10
4. Baseplate	II-11
5. Column	II-15
6. Lower-Ring Assembly	II-16
7. Distributor Frame	II-17
8. Engine-Extension Subsystem	II-17
9. Ground Plane	II-20
10. Detuning Wing	II-21
11. Antenna Mounts and Clamp Deflectors	II-22
12. Miscellaneous Structural Parts	II-23
C. Thermal Design	II-23
1. General	II-23
2. Design Discussion	II-24
D. Mechanical Integration	II-28
1. Component Arrangement	II-29
2. Component Mounting	II-30
3. Hardware	II-31
4. Assembly Techniques	II-32
5. Dynamic Balancing and Inertia Measurement	II-32

TABLE OF CONTENTS (Continued)

Section	Page
E.	Handling Procedures II-36
1.	General II-36
2.	Lifting Sling II-36
3.	Workstands II-37
4.	Turning Fixture II-37
5.	Layout and Drill Stand II-37
III	SPACECRAFT ELECTRICAL DESIGN III-1
A.	General III-1
B.	Mercury-Bombardment-Engine Subsystem III-5
1.	Description III-5
2.	Neutralizer Voltage Control Unit (NVCU) III-6
C.	Cesium-Contact-Engine Subsystem III-10
D.	Telecommunications Subsystem III-10
1.	General III-10
2.	Description III-11
3.	Signal Conditioning III-14
4.	Commutators III-19
5.	Subcarrier-Oscillator (SCO) Package III-24
6.	RF Transmission Equipment III-26
7.	Antenna Equipment III-28
E.	Command and Control Subsystem III-40
1.	General III-40
2.	Subsystem Description III-40
3.	Command Subsystem III-41
4.	Auxiliary Command Unit III-51
5.	Command Programmer III-56
F.	Power Subsystem III-56
1.	General III-56
2.	Batteries III-56
3.	Power-Switching Unit III-57
G.	Sensory Subsystem III-64
1.	General III-64
2.	Sun Sensors III-65
3.	Radial Accelerometer III-67
4.	Ion-Beam Probe III-67
H.	Electrical Integration III-70
1.	Wiring and Cabling III-70
2.	Fuse Block III-75

TABLE OF CONTENTS (Continued)

Section		Page
IV	SPACECRAFT DYNAMICS	IV-1
	A. Introduction	IV-1
	B. Measurement of Engine Thrust	IV-2
	1. General	IV-2
	2. Thrust Measurement Systems	IV-5
	3. Thrust Measurement Errors	IV-8
	C. The Precession Damper	IV-10
	1. General	IV-10
	2. Functional Description	IV-10
	3. Design Analysis	IV-11
	4. SERT T-3 Nutation Damping Characteristics	IV-14
V	GROUND EQUIPMENT DESIGN AND DEVELOPMENT	V-1
	A. General	V-1
	B. RCA Laboratory Test Station	V-1
	1. Description	V-1
	2. Development	V-5
	3. Checkout Control Equipment Rack	V-9
	4. Telemetry Receiving and Decommuation Equipment Racks	V-10
	5. Data Presentation and Recording Equipment Racks	V-11
	6. Command Test Equipment Rack	V-12
	7. General Test and Checkout Equipment	V-13
	C. Wallops Island Launch Checkout Equipment	V-15
	1. General	V-15
	2. Electronics Van	V-15
	3. Blockhouse and Terminal Building Equipment	V-15
	D. Flight Monitoring and Control Equipment	V-20
	1. General	V-20
	2. Spin-Rate Equipment Rack	V-20
	3. Command Programmer Equipment Rack	V-21
	4. Meter Panel	V-23
VI	TESTING PROGRAM	VI-1
	A. Introduction	VI-1
	B. Component Testing	VI-2
	1. General	VI-2
	2. Performance Measurements	VI-2

TABLE OF CONTENTS (Continued)

Section	Page
C. Systems Development Testing	VI-17
1. General	VI-17
2. Nutation Test	VI-17
3. Systems Electrical Development Tests	VI-18
4. Thermal-Vacuum Tests	VI-20
5. Qualification Vibration Testing, Model T-1B-1	VI-20
D. System Test Program	VI-24
1. General	VI-24
2. Prototype Model T-1B-3	VI-25
3. Flight Acceptance Testing, Flight Model T-3	VI-36
4. Performance, Prototype Model and Flight Model	VI-38
VII RELIABILITY ANALYSIS	VII-1
A. Introduction	VII-1
B. Failure Mode and Effects Analysis of SERT I	VII-1
C. Failure Mode and Effects Analysis of SERT I Ground Support Equipment	VII-5
D. Reliability Stress Analysis	VII-6
E. Summary of Reliability Analysis	VII-11

TABLE OF CONTENTS (Continued)

Appendix		Page
A	Analytical Determination of SERT Balance and Moments of Inertia (Configuration C)	A-1
B	Signal-Conditioning Data	B-1
C	Telecommunications Analysis	C-1
D	Telecommunication Accuracy Determination	D-1
E	Spin Rate Change Due to Ion Engine Thrust	E-1
F	Spin Rate Electronics and Communication Detection Error	F-1
G	Thrust Measurement Errors	G-1
H	Effect of Thermal Expansion on Moment of Inertia and Spin Rate	H-1
J	Modulation of Spin-Period Measurements Due to Nutation	J-1
K	The Treatment of Spin-Period Data	K-1
	Abstract	L-1
	Distribution	L-3

LIST OF ILLUSTRATIONS

Figure		Page
I-1	The SERT I Spacecraft	xii
I-2	SERT Spacecraft Inside the Scout Heat Shield	I-5
I-3	Location of Major Subsystems and Components in the SERT I Spacecraft	I-6
I-4	Artist's Concept of the SERT Spacecraft in Flight	I-8
I-5	Simplified Block Diagram of the SERT I Electrical System	I-10
I-6	Simplified Block Diagram of the SERT Ground Equipment	I-12
I-7	SERT I Mission Profile	I-14
II-1	SERT I Mechanical Configuration	II-2
II-2	SERT I Component Layout	II-3
II-3	SERT I Structure	II-4
II-4	Baseplate	II-5
II-5	Distributor Frame	II-5
II-6	SERT Mechanical Survey Models	II-8
II-7	Comparison of Apparent Dynamic Responses of Power Supplies for the Mercury-Bombardment Engine	II-12
II-8	Dynamic Response of Radial Accelerometer Mounted With and Without Urethane Isolators	II-13
II-9	SERT Static Load Test	II-15
II-10	Engine-Extension Subsystem Mounted on the SERT Structure	II-18
II-11	Antenna Ground Plane Wires Shown Being Stowed in the Lower Ring	II-21
II-12	SERT T-3 Spacecraft on the Balance Machine	II-33
II-13	Special Adapter for Spin-Axis Moment-of-Inertia Measurements	II-34
II-14	Box Frame and Standard for Transverse-Axis Moment-of- Inertia Measurements	II-35
II-15	SERT Spacecraft, Suspended by the Lifting Sling, Being Placed in the Shipping Container	II-36
III-1	Functional Block Diagram of the SERT System	III-3
III-2	Mercury-Bombardment Ion Engine	III-6
III-3	Simplified Schematic Diagram of the Neutralizer Voltage Control Unit	III-8
III-4	Neutralizer Voltage Control Unit	III-9

LIST OF TABLES

Table		Page
I-1	Government-Furnished Equipment (GFE) on the SERT I Spacecraft	I-1
I-2	SERT I Subsystem Weight Breakdown	I-5
I-3	SERT I Flight Sequence	I-15
I-4	SERT I Commands	I-17
I-5	SERT I Configuration Growth	I-21
III-1	SERT I Commands and Tones	III-43
V-1	RCA Laboratory Test Station Equipment Racks	V-6
VI-1	Summary of Environmental Tests	VI-3
VI-2	SERT Component Test Program	VI-4
VI-3	Prototype-Model Vibration Test Sequence	VI-23
VI-4	Flight-Model Vibration Test Sequence	VI-37
VII-1	Summary of Results from Reliability Analysis of SERT I	VII-3
VII-2	Summary of Results from Reliability Analysis of SERT I Ground Support Equipment	VII-7
VII-3	Summary of Results from Reliability Analysis of Reliability Estimate and Parts Application Review	VII-8
A-1	SERT Balance and Moment of Inertia Computation - T-3 Spacecraft	A-5

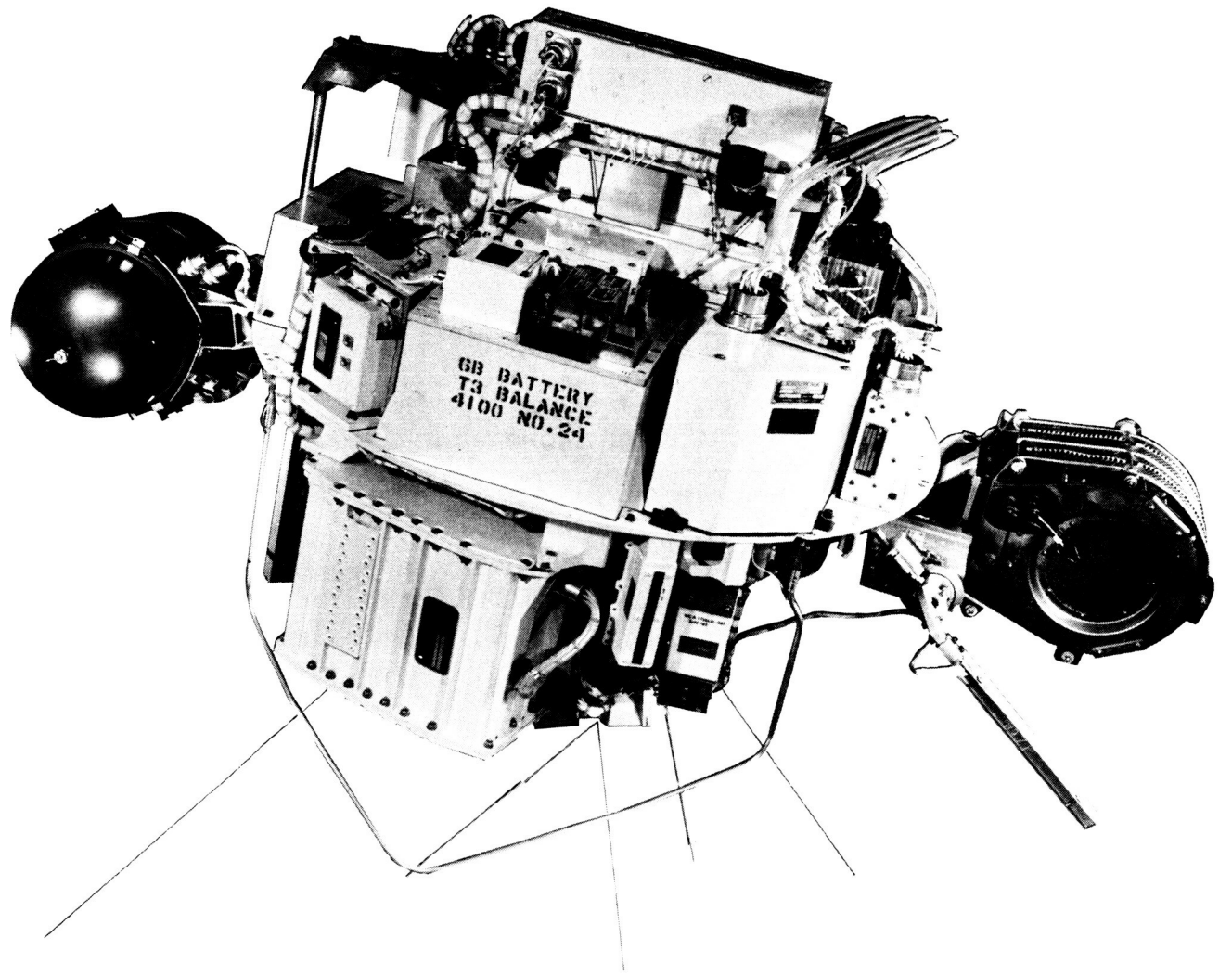


Figure I-1. The SERT I Spacecraft

SUMMARY REPORT on the DEVELOPMENT OF THE SERT I SPACECRAFT

SUMMARY

This final report describes the development of the spacecraft system for the SERT program. The program was carried out by the Astro-Electronics Division (AED) of RCA for the Lewis Research Center (LeRC) of the National Aeronautics and Space Administration under Contract No. NAS 8-2449. Specifically, RCA designed and built three prototype and two flight models of the SERT spacecraft, designed portions of the ground checkout and flight monitoring equipment, and provided assistance in testing and prelaunch checkout of the spacecraft. This report concerns work performed from the initiation of the contract in July, 1961, to the flight on July 20, 1964. Since the details of the flight and the analysis which followed are beyond the scope of this document, this information is not given herein. For such information, the reader should consult NASA report No. TN D-2718.

SECTION I INTRODUCTION

A. GENERAL

Ion-propulsion development, up to the initiation of the SERT program, had been exclusively concerned with analytical studies and laboratory testing of research engines. The success achieved in these areas led to a desire to operate these devices in the space environment in order to evaluate phenomena not readily amenable to ground testing and to determine the existence of unknown phenomena directly connected with the space environment. NASA, therefore, initiated the SERT program, with the aim of conducting a short-term space test of ion propulsion engines.

Two ion-engine systems representative of approaches under study were to be flown: a mercury-bombardment ion engine, developed by the NASA Lewis Research Center and a cesium-contact ion engine, developed by the Hughes Research Laboratory under contract to the Lewis Research Center. The engines to be flown would be research designs modified for the purposes of the test.

The major objective of the test was to study the behavior of ion-beam neutralization, without which, in general opinion, thrust is unobtainable. It was felt that limitations in vacuum-chamber testing, e.g., wall effects and incomplete vacuum, may have affected the successful neutralization achieved to date.

B. THE SERT I MISSION

The mission specified for the SERT I spacecraft (Figure I-1) was to test the mercury-bombardment and cesium-contact ion engines in a space flight. As conceived, the spacecraft would carry the two ion engines, each with its own power-conversion equipment, in addition to the power, communications, control, and sensory equipment necessary to in-flight operation of the engines and transmission of flight data. A one-hour flight with a ballistic trajectory was considered sufficient to sequentially operate the two engines and obtain the desired test data. For this flight, a standard 4-stage Scout, utilizing an ABL X258 fourth stage, was selected as an economical, available launch vehicle having the necessary performance characteristics.

The NASA Scout launch facility at Wallops Island, Virginia, was designated as the launch site, and the flight was to end with re-entry into the atmosphere over the Atlantic Ocean. The TIROS communication facility at Wallops Island was to be utilized for the command and telemetry functions, with the down-range station at Bermuda furnishing additional tracking and data-retrieval support.

C. THE SERT I SYSTEM

1. System Requirements

The SERT I system was designed to meet the specific requirements of the flight-test mission. For the spacecraft, the principal design and interface requirements, established at the outset of the program, are as follows:

- The spacecraft must provide a method for measuring ion-engine thrust during flight;
- It must contain and support the two ion engines for satisfactory in-flight operation;
- It must contain the power sources and power conversion equipment necessary to the in-flight operation of the ion engines;
- It must have the capability for complete self-programmed and remote control of in-flight system operation;
- It must provide the means for obtaining in-flight performance data;
- Provision must be made for the integration of Government-Furnished Equipments (GFE) into the spacecraft system (See Table I-1);

TABLE I-1. GOVERNMENT-FURNISHED EQUIPMENT (GFE) ON THE
SERT I SPACECRAFT

Mercury-Bombardment-Engine DC Power Supply
Mercury-Bombardment-Engine AC Power Supply
Cesium-Contact-Engine Inverter
Cesium-Contact-Engine AC Power Supply
Cesium-Contact-Engine DC Power Supply
Cesium-Contact-Engine Control Box
Mercury-Bombardment-Engine Neutralizer Power Supply and Transducer
Main Batteries (2)
Telemetry Battery
Programmer
Mercury-Bombardment-Engine Magnetic-Field Supply and Transducer
Commutators (2)
Radial Accelerometer
Flyaway Mounting Block
Cesium-Contact Ion Engine
Mercury-Bombardment Ion Engine

- It must be designed to fit within the launch-vehicle heat shield and to mate with, and separate from, the final stage;
- Its weight must not exceed the limits set by launch-vehicle stress and mission time-of-flight requirements;
- It must provide a satisfactory thermal environment for the components during mission lifetime and ground testing;
- The spacecraft and its components must be designed to withstand the launch and flight mechanical environment as well as handling loads to which it would be subjected; and
- The spacecraft system, subsystems, and components must be designed to provide a high degree of assurance of mission success.

The general design and interface requirements of the SERT ground equipment, designed to support the spacecraft system, are as follows:

- On-site checkout of the flight spacecraft;
- Go/No-Go checkout of the spacecraft during launch operations; and
- In-flight monitoring and control of spacecraft operation.

2. System Description

a. Spacecraft Configuration

The SERT spacecraft configuration was dictated primarily by mission requirements. Launch vehicle considerations further dictated the maximum physical configuration of the spacecraft.

To achieve the major objective of the test, i. e. , proof of ion-beam neutralization, a measure of the thrust produced was mandatory. A thrust of 0.006 pound, as was expected from the mercury-bombardment engine, would produce a linear acceleration of $1.7 \times 10^{-5}g$ on a 350-pound spacecraft. Because of the difficulties associated with the measurement of so small a linear acceleration, it was decided to apply thrust so that the angular momentum of the spacecraft, rather than the linear momentum, would be varied. Accordingly, a spin-stabilized spacecraft, with the ion engine mounted to apply torque about the spin axis, was selected. With this arrangement, thrust can be measured through detection of the rate of change of spacecraft spin rate. A very significant feature of this technique is the time integration of thrust by the spinning spacecraft. Because the spin-rate data was critical to the mission, redundant methods of measurement (sun sensors, radial accelerometers, and rf signal-strength variations) were employed.

The overall spacecraft, 30 inches in diameter and 28 inches in height, was designed to fit within the 34-inch heat shield of the Scout launch vehicle with internal clearances of at least 1 inch to allow for movement under dynamic stresses (see Figure I-2).

The spin-stabilized spacecraft selected utilized a circular, ribbed baseplate, which provided (1) symmetry about the spin axis, (2) availability of top and bottom surfaces for component mounting, and (3) structural efficiency proven in other spacecraft. The baseplate was mounted atop a hollow column to provide clearance between the Scout fourth stage and the components mounted under the baseplate.

For stability about the spin axis, the moment of inertia about that axis had to be larger than that about any other axis. To achieve this, the heavier components were mounted toward the outside of the baseplate. This mounting arrangement was also favorable with regard to thermal design because radiation from the larger components (having the greatest internal energy dissipation) was unobstructed. Although total weight (375 pounds) was a secondary consideration in this non-orbital spacecraft, it did affect the system configuration; the subsystem weights are given in Table I-2.

The ion engines were mounted on arms, hinged at the outer edge of the baseplate, which permitted them to be stowed below the baseplate during launch. After separation from the fourth stage, the engines would extend to positions well beyond the heat shield limitation. The extension was required (1) to minimize interference between the ion-engine exhaust and the spacecraft; (2) to reduce thermal coupling from the hot engines to the spacecraft; and (3) to increase the torquing moment arm of the engines. Figure I-3

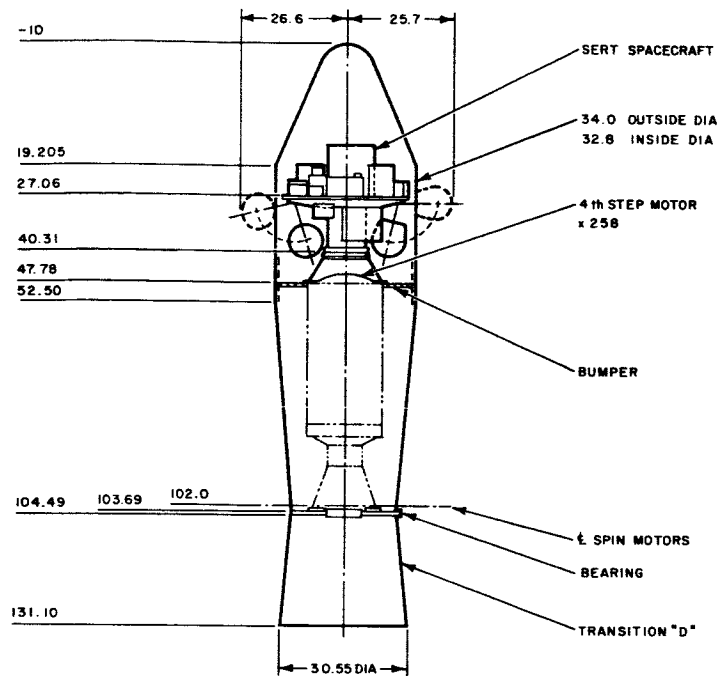


Figure I-2. SERT Spacecraft Inside the Scout Heat Shield

TABLE I-2. SERT I SUBSYSTEM WEIGHT BREAKDOWN

Mercury-bombardment-engine subsystem	94.91
Cesium-contact-engine subsystem	53.90
Telecommunications subsystem	33.72
Command and control subsystem	18.04
Power subsystem	73.75
Sensory subsystem	9.66
Structure (including distributor frame, ground plane, and detuning wings)	26.90
Miscellaneous mounting brackets (including engine extension subsystem)	21.98
Harness and squibs	17.57
Precession dampers	2.48
Balance weights	8.34
Potting, tacking, and miscellaneous parts	13.75
Total spacecraft weight	375.00

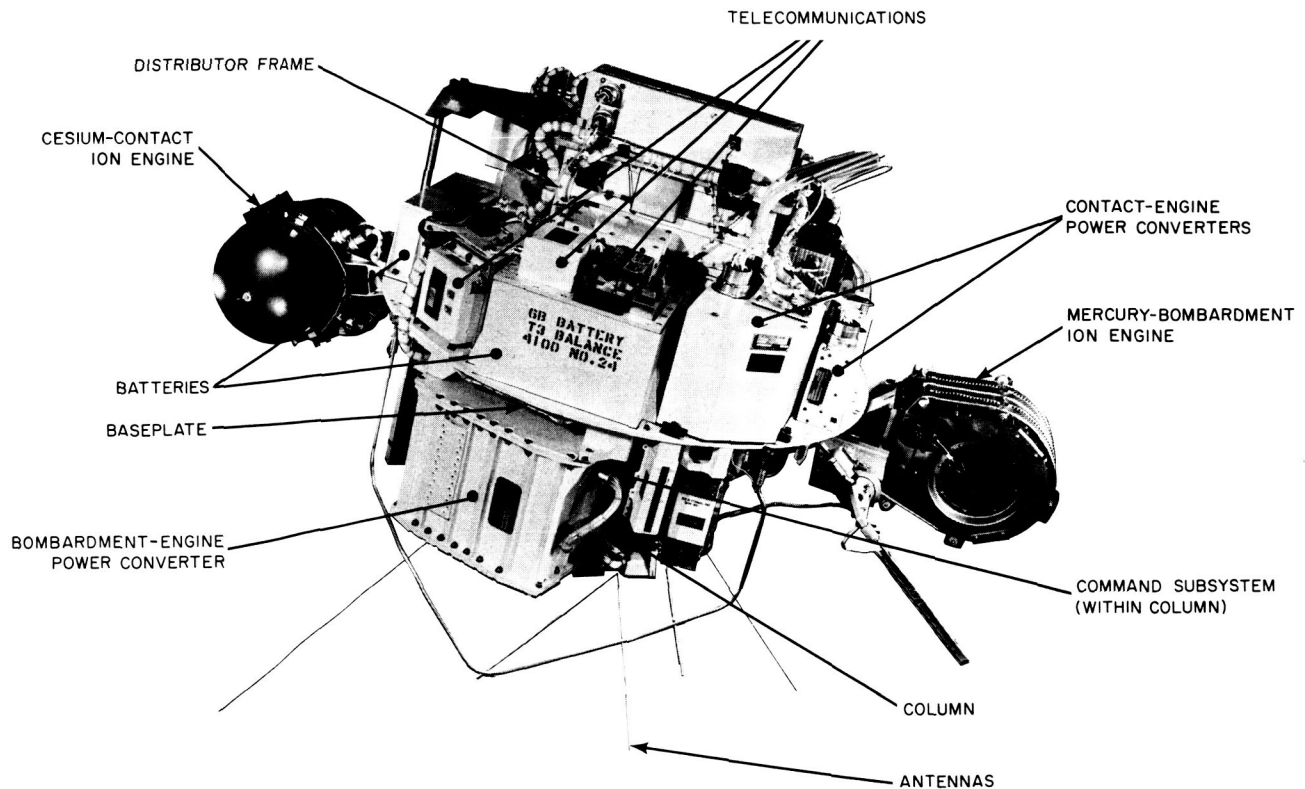


Figure I-3. Location of Major Subsystems and Components in the SERT I Spacecraft

shows the SERT I spacecraft with the engines in the extended position; also shown in the figure are some of the major component locations.

The electrical system was also developed in direct response to mission requirements. A major consideration, in view of cost and development time factors, was the use of off-the-shelf hardware wherever possible. The requirement for high power (up to 1.5 kw) for less than one hour gave rise to the selection of "one-shot," silver-zinc batteries (GFE) as the prime spacecraft power source. The use of solar power was discounted immediately because of the power-weight-time tradeoff, and rechargeable batteries such as nickel-cadmium or silver-cadmium were rejected because of their less favorable energy-to-weight ratio. The long-term multiple-use advantage of rechargeable batteries was also rejected in favor of the use of external power supplies for most test purposes. The requirement for dc-dc power converters to provide the high voltages necessary for ion-engine operation evolved as a result of the battery selection. Direct approaches of obtaining high voltages (e. g. , from a battery array) were rejected because of the many developmental problems and the unfavorable weight trade-off.

Selection of a simple pam-fm-fm telemetry system rather than one using a more sophisticated and efficient approach (e. g. , digital transmission) was based on the

minimum development cost and time required (most of the hardware could be obtained off-the-shelf) and on the adaptability with the ground station at the Wallops Island launch site. An on-board preset programmer for primary mission control was selected because of its simplicity and reliability compared with variable programming or complete control via ground command. In addition, the possibility of ion-engine-induced noise jamming a ground command system was a major consideration in favor of the preset programmer. A relatively simple command system with excellent noise-rejection characteristics was added to provide back-up ground control for the mission. It provided primarily for emergency shut-off of either of the two engine subsystems and activation of the other, and could also be used to direct mission operations in the event of programmer failure.

The engine subsystem power-switching function was designed with interlocks to prevent simultaneous operation of the two ion engines. Such operation would cause major electrical malfunctions as a result of the excess power demands and would also prevent successful measurement of engine thrust. To protect against draining battery power as a result of short circuits within the engine subsystems, special vacuum-safe-fusing was developed and added to the system.

The power and telemetry subsystems were specifically designed to be operable during the launch environment to provide a record of spacecraft operation.

b. Spacecraft Mechanical System

The mechanical subsystems of the SERT I spacecraft include the spacecraft structure, the engine-extension subsystem, the precession dampers, and the antenna ground plane and detuning wings. The function and salient features of each mechanical subsystem are described in the following paragraphs; design details are discussed in Section II.

- (1) **Spacecraft structure:** The main member of the structural and component arrangement is the 30-inch-diameter baseplate to which the majority of components are mounted, top and bottom. The distributor frame, located at the top center of the baseplate, is an open structural box, which contains additional components, supports the main routing of the spacecraft wiring harness, and acts as an anchor for top-component vibration braces. The third major structural element is the column, the hollow cylindrical member which allows space between the baseplate and the rocket fourth stage for mounting components on the underside of the baseplate. In addition, the column houses some of the command-subsystem components.
- (2) **Engine-extension subsystem:** The engine-extension subsystem provides mounting for the ion engines and implements their deployment to the operating position after separation from the Scout vehicle. The subsystem contains hinged ion-engine supporting arms, hydraulic

dampers, and various coupling and attaching hardware. The hydraulic damper is required to retard the unfolding motion caused by centrifugal force of the spinning spacecraft and to reduce the limit impact shock.

- (3) Precession dampers: Two redundant, mechanically-tuned precession dampers remove excess nutational motion from the spinning spacecraft by dissipating kinetic energy in the form of frictional heat.
- (4) Antenna ground plane and detuning wings: The antenna ground plane, (identifiable in the artist's concept, Figure I-4) is a radial array of wires located at the base of the spacecraft column. It is folded within a slot before launch and is extended after spacecraft separation. The ground plane serves to remove large nulls or asymmetries in the antenna patterns, which result from the rather distended exterior of the spacecraft. The detuning wings (also shown in Figure I-4) are a pair of metal loops extending from the baseplate at diametrically opposite locations 90 degrees from the ion-engine mountings. These loops, which extend as a result of centrifugal force, assist the antenna ground plane in removing large nulls from the antenna patterns.

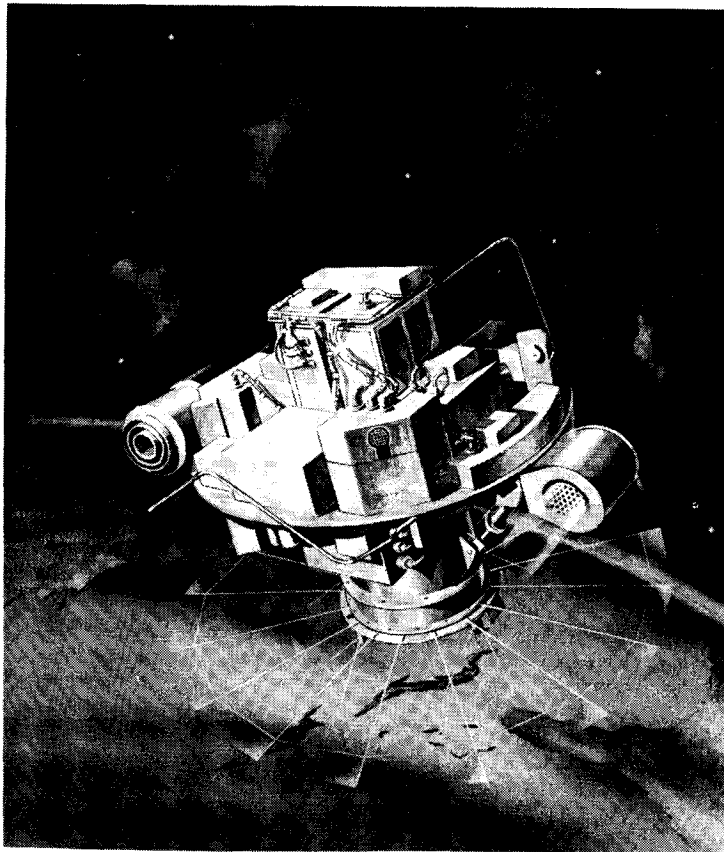


Figure I-4. Artist's Concept of the SERT Spacecraft in Flight

c. Spacecraft Electrical System

A block diagram of the SERT I electrical system is presented in Figure I-5. The electrical subsystems are described generally in the paragraphs that follow. The function, operation, and design of these subsystems and components are discussed in detail in Section III.

- (1) **Mercury-bombardment-engine subsystem:** This subsystem consists of the ion engine and the auxiliary equipment necessary to convert spacecraft primary power into the special forms required for engine operation. Its complement is as follows:
 - Mercury-bombardment ion engine;
 - AC and DC power supplies, for power conversion;
 - Special battery supplies, to provide special potentials; and
 - Neutralizer voltage control unit, for experimental variation of engine operating parameters.

- (2) **Cesium-contact-engine subsystem:** This subsystem includes the ion engine and its electrical support equipment:
 - Cesium-contact ion engine;
 - Inverter, DC power supply, and AC power supply for conversion of primary spacecraft power; and
 - Control box, for necessary subsystem control functions. The control box also provides mounting for the E-field-meter sensor.

- (3) **Telecommunications subsystem:** This subsystem processes, multiplexes, and transmits flight-telemetry data to the ground receiving stations. For increased reliability, all active elements are redundant. The major components of this subsystem are:
 - Signal conditioners, which convert spacecraft data outputs into signals compatible with the multiplexing equipment;
 - Commutators, for time-multiplexing of spacecraft telemetry data;
 - Subcarrier oscillators and rf transmitters, which frequency-multiplex the multiple channels of telemetry data and convert them to modulated power;

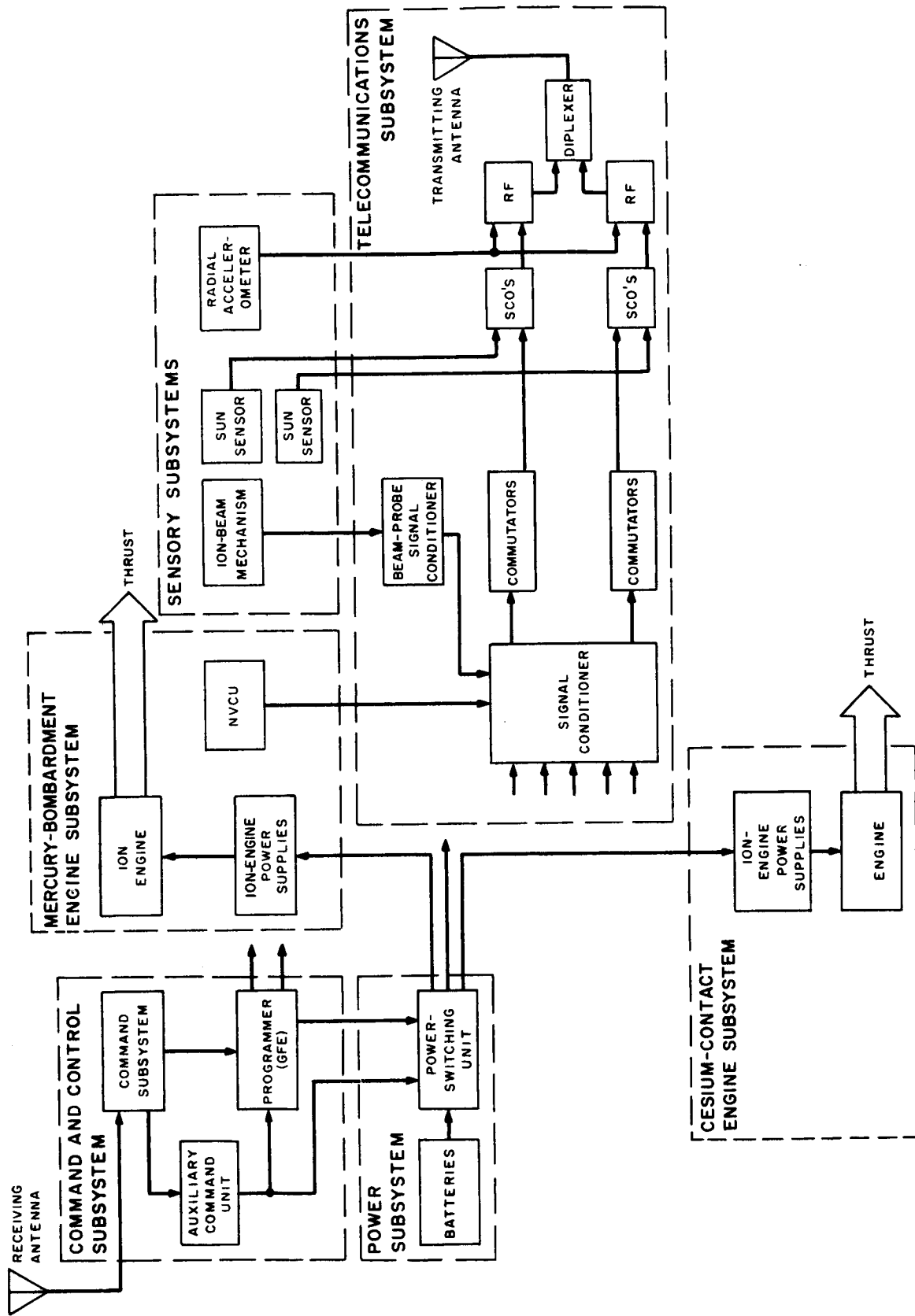


Figure I-5. Simplified Block Diagram of the SERT I Electrical System

- Diplexer and transmitting antenna, which combine the outputs and radiate these signals to the ground receiving stations.
- (4) **Command and control subsystem:** This equipment consists of the programmer, which controls the in-flight sequencing of spacecraft operations, and the command subsystem and auxiliary command unit, which decode and implement ground commands.
 - (5) **Power subsystem:** The power subsystem consists of batteries, which provide primary spacecraft power, and the power-switching unit, which switches power to the various subsystems at the direction of the command and control subsystem.
 - (6) **Sensory subsystem:** These subsystems measure special in-flight operating parameters which are transmitted to the ground stations via the telecommunications subsystem. It consists of:
 - Sun sensors, which detect successive sun crossings as required for spin-period measurement;
 - Radial accelerometer, for measurement of spin rate through detection of changes in radial acceleration; and
 - Ion-beam probe and mechanism, which is a device for mapping the energy profile of the mercury-bombardment-engine exhaust.

d. Ground Systems

The ground equipment for the SERT mission consists of those facilities necessary for prelaunch and launch support and for in-flight monitoring and control. A simplified block diagram of the SERT I ground equipment is shown in Figure I-6.

The major elements of this equipment, and their functions, are as follows:

- Electronics Van, a mobile van which contains all equipment necessary for launch-site checkout of the spacecraft;
- Blockhouse, Terminal Building, and Launch-Tower Equipment, which consists of the control equipment and external power sources necessary for immediate prelaunch checkout and control of the spacecraft; and
- Telemetry Building Equipment, located in the Telemetry Building at Wallops Island, which receives in-flight telemetry data and generates and transmits commands to the spacecraft in flight.

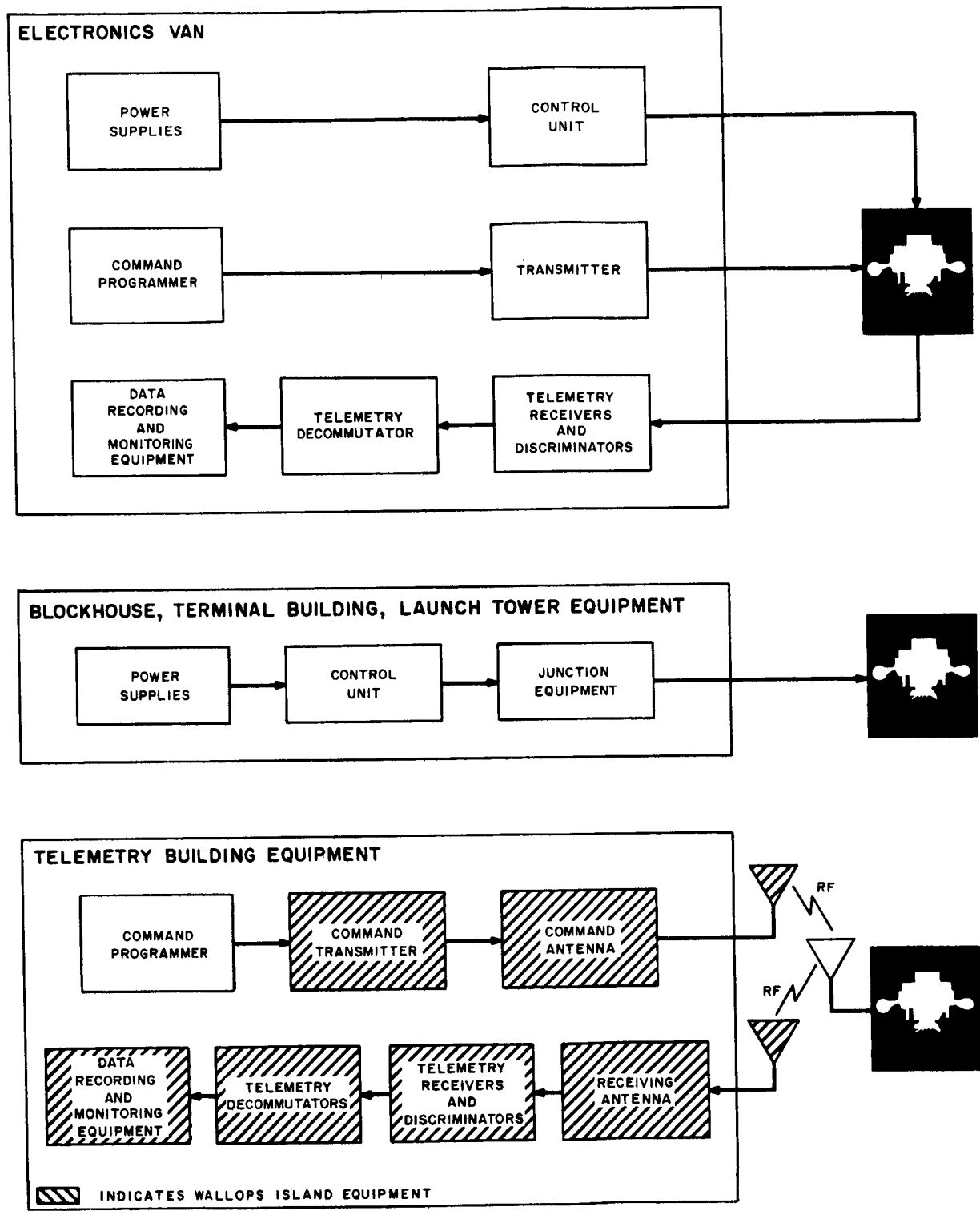


Figure I-6. Simplified Block Diagram of the SERT Ground Equipment

D. SYSTEM OPERATION (MISSION PROFILE)

The basic SERT I mission requirements have been defined as the alternate operation of the two ion engines in the space environment and the transmission of data sufficient to describe the operation of the engines and the spacecraft. As programmed, the mission was to consist of the following:

- Prelaunch operations, consisting of those events and test sequences occurring before Scout lift-off (T -0:00 time);
- Launch, all events occurring from the time of lift-off through spacecraft separation at T +5:02 (minutes, seconds);
- Cesium-Contact-Engine operation, from separation through T +27:15;
- Mercury-Bombardment-Engine operation, from T +27:15 to destruction at re-entry (approximately T +53:05).

The basic operational sequence of the mission is shown in Figure I-7. A more detailed description of the flight plan follows.

Flight operations are initiated approximately 18 minutes before launch when an external signal, fed to the spacecraft through the "flyaway" umbilical, activates the cesium-contact-engine subsystem, providing the time needed for warm-up of the cesium boiler. The power required during the prelaunch cycle for all spacecraft functions is supplied from an external source through the "flyaway" umbilical; some additional power is also provided, as needed, to bring the batteries up to full charge. Also included are provisions to bring the internal battery voltage down to acceptable levels, using externally-located resistor banks.

The spacecraft is fully activated at approximately T -40 seconds, when the programmer is started and power demand is switched to the internal supplies. The telecommunications and the command and control subsystems are fully activated, and the cesium-contact-engine subsystem warmup is continued on internal power. Full heater power to the cesium-contact-engine subsystem is switched on during launch-vehicle burning. After Scout fourth-stage burn-out, the spacecraft separation signal is fed from the programmer to the Scout separation mechanism ($t_{\text{prog}} = 5 \text{ min, } 31 \text{ sec}$). A simultaneous signal uncages the precession dampers. At this point in time, the spacecraft is spinning at approximately 100 to 120 rpm, the spin imparted to the last stage before ignition. Within several seconds of separation, the following sequence of events is directed by the programmer:

- (1) Engines extended: The programmer signal closes a relay (in the power-switching unit) to fire the two explosive pin-pullers holding the ion engines in the retracted position. With the pins pulled, the ion engines, under the influence of centrifugal force, move to the extended position in less than a second. The change in spin-axis moment of inertia results in a decrease in spin rate of approximately 20 percent.

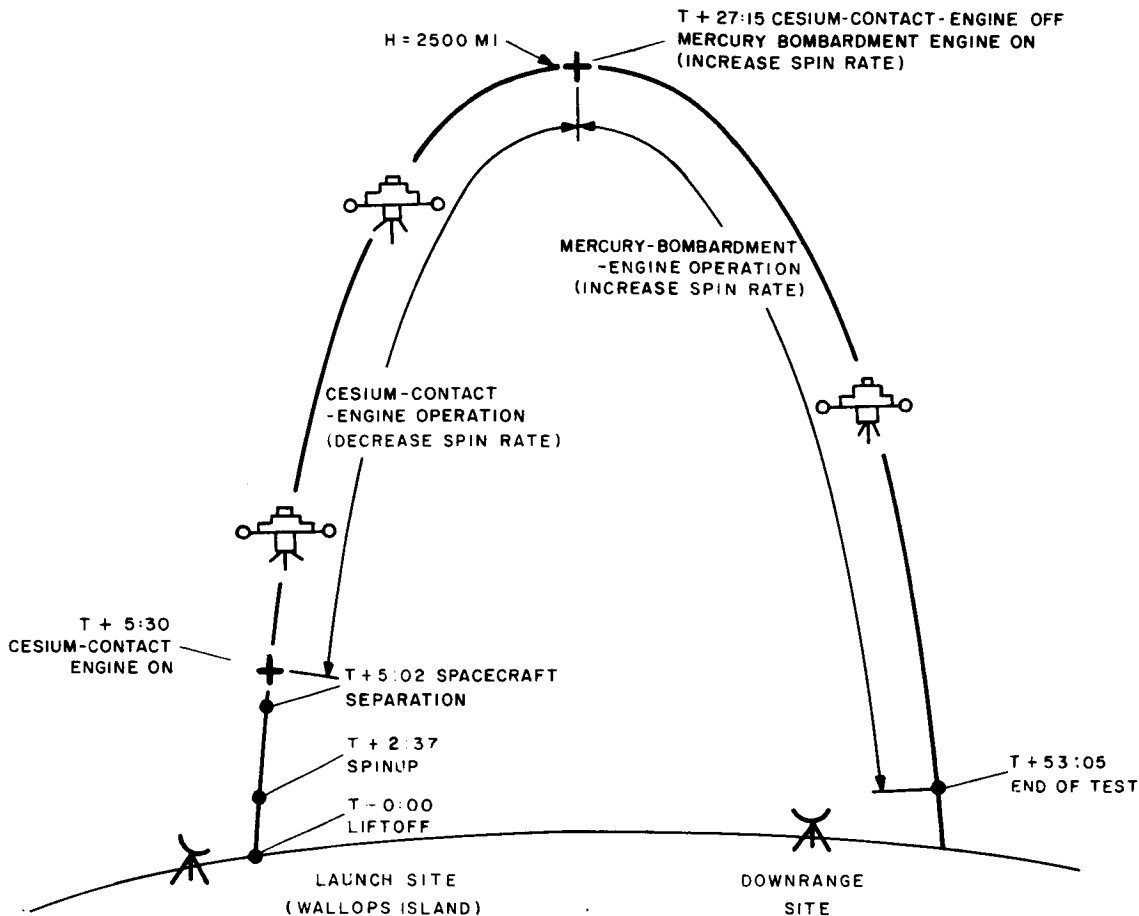


Figure I-7. SERT I Mission Profile

- (2) Pod-door release: An electrical signal sent to the cesium-contact-engine subsystem results in the release, under the influence of centrifugal force, of the door covering the exhaust (down-stream) end of the cesium-contact-engine pod. Removal of this door prepares the cesium-contact-engine, hermetically sealed and evacuated before flight to prevent contamination, for immediate operation.
- (3) Ground plane release: After the engines are extended, the radial array of wires which make up the antenna ground plane is deployed.
- (4) Cesium-contact-engine high-voltage On: The programmer then directs start of the cesium-contact-engine operation.

The complete flight sequence under programmer operation is given in Table I-3. Ion-engine current, voltage, and other operational parameters are conditioned and transmitted to the ground throughout the period of engine operation. Thrust measurement is provided by spin-rate data which is generated and transmitted through the entire flight.

TABLE I-3. SERT I FLIGHT SEQUENCE*

Real Time		Programmer Time	Description of Event
T -20'	Prelaunch	-	RF and telemetry On
T -18'		-	Cesium-contact-engine subsystem On
T -15' to 3'		-	Battery charging and payload telemetry evaluation
T -2'		-	Cesium-contact-engine superheater cutback confirmed by telemetry
T -40" to 35"		-	Activate Payload, confirm by telemetry
T -0		35" to 40"	Lift-off, confirm by payload control console
-		1'59"	Confirm full heat
-		5'31"	Confirm separation
-		5'33"	Confirm engines extended
-		5'35"	Confirm pod-door signal
-	Launch	5'44"	Confirm ground-plane signal
-		5'59"	Confirm cesium-contact-engine high voltage On
-			Describe engine operation and use command No. 2, 7, and 8 as required (Table I-4)**
-		12'29"	Confirm cesium-contact-engine subsystem auto program
-		13'29"	Confirm command No. 1 Armed
-		20'0"	Send and hold command No. 2
-		20'20"	Confirm cesium-contact-engine trap neutralizer operation — Describe operation
-		21'	Release command No. 2. Use commands No. 1, 2, 7, and 8 as required
-		26'34"	Confirm trap neutralizer study completed
-		26'39"	Confirm cesium-contact-engine high voltage Off
-	Cesium-Contact - Engine Subsystem Operation	27'38"	Confirm cesium-contact-engine subsystem Off
-		27'39"	Confirm cesium-contact-engine subsystem interlock Off
-		27'44"	Confirm mercury-bombardment-engine subsystem On — Describe engine parameters
-		27'46" to 39'41"	Observe boiler warm-up and send command No. 7 as required — Call out engine light, and continue to describe engine operation
-		39'44"	Confirm probe study and describe operation
-		41'43"	Confirm NVCU study and describe operation — use command No. 7 as required
-		47'33"	Confirm NVCU study completed
-		47'34"	Confirm probe survey started and mercury-bombardment engine neutralizer Off — describe operation
-		49'34"	Confirm probe survey started and mercury-bombardment engine neutralizer On
-		51'34"	Confirm probe survey started and mercury-bombardment engine neutralizer Off—describe operation
-	Mercury-Bombardment-Engine Subsystem Operation	53'34"	Confirm mercury-bombardment-engine neutralizer On

*This Table is drawn from NASA-LaRC memorandum Subject: SERT I Launch Flight Events, dated June 29, 1964.
 **Command sequences are included to indicate approximately where in the flight program they are "windowed" and would be utilized if so required.

During the cesium-contact-engine operational sequence, a number of experiments are performed during which certain engine parameters are varied. The command subsystem is used during this period to provide in-flight ground direction of the experimental investigations. The programmer then directs the power-switching unit to deactivate the engine subsystem after its sequence of operation is completed.

Power is then provided to the mercury-bombardment-engine subsystem at $t_{\text{prog}} = 27$ min., 44 sec., initiating its operational sequence. After several minutes of boiler warm-up, engine operation and thrust development should commence. The command subsystem may be used at this point, and later, to assist in engine start through interruption of its magnetic field. During periods of mercury-bombardment-engine operation, the effect of neutralizer potential on engine performance is studied through programming of the neutralizer voltage control unit (NVCU): the intensity of the ion beam is mapped with the aid of the ion-beam probe mechanism, and operation with the neutralizer voltage removed is attempted. Mercury-bombardment-engine operation is programmed to continue through flight termination.

The flight sequence, as described above, will be followed if flight operations proceed as intended. However, because of the possibilities of unexpected operation and/or in-flight failures, an independent method of operation using the command subsystem and auxiliary command unit was devised. The command subsystem can be utilized to provide three different approaches to flight direction:

- (1) Assist ion-engine operational sequencing within the basic program, that is, control of cesium-contact-engine neutralizer study, interruption of mercury-bombardment-engine magnetic field;
- (2) Direct programmer to advance from cesium-contact to mercury-bombardment-engine operation, or vice-versa; and
- (3) Completely direct in-flight operations and sequencing in the event of programmer failure.

In summary, operation of the SERT I system consists basically of the alternate functioning of either of the two ion-engine subsystems, with continuous telemetering of in-flight data. Flight sequencing is achieved with the programmer, the command subsystem, or a combination of the two. Operations commence shortly before lift-off and continue until the spacecraft is destroyed after re-entering the Earth's atmosphere.

Total time of flight above the sensible atmosphere is approximately 50 minutes; launch is easterly with an impact somewhere in the middle or south Atlantic. A peak altitude of 2500 to 3000 nautical miles and a maximum communications range of 3000 nautical miles are anticipated.

The third approach includes the generation of basic flight-operating signals, paralleling those emanating from the programmer: cesium-contact-engine full-heat, separation, engines unfold, cesium-contact-engine pod-door release, ground-plane release, cesium-contact-engine dc on, and cesium-contact-engine Off/mercury-bombardment engine On. A listing of the command subsystem functions is presented in Table I-4.

TABLE I-4. SERT I COMMANDS

Command No.	Mode-I Function	Mode-II Function
1	Cesium-contact-engine neutralizer potential program stop	Same as mode I
2	Cesium-contact-engine feed-valve closed	Same as mode I
3	Arm squibs	Select mode I*
4	Separation and damper squibs	Same as mode I
5	Unfold squibs	Cesium-contact-engine subsystem Off/mercury-bombardment-engine subsystem On
6	Cesium-contact-engine full heat On	Same as mode I
7	Select mode II* Cesium-contact-engine pod door Off Cesium-contact-engine boiler Off Mercury-bombardment-engine magnetic field interrupt	Same as mode I
8	Cesium-contact-engine dc On Ground plane squibs Cesium-contact-engine boiler Off and feed valve closed	Same as mode I
9	Programmer Advance (to mercury-bombardment-engine subsystem operation)	Same as mode I
10	Mercury-bombardment-engine subsystem Off/ Cesium-contact-engine subsystem On	Same as mode I
*Refer to Table I-3		

E. SYSTEM DEVELOPMENT

This section will describe, in some detail, the development of the SERT I spacecraft system at RCA, from the inception of the program in mid-1961 until the delivery of the T-3 flight spacecraft in mid-1964. As originally conceived, SERT I consisted of the basic elements necessary to the steady-state operation of the ion engines:

- The mercury-bombardment and cesium-contact ion engines,
- Mercury-bombardment-engine power converters,
- Cesium-contact-engine power converters,
- A power subsystem,
- Telecommunications, and
- A programmer.

In this early concept, in-flight sequencing was to be performed by the programmer alone; no experiments were considered during engine operation; and spin-rate sensing was provided by the sun sensors only. The weight of this original configuration was estimated at approximately 250 pounds. During the initial growth and development cycle of late 1961 and early 1962, NASA decided to expand the basic mission and the operational flexibility by adding the following equipment:

- The command subsystem,
- The cesium-contact-engine control box,
- The neutralizer voltage control unit, and
- The mercury-bombardment-engine probe.

The command subsystem, as conceived, was to provide two types of control: (1) ground control of a cesium-contact-engine sub-program in which system optimization would be studied, and (2) a limited degree of system control to be used in overriding the programmer. High noise immunity was a primary requirement for the command subsystem since it was felt that generation of an rf noise field by the ion engines was probable. Further protection against inadvertent commands being generated by this noise was included in the system design by linking the command subsystem to the programmer to provide "windows," or limited time periods, during which the command subsystem was to be functional. Programmer back-up consisted of all events up to and including turn-on of the cesium-contact engine, and advancing or resetting the programmer to either the cesium-contact or the mercury-bombardment-engine-subsystem cycles. These latter commands were those "windowed" by the programmer. The cesium-contact-engine control box was added to perform needed control and sub-programming functions in the cesium-contact-engine subsystem, and also served as a mounting for the E-field meter. The mercury-bombardment-engine subsystem was supplemented with the neutralizer-voltage control unit (NVCU) as an

experiment to determine the effect of neutralizer potential on engine operation. Similarly, the ion-beam probe was conceived as an experiment to map the energy within the beam of the mercury-bombardment engine.

No major configuration changes were required to accommodate the above equipment. The command subsystem was designed to fit the interior of the column structure; the cesium-contact-engine control box was located atop the engine AC power supply; the NVCU was integrated above the distributor frame; and the ion-beam probe equipment was mounted in the space beneath the baseplate.

A number of important system concepts evolved during this development period. Of special interest are the following:

- (1) The special nature of the ion engines makes them subject to damage if activated in air. Hence, it became necessary to develop engine simulators, or "electrical dummy engines," to be used during system and subsystem testing. Because of the excessive weight, size, and reliability-degradation of high-voltage and high-current switches, a design approach was adopted in which the need for such switches was obviated by interchanging the engine input lead between the engines and the simulators. Similarly, the power input leads for the engine subsystems were interchanged between the spacecraft batteries and an external source. Under this philosophy, final checkout of the SERT ion-engine power converters cannot conveniently be conducted any later than 8 hours before launch, at which time final mating of the heat shield to the Scout rocket is to be accomplished.
- (2) Usually, the signal and power for activating the separation squibs to release the spacecraft separation clamp are provided aboard the Scout fourth-stage. For SERT I, it was decided to save approximately 10 pounds by providing both signal and power from the spacecraft. This decision was felt to be logical since (a) the programmer, which provided the separation signal, was important to mission success in any case, and (b) the spacecraft already contained adequate squib-firing power.
- (3) Scout generally provided a "clamp-catcher" on the final stage to prevent the separation clamp from striking the spacecraft during separation. However, to accommodate this device, the antenna whips would have to be mounted away from the base of the spacecraft column; therefore, to achieve the better antenna performance available with the optimally-positioned antennas, special "clamp-deflectors" were designed to mount at the base of the spacecraft and the "clamp-catcher" was not used.
- (4) Thermal analysis early in the program revealed that, unless special provisions were made, the cesium-contact-engine-subsystem inverter would overheat during the programmed flight, if the spacecraft temperature exceeds 70° F. It was decided, therefore, to cool the spacecraft during the immediate prelaunch phase using dry air or nitrogen ducted to the heat shield.

- (5) Immediate in-flight operation of the cesium-contact-engine subsystem dictated the addition of a pre-heat cycle during the final countdown. To alleviate drain of the main battery power source, it was decided to introduce external power through the "flyaway" umbilical. External power for the telecommunications subsystem was also provided.

The first complete spacecraft (configuration A of Table I-5) was thus evolved to include the subsystems and special system characteristics described above. The mechanical design and integration approach was to place those components having the greatest thermal dissipation at outboard locations (so as to maximize heat radiation to space) and also to arrange components, especially the batteries, for ease of installation and removal. As described in paragraph II-D, balance and moment of inertia requirements were also critical factors in establishing component arrangements.

The first operating SERT model of the A configuration was an electrical prototype model, designated T-2. Its assembly and operation were preceded by a series of mechanical tests performed on two mechanical models identified as T-1A (static test model) and T-1B (dynamic test model). The T-1A and T-1B models served to verify the basic mechanical integrity of the spacecraft design.

During early electrical testing of the T-2 model, considerable difficulty was experienced in attaining successful operation of the power-switching unit (PSU). Because of the requirement to switch the 20- to 30-ampere ion-engine-subsystem current in a relatively small space, the original design of the PSU employed silicon-controlled rectifiers (SCR's) for major switching. However, the unusual load characteristics of the ion-engine power converters and the transients induced into the system by these components caused inconsistent operation of the SCR's in the power-switching unit. The problem was solved after it was determined that the high currents could be controlled at the inversion circuits within the ion-engine power converters. The PSU was then redesigned with relays replacing the SCR's; these relays provided low-current switching needed to control the aforementioned inversion circuits.

During the latter stages of T-2 development, NASA requested RCA to study the feasibility of adding several additional equipments to the existing design and to investigate the structural modifications necessary (1) to support these additional components, and (2) to reduce vibration amplifications in the area of some of the ion-engine equipment. The new components under consideration were (1) an accelerometer for thrust measurement, (2) a calibration device for in-flight moment of inertia determination, and (3) a system for measuring rf noise created by the ion beam. In consideration all program factors, it was decided after completion of the study (Reference I-1) to add only the radial accelerometer to the spacecraft. This device measured acceleration radial to the spacecraft spin axis; its output, being a frequency proportional to acceleration, provided the accuracy necessary for precise measurement of spin-rate variation (and thrust).

TABLE I-5. SERT I CONFIGURATION GROWTH

Configuration	Weight	Major Elements	Changes
A (T-2)	304 lbs	Final configuration minus: radial accelerometer; auxiliary command unit; ion-beam-probe power supply; sun-sensor voltage regulator; diplexer ballast load; and fuse block	---
B (T-1B-2)	323 lbs	Final configuration minus: auxiliary command unit; ion-beam-probe power supply; sun-sensor voltage regulator; diplexer ballast load; and fuse block.	Addition of radial accelerometer; relocation of communications components. Weight growth in cesium-contact-engine subsystem, power-switching unit, engine-extension subsystem, and mercury-bombardment engine.
C (T-3) (T-1B-3)	375 lbs	Final Configuration	Addition of auxiliary command unit, ion-beam-probe power supply, sun-sensor voltage regulator, diplexer ballast load, fuse block, and balance weights; weight growth in mercury-bombardment-engine power supplies.

The accelerometer output would directly modulate the rf transmitter without interfering with the existing subcarriers. The device was procured by NASA and provided to RCA for integration aboard the spacecraft.

The T-2 model was delivered to NASA for use in vacuum testing of the ion-engine subsystems integrated with the spacecraft system. Concurrently, RCA conducted a vibration testing program on the T-1B mechanical model, revised to represent the new B configuration (Table I-5). The results of this testing are described in paragraph II-B. This model was later modified to serve as a vibration-qualification test bed for SERT subsystems, and, in this configuration, was identified as T-1B-2.

Because of difficulties with the ion-engine subsystems, uncovered during T-2 vacuum-chamber testing, NASA introduced design modifications to the component equipment and to the overall system as well. Consequently, NASA requested RCA to consider the design changes necessary to accommodate larger and heavier mercury-bombardment-engine power converters. A reduced vibration environment was also specified as a result of the refinement of flight data on the Scout vehicle. RCA determined, after study (Reference I-2) of the mechanical and thermal environmental changes, that the new power converters for the mercury-bombardment ion engines could be integrated with some shift of equipment locations (for example, moving the subcarrier oscillators from the side of the mercury-bombardment-engine power converters to positions atop the main batteries) and with an increase in the structural support provisions for these converters. Major structural rework, however, was found to be unnecessary.

Further system modifications arose from continued T-2 testing by NASA and from a system reliability investigation conducted by the system contractors under NASA direction. These modifications included the following:

- (1) The electronic commutators in the telecommunications subsystem were replaced with mechanical commutators. This was necessary to prevent commutator damage resulting from system transient overvoltages induced by high-voltage arcing in the ion engines.
- (2) The signal conditioner circuitry was modified to both accommodate the mechanical commutators and to improve reliability. Protection against ion-engine-induced transients was also added.
- (3) The auxiliary command unit, which provides complete ground control of system operation, was added to the command and control subsystem. Additional command functions found to be useful during T-2 testing were also implemented through this modification. Special diode networks were later added, at NASA request, to modify several command functions for the cesium-contact-engine and mercury-bombardment-engine subsystem.

- (4) Special explosion-proof fusing was developed and incorporated in the system to protect against complete system failure due to in-flight short-circuiting of the main power source by either of the two ion-engine subsystems.
- (5) To protect against inductive transfer of voltage transients, the harness was separated into three major sections: signal, high voltage, and high current.

The configuration, modified to include the enlarged mercury-bombardment-engine power converters, was subjected to an investigation of mechanical integrity and vibration-resonance characteristics using a new mechanical model identified as T-1D (shown being tested in Figure II-6). Subsequently, the flight prototype spacecraft (T-1B-3) was integrated to the final configuration (Table I-5) and subjected to an electrical test program, a vibration qualification program, and a thermal calibration at RCA. It was then shipped to the Lewis Research Center where it was subjected to thermal-vacuum and transient-vacuum qualification tests with operating ion engines. During the thermal-vacuum testing, ion-engine subsystem malfunctions were traced to high-voltage breakdown within the ion-engine power-supply connectors. These connectors were conventional designs, modified for high-voltage applications. This problem was resolved by encapsulating the high-voltage leads directly within the existing component receptacles. At this time, RCA and NASA conducted concurrent investigations and development programs concerning high-voltage terminations and disconnects. Although a qualified high-voltage disconnect emerged from the evaluation and it appeared as though a successful encapsulation technique was developed, the investigation revealed some uncertainty as to the aging and repetitive thermal-cycling effects on the encapsulation.

Shortly after T-1B-3 testing, the flight spacecraft (T-3) was integrated to the T-1B-3 configuration and was acceptance tested at RCA and the Lewis Research Center. It was then shipped to the Wallops Island launch site where final checkout and prelaunch preparations were accomplished. The final full systems test was conducted just before Scout integration; the engine leads were then removed from the ion-engine simulators and installed on the flight engines for the last time. This operational modification also deleted the requirement for utilizing the electronics van during final launch operations; rather, final spacecraft systems confirmation was obtained via telemetry using the ground receiving station at the Wallops Island Telemetry Building.

REFERENCES

- I-1 RCA Document SPO-10, "A Study of the Addition of New GFE Components to the SERT Capsule," Contract NAS 8-2449, Oct 3, 1962.
- I-2 RCA Document SPO-58, "A Study of the SERT Capsule of Modifications to the LeRC Engine Power Supply System," Contract NAS 8-2449, Jan 23, 1964.

SECTION II

SPACECRAFT MECHANICAL DESIGN

A. GENERAL

The complete SERT I spacecraft, at a diameter of 30 inches and a height of 28 inches, was designed to fit within the 34-inch heat shield of the Scout rocket with internal clearance of approximately 1 inch. The components are mounted directly to the top and bottom of the spacecraft baseplate, inside the hollow supporting column beneath the baseplate, and hinged along side the structure to provide an extremely compact 375-pound spacecraft. The high density of the spacecraft coupled with its very high heat power (600 watts) dictated a component layout in which thermal considerations were paramount.

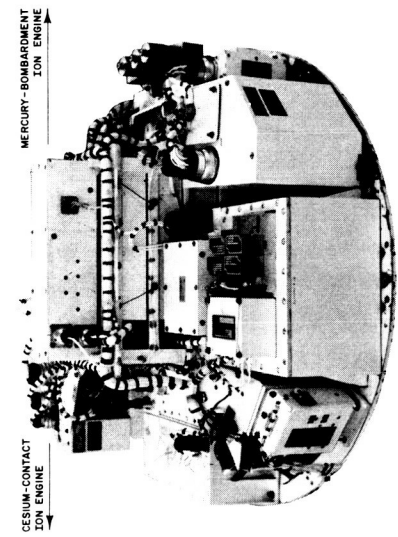
This section describes (1) the design, construction, and development of the SERT structure and the mechanical subsystems required to support spacecraft operation; (2) the thermal considerations which influenced the spacecraft design; (3) the various factors which govern the selection of component arrangement and mounting; and (4) the methods used in fabricating and handling the spacecraft and performing mechanical measurements. The mechanical configuration of the SERT I spacecraft is shown in Figure II-1; Figure II-2 shows the location of components on the top side of the baseplate.

B. STRUCTURE

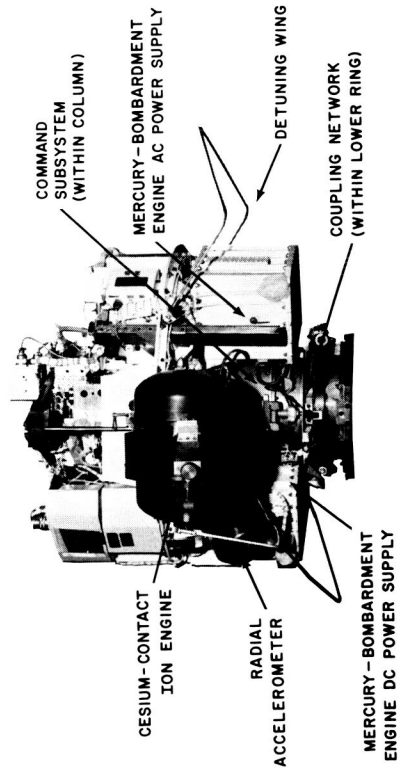
1. General Discussion

The SERT I structure consists of four major assemblies — the lower ring, the center column, the baseplate, and the distributor frame — which form an integrated structural member (Figure II-3) supporting all the components mounted on the baseplate and providing, at the lower ring, an interface for mounting the spacecraft to the adapter section of the fourth stage of the Scout rocket.

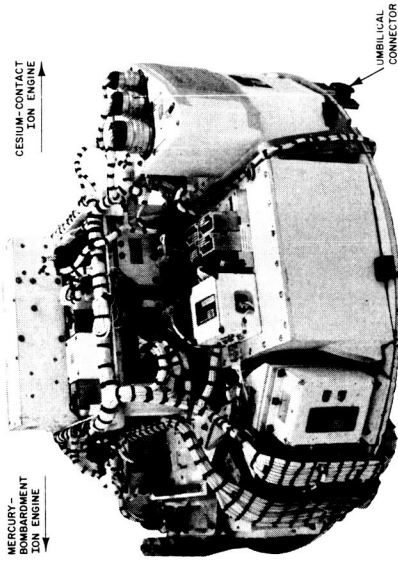
The lower ring is essentially a hollow cylinder, 3.940 inches high, with flanges at both ends. The top flange is a simple, radially orientated rib of constant diameter and height. The bottom flange, however, is more complicated in shape. It is on this bottom flange that pads of various sizes and orientations are machined for the attachment of the deflectors for the rocket quick-disconnect clamp and the antenna mounts. In addition, a radially deep, annular groove is machined on the outer surface (edge)



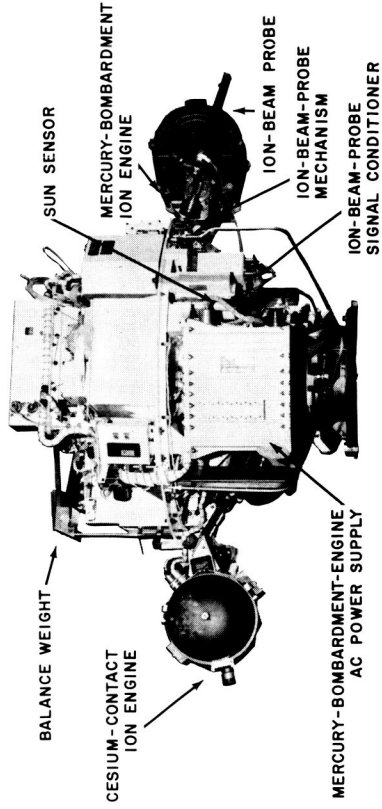
TOP VIEW (-X SIDE)



SIDE VIEW (-X SIDE)



TOP VIEW (-Y SIDE)



SIDE VIEW (-Y SIDE)

Figure II-1. SERT I Mechanical Configuration

NASA CR-54243
AED R-2565

ERRATA SHEET
for the
SUMMARY REPORT
on the
DEVELOPMENT OF THE SERT I SPACECRAFT

prepared for
NATIONAL AERONAUTICS AND SPACE ADMINISTRATION
CONTRACT NAS 8-2449

by the
RADIO CORPORATION OF AMERICA
ASTRO-ELECTRONICS DIVISION
PRINCETON, NEW JERSEY

Errata:

Page II-2, Figure II-1 The "TOP VIEW (-X SIDE)" should be "TOP VIEW (+Y SIDE)," and the "CESIUM-CONTACT ION ENGINE" and the "MERCURY-BOMBARDMENT ION ENGINE" callouts are reversed. In the "TOP VIEW (-Y SIDE)" the "CESIUM-CONTACT ION ENGINE" and the "MERCURY-BOMBARDMENT ION ENGINE" callouts are also reversed.

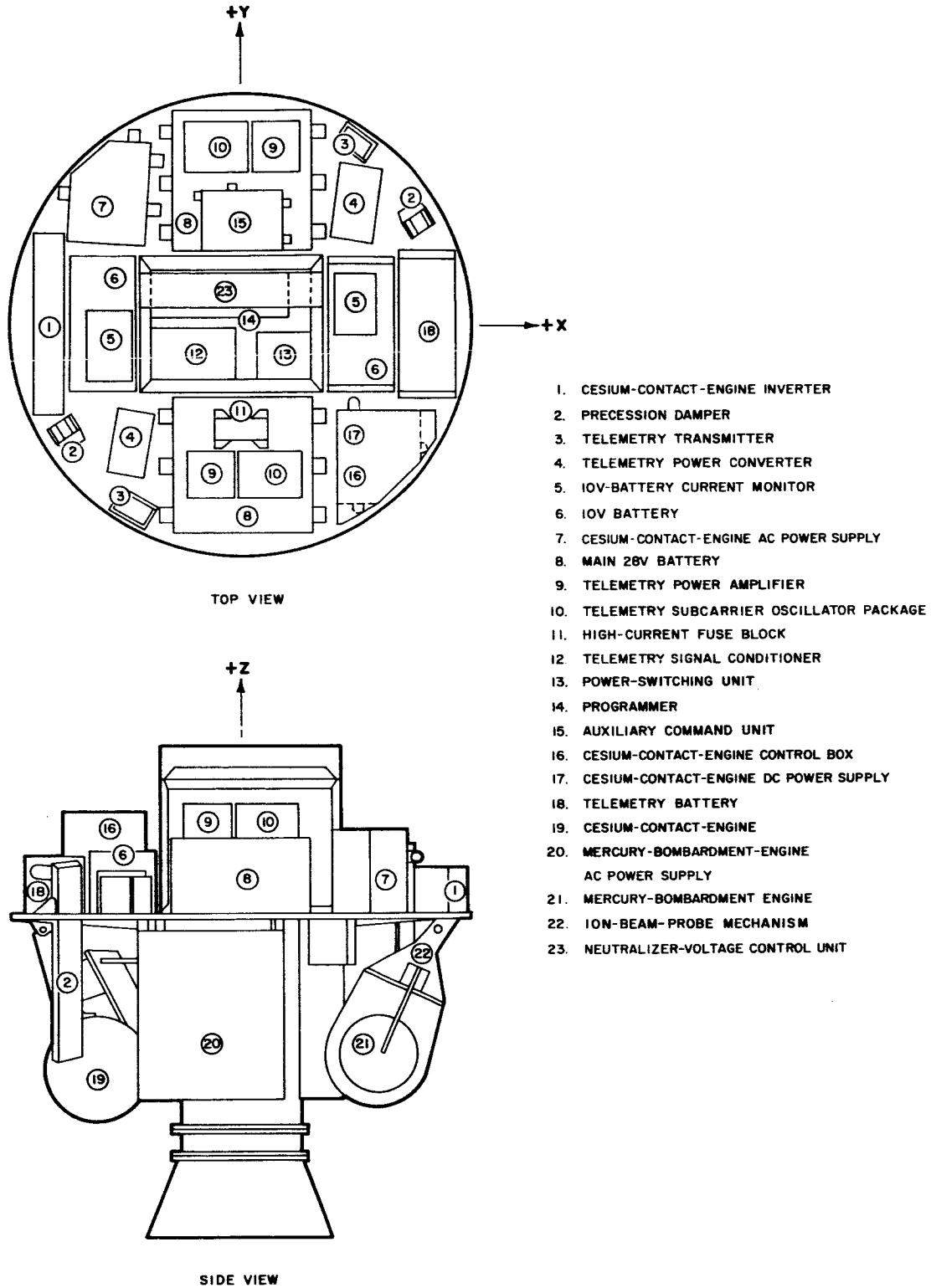


Figure II-2. SERT I Component Layout

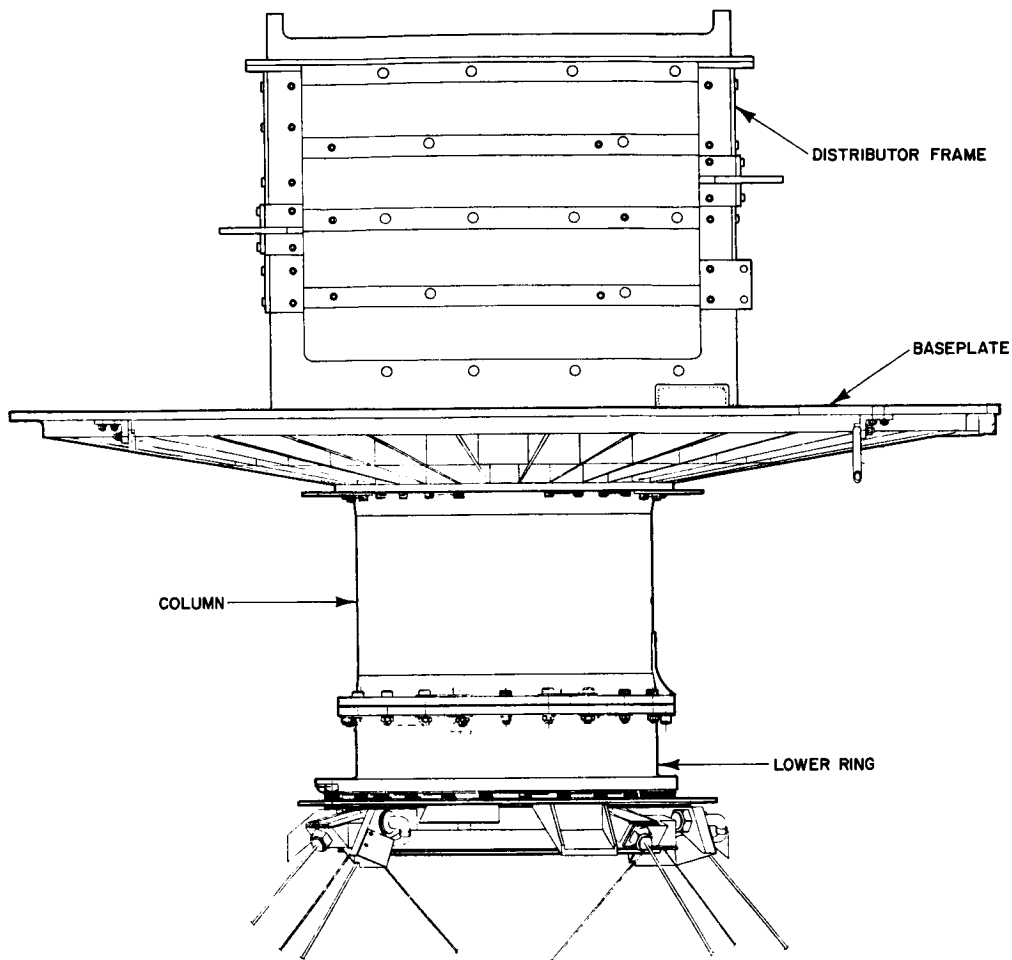


Figure II-3. SERT I Structure

of this flange for storing the antenna ground-plane wires until they are extended during flight. Lastly, an interface is provided to which the adapter of the fourth-stage rocket is attached. For a more detailed description of the lower-ring assembly, refer to Paragraph II-B. 6.

The center column is a thin-wall, flanged, cylinder. The lower flange of the center column is bolted to the top flange of the lower ring and its upper flange is bolted to the hub of the circular baseplate. The height (6.763 inches) of the column is dictated by the critical heights of some spacecraft components. That is, the components mounted on the top side of the baseplate can not exceed the envelope defined by the spacecraft heat shield, and the components suspended from the bottom of the baseplate can not interfere with other components mounted on the lower-ring assembly. The space inside the column is utilized to house the antenna diplexer and the command subsystem. For more details, refer to Paragraph II-B. 5.

The baseplate (Figure II-4) is essentially a circular flat plate reinforced by a cylindrical hub at the center and thirty-two radial ribs of tapering height. The baseplate

is further strengthened by two reinforcing rings concentric with the hub; the first one is located near the periphery of the baseplate, the other about mid-way between the hub and the first ring. The entire baseplate is machined from a forging of magnesium alloy AZ-80A-T5. This method of fabrication was chosen because of its inherent advantage, among others, of being able to provide generous fillet radii between intersecting structural members, thus minimizing effects of stress concentration. This was a major consideration in the design of the baseplate for vibratory loads. The baseplate is described in more detail in Paragraph II-B.4.

A distributor frame (Figure II-5) is mounted on the top of the baseplate at its center. To this frame, electronic components such as the neutralizer voltage control unit, programmer, signal conditioner, and power-switching unit are attached. The four corner posts of the distributor frame are reinforced for the attachment of the brackets which are used to restrain lateral motions of some components located at the outer edge of the baseplate.

Mounted on the major assemblies described above are various secondary structural members which support several spacecraft components:

- Supporting brackets for each of the two ion engines and their associated arms and hydraulic dampers are attached to the baseplate at the machined bosses on the bottom.
- Miscellaneous brackets for the mounting of the detuning-wing assemblies and ion-beam probe mechanism are bolted to the bottom of the baseplate at its rim.

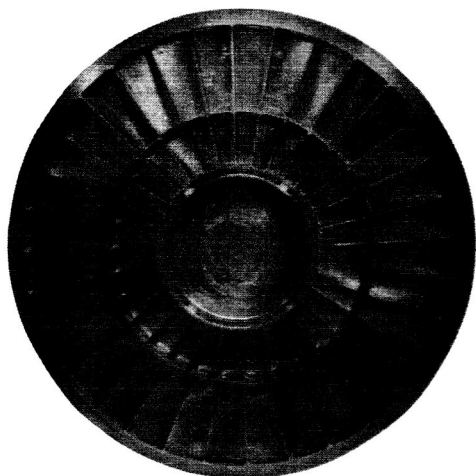


Figure II-4. Baseplate

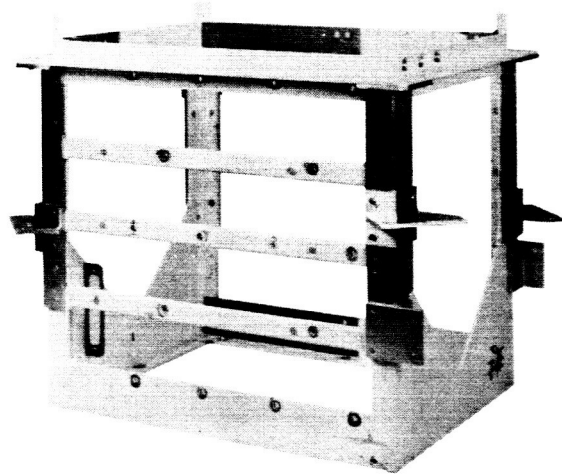


Figure II-5. Distributor Frame

- A strut and a stabilizing bracket, attached to the center column at its upper and lower flanges, provides mounting for the accelerometer.
- The supports for the locking devices of the hydraulic damper assemblies are mounted on the lower flange of the center column.

The SERT I structure supports a total spacecraft weight of 375 pounds, with most of the weight held by the baseplate. The structure was originally designed for a gross weight of 300 pounds and a vibration load of 53.5 g in the thrust axis; this load corresponds to a 10.7-g input in the critical frequency range of 50-500 cps, multiplied by an estimated amplification factor of 5.0. Vibration loading in the lateral direction, shock loading, and acceleration loading are less critical than thrust-axis vibration. Throughout the program, additional weight could be accommodated with no major structural modifications because of a reduction in the specification vibration level. A more detailed presentation of design loads on the SERT I structure can be found in Reference II-1.

Under the action of loads in the thrust direction, the SERT I structure transmits the loads to the fourth-stage interface by means of bending and shear in the baseplate and direct, axial, tension, and compression in the column and the lower ring. For laterally applied loads, the structure acts as a cantilever beam fixed at the fourth-stage interface (the vibration facility interface, upon which the design is postulated). However, there is some minor local bending in the baseplate due to the transverse loads on the baseplate-supported components.

Dynamically, the SERT I spacecraft is a multi-degree-of-freedom system: the response of the spacecraft, in general, and some components, in particular, to an applied excitation force is of such a complex nature that an accurate theoretical analysis becomes very involved. However, by treating the spacecraft as a simple mass-spring-dashpot system, a natural frequency was determined which agreed very well with the average natural frequency found in subsequent vibration tests. In this simple system, assuming the spacecraft to be a single mass — with the baseplate, the center column, the lower ring, and the rocket fourth-stage adapter acting as springs in series — and assuming a low critical damping ratio of 0.05 for the dashpot, the natural frequency is 89.5 cps. It should be noted that this natural frequency is essentially dictated by that of the baseplate which has a much lower spring constant than the other structural members.

The weights of the major structures are 10.4 pounds for the lower ring and the column, 10.7 pounds for the baseplate, and 4.87 pounds for the distributor frame.

2. Development of the Structure

The development of the SERT I structure is described in the following section. It parallels, to some extent, the configuration changes described in section I-E.

The mechanical performance of configuration A, the original design, was evaluated in a series of model tests consisting of (1) static load tests of the baseplate, (2) determination of vibration resonance for the entire structure, and (3) structural integrity

tests at prototype vibration levels. The static load tests (refer to Paragraph II. B. 4. c) verified the capability of the structure to withstand anticipated loads. For the configuration-A vibration testing, a model of the spacecraft, designated T-1B, was developed, utilizing dummy weights to simulate the components. For instrumentation of this model, dynamic strain gages and accelerometers were used (Figure II-6). During the resonance surveys (References II-4 and II-10), most components exhibited amplification factors of eight-to-one, or less, with some components being slightly higher. The integrity of the basic structural design was satisfactorily demonstrated in a vibration test at full prototype level.

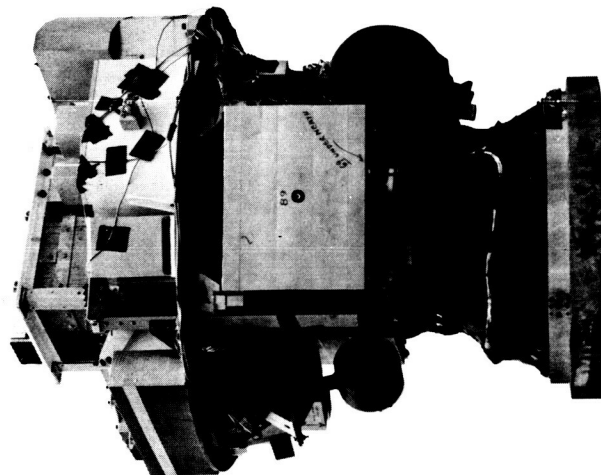
The basic structure remained essentially unmodified for the B configuration, although the component layout was changed to accommodate new components (especially the radial accelerometer) and additional connecting brackets. The vibration survey model T-1B was integrated to the new B configuration, and a vibration evaluation was performed, with the major aim the reduction of amplifications at the power supplies for the mercury-bombardment and cesium-contact ion engines.

The structure was further evaluated for the B configuration during a vibration qualification test performed on model T-1B-1. This model, shown being tested in Figure II-6, was integrated with "live" components and differed from a flight spacecraft only in that a full harness was not integrated. As discussed in References II-11 and II-12, the structural behavior was satisfactory and essentially unchanged from the testing conducted on the T-1B model.

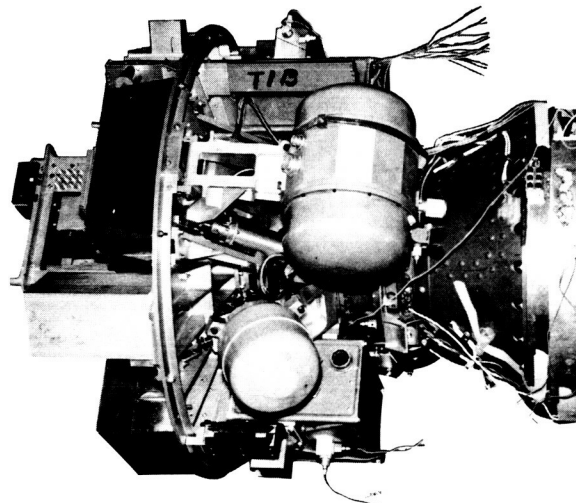
Further component rearrangements and the modification of component attachments were required to accommodate the C configuration, but no major structural modifications were necessary. In particular, the number of attachment points, or underside mounting blocks, required for the heavier mercury-bombardment-engine power supplies were increased from four to six. A high-frequency vibration isolation system for the radial accelerometer was also designed and integrated.

The new configuration was incorporated in a vibration model, designated T-1D, shown being tested in Figure II-6.

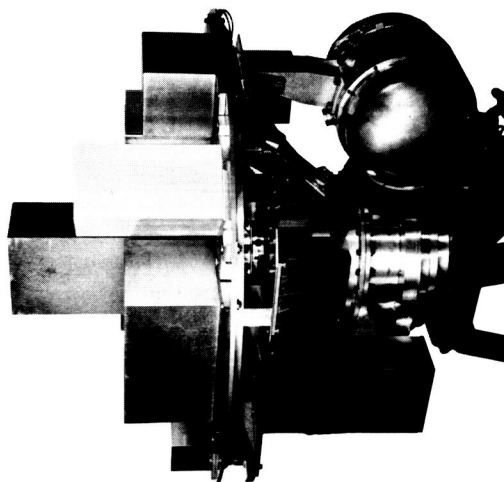
The purposes of the T-1D tests were first to evaluate the effects of the modifications on the vibration characteristics of the structure, then to prove the structural integrity of this T-1D configuration under the prototype loading condition, and finally to determine the ultimate strength of the structure by test to destruction. The testing consisted of a series of survey runs, complete prototype tests in the thrust and the lateral directions, and higher g-level tests in the critical thrust direction. The T-1D model successfully met all the prototype vibration test requirements and passed the 8-, 10-, and 12-g runs during the high g-level testing, which was finally terminated after the 14-g run when the Scout separation mechanism cracked. A detailed report of the T-1D vibration testing is given in Reference II-2.



T-1D Model



T-1B (Modified) Model



T-1B Model

Figure II-6. SERT Mechanical Survey Models

Immediately after the T-1D vibration testing, a prototype model, designated T-1B-3, was assembled with all the live components, representing all modifications to the T-1D model; additionally, this model contained a few new items such as the ion-beam-probe power supply, the fuse block, the auxiliary command unit, and the diplexer ballast load. The T-1B-3 model was then subjected to prototype-level testing in February, 1964; the structure proved capable of carrying the heavier load. The dynamic responses of all instrumented components were in very good agreement with those obtained in past tests, with the exception of the response from cesium-contact DC power supply and control box. Here, the X-Y plots indicated some abnormally large responses over the frequency band from 80 to 100 cps. Responses of this nature were not evident in all the previous tests. An examination of the baseplate after the test did not reveal any local pull-out in the region where this component was mounted; however, it was found that the covers for this component were not rigidly connected to the mounting bases. Being mounted on these covers, the accelerometers thus register large excursions at the critical frequency range.

Upon completion of the T-1B-3 vibration testing, the entire spacecraft, with the Scout separation mechanism, was attached to the spin-test rig. The spacecraft was spun at 170 rpm and the ion engines were deployed. The deployment of the ion engines to the stops was accomplished with a smooth motion apparently without any shock. After the spin test, some slight leakage of the water-glycerine fluid used in the hydraulic damper assembly of the engine deployment system was discovered. This small amount of leakage (less than 1 c.c.) would not create an unfavorable environment for the operation of the ion engines in outer space as some of the escaped fluid evaporates immediately. The fluid which deposits on the structure produces some vapor pressures, but these pressures would not be sufficient to reduce the vacuum enough to cause arc-over in the high-voltage circuit of the ion engines. A more detailed discussion of the effects of the damper fluid leakage on the performance of the spacecraft is given in Reference II-3.

Regarding the spin test, two specific points of interest are worthy of note: (1) the operation of the release mechanism of the engine deployment system was successfully demonstrated; and (2) the ability of the baseplate to withstand the dynamic loads caused by engine deployment was also demonstrated.

During the T-1D vibration tests, the locking device in the release mechanism had developed some degree of binding to the extent that release of the engines from their locked positions could be hindered. Even though it was firmly believed that the binding had been developed in the higher-than-prototype-g-level runs, various parts of the locking device were modified in the T-1B-3 model to increase their strength, thus improving the reliability of the deployment system. These parts were then subjected to the T-1B-3 prototype vibration testing; they functioned flawlessly in the subsequent spin test. Examination of these parts after the spin test revealed no yielding whatsoever. The modifications to the locking device are discussed in Paragraph II-B. 8.

3. Vibration Characteristics

The SERT I spacecraft is a multi-degree-of-freedom system, and as such, the response of the structure, in general, and some components, in particular, to an applied force is of a very complex nature. Extensive vibration testing, therefore, was considered a major phase of the design and development program. Three comprehensive vibration tests were conducted, corresponding to configurations A, B, and C.

The first test was performed on the T-1B model which incorporated all the prototype structural parts in the spacecraft but no "live" components; the components were replaced with dummy weights. The purpose of this test was to establish the transmissibility of major components, with sinusoidal or random-noise input excitations applied at the base of the column. In addition, this test, in which the spacecraft was vibrated to prototype specifications, was to prove the structural integrity of the baseplate, the column, and the lower ring. The major prototype condition was a sine-wave sweep of 10.7-g amplitude in the critical frequency range of 50-500 cps, representative of the ABL X-248 Scout last stage. The results demonstrated that the amplification of most components was less than eight-to-one and that the baseplate and column were capable of withstanding the prototype vibration level without exceeding the allowable stresses. However, few components did show slightly higher amplification due to the method in which they were mounted on the structure. Subsequent improvements made on these components alleviated this condition.

Based on the outputs shown in the response curves during the vibration testing, the power supplies for the mercury-bombardment and cesium-contact engines were component-tested by NASA. The test results indicated that some improvement in their environment was necessary. Consequently, braces were added on the T-3 (flight) spacecraft to restrain the lateral movement of the critical components. Furthermore, an accelerometer was added to the design, requiring a supporting strut and some rearrangement of the components. The T-1B model was then modified to the B configuration, and was subjected to a series of vibration tests during December, 1962, and January, 1963.

The purpose of these tests were (1) to determine the dynamic vibration responses of the spacecraft components, including the newly added accelerometer with the new spacecraft configuration, and (2) to attempt to improve the vibration environment of certain GFE and of other spacecraft components affected by the changes in configuration.

During this evaluation, two methods of improving the vibration environment were considered: (1) the increase of the structural rigidity in accordance with suggestions set forth by NASA, and (2) the use of supplemental braces or brackets between components to reduce excursion during vibration.

The results showed that the first approach, which provided a more rigid structure through the addition of diagonal struts from the base of the column to the baseplate,

did not improve the vibration environment. The second method reduced the vibration transmissibility considerably for all components, particularly with regard to lateral excitations. Most components had an amplification ratio of five-to-one, or less, and the greatest amplification ratio was approximately eight-to-one.

Full prototype-level testing was then successfully performed using a reduced specification (6.0 g's from 50-500 cps) as a result of refinement of flight data on the Scout vehicle. More detailed information is given in Reference II-5.

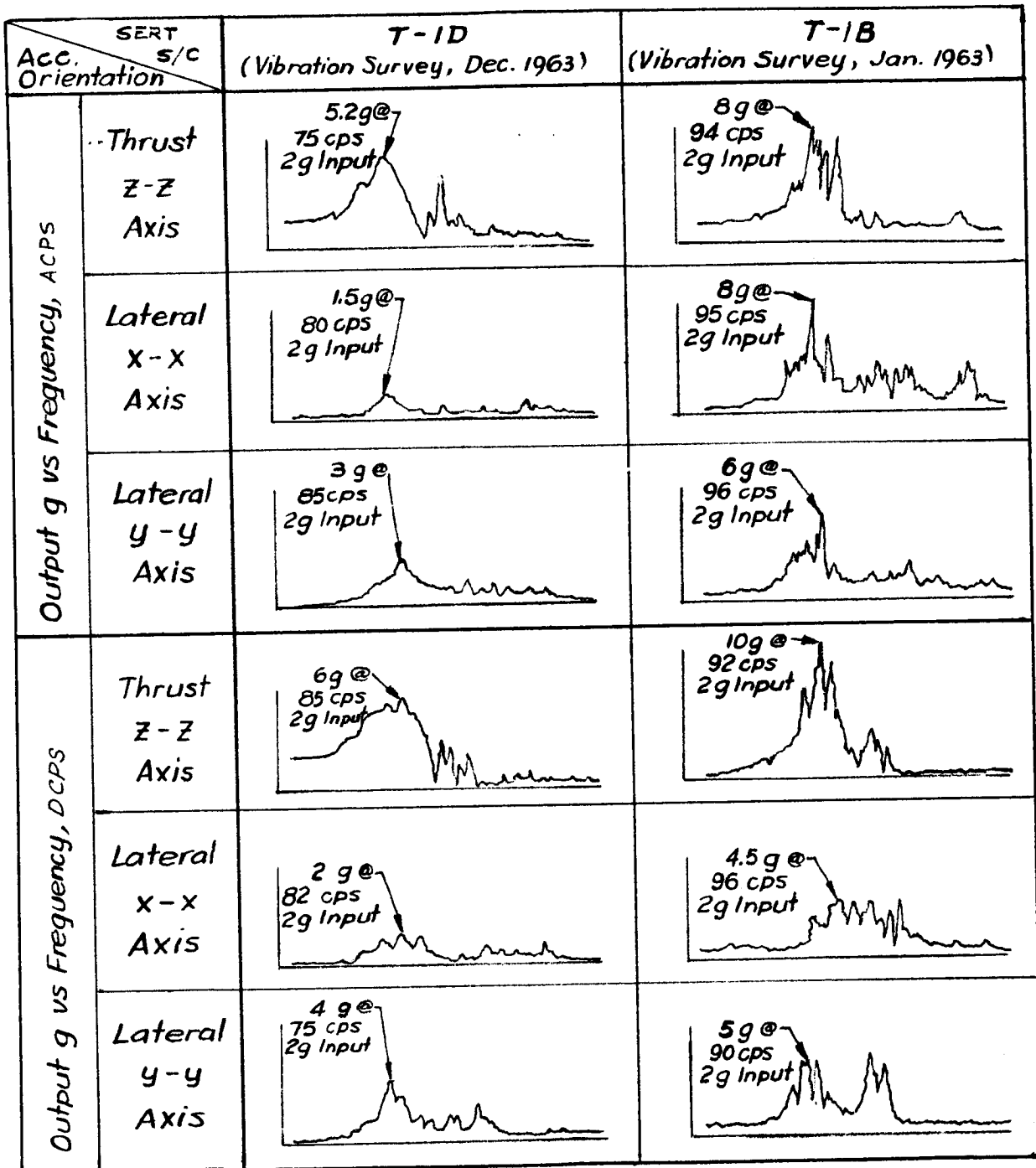
In addition to the vibration tests previously discussed, two more full-scale vibration tests were conducted after the SERT spacecraft was revised to the T-1D and T-1B-3 configurations, respectively. The T-1D configuration was basically the same as the T-1B configuration, modified to incorporate larger and heavier power supplies for the mercury-bombardment ion engines and to introduce vibration-isolator pads between the mounting feet of the radial accelerometer and its mounting bracket. These pads were designed to isolate the radial accelerometer from excessive dynamic responses which had been observed previously during the T-1B vibration surveys in the critical frequency range of 300 to 2000 cps. Vibration-test results showed that the natural frequency of the SERT structure was reduced by these changes and that the isolator pads effectively isolated the accelerometer.

A comparison of the vibration responses to thrust-axis inputs for the T-1B (modified) and T-1D models is shown in Figure II-7; the responses were measured at the AC and DC power supplies of the mercury-bombardment-engine subsystem. For both models, the transmissibilities are less than 5 to 1, although those for the T-1D are less than those for the T-1B. Of particular note are the characteristic fundamental baseplate frequencies for the T-1B model (90-100 cps) and the T-1D model (75-85 cps). The reduced value for the T-1D model is related to the increase in spacecraft weight. Figure II-8 illustrates the vibration improvement obtained for the radial accelerometer with the high-frequency isolator system. (See Reference II-2 for more details).

4. Baseplate

a. General

The baseplate (RCA Drawing No. 1173773, Rev. E) is machined from an AZ-80A-T5 magnesium forging. Magnesium alloy was chosen as the material for the baseplate because of its excellent machinability and its high damping capacity, i. e., its capacity to absorb vibrations, thus reducing stresses. The baseplate is basically a reinforced, circular, 0.090-inch-thick flat plate, 30 inches in diameter. The reinforcement consists of a center hub, approximately 10 inches in diameter; two cylindrical rings, which are concentric with the hub; and 32 radial ribs. The two cylindrical rings are located at radii of 8.5 and 14 inches. The center hub, which has a flange containing 32 equally spaced tapped holes is used to attach the baseplate to the center column. An annular groove with closely controlled tolerances is machined on the flange; this groove accepts the annular tongue on the mating flange of



Note: Output responses shown above are apparent G peak values.

Figure II-7. Comparison of Apparent Dynamic Responses of Power Supplies for the Mercury-Bombardment Engine

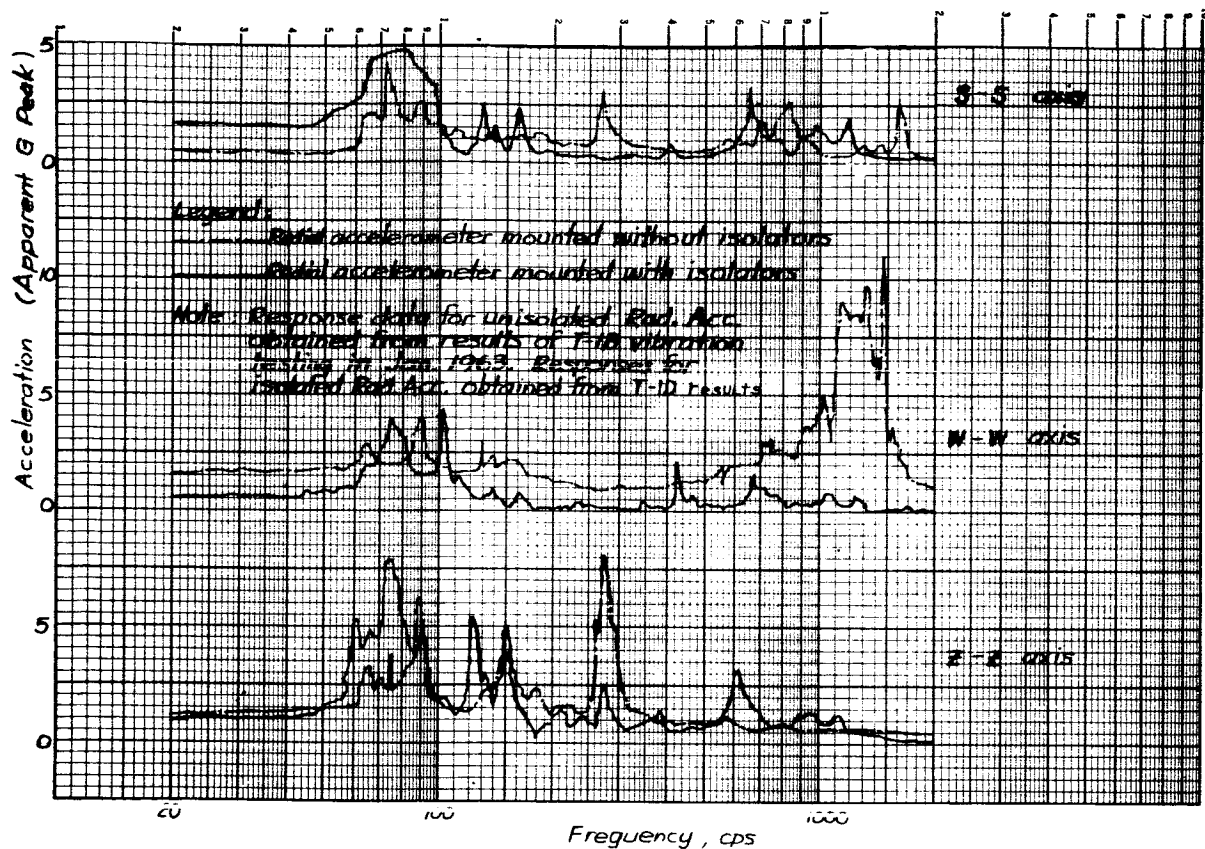


Figure II-8. Dynamic Response of Radial Accelerometer Mounted With and Without Urethane Isolators

the center column. This tongue-and-groove arrangement relieves the mounting bolts of transverse shear force due to lateral loads on the structure.

The 32 radial reinforcing ribs (thickness 0.1 inch) taper from a height of approximately 2.5 inches at the hub to 0.75 inches at the edge of the baseplate. At the various intersections of the ribs, rings, and center hub, generous fillets (typical radius 0.25 inches) are provided. All material thicknesses throughout the baseplate were determined on the basis of strength requirements and also upon limitations imposed by the contour milling process used to fabricate the baseplate. Figure II-4 is a photograph of the baseplate, showing some of the above details.

Groups of reinforced bosses are machined on the bottom side of the baseplate. The bosses allow attachment of the supporting brackets for the hydraulic-damper assemblies and distribute the hydraulic-damper load into the reinforcing radial ribs. The thickness of the ribs in these regions is increased from the typical value of 0.105 inch to 0.150 inch for the transmission of these highly localized damper loads.

b. Functional Description

The baseplate is a supporting platform for nearly all the spacecraft components, most of which are mounted on the top surface, although a few are suspended from the bottom. To maintain spin stabilization, the components must be arranged so that a favorable ratio of the mass moment of inertia about the spin axis to that about the lateral axis can be achieved. Fortunately, to satisfy thermal requirements, most of the heavier components were located toward the outer portion of the baseplate; hence, the favorable ratio was attained. This, however, introduced bending in the baseplate. The maximum bending moment is caused by vibratory load on the components due to excitation in the thrust axis and occurs at the junction of the center hub and the radial ribs. This bending moment is counteracted by a couple. One of the radially orientated couple forces acts on that portion of the baseplate inside the center hub; the other acts on the lower flange mating with the center column. The vibratory load on all the baseplate-supported components in the thrust direction is then transmitted to the center column, through the hub, as tension and compression.

Besides electronic components, the baseplate also supports the hydraulic-damper system for the ion engines, the precession dampers, and other miscellaneous items such as detuning-wing assemblies and ion-engine stops. To permit brackets for supporting these items to be attached, the outer rim of the baseplate (beyond the 28.00-inch-diameter reinforcing ring) is 0.250 inch thick instead of 0.090 inch as in the remaining portion of the baseplate.

c. Development

Before the vibration tests on the T-1B and on the modified T-1B models, the baseplate was subjected to static load tests on March 2, 7, and 14 of 1962. A whiffle-tree arrangement, in which a series of bars, plates, and rods were assembled on the baseplate, was used (See Figure II-9). The bars, plates, and rods were so connected that a load in a rod attached to a hydraulic jack would load each simulated component plate in proportion to the total force. This type of loading would apply for any level of g-load.

The first static test was basically a verification of correct assembly of the whiffle-tree arrangement; the load applied was 2g. The second test was carried out for a 20-g load with stress coat applied to the entire surface area of the baseplate, except the top surface and bolt holes. Stress coat was used in this test to indicate areas of high stress so that strain gage could be placed in these areas for the final static test. In the last test on the baseplate, static loads of 10, 20, 25, 30, and 33 g were applied. The maximum stress was found to be 14,000 psi (less than half the strength of the baseplate material, AZ-80A-T5 magnesium alloy). A detailed account of the baseplate static testing is given in SERT Logbook No. SL-20 (Reference II-6).

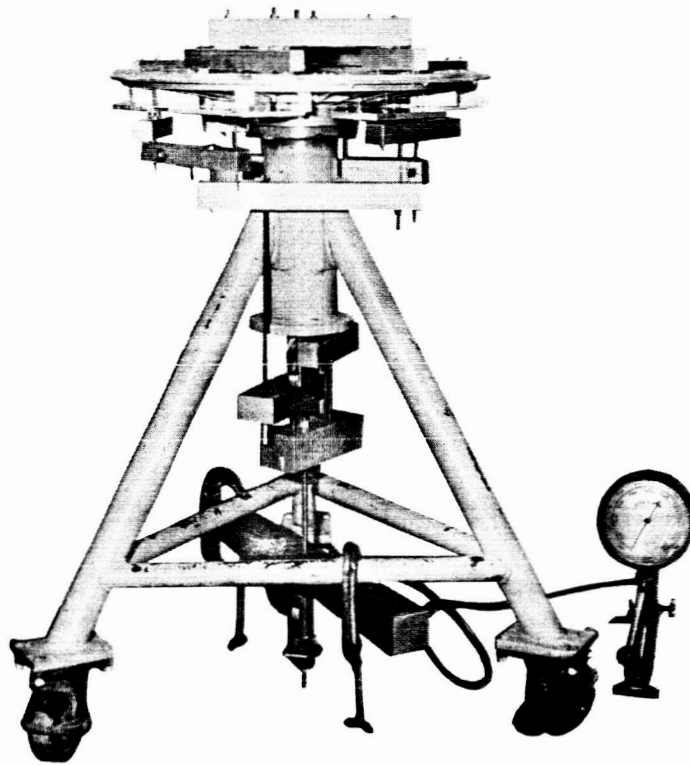


Figure II-9. SERT Static Load Test

5. Column

a. General

The column assembly (RCA Drawing No. 1706516, Rev. B.) essentially consists of the column (RCA Drawing No. 1703092, Rev. E.) and the hydraulic-damper-locking brackets. The column is machined from an annealed forging of 7075 aluminum alloy to form a thin-wall cylinder with end flanges. The rough machined piece is then fully heat-treated and final machined to obtain a wall thickness of 0.060 inches. This sequence was used to avoid cracking of the workpiece during machining. Had the column been fully heat-treated, the removal of the large amount of the core material to form the thin-wall cylinder would produce high internal stresses and consequently result in cracking of the wall.

The column has an inside diameter of 8.750 inches and an overall height of 6.763 inches. A smooth transition from the thin wall to the upper and lower flanges is accomplished by incorporating a gradual taper of the wall at each junction with the flange. The taper minimizes effects of stress concentration and reduces the discontinuity stresses.

The upper flange of the column matches with the baseplate mounting flange in the center hub. The tongue part of the annular tongue-and-groove shear joint is on the top surface of this flange. This shear joint was designed to relieve the flange bolts of transmitting lateral loads in shear. The lower flange matches with the lower-ring mounting flange. There are 21 holes spaced on the basis of 24 equally spaced holes on a 9.600-inch bolt-circle diameter. Mounting brackets for the locking devices of the ion-engine hydraulic dampers are attached to the column wall and to this flange at two locations.

The height of the column is determined by the space required for accommodating various components mounted below the baseplate and by the spacecraft heat shield, which fixes the ceilings of the components mounted on top of the baseplate.

b. Functional Description

The column assembly, which supports the component-laden baseplate, is the main load-carrying member of the structure. It was designed to withstand vibratory loads in all directions: for excitation in the thrust direction, the column acts as a tension and compression member; for lateral excitations, the column acts as a cantilever beam. The rigidity of its lower flange is utilized to support the hydraulic-damper locking devices which react to the static, compressive load acting on the hydraulic cylinders caused by the centrifugal force on the stowed ion engines. The mounting brackets for the accelerometer are supported from the column by bolts in both upper and lower flanges of the column.

c. Development

There has been no development work done on the column since its original conception. However, at NASA'S request design studies of a cast column with built-in supports for the mercury-bombardment-engine power supplies was made. Feasibility of a thick-wall column was also investigated. These studies were part of an effort to reduce the amplification factor of some electronic components. These studies, however, did not develop into hardware stages as other effective means of reducing amplification had been found.

6. Lower-Ring Assembly

The lower-ring assembly (RCA Drawing No. 1703117, Rev. F.) could be considered as the foundation of the SERT structure. It supports the column and baseplate at the top and connects with the adapter of the fourth stage of the Scout rocket at the bottom. Aside from being a major load-transmitting structural member, the lower ring provides storage space for the antenna ground-plane wires, the flange for attaching the antenna coupling network and the command subsystem, various bosses and pads for mounting the antennas and the deflectors for the separation clamp of the rocket fourth stage. Because of its multi-purposed design features, the ring is a rather complicated machined piece.

Basically, it is a hollow cylindrical housing 3.940 inches high. Its top flange matches with the column lower flange; the two flanges are joined by twenty-one 8-32 bolts. The top flange also extends radially inward to form a mounting surface with eight tapped holes for the antenna diplexer mounting plate.

The upper two inches of the cylindrical housing has a constant wall thickness of 0.150-inch. The wall thickness then increases sharply so that the cylinder becomes a thick ring for the remaining height of the housing. From this thick ring, mounting pads, flanges, and radially deep annular grooves are machined.

The material for the lower ring is 2014 T-6 aluminum alloy. This material was chosen because of its excellent machinability and strength. For added reliability, steel-thread inserts are used in all tapped holes in the mounting pads and flanges. The lower-ring assembly was subjected to two prototype vibration tests and several vibration surveys in which the structural integrity was successfully demonstrated.

7. Distributor Frame

The distributor frame (RCA Drawing No. 1703282) is a welded frame of aluminum angles and plates (See Figure II-5). It provides mounting for various components, including the programmer, the neutralizer voltage control unit, the signal conditioner, and the power-switching unit. In the first T-1B vibration test, a 12-to-1 amplification factor existed at the programmer. The frame was modified by the addition of stiffening gussets, and a vibration test was conducted on the stiffened frame. This test showed a decrease of amplification from 12-to-1 to 3-to-1.4 (Reference II-7).

In order to reduce amplification at some components mounted on the baseplate, lateral braces were installed. These braces connect the components to adapter angles on the distributor frame which were, in turn, attached to the reinforced corner posts. The frame was adequate for withstanding the stress and strain imposed by the additional lateral braces.

The distributor frame was also modified to add a supporting bracket to each of its two vertical posts closest to the cesium-contact-engine inverter. These brackets connect an added lateral tie bracket for this inverter to the distributor frame. It was felt that this inverter, which had recently been increased in its height and weight, might need a structural tie to restrain its lateral movement during vibratory excitation. All of the modifications were made before T-1B vibration testing.

8. Engine-Extension Subsystem

a. General

The SERT engine-extension subsystem consists of the ion-engine supporting arms, the hydraulic-damper subsystem, and the brackets for mounting these arms and dampers.

The damper subsystem is used in conjunction with the ion-engine-supporting-arm mechanism for the purpose of retarding the motion of, and hence reducing the shock loads on, the two ion engines during the unfolding operation. This operation utilizes the centripetal forces acting on the engines due to the spinning of the spacecraft. These forces create unbalanced moments at the hinge points of the engine supporting arm causing the engines to leave their stowed positions after they are unlocked by the firing of an exploding pin puller.

The SERT hydraulic-damper subsystem is a self-contained assembly consisting of three hydraulic-damper subassemblies interconnected by flexible hydraulic hoses. The major parts in the damper subassembly are the cylinder, end caps, piston, sealing diaphragms, and the flow-regulating valves built into the end caps. The hydraulic-damper subsystem is so assembled that the upper chamber of one damper subassembly is connected to the lower chamber of another. By connecting the three dampers in this manner, a self-contained, synchronized, hydraulic-damper subsystem is achieved. The subsystem is filled with a hydraulic fluid mixture of 50-percent (by volume) water and 50-percent glycerol. At this ratio, the freezing point of the mixture is below the lower limit of the operating temperature.

The hydraulic-damper subsystem is so arranged that there are two dampers on the cesium-contact-engine side and one on the mercury-bombardment-engine side. This arrangement was made according to the space available in the spacecraft. Thus, the hydraulic dampers, the engine supporting arms, and the brackets form a linkage system which prescribes the movement of the ion engines during extension. Figure II-10 shows the engine extension subsystem attached to the SERT structure. A detailed report concerning the design and development of the hydraulic-damper subsystem is given in Reference II-8.

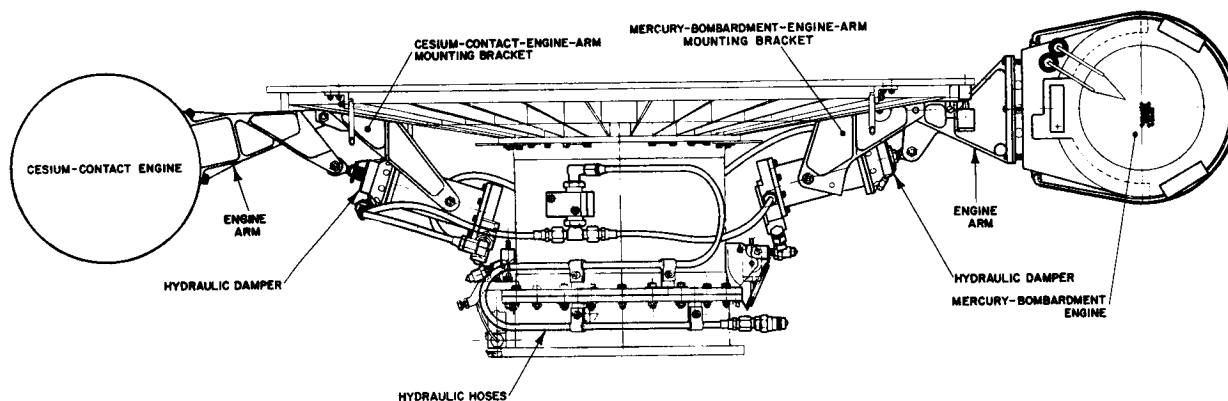


Figure II-10. Engine-Extension Subsystem Mounted on the SERT Structure

b. Development

The hydraulic dampers for the engine-extension subsystem had two major development problems of interest. The first problem was caused by the high fluid-pressure shock occurring just after the ion engines pass through the mid-point of the arc prescribed by the center of the unfolding engines. At this mid-point, the hydraulic-damper cylinders have just completed the first half of the total stroke and are about to reverse and start the second half of the stroke. It was found, by analyses which were later substantiated by tests, that at the beginning of the second half of the stroke, a high-pressure shock with peak values close to 1000 psi was developed. This shock caused the damper diaphragms to rupture during two spin tests. This problem was solved by changing the diaphragm fabric material from nylon to the stronger dacron and modifying the valving in the hydraulic subsystem to reduce peak pressure.

The other development problem worthy of note is that of the free play in the hydraulic subsystem which would develop after long periods of shelf life. Qualified hydraulic-damper subsystems initially having no free play* were found to have as much as 0.25 inch of free play after the subsystem had been placed on a storage shelf for about three months. There was no evidence of any leakage anywhere in the subsystem; however, comparative weighings of a subsystem with free play and a subsystem completely filled (no free play) indicated that the latter was heavier. The weight difference corresponded closely to a calculated value which was based on the volume of fluid for the two subsystems, thus indicating loss of fluid in the subsystem. A series of tests were then performed to determine the cause or causes of fluid loss. Helium leak tests were performed, but no leakage was detected. Specific gravity checks indicated some loss of water content in the hydraulic fluid from the subsystem having the free play. Further investigation disclosed that the elastomer material (fluorinated silicone) of the diaphragms is somewhat permeable, allowing a slight amount of fluid to be lost. During over-extended storage periods, the amount of fluid lost becomes significant. Tests run on the T-1B system have shown that no air enters the subsystem as the original volume of fluid decreases.

The following corrective actions were taken:

- Additions to the hydraulic subsystem were made to allow each of the three pairs of chambers to be recharged from a common fitting at any time. Disassembly of the hydraulic subsystem, or removal of any components from the spacecraft, would not be required for the charging operation.
- The subsystem would be completely filled under pressures from 40 to 50 psig during initial assembly.

*Free relative movement between the piston and the cylinder of any one hydraulic damper while the piston and cylinder of the two remaining dampers are held stationary.

- Distilled water would be used, eliminating from the fluid many of the unknown impurities normally found in tap water. The possibility of introducing dissolved air into the subsystem is also reduced through the use of distilled water.

Hydraulic-damper hardware was then modified to incorporate the design features necessary for the charging operation.

The release mechanism of the deployment system for the ion engines is connected to two brackets mounted on the lower flange of the column assembly. Various parts in this release mechanism yielded during the T-1D vibration tests. The yielding occurred at the holes which hold the retractable pin in the explosive pin puller and the hinge pin. It was evidently caused by excessive bearing stresses on the brackets and the associated parts of the release mechanism during the high g-level runs. The lateral displacement of bracket lugs and their mating clevis links under the bearing load was large enough to cause binding between the parts of the release mechanism. Thus, the deployment of the ion engines could be seriously affected. Even though this did not happen at levels below prototype level, the pertinent parts of the release mechanism were modified to provide an extra margin of safety. The modifications, in essence, consisted of the following:

- For parts formerly made of 6061-T6 aluminum alloy, the material was changed to 7075-T6 alloy, resulting in an increase of 50 percent in bearing yield strength.
- Stainless steel (18-8 type) pins were replaced by pins made of hardened stainless steel (17-4PH), increasing the yield strength by a factor of three; and
- The pin of the explosive pin puller was lengthened slightly to insure that this pin and the supporting lugs of the brackets mounted on the column were fully engaged, resulting in increased bearing area, hence decreased bearing stresses.

These modifications were incorporated in the T-1B-3 model which subsequently passed first the prototype vibration tests and then the spin test.

9. Ground Plane

The antenna ground plane is formed by 24 spring wires each 0.042 inches in diameter. These wires extend radially outward to an envelope of 46.2 inches diameter. The 24 wires are connected by a stranded wire at a point 3.25 inches from the outer tip of each wire. The other end or the inner tip of the wire is formed into a short helical

coil spring. The coiled end of each wire is inserted into the radially deep annular groove in the lower ring assembly, and the 24 wires are initially stowed in this groove. The inner tip of the ground-plane wire is attached to the lower ring by installing a spring pin through the coiled end of the wire and into the matching holes in the lower-ring assembly. The wires are stowed by wrapping them progressively in the groove, a portion of wire length at a time, until the entire length of each wire is tightly stored in the annular groove (See Figure II-11). A hoop clamp is then used to retain the wires in the groove, which are now under the stress and strain as a result of the wrapping. With the helical coil at the point of attachment to the lower ring, the torsional strain of the coil makes the wrapping of the wire possible without overstress. A packaging procedure for the ground plane wires is specified in Reference II-9.

Deployment of the ground plane occurs after the engines are unfolded and is triggered by the same signal that blows loose the door to the cesium-contact-engine pod. Upon firing of an explosive pin puller, the hoop clamp is disconnected and dislodged from the lower ring assembly under the combined effects of the strain energy of the wrapped wires and its own centrifugal force. The ground plane wires likewise spring out from the storage groove and form a lateral plane to shape the antenna pattern. (Refer to paragraph III-D. 7.)

10. Detuning Wing

The detuning wing is a piece of 6061-T6 aluminum tubing of 0.250 inch, O.D., by 0.035 inch, wall thickness, bent into a modified "U" shape of three-dimensional bends. Its developed length is approximately 45 inches, with the semi-circular part having a mean radius of about 11 inches. It is attached to the outer edge of the baseplate by means of small hinges riveted to the open ends of the "U." Two nearly diametrically opposite detuning wings are used in the spacecraft located approximately 90 degrees from the ion engines. During launch, the wings are pendant beneath the baseplate. After the heat shield is jettisoned and spin-up of fourth-stage rocket and spacecraft



Figure II-11. Antenna Ground Plane Wires Shown Being Stowed in the Lower Ring

is accomplished, the wings are free to move outward, by the action of centrifugal forces, to the horizontal position where they function as part of the antenna subsystem. A urethane bushing was incorporated in the hinge design to reduce the bending stresses in the wing upon contact of the wing hinge stops with the baseplate.

11. Antenna Mounts and Clamp Deflectors

a. General

The antenna mount, machined from 6061 aluminum alloy, serves a two-fold purpose: first, it provides mounting for the antenna whips; and, second, it forms a part of the deflector system which protects the spacecraft during fourth-stage vehicle separation. There are four antenna mounts for the eight whips in the antenna array. Teflon inserts serve to protect the two antenna whips on each mount. There are three different pairs of 6061 aluminum clamp deflectors (five pairs total). Three pairs of clamp deflectors are bolted to the pads on the lower ring; the remaining two pairs of deflectors are riveted to the protruding flange on the lower ring. The deflectors are placed around the periphery of the lower portion of the lower-ring assembly to shield the components below the baseplate from the separating clamp parts that are jettisoned during fourth-stage vehicle separation.

b. Development

Three separation tests were conducted to determine, among other things, the adequacy of the clamp deflector design. The first tests were conducted on July 2, 1962. The separation tests were performed on a table rotating at 180 rpm with the two halves of the separation system clamped together. It was noted that during separation the short antennas mounted closest to the explosive nut on the separation clamp were bent outwards slightly (about 1 inch) at the tip. As a result, an extra deflecting surface was added on the bottom of the antenna mount. The additional deflector was made of aluminum and was riveted to the original antenna mount. The modified deflector system was subjected to testing on August 21, 1962. The purpose of the second series of tests was to determine whether the additional deflectors adequately protected the antennas. The test indicated that the new deflectors did protect the short antenna and that none of the antennas were hit by the clamp parts. The third series of tests was performed on March, 1963. The purpose of these tests was to determine the adequacy of the teflon block which replaced the added aluminum deflectors tested in the second series of testing. (The aluminum deflectors were interfering with the electrical operation of the whip antennas.) Test results indicated that the teflon blocks on the antenna mounts functioned satisfactorily.

12. Miscellaneous Structural Parts

The miscellaneous structural members of significance are the supporting brackets for the radial accelerometer and the lateral braces for the power supplies of the cesium-contact and mercury-bombardment engines, the cesium-contact-engine inverter, and the precession dampers.

There are two supporting brackets for the radial accelerometer. The main bracket to which the accelerometer is attached by three equally spaced bolts is machined from aluminum-bar stock. The lower end of the strut is bolted to the lower flange of the center column assembly; the upper end is connected to a second bracket which, in turn, is bolted to the column upper flange. An adapter plate with two sets of three equally spaced holes is placed between the main bracket and the radial accelerometer.

The plate is mounted to the main bracket with screws through one set of holes. The radial accelerometer is mounted to the second set of holes by means of adjustable screws. These screws are machined to incorporate a shoulder with a spherical surface on one side so that, during assembly, the shoulder would contact a matching spherical seat machined in the adapter plate. This arrangement allows the radial accelerometer to be aligned so that its longitudinal axis passes through the center of gravity of the spacecraft. To provide a favorable vibration environment for the radial accelerometer, urethane isolators are used between the accelerometer and the adapter plate at each mounting point.

The lateral braces for the cesium-contact-engine power supplies and the precession dampers are made of 0.09-inch-thick aluminum plate. The braces for the cesium-contact-engine inverter and the mercury-bombardment-engine power supplies are machined; these braces are 0.060 inches thick and have a flange for mounting. The basic function of the lateral braces is to restrain these components (which are either radially remote on the baseplate, stabilized at the center column, or mounted to the baseplate with a large overhang from the mounting surface) from rocking during vibration. The restraint is provided by attaching the components to one end of the brace which is connected to one of the reinforced posts of the distributor frame.

C. THERMAL DESIGN

1. General

The thermal design of the SERT I spacecraft imposed several restrictions related to component location, mounting, and surface finish. Many component arrangements were analyzed to arrive at an arrangement which would be compatible with the other engineering requirements as well as the thermal requirements that had to be satisfied. Since the electrical power dissipation levels were much higher than normally encountered in satellite design, many design techniques for maintaining a satisfactory temperature level were investigated. Due to the level of thermal activity, contact resistance

at the interface between components and the baseplate had to be minimized, and special surface finishes had to be employed to reduce the external heat loads. Since the flight profile called for a one-hour flight, with portions of the flight within the Earth's atmosphere, heat inputs due to aerodynamic heating during ascent and coast flight were investigated. Also studied were the need for ground cooling and the problem of electrical breakdown due to outgassing of materials.

2. Design Discussion

a. Analytical Study

The thermal design criteria established a temperature range of 0°C to 70°C as the satisfactory operational range of the spacecraft components. The exceptions to this temperature range of operation were the main battery (15°C to 49°C) and the command subsystem (0°C to 60°C). Each component would be activated for a minimum duration of a half hour and a maximum of an hour at full power.

Since the component locations and power levels were uncertain at the start of the SERT program, a simplified approach to the thermal analysis was taken. The thermal inertia and power dissipation level of each component was calculated for several different locations until an optimum component thermal configuration was obtained. Having fixed the component location (Figure II-2) and power level, a more detailed analysis was required to determine the heat transfer between components and the need for placing additional heat sinks in the telemetry equipment.

A digital computer program was prepared to determine the transient heat transfer between components. Also accounted for within the program was the heat input due to solar energy, albedo, and Earth-emitted radiation. The program also included the radiation and conduction coupling between components.

The mathematical expression used in the digital computer program is as follows:

$$M_i C_{p_i} \frac{dT_i}{d\theta} = \Gamma \left[A_{\rho_i} \alpha_i \rho_i(\theta) + A_{s_i} \alpha_i S \cos \beta_i(\theta) \right] + A_{u_i} \epsilon_i u_i(\theta) \\ + Q_i(\theta) - \sum_{j=i}^n R_{ij} \sigma (T_i^4 - T_j^4) - \sum_{j=i}^n K_{ij} (T_i - T_j) - A_{R_i} \epsilon_i \sigma T_i^4 \quad (\text{II-1})$$

where

M_i is the mass of the i-th body,

C_{ρ_i} is the specific heat of the i-th body,
 T_i is the temperature of i-th body,
 T_j is the temperature of j-th body,
 θ is time,
 Γ is a control set (1.0 during day operation and zero during night operation),
 A_{ρ_i} is the area receiving albedo,
 α_i is solar absorptivity,
 $\rho_i(\theta)$ is albedo (variable with time),
 A_{S_i} is the area receiving solar energy,
 S is direct solar energy,
 $\beta_i(\theta)$ is sun angle (variable with time),
 A_{μ_i} is the area receiving earthshine,
 ϵ_i is emissivity,
 $u_i(\theta)$ is earthshine (variable with time),
 $Q_i(\theta)$ is internal power generation (variable with time),
 R_{ij} is the radiative coupling factor,
 K_{ij} is the conductive coupling factor,

σ is the Stefan - Boltzman = n constant (3.657×10^{-11} watts/in² °K⁴),
and

A_{R_i} is the area radiating to free space.

The radiative coupling factor can be defined in the following manner:

$$Q_{1-2} = A_1 \epsilon' \phi_{1-2} \sigma (T_1^4 - T_2^4) \quad (\text{II-2})$$

where

Q_{1-2} is the radiative coupling factor between bodies 1 and 2,

A_1 is the area of the first body,

ϵ' is some function of the emissivity of both bodies,

ϕ_{1-2} is the angle factor from first body to second body,

T_1 is the absolute temperature of first body, and

T_2 is the absolute temperature of second body.

The coupling factor from the first body to the second body (R_{1-2}) is therefore:

$$R_{1-2} = A_1 \epsilon' \phi_{1-2} \quad (\text{II-3})$$

and the conductive coupling (K_{1-2}) factor is simply:

$$K_{1-2} = \frac{k}{\ell} A_c \quad (\text{II-4})$$

where

k is the conductivity of the material,

A_c is the conduction area, and

ℓ is the length of conduction path.

Equation (II-3) is used to calculate the contact resistance between the SERT baseplate and the component interface. The thermal conductance due to this contact resistance replaces the k/l in the above expression, and the component contact area replaces the A_c term.

The value of the direct solar flux, average albedo, and earthshine inputs for the transient state were calculated for each surface. The actual power profile of each component is included in the analysis.

The increase in compartment temperature due to aerodynamic heating during launch was computed for launch attitude angles of 85 degrees and 78 degrees. For the 85-degree launch-attitude angle, the spacecraft temperature increases 8.5°C before second-stage burnout. Upon ejection of the heat shield, the spacecraft decreases 4°C at fourth-stage burnout; this leaves a net increase of 4.5°C during launch. For the 78-degree launch-attitude angle, the net increase is 45°C ; this is due to direct aerodynamic heating on the components when the heat shield is ejected at this lower trajectory angle. However, the launch attitude angle of 85 degrees was selected to avoid any severe problems.

Prelaunch cooling of the entire spacecraft to an initial temperature of 10°C was suggested. This initial condition maintains all components below the 70°C temperature limit and removes the need for placing additional heat sinks in the telemetry equipment.

In the above paragraphs, only the technique of predicting component temperature was discussed. However, the surface properties of the components directly affects the component operating temperature.

Since the SERT spacecraft is a high-power dissipating system, a coating that would allow maximum thermal radiation and minimum thermal absorption was selected. The possibility of arcing due to the presence of the 5000-volt potential (above ground) imposed additional restrictions on the type of materials used within the SERT components as well as those used for surface coatings.

To comply with this additional restriction, materials having low-outgassing properties were selected. An analysis was made to determine the arc-over problem due to outgassing of the Tilecote surface material. Using the vacuum test data given in Reference II-13, it was shown that, for an assumed weight-loss rate of epoxy paint (component surface coating) of 5 percent per hour, the computed vapor pressure of 2.1×10^{-4} mm Hg, at a point adjacent to the component surface, was well below the pressure level (4.6×10^{-3} mm Hg) required to produce an arc across a 100-mm gap at 5000-volt potential. Since the entire engine testing is performed above a 200-mile altitude (ambient pressure of 10^{-8} mm Hg), the assumption that the computed vapor pressure would exist between points of high potential (engine and components) produces the most conservative estimate of arc-over probability.

b. Test Program

To augment the study of arc-over due to outgassing at low pressure, a series of tests were conducted at appropriately low pressures (10^{-5} mm Hg) to determine if electrical breakdown on the SERT spacecraft would occur. These tests simply employed two brass electrodes separated by a known distance. The potential difference between the two electrodes was varied and the breakdown voltage (if breakdown did occur) was noted. Test results indicated that at a pressure of 10^{-5} mm Hg, a potential difference of 30,000 volts across an 0.3 inch gap did not result in breakdown. It then follows that 5000 volts across the gap of 0.0625 inches (minimum internal distance between surfaces of the mercury-bombardment-engine) will not break down at 10^{-5} mm Hg. A detailed discussion of the test is presented in Reference II-21.

In conjunction with the digital computer thermal analysis program, a test program was initiated to check the temperature of the high-power-dissipating components. Thermal models of the telemetry equipment, main battery, and mercury-bombardment-engine converter were fabricated and assembled to a simulated baseplate as the flight hardware would appear in the actual spacecraft. These tests were performed to corroborate the temperature predicted by the computer program and to indicate the extent of conduction coupling and contact resistance between components.

The tests were conducted with the components in a glass bell jar evacuated to 5×10^{-5} mm Hg; the walls of the bell jar were at room temperature. Each component was operated at the duty cycle that it would experience in actual flight. Since the chamber walls were not cooled, the environment that the spacecraft was subjected to did not simulate the actual conditions. However, the temperature rise of each component would be similar to that which occurs in the actual environment.

Results of the test program indicated that the components would not exceed the 70°C maximum temperature limit. A few of the component arrangements tested did exceed this limit; however, these arrangements were not incorporated in the final component configuration. A complete discussion of results and test data is given in Reference II-22.

D. MECHANICAL INTEGRATION

The primary purpose of the mechanical integration task was to ensure the mechanical integrity of the spacecraft. This task comprised the design of the mechanical arrangement of the assemblies, subassemblies, and the components within the spacecraft; the design of fixtures and jigs, where necessary, for proper weight and balance; and the coordination and incorporation of all mechanical mounting changes in the spacecraft. Mechanical integration procedures were evolved as needed to provide maximum flexibility for incorporating design changes or modifications throughout the course of the program without detrimentally affecting the overall program schedule.

1. Component Arrangement

The arrangement of components on the spacecraft structure was necessarily a compromise among a number of design factors. However, among these, the requirements set by last-stage rocket dispersion limits for static balance (50 ounce-inches) and dynamic balance (200 ounce-inches²) in the engines-folded condition were paramount and were to be met with a minimum of balance weights. The other design considerations were as follows (in order of importance):

a. Engine Clearance

The component arrangement necessarily respected the volume required for the uninhibited movement of the ion engines from their folded to extended positions.

b. Thermal

High-power-dissipating components had to be mounted at the baseplate periphery with as little obstruction to space as possible. Furthermore, these components were not to be located adjacent to each other. For example, cesium-contact-engine subsystem components were kept as far as possible from mercury-bombardment-engine subsystem components. Good thermal-conduction paths were also maintained between heat-generating and heat-absorbing components and the spacecraft baseplate. Note particularly that only non-dissipating components (programmer, power-switching unit, signal conditioner) are located on the distributor frame. The command subsystem was specifically designed for location within the column structure where a temperature environment between 0°C and +60°C could be guaranteed.

c. Structural

It was necessary not only to provide as much equalization of the load across the total baseplate surface as possible, but also to arrange the components so that the load from the mounting points could readily be transferred through the baseplate skin to the ribs. In the case of the underside components, it was necessary to place the mounting feet such as to avoid unduly loading a particular rib. Load-transferring blocks were often used to provide the necessary equalization.

d. Accessibility

Often, the large number of components packaged in the small space provided by the spacecraft would make accessibility extremely difficult; however, special consideration was given to the batteries, all component connectors, measurement

points, and adjustment points. Wherever possible, access to mounting hardware was arranged so that a minimum of special tooling would be required.

e. Harnessing

While it was desirable, for mechanical integrity, that the harness be fastened rigidly to the structure wherever possible, the shortage of available baseplate area often made it necessary to run the harness across components, using existing bracing or adding special bracing wherever possible. Assembly and disassembly times were greatly affected by the large number of constraints created by the harness.

Of particular note in the final configuration is the location of a number of components atop the batteries. Space availability was at such a premium that this arrangement became necessary. The battery covers utilized were specially designed by RCA to provide the required component mountings, structural integrity, and satisfactory thermal conductivity.

Individual component layouts were prepared for each of the three major configurations evolved during the program. Accompanying each layout was a computation report in which the weight and balance was validated, based upon the latest component information (e.g., size and weight). The design process involved a series of sample layouts and computations during which the effect of component movement on both the layout and balance would be analyzed in order to select an arrangement that would minimize balance weight while still satisfying all of the design considerations. The weight, balance, and moment of inertia computations for the final configuration are presented in Appendix A.

2. Component Mounting

Various methods of locating and accurately drilling component mounting holes were considered. The use of a metal drilling template was discounted because it was not readily adaptable to subsequent relocation of components and excessive time was required to locate new hole centers using coordinate dimensioning. The laying out of the component arrangement on each baseplate using the surface-plate and height-gage method was abandoned because the time involved was prohibitive; in addition, this method involved the scoring of the baseplate with a scribe, which, in turn, increases the probability of failures under vibration due to the high stress concentration at the scribed marks.

To locate holes on the topside of the baseplate, the final decision was to use Mylar film to make a "primary master" layout of the baseplate and component arrangement; Mylar has excellent dimensional stability and any layout changes can easily be incorporated. The "primary master" is never used; instead, a working

"secondary master" was photographically reproduced. The "secondary master" was taped onto the surface of the baseplate, and the hole locations were transferred from the "secondary master" to the baseplate with a center punch.

To prevent "hole drift" during drilling, a drill bar and slip-drill bushings were used. A trammel point with the center-punch mark as a guide was used to locate the drill bar. The drill bar was then clamped to the baseplate and the desired size of the hole obtained by stepwise increase in the size of the slip-drill bushings used.

For the underside of the baseplate, the mounting of components presented similar problems of location plus the added complication of a conical, ribbed surface. The design of the baseplate was predicated on the loads being distributed to at least two of its ribs for each point of attachment. The mounting accuracy required to insure load distribution over a large area without inducing preload stresses in the ribs dictated the use of machined aluminum blocks; sheet metal attachments would be unacceptable. These aluminum blocks were machined to within 0.005 inch of the final dimension and then hand filed and fitted to the exact rib spacing. The criteria for fitting these blocks was established as a minimum of 75 percent of the surfaces in contact and the area of contact so distributed that no less than 40 percent of the contact is obtained in one half of the total block area. Most blocks were designed and fitted in such a manner that the loads were distributed among two ribs and the baseplate surface; lightly loaded blocks were secured to one rib and the baseplate surface. In order to obtain equal load distribution on the mounting blocks for the heavier components, these blocks were made 0.100 inch longer and were finish machined after installation on the baseplate. This generated a single plane for component mounting. Special jigs and templates were used to locate component mounting holes in these blocks.

3. Hardware

The initial selection of hardware comprised mainly socket-head cap screws made from Type-304 stainless steel and thin hexagonal locknuts (of the internal-external wrenching type) made from Type-A286 corrosion-resistant steel. As the component arrangement became more complex and the amount of available mounting space lessened, the mounting hardware became more inaccessible; this problem was solved by replacing the thin hexagonal locknuts with either two-lug miniature floating anchor nuts (NAS 1068) or corner anchor nuts (NAS 698).

Another problem that evolved was the tendency for the nut to behave as a die which would cut the threads of the bolt when the bolt was removed during disassembly; the resulting chips from the bolt caused the bolt to "freeze" in the nut. (Locking is accomplished by distorting the back of the threaded section of the nut.) The problem was solved by changing the specified bolt material from the softer stainless steel to a much harder alloy steel, thereby negating the die-cutting tendency of the nut.

Vibration testing revealed that bolts threaded into tapped holes, as opposed to anchor nuts, had a tendency to loosen, even though they were installed with split lockwashers and "locktite" applied to the threads. This was particularly true where the bolt loading was primarily a tension loading. To remedy this situation, lockwire was installed in all bolts not assembled into locking-type nuts.

4. Assembly Techniques

Consistent with the adopted mechanical integration philosophy of providing maximum flexibility, the simple assembly techniques employed were developed as the project progressed and as the need arose. To alleviate the difficulties encountered with installing lockwire in certain cramped locations, the bottom side of the spacecraft baseplate was partially assembled before the top. In assembling the top side of the baseplate, it was advantageous to start from the center and work toward the periphery. As each mounting bolt was installed, it was torqued to its specified limit and marked with a small dot of red dye. The dye was applied in such a manner that any loosening of the bolt was immediately apparent. The torque values for most applications were as follows:

<u>Bolt Size</u>	<u>Torque Value (in. -lb.)</u>
No. 6	14
No. 8	25
No. 10	42
1/4 in.	101

These values were established in consultations with the Structural Analysis Group at RCA and were set at approximately 90 percent of the mean tensile yield stress of the bolt using the thread root-area as the design criteria. There were, of course, special torque requirements for mounting bolts whose application deviated from the norm.

As an added precaution against bolt fatigue or surface galling, mounting bolts that had been installed and then removed for any reason were discarded; new bolts were used for re-installation. This procedure was also applied to non-captive lock-nuts, but, as an exception, the aluminum flat washers were not replaced unless they showed excessive deformation or wear.

5. Dynamic Balancing and Inertia Measurement

Dynamic and static balancing of the SERT flight spacecraft (T-3) was performed on a vertical two-plane balance machine; a photograph of the T-3 spacecraft on the

machine is shown in Figure II-12. The balancing operation was performed in two separate phases:

a. Engines Folded

In this condition, the spacecraft was dynamically and statically balanced to accuracies of 158.7 ounce-inches and 36.9 ounce-inches, respectively and permanent balance weights were installed.

b. Engines Extended

Subsequent to the engines-folded balancing, the static and dynamic unbalance of the spacecraft created by extension of the engines were determined by the addition of temporary balance weights. The results showed that the reorientation of the spin axis due to engine extension was less than 1 degree.

Detailed descriptions of the measurements and the results are presented in References II-15 and II-16.

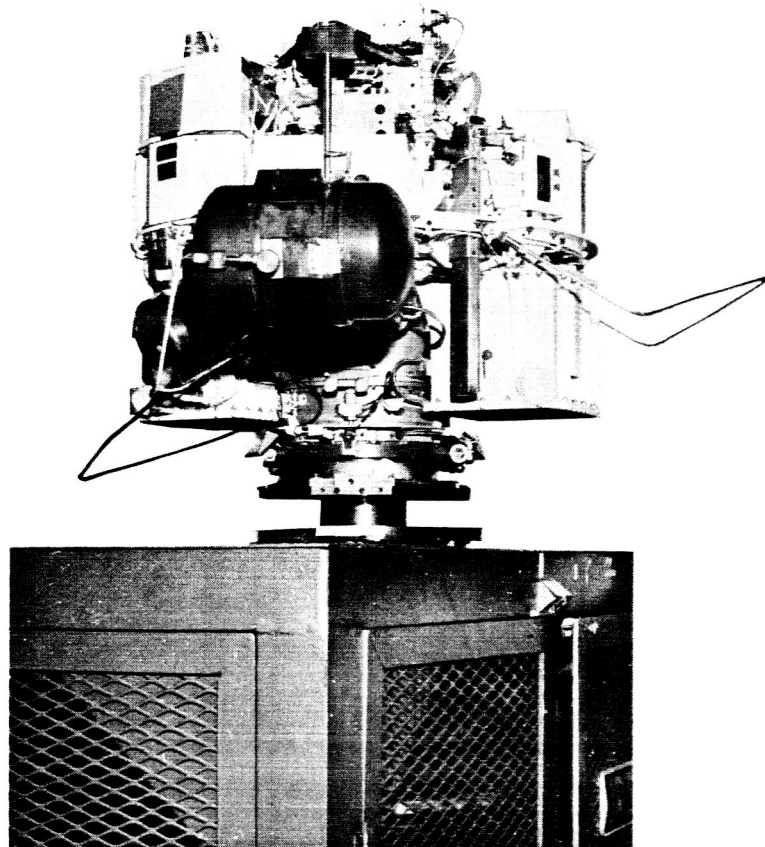


Figure II-12. SERT T-3 Spacecraft on the Balance Machine

Moments of inertia were measured using the bifilar pendulum facility located at AED (originally developed for the NASA Relay* program). The following moment of inertia measurements were made:

- (1) Spin Axis, Engines Folded.
- (2) Spin Axis, Engines Extended.
- (3) Three Transverse Axes (45 degrees apart), Engines Extended.

For the measurements of (1) and (2), the spacecraft was mounted in an inverted position with the base ring fastened to a special adapter (shown in Figure II-13). Before installing the spacecraft on the adapter, a standard, approximating the size and weight of the spacecraft, was used to make calibration measurements. As shown in Reference II-17, a measurement accuracy of better than 0.2 percent is possible.

The spacecraft was then mounted in a special box frame for the transverse-axis measurements. As with the spin-axis measurements, a calibration using the standard was also performed. Figure II-14 shows the standard and box frame installed on the pendulum.

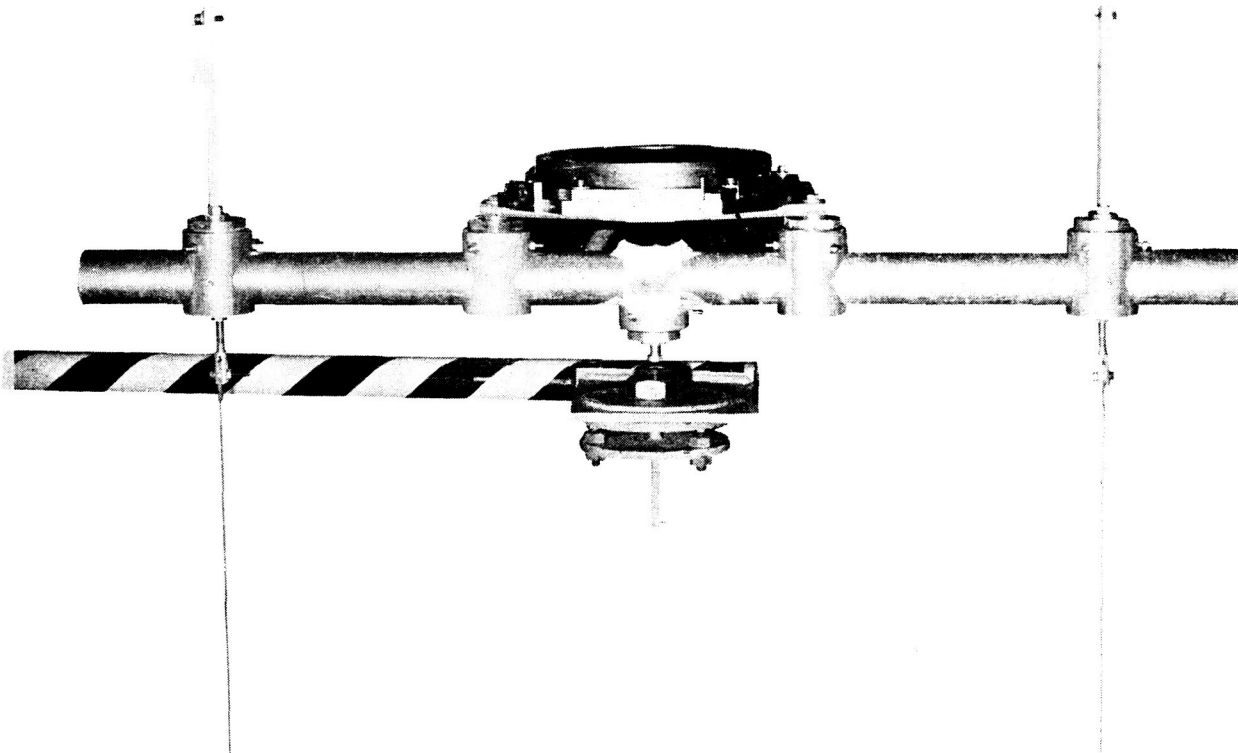


Figure II-13. Special Adapter for Spin-Axis Moment-of-Inertia Measurements

*The Relay Satellite was designed and built by the Astro-Electronics Division of RCA for NASA under Contract No. NAS 5-1272.

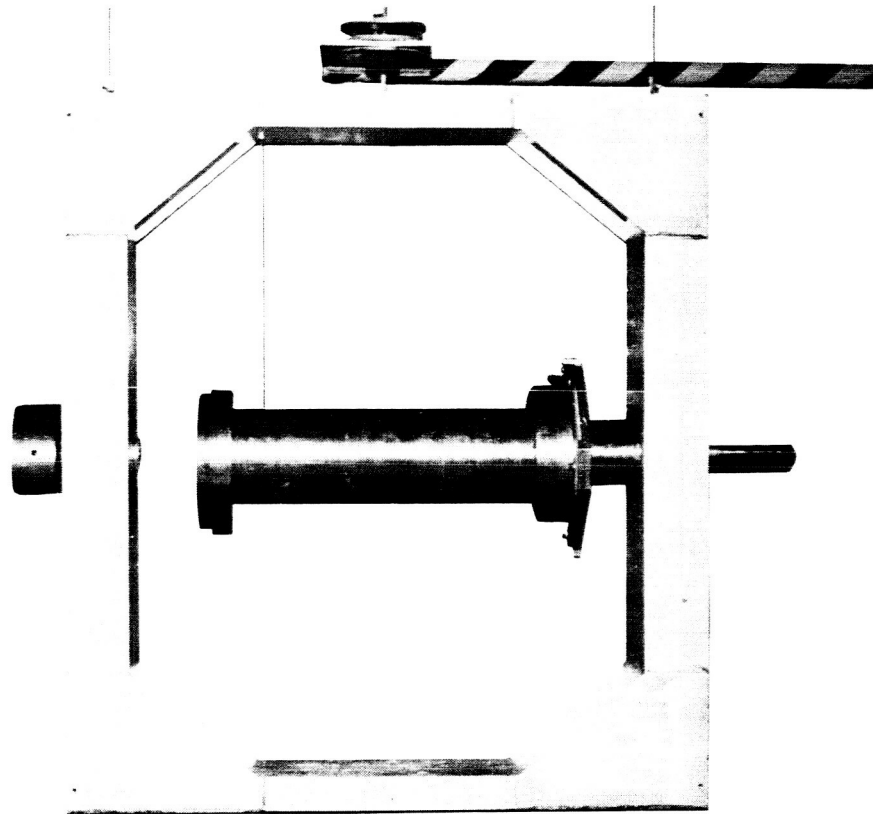


Figure II-14. Box Frame and Standard for Transverse-Axis Moment-of-Inertia Measurements

The results of the moment of inertia measurements are presented in References II-18, II-19 and II-20. The following is given in summary:

$$\begin{aligned}
 I_{(\text{spin axis})} &= 10.41 \text{ slug-ft}^2 \\
 I_{(\text{transverse}) (\text{max.})} &= 8.33 \text{ slug-ft}^2 \\
 I_{(\text{transverse}) (\text{min.})} &= 7.36 \text{ slug-ft}^2
 \end{aligned}$$

The axis of maximum transverse inertia is located 82 degrees counterclockwise from the mercury-bombardment-engine location (+X) as viewed from above the baseplate.

E. HANDLING PROCEDURES

1. General

The fully assembled SERT spacecraft was difficult to handle not only because of its bulkiness and considerable weight but also because the areas for grasping the spacecraft were severely restricted by its complexity. Mostly, lifting of the spacecraft was accomplished by hand-operated chain hoists of one-half-ton capacity. On some occasions, however, electrically operated, overhead traveling cranes were used.

2. Lifting Sling

The sling used for lifting the spacecraft during various stages of its integration and test cycle consisted of three felt-covered aluminum clamps secured to the base-plate outer flange at equally spaced intervals. Each clamp had a length of one-quarter-inch-diameter wire rope spliced to a standard eye bolt which screwed into the clamp body. The other end of these wire ropes was spliced to a lifting ring of suitable size to fit over the hook of the chain hoist. Approximately mid-way between the end points of the wire ropes a spreader ring was installed to insure that these ropes did not damage the spacecraft components. The entire assembly is shown in Figure II-15.

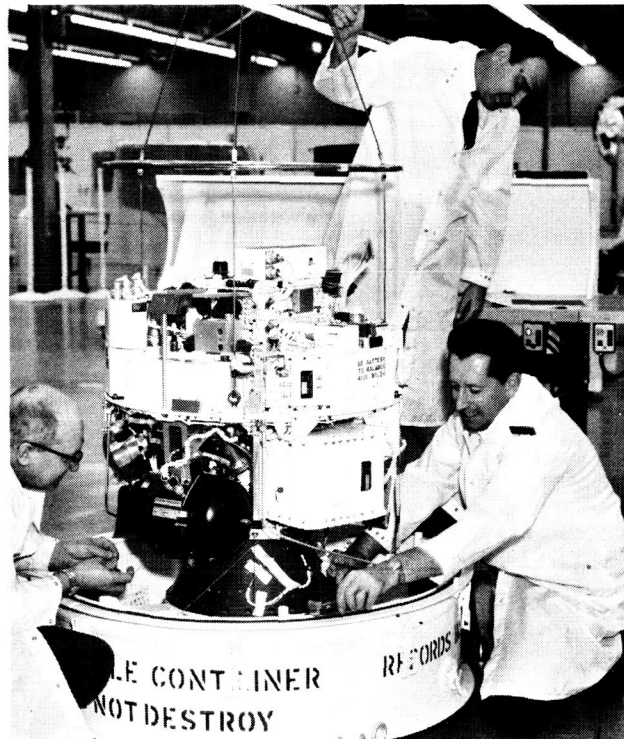


Figure II-15. SERT Spacecraft, Suspended by the Lifting Sling, Being Placed in the Shipping Container

3. Workstands

Most of the integration and some of the testing of the spacecraft was performed with the spacecraft mounted on a modification of a standard spacecraft workstand used by RCA. This modification affected the way in which the spacecraft was mounted; three different arrangements were required:

- One arrangement utilized a ring with a hole pattern and centering counterbore suitable for mating with the lower surface of the column assembly.
- Another arrangement consisted of a ring simulating one-half of the rocket mounting adapter, thus allowing the spacecraft to be mounted using the separation clamps.
- The third arrangement used a large flat plate whose outside diameter was slightly smaller than the inside diameter of the lip on the base of the separation mechanism. This plate was drilled to simulate the hole pattern of the separation mechanism mounting.

4. Turning Fixture

This fixture was designed and used for inverting the integrated spacecraft before performing the inertia measurements. The fixture consisted of three baseplate clamps similar to those on the lifting sling. Each clamp supported a solid aluminum rod which extended both above and below the spacecraft; these legs were braced, at top and bottom, with triangular-shaped brackets. The clamps and legs were assembled to the spacecraft and enclosed it like a cage. The entire assembly could then be placed on the floor and carefully tipped to the proper position for installation on the bifilar pendulum for inertia measurement. The process is reversed to replace the spacecraft on the workstand.

5. Layout and Drill Stand

The layout and drill stand, which was used to hold the baseplate during location and drilling of mounting holes, consisted of a triangular base with three upright posts, cross-braced to provide the required stability. The upright posts were notched and lined with felt to provide a nest for the baseplate. Felt-covered clamps were used to secure the baseplate to the posts and to prevent it from shifting or tipping. This stand was fabricated of wood and outfitted with casters for mobility. It supported the baseplates with either the top side or bottom side up and readily allowed the installation of the Mylar drill template (Paragraph II-D. 2).

REFERENCES

- II-1 RCA Report ESAR S-1, "SERT Structural Stress Report," Contract NAS-8-2449.
- II-2 RCA Report AED R-2388, "Vibration Test Report of the SERT T-1D Capsule," Contract NAS-8-2449, Jun 4, 1964.
- II-3 RCA Memo, E. A. Jackson to L. E. Golden, "Effect of SERT Damping Fluid," Mar 11, 1964.
- II-4 RCA Report IM-B-105, "Project SERT Vibration Survey Mechanical Model (T-1)," Contract NAS-8-2449, Jun 15, 1962.
- II-5 RCA Document TM-1401 AED R-1977, "A Report on Supplemental Vibration Testing of the SERT I Capsule," Contract NAS-8-2449, Jun 25, 1963.
- II-6 SERT Logbook SL-20, "Static Load Test, SERT Baseplate."
- II-7 Project SERT Vibration Survey Data of SERT Distributor Frame.
- II-8 RCA Document SPO-41, "A Report on the Design and Development of the SERT Hydraulic Damper System (Engine Extension System), Contract NAS-8-2449, Jul 12, 1963.
- II-9 RCA Document SPO-87, "A Report on the Ground Plane Packing Procedure for the SERT Capsule," Contract NAS-8-2449, Jul 22, 1964
- II-10 T-1B Vibration Survey Data, Jan 29, 1963.
- II-11 RCA Report AED R-1894-2, "SERT T-1B-1 Capsule Qualification Vibration Test Report," Contract NAS-8-2449, Mar 14, 1963.
- II-12 RCA Report, "T-1B-1 Prototype-Level Vibration Test Data," Contract NAS-8-2449, Mar 8, 1963
- II-13 Edited by F. J. Clauss, First Symposium Surface Effects on Spacecraft Materials, John Wiley and Sons, 1960.
- II-14 J. J. Thomson, Conduction of Electricity Through Gases, Cambridge University Press, 1906.
- II-15 RCA Document SPO-80, "T-3 Balance Report," Contract NAS-8-2449, Jun 1, 1964.
- II-16 RCA Document SPO-81, "T-3 Supplementary Balance Report," Contract NAS-8-2449, Jun 1, 1964.

- II-17 RCA Technical Memorandum TM-1501, "Moment of Inertia Measurement by the Use of the Bifilar Torsional Pendulum," Contract NAS-8-2449, Sep 10, 1962.
- II-18 RCA Document SPO-82, "Measurement of Spin Axis Moment of Inertia - SERT T-3 Capsule," Contract NAS-8-2449, Jun 1, 1964.
- II-19 RCA Document SPO-83, "Measurement of Transverse Moment of Inertia - SERT T-3 Capsule," Contract NAS-8-2449, Jun 1, 1964.
- II-20 RCA Document SPO-84, "Supplementary Inertia Measurement Report - SERT T-3 Capsule," Contract NAS-8-2449, Jun 10, 1964.
- II-21 RCA Technical Memorandum TM-1301, "Electrical Breakdown on the SERT Capsule," Contract NAS-8-2449, Sep 7, 1962.
- II-22 RCA Test Report, "Test Report - SERT Thermal Model," Nov 15, 1962

SECTION III

SPACECRAFT ELECTRICAL DESIGN

A. GENERAL

Presented in Section I were the general requirements of the SERT I electrical system and the major subsystems necessary to implement these requirements. This section is devoted to an expansion of the system discussion and to the detailed description of each subsystem, including its concept, operation, development, and component hardware. The descriptive material presented for those subsystems not developed under RCA's responsibility is necessarily brief but is included for completeness.

Figure III-1 is a functional block diagram of the SERT I electrical system. The major subsystems are as follows:

- Mercury-Bombardment-Engine Subsystem,
- Cesium-Contact-Engine Subsystem,
- Telecommunications Subsystem,
- Command and Control Subsystem,
- Power Subsystem, and
- Sensory Subsystem.

Power for the mercury-bombardment-engine subsystem is provided by the power subsystem as inputs to the ac and dc power supplies, which convert the basic 28 and 56 volts into the various potentials needed for engine operation. The neutralizer voltage control unit is controlled by the programmer of the command and control subsystem. Subsystem performance data is routed, as dc and ac voltages, to the signal conditioner of the telecommunications subsystem. The ion-beam probe and mechanism and the beam-probe signal conditioner, although part of the sensory subsystem, are operated in conjunction with the mercury-bombardment engine.

Power for the cesium-contact-engine subsystem is provided directly to the inverter where it is conditioned and applied to the remaining subsystem components. The control box provides timed signals to implement parameter variations. Subsystem performance data is routed through the spacecraft harness to the signal conditioner of the telecommunications subsystem.

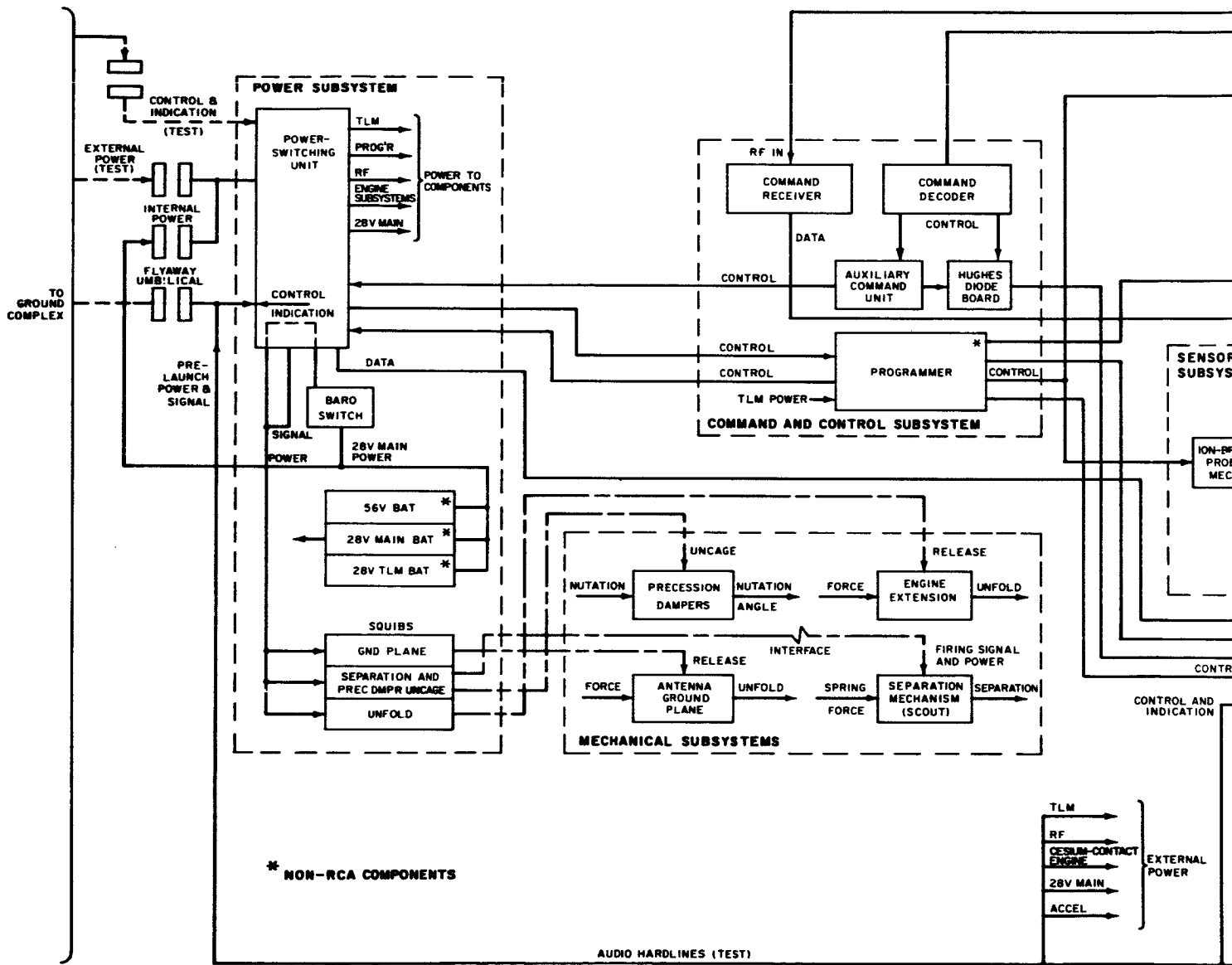
As shown in Figure III-1, there are two separate and redundant active-element links in the telecommunications subsystem, each link consisting of a commutator, sub-carrier oscillator package, transmitter, converter, and power amplifier. Sub-system power, although not specifically shown, is provided completely by the 28-volt telemetry battery within the power subsystem. Power regulation and conversion, as required, is performed independently by each of the various components, with the exception of the telemetry transmitters and rf power amplifiers which receive regulated power from the dc-to-dc converters. Control inputs are not necessary since the subsystem operates in one mode through the entire flight. Data inputs from the other subsystems are provided at several points: at the signal conditioners, for the commutated data links; and directly into the subcarrier oscillators, for the real-time links. The telecommunications subsystem output is the modulated rf power from the SERT transmitting antenna. As shown in Figure III-1, the receiving antenna signal is fed into the coupling network before it reaches the command and control subsystem.

Allocations of the various data to the 86 commutated data channels were established by NASA in conjunction with the major subcontractors to provide some redundant data in each of the communications links. Specifically, 12 critical ion-engine parameters were selected for redundant transmission. Channel allocations adopted for the mission are listed in Appendix B.

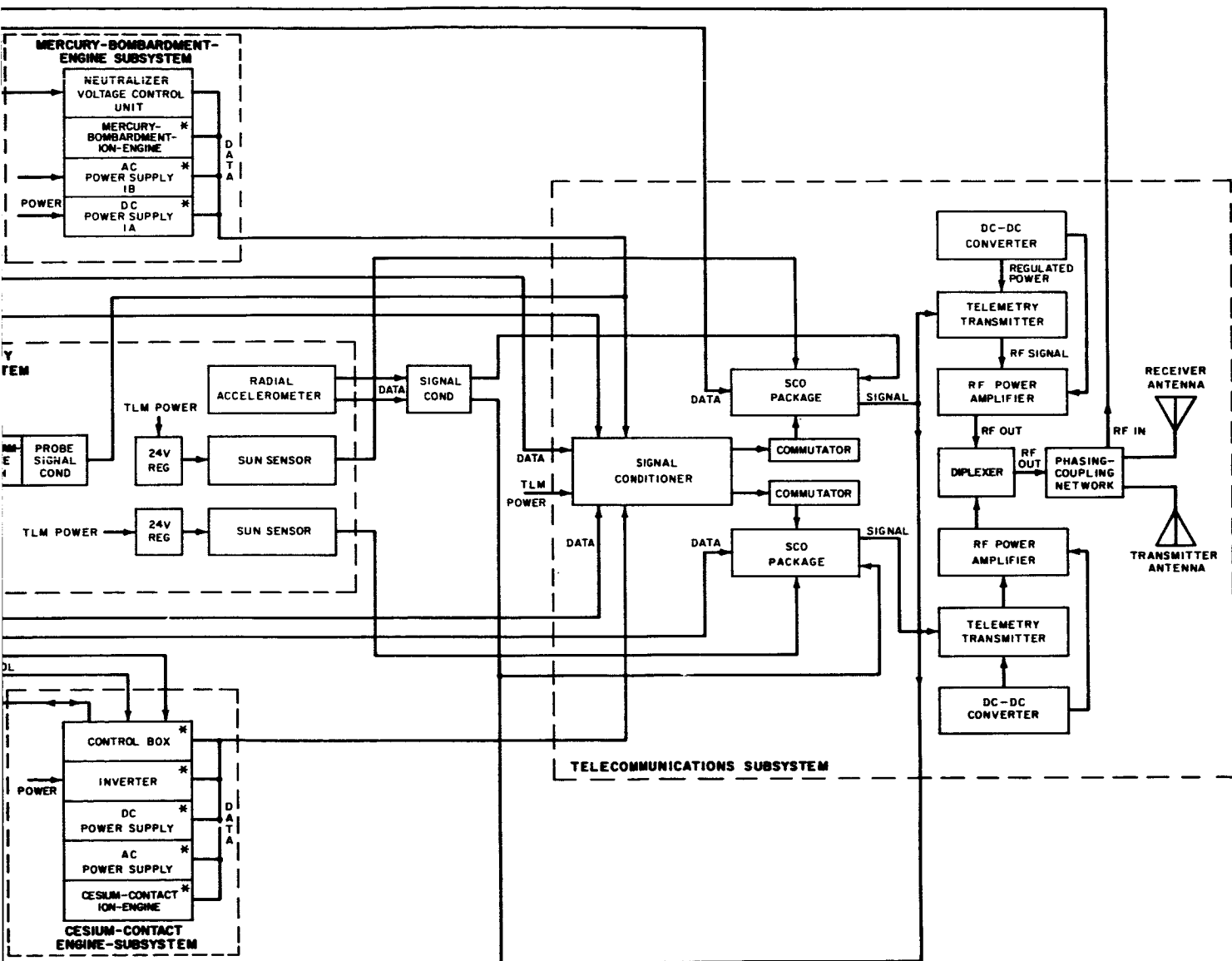
The command and control subsystem performs the in-flight programming and control function of the spacecraft. In general, control interfaces with the other subsystems are in the form of relay closures. This type of interface was selected early in the program because of its basic simplicity and because it permitted separation of subsystem design details. Power for the subsystem is provided from the 28-volt telemetry battery.

The power subsystem was designed to provide power to the power-switching unit either from the spacecraft batteries (in flight) or from an external power supply (during test). Control is provided from the command and control subsystem, although external control during testing is provided through the "flyaway umbilical." The power-switching unit also provides state and power information to both the telecommunications subsystem and to the ground test complex. The squib-firing functions for engine unfolding, ground-plane release, precession damper uncage, and spacecraft separation are also contained within the power-switching unit, although control signals are provided by the programmer. A barometric switch is in series with these functions to prevent squib firing before lift-off.

The sensory subsystem provides spin-rate and mercury-bombardment-engine data to the telecommunication subsystem. Power from the 28-volt telemetry battery (through the power-switching unit) is provided continuously to all sensors except the beam probe which operates only when the mercury-bombardment-engine is activated.



III-3



III-4

Figure III-1. Functional Block Diagram of the SERT System

B. MERCURY-BOMBARDMENT-ENGINE SUBSYSTEM

1. Description

The heart of this subsystem is the ion engine (Figure III-2) which operates on the electron-bombardment ionization principle. This engine has a self-contained fuel supply and is capable of producing thrust upon the application of electrical power. The engine, its power supplies, and power-control equipment were designed and built by the NASA Lewis Research Center. In response to NASA specification RCA developed the neutralizer-voltage control unit (NVCU) which is used to aid in studying the effects of variations in neutralizer voltage on engine operation. The NVCU is discussed, in detail, in paragraph II-B.2. The other components are not discussed in detail; however, for completeness, a brief description is given in the paragraphs that follow.

a. DC Power Supply

This component, which contains solid-state circuitry throughout, uses the 28- and 56-volt dc power from the power subsystem to generate the high dc potentials needed for engine operation. The 56-volt power is converted into ac by an inverter, and special insulated transformers are used to step-up this voltage to levels which can then be rectified and filtered to provide the required high dc potentials. In combination with the ac power supply, this unit contains overload circuits designed to protect it against shorting or arcing at the outputs.

b. AC Power Supply

This unit converts spacecraft primary power into high ac voltages which are applied to the engine boiler and the cathode heater.

c. Magnetic Field Power Supply (Battery)

This battery provides power to the engine magnetic field coils. A special fiber-glass case isolates the battery, which is at the high dc potential of the dc power supply, from ground. The battery is of the zinc silver-oxide type discussed further in paragraph III-F; it is rated at 6 volts (nominal), 20 amperes, and 12 ampere-hours.

d. Neutralizer Power Supply (Battery)

This battery is the power source for the engine neutralizer filament. As with the magnetic field battery, this battery is fiber-glass-cased and can be isolated above ground at high potentials. The two batteries are identical in external appearance. This battery is rated at 10 volts (nominal), 20 amperes, and 12 ampere-hours.

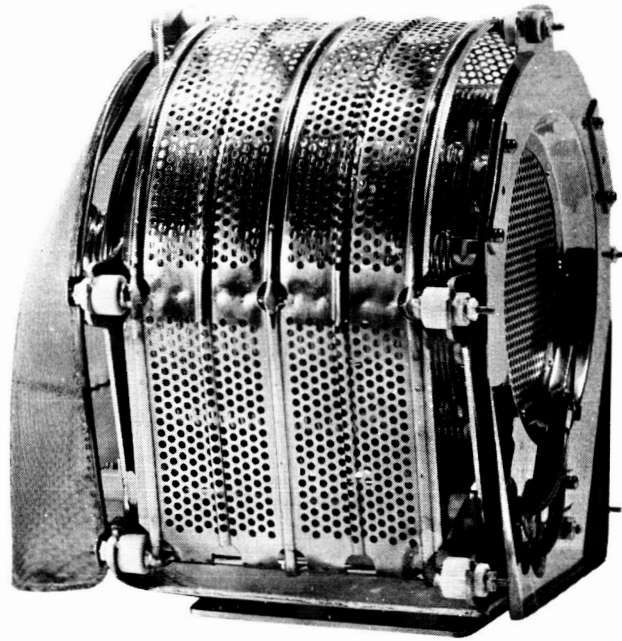


Figure III-2. Mercury-Bombardment Ion Engine

2. Neutralizer Voltage Control Unit (NVCU)

a. General

The mercury-bombardment-engine neutralizer is a heated filament, placed in the ion-engine exhaust, which serves to neutralize the ion beam by injecting electrons. The neutralizer-voltage control unit (NVCU) is an electromechanical device which, on command, varies the resistance between this filament and spacecraft ground along the path of ion-beam neutralization current, thus varying the neutralizer potential. During most of the engine operation, the NVCU remains shorted, allowing only the voltage necessary for neutralization-current measurement to be developed. When, for experimental purposes, the neutralizer potential is to be varied, the onboard programmer directs the ordered sequencing of resistances; two such sequences are performed during flight.

b. Functional Description

Within the NVCU, resistances are selected by relays which are controlled by a pulse-operated stepping switch. Initially, the resistance of the NVCU is 13 ohms; during sequencing, this resistance is increased in five 800-ohm steps to

4000 ohms. Since the anticipated neutralizer current is to be constant at 300 milliamperes, the voltages developed at this filament range from approximately 4 volts to 1200 volts. A simplified schematic diagram of the circuit designed to accomplish this switching is shown in Figure III-3. This circuit is divided into two parts: the control circuit and the switching circuit.

The control circuit consists of a 12-contact stepping switch and an array of diodes. At each position of the switch, 28-vdc power is applied to the switching circuit through one or more of the diodes. In the switching circuit, the outputs of these diodes are applied to one or more of the three relays which short various portions of a resistive divider network to produce the desired resistances. Because of the high-voltages produced in this circuit, high-voltage relays and wiring and high-power resistors are used.

The NVCU also provides a prelaunch signal through the umbilical confirming that the stepping switch is in position one. Position one is the start of the sequence and corresponds to that state in which all three high-voltage relays are energized leaving a total resistance of 13 ohms in the neutralizer circuit.

For testing and preflight checkout, the unit has test points to allow monitoring of the position of the stepping switch, and it also has provisions for externally controlling the stepping switch. In addition, the NVCU provides two outputs to the telecommunications subsystem; these outputs, representing neutralizer voltage and current, are telemetered to the ground station throughout the entire mercury-bombardment-engine operating cycle.

The power resistors (R1, R2, and R3) were selected for the largest physical size to fit the available space so that no resistor would exceed the maximum temperature rating of 300°C during the two pre-established identical sequences of resistor switching. Resistors R4 and R5 were more conservatively rated since little volume and space was required for the power dissipated.

c. Mechanical Description

The NVCU, mounted physically separate from the mercury-bombardment-engine subsystem, is 11.75 inches long, 3 inches wide, and 3.75 inches high; it weighs three pounds (Figure III-4). All of the electrical components in this unit are mounted on the 11.75- and 3.75-inch faces, and the unit is mounted to the spacecraft distributor frame along the 3- and 3.75-inch faces.

d. Development

In the development of the NVCU, two problems were encountered: (1) the selection of the stepping switches and (2) the selection of the high-power resistors. Extensive testing programs were required before the final selections were made.

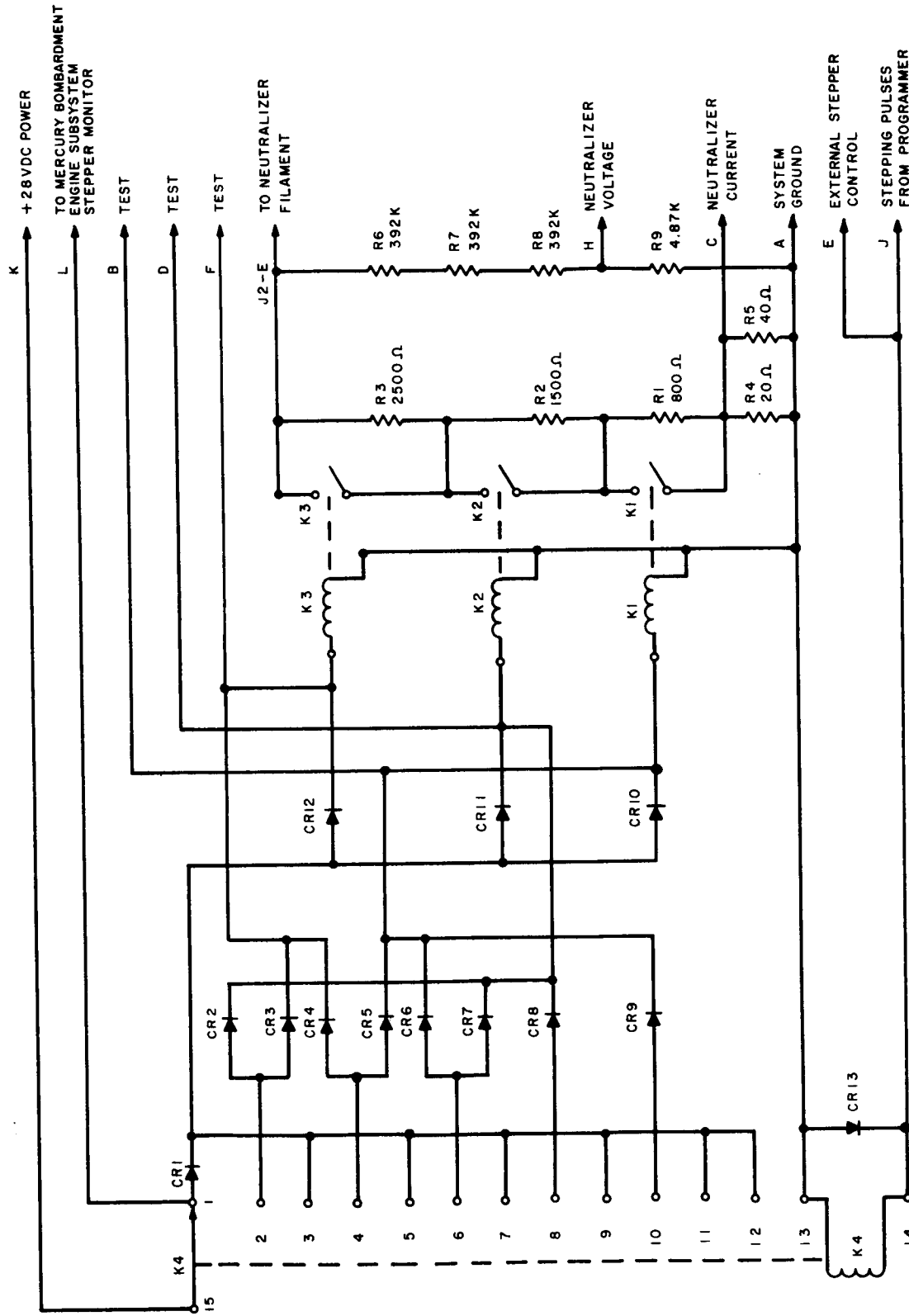


Figure III-3. Simplified Schematic Diagram of the Neutralizer Voltage Control Unit

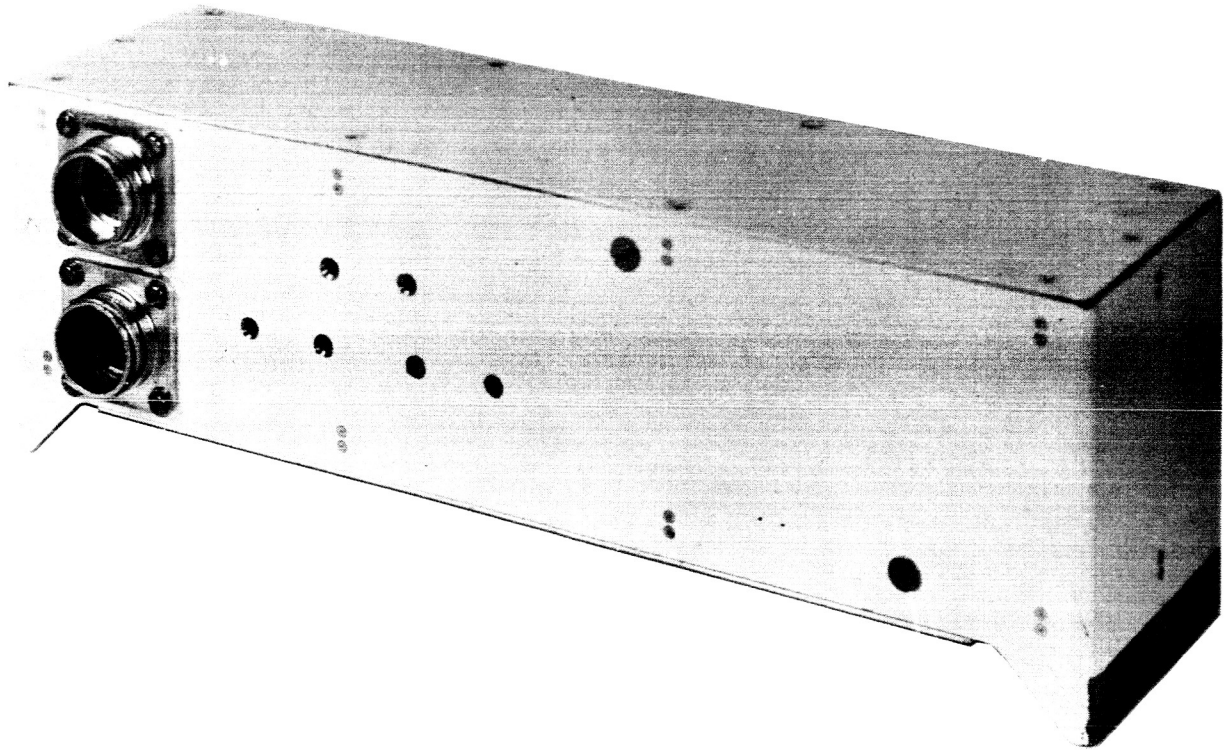


Figure III-4. Neutralizer Voltage Control Unit

During the stepping switch development, the design of a solid-state switch as well as the application of three mechanical switches available in the industry were considered. The former approach was abandoned after investigations of mechanical switches showed them to have greater noise immunity and simpler development requirements. After an extensive evaluation program, which included much environmental testing, a switch designed to meet the special environmental requirements, was selected.

The major problem in the development of the high-power resistors involved high-voltage breakdown during vacuum-testing under operating conditions. In order to meet the high power requirement, the resistors were designed with the resistive element wound on a grooved ceramic core and totally enclosed within a cast-metal heat sink.

During vacuum testing, the air entrapped in the grooves between the resistive winding and the metal heat sink would outgas producing critical pressures within the groove cavities, setting up the conditions for electrical breakdown (arcing). These breakdowns would generally occur after one or more hours exposure to vacuum. The problem was solved by potting the ends of the resistors with R. T. V. which sealed the joint between the ceramic former and heat sink thus preventing the escape of entrapped air. The flexible R. T. V. potting material was used to prevent cracking due to differential expansions caused by the heating and cooling of the resistor during its duty cycle. At least 9 hours of reliable operation was achieved during vacuum testing on several resistors.

A further modification to the unit resulted from operational tests with the mercury-bombardment engine. This modification required separation of the high- and low-voltage inputs into two connectors.

C. CESIUM-CONTACT-ENGINE SUBSYSTEM

Essentially, the requirements for this subsystem are the same as those for the mercury-bombardment-engine subsystem: to produce thrust when power is applied. A photo of the cesium-contact engine is shown in Figure III-5. The design of this subsystem and its components, however, is quite different. Since none of this subsystem was RCA's responsibility, a detailed description is not given; for completeness, however, a brief description of each of the components follows:

- (1) Inverter: This component converts the 56-volt battery power from the power subsystem to regulated ac; the 28-volt supply provides the power necessary to operate the inverter. All of the inversion circuits are transistorized.
- (2) DC Power Supply: This component accepts the ac voltage from the inverter, steps it up using transformers, and rectifies it to provide the high dc potentials required for engine operation.
- (3) AC Power Supply: Primarily, this component conditions the ac voltage from the inverter power for the cesium-contact-engine heaters. It also provides many of the auxiliary voltages needed for subsystem operation.
- (4) Control Box: This component serves as a subprogrammer for the cesium-contact engine subsystem, controlling all heater sequencing and experimental programming. It also contains the overload protection capability for the entire subsystem. In addition, the control box provides mounting for the E-Field sensor.

D. TELECOMMUNICATIONS SUBSYSTEM

1. General

The telecommunications subsystem provides a means of monitoring, conditioning, and transmitting flight data from the SERT spacecraft. This data is in a format which can be received and reduced by standard telemetry ground stations and which is particularly suited to the capabilities of the Wallops Island Launch Station. The entire system, including ground equipment, is capable of data presentation with an accuracy of greater than 5 percent.

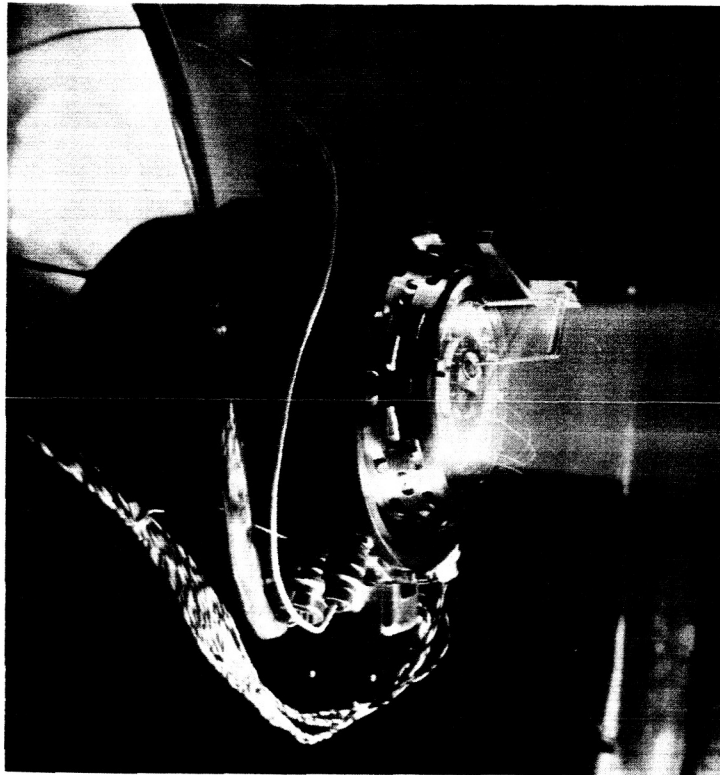


Figure III-5. Cesium-Contact Ion Engine

2. Description

The telecommunications subsystem includes all equipment for conditioning, multiplexing, and transmitting the experimental data and spacecraft housekeeping (operating) data. The subsystem has two independent active-element links. In the event of a failure in either link, sufficient data would be retrieved through the remaining link to ensure partial mission success. The subsystem block diagram is shown in Figure III-6.

The signal conditioning equipment converts the data inputs, to be later time-division multiplexed by the commutators, into dc signals with a dynamic range of 0 to 5 volts. In addition, this equipment generates the pedestal reference voltages for the commutators. The signal conditioning equipment is discussed in detail in paragraph III-D.3.

Two 45-segment PAM commutators and two subcarrier-oscillator (SCO) packages compose the multiplexing equipment. Eighty-six channels of ion-engine experimental data and spacecraft housekeeping data are time-division multiplexed by the commutators and fed to the SCO packages to modulate the 10.5-kc subcarriers. Continuous

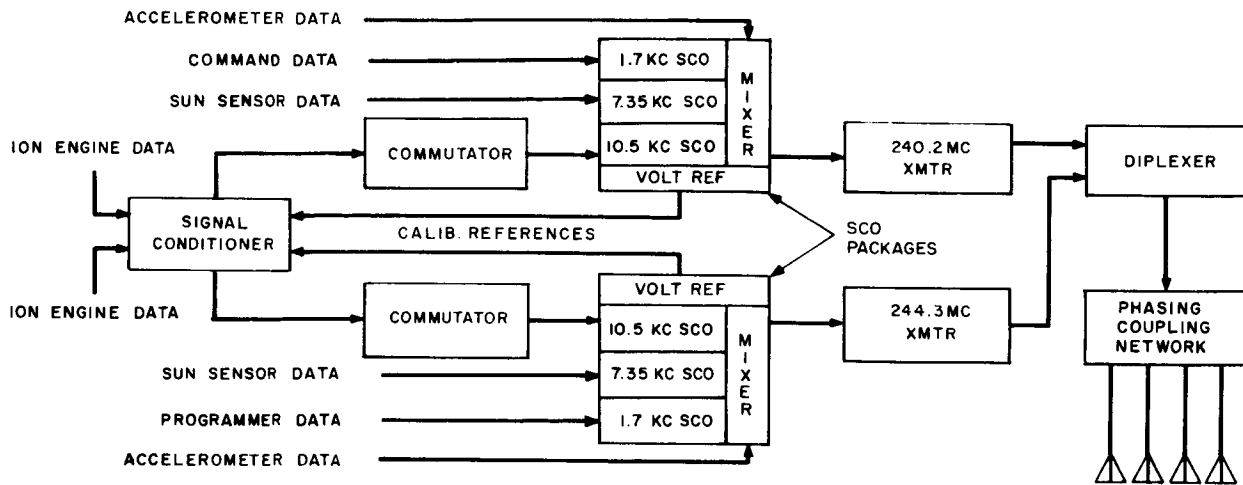


Figure III-6. Block Diagram of the SERT Telecommunications Subsystem

sun-sensor spin-rate data modulates the 7.35-kc subcarriers, and continuous on-board-programmer milestone information and command-backup-signal-decoding confirmation modulate the 1.7-kc subcarriers. The outputs of the SCO's are summed with each other and with the low-frequency accelerometer data to frequency modulate the transmitting equipment. For details, refer to paragraphs III-D. 4 and III-D. 5.

The outputs of the two 10-watt fm transmitters, one operating at 240.2 megacycles and the other at 244.3 megacycles, are first diplexed and then phase shifted to quadrature feed four quarter-wavelength antennas which produce a circularly polarized radiation pattern. Details of the transmitters are given in paragraph III-D.6; the antennas are discussed in III-D.7.

The analytical design of the SERT telecommunications subsystem is summarized below and is described in detail in Appendix C.

- (a) The selection of a multiple-subcarrier, pam-fm-fm system was based upon the following:
 - (1) Compatibility with existing Wallops Island facilities,
 - (2) Simplicity,

- (3) Compatibility with data requirements, and
- (4) Minimum equipment development requirements.

Two redundant active links were required to ensure reliable transmission of the ion-engine-performance data and spin-rate information. Programmer and command-subsystem status were considered to be of secondary importance; therefore, this information was not redundant, saving considerable power and weight.

(b) RF bandwidth requirements were based upon the sum of:

(1) Data bandwidth (10.5kc SCO)	22.6 kc
(2) Doppler Shift (at separation)	6.2 kc
(3) Frequency stability (+0.01%)	49 kc
	77.8 kc

A standard receiver i. f. bandwidth of ± 100 -kc was therefore selected.

- (c) As detailed in Appendix C, the communications link calculation for (1) a 4000-mile slant range, (2) a selected standard-band frequency of 245mc, (3) a circularly polarized isotropic spacecraft antenna, and (4) a specified antenna at Wallops Island shows that a 10-watt transmitter will provide a margin of 15db above fm threshold (without phase-lock loop). This margin was considered desirable in view of the unknown effects of the ion beam (Reference III-1).
- (d) The 10.5-kc subcarrier was selected on the basis of the commutated data and bandwidth requirements; the other subcarrier frequencies were selected to be (1) below 10.5 kc (minimizing bandwidth), (2) compatible with IRIG standards, and (3) capable of meeting the data-transmission requirements. The sub-carrier signal-to-noise levels are very satisfactory (greater than 41 db at receiver threshold) and do not contribute significantly to the system error. In particular, the error in the 10.5-kc channel is less than 0.33 percent and less than 2.2 microseconds in the 7.35-kc link.
- (e) Error analyses were performed in the telecommunications subsystem to verify that data accuracy was better than the required 5 percent (see Appendix D). The analyses revealed the following:

<u>Channel</u>	<u>Error</u>
Commutated channels	3.3 percent (without calibration)
Sun Sensor channels	23 microseconds
Programmer and command channels	3.5 percent (without calibration)

3. Signal Conditioning

a. General

The SERT signal-conditioning equipment converts the data inputs which are to be time-division multiplexed into dc signals with a dynamic range of 0 to 5 volts. The bulk of the conditioning is accomplished within a central unit (signal conditioning box). Four outlying components — two dc amplifiers, a box containing five ac amplifiers, and an accelerometer signal conditioner — complement the central unit. A block diagram is shown in Figure III-7.

Two of the complementary units, the dc amplifiers, convert 0- to 50-millivolt shunt potentials, representing main-battery and telemetry-battery-current, obtained within the power-switching unit into voltages within a 0- to 5-volt range. These amplifiers plug into the central unit, and their outputs are sampled by the commutators.

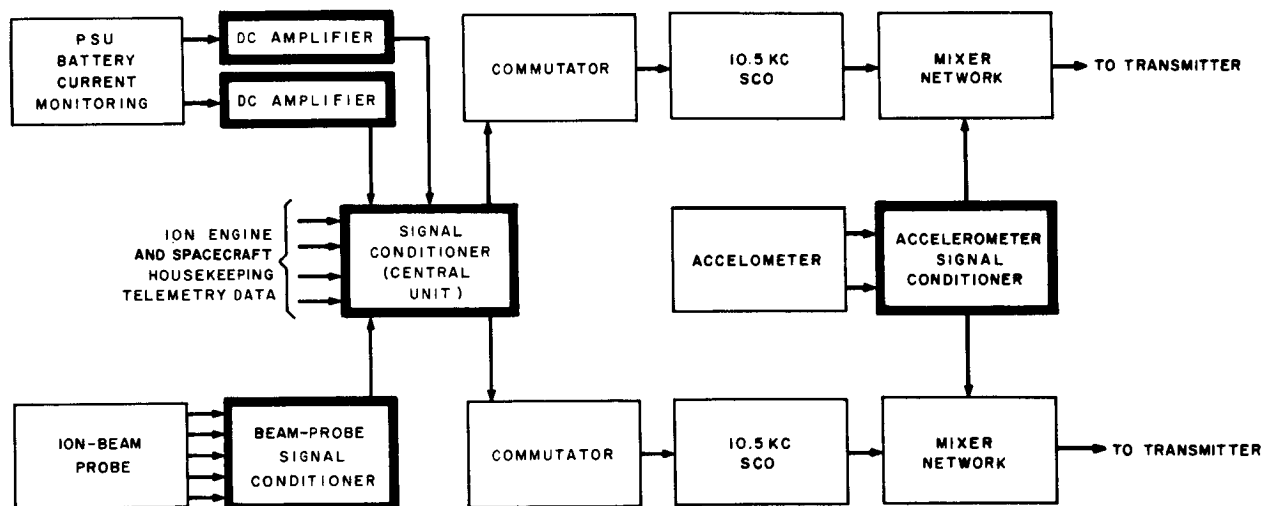


Figure III-7. Block Diagram of the Signal Conditioning Equipment

The third complementary unit, the ion-beam-probe signal conditioner, which contains five ac amplifiers and associated circuitry, converts millivolt-range ac signals, which are isolated above ground into dc voltages in the 0- to 5-volt range. These ac signals represent ion-beam current information that is obtained from five hot-wire anemometer probes which are positioned in the exhaust path of the mercury-bombardment engine. The ion impingement on the wires results in a corresponding resistance change and a resultant voltage variation. This voltage variation is transformer coupled to one leg of an ac bridge. Transformer coupling is used to isolate the signal-conditioning equipment from any high potentials which may be induced into the sensing circuits by the ion beam. The signals are amplified, rectified, and fed to the central unit to become five of the time-division multiplexed data channels.

The fourth supporting unit, the accelerometer signal conditioner, consists of adjustable resistive circuit which provides impedance matching between the two accelerometer outputs and the mixer circuits in the SCO packages. Since the conditioner outputs directly modulate the transmitters by way of the mixer, the adjustments serve also to set the deviation ratio.

The central unit itself contains all of the electronic circuitry required to convert the remaining data inputs into signals which have an amplitude range of 0 to 5 volts dc. The time-division multiplexers, or commutators, which are physically attached to the central unit, sample these signals and feed the resultant wave-train back to the central unit where noise spikes are filtered. The wave-train then modulates the 10.5-kc subcarrier oscillators.

b. Signal Conditioner (Central Unit)

The electrical networks in the central unit condition 86 channels of ion-engine performance and spacecraft housekeeping data: twenty-eight channels for the mercury-bombardment engine, thirty-five channels for the cesium-contact engine, nine channels of temperature-level data, six battery-condition channels, five calibration channels, one channel for confirmation of spacecraft separation and ion engine deployment, and one channel which indicates the back-up-command mode.

The central unit consists of six component boards, a potentiometer assembly, two dc-dc converters, two dc amplifiers, and the associated harness wiring. The unit is approximately 11-1/2 x 6-1/4 x 4-1/2 inches and weighs approximately five pounds. The design and development of the unit was in accordance with the specifications of RCA Technical Memorandum TM-1105 "SERT Signal Conditioner Data," (Reference III-2).

The unit was developed using solid-state circuitry and resistive dividers, mounted on plug-in module boards. In this way, specification changes could be readily handled by module board changes rather than overall assembly changes.

The first central units were designed to mate with the electronic commutators which were mounted on each of the chassis. Because of difficulties encountered during T-2 system testing at the Lewis Research Center, it became necessary to redesign the central unit to accommodate mechanical commutators (paragraph III-D.4). In addition, the two dc amplifiers, previously located in the power-switching unit, were relocated on the signal conditioner (paragraph III-D.2). Both of the dc amplifiers were mounted on one end such that electrical adjustments could be made while the central unit was installed on the spacecraft. As before, the commutators were mounted on each end of the chassis.

For simplicity and reliability, the use of passive, purely resistive networks was emphasized in the design of the central unit. Two types of purely resistive divider circuits were used to obtain the 0- to 5-volt output: 0 to 30 volts by 6 dividers and

0 to 6 volts by 5 dividers. In addition, all of the temperature sensing networks utilized the resistive-change characteristics of the temperature sensors in a purely resistive network to obtain a 5-volt output for the corresponding lower temperature limit.

Some of the conditioning requirements dictated the use of several types of active low-level circuits. These included a 5-to-1 AGC amplifier, high-gain dc amplifiers for monitoring the cesium-contact-engine beam-probe currents, a rectifier network for the mercury-bombardment-engine mercury-heater temperature, and negative-bias-voltage generators. All of these circuits were designed using solid-state circuitry. Reference III-3 (TM-1103 "SERT Signal Conditioner") provides detailed information as to the channel-by-channel circuit configurations. Reference III-4 (SPO-11, "SERT Signal Conditioner Scale Factors") supplements TM-1103 to provide channel-by-channel scale-factor information. Several typical signal-conditioning circuits are shown in Figure III-8.

The introduction of mechanical commutators in place of the solid-state electronic commutators resulted in some redesign and additional electronic circuitry in the central unit. The mechanical commutator was chosen by NASA who instructed RCA to study the incorporation of the device into the telecommunications subsystem. The results of this study are given in Reference III-5.

The battery-current-monitor dc amplifiers were moved from the power-switching unit to the top of the central unit in conjunction with the commutator changes. The smaller volume of the mechanical commutators (compared to the solid-state commutators) made this change possible. The advantages of such modifications were:

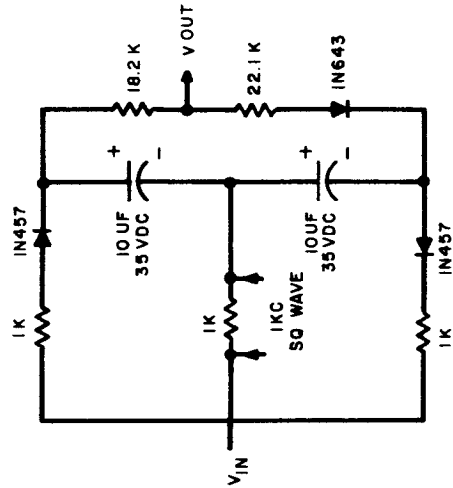
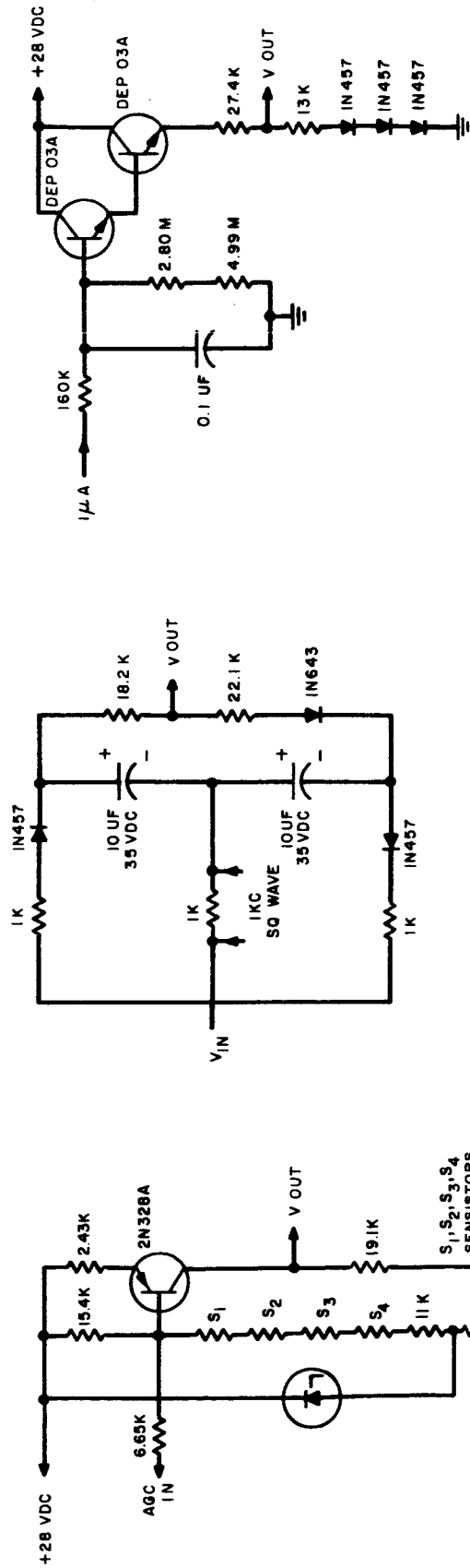
- (1) Amplifiers could be changed without disassembly of part of the spacecraft.
- (2) Adjustment of the zero set and gain of the dc amplifiers could be accomplished with greater ease.

The changes to the central unit resulting from the above modifications were:

- (1) Addition of two low-pass filters to protect the input of the dc amplifiers;
- (2) Addition of a low-pass filter and level-limiting circuits on the output of the commutators to protect the 10.5-kc SCO inputs; and
- (3) The design and manufacture of a dc-dc converter to provide redundant pedestal voltages for the mechanical commutators.

c. DC Amplifier

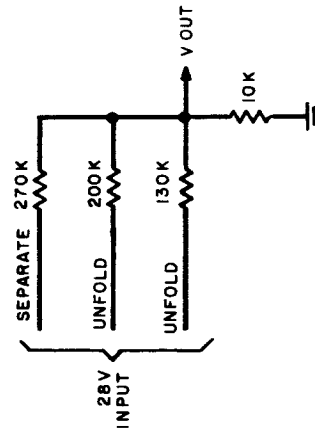
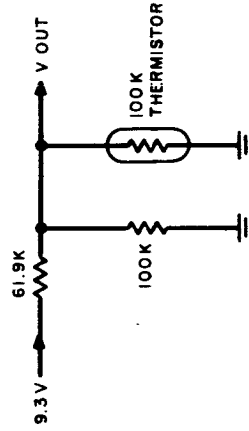
The battery-current-monitor dc amplifiers were developed to facilitate telemetry measurements of the main and telemetry battery currents. Current shunts,



COMMAND RECEIVER AGC AMPLIFIER

MERCURY HEATER MONITOR

BEAM-PROBE AMPLIFIER CESIUM - CONTACT ENGINE



TEMPERATURE MONITOR

EVENT MONITOR

Figure III-8. Typical Signal - Conditioning Circuits

mounted in the power-switching unit (PSU) and connected in series with the ground (negative) leads of the two battery systems, provide voltages in the 0- to 50-millivolt range, which are directly proportional to the current flow. Since the dc amplifier provides linear operation with a gain of 100 over the entire input range, the output is in the 0- to 5-volt range required for the telecommunications subsystem.

The amplifiers initially selected for use were subcontracted; these amplifiers passed the qualification and acceptance test programs only after considerable difficulty. Among the failures encountered were loss of output, zero off-set, and drift.

During subsequent live ion-engine testing on the prototype spacecraft (T-2) at the Lewis Research Center further failures occurred. These failures were caused by high-voltage transients (spikes) which exceeded the allowable levels at the input of the amplifiers. The transients were caused by high-current surges induced during ion-engine arcing.

A redesign of the amplifier was then initiated; the two objectives of this redesign were to (1) incorporate a low-pass filter at the amplifier input and (2) to improve overall reliability, including the zero-set and drift-stability characteristics. In addition, the dc amplifiers could now be moved from the PSU to the top of the signal conditioner (central unit), thus providing better access. Throughout the redesign, the original envelope, method of mounting, and connector and connector-pin arrangements were maintained.

Specifications for the redesigned amplifiers were sent to twenty-four manufacturers, and three companies responded. The amplifiers selected passed the qualification and acceptance test programs without difficulty and were incorporated on the T-1B-3 and T-3 spacecrafts.

It was found to be impractical to incorporate the input low-pass filters within the envelope of the amplifier. Therefore, an external filter was built into the signal conditioner (central unit). However, some special input-power filtering was provided within the amplifiers.

d. Ion-Beam-Probe Signal Conditioner

In the original design of the ion-beam-probe signal conditioner, the fine ion-beam-probe resistance elements were made of 0.4-mil wire with a resistance range of 12 to 20 ohms from engine-off to maximum-beam-density conditions. The conditioning circuitry was designed to meet these parameters. During live ion-engine testing at the Lewis Research Center, it was found that the 0.4-mil wire eroded too fast when swept through the ion-beam. The wire size was increased to 0.6 mils which reduced the off-to-full beam resistance to a variation of 5 ohms and a range of 9 to 14 ohms.

In the original design, the low side of all five transformer secondaries were grounded and the high sides were connected directly to the input of the ac amplifiers. With the new resistance wire, the amplifier was not sensitive enough to provide a 0- to 5-volt telemetry signal. In order to increase the sensitivity, the transformers were redesigned and used as inductance legs of five separate ac bridges, and the amplifiers were now driven by the outputs of these bridges. The gain of each amplifier was increased by reducing the emitter resistance of the input stage from 330 ohms to 27 ohms. The overall sensitivity of the final circuit is 2 volts output for each ohm of sensor resistance change. A schematic diagram of this circuit is shown in Figure III-9; a photo of the unit is shown in Figure III-10.

e. Accelerometer Signal Conditioner

The accelerometer signal conditioner is composed of two simple resistive matching circuits; each provides impedance matching between an accelerometer output and the telemetry-signal mixer circuits in the SCO package. A 20 kilohm trimpot provides a voltage level adjustment of each signal. Since the conditioner outputs directly modulate the transmitters by way of the mixer, the adjustments serve to set the deviation ratio. A schematic diagram is shown in Figure III-11.

The parts are mounted on a fiber-glass board which is mounted to a bracket (Figure III-12). The bracket bolts to one of the spacecraft baseplate ribs with the trimpot adjusting screws exposed.

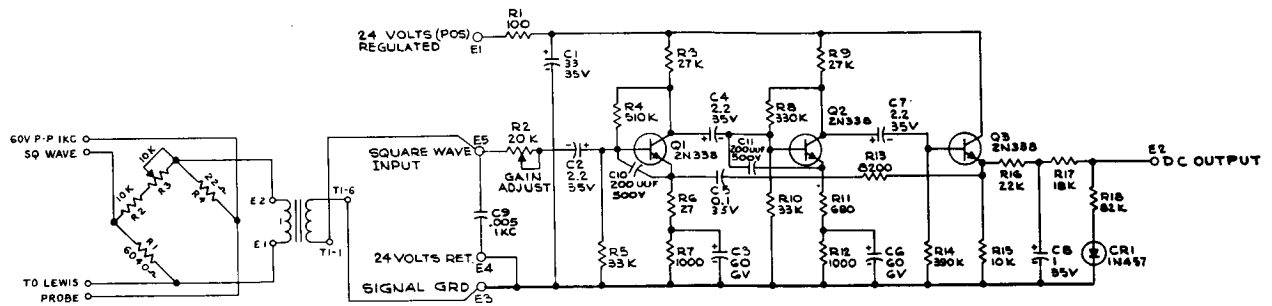
4. **Commutators**

a. Functional Description

The commutators provide the means of monitoring 86 channels of spacecraft performance data. SERT uses two 45 x 2 commutators (one for each transmission channel) which accept inputs directly from the signal conditioning equipment (paragraph III-D.3) to time-division multiplex this data. Data channels 1 and 2 carry calibration voltages, 3 through 43 performance data, and 44 and 45 sync. The commutator operates at a rate of two frames per second, and the output pulse trains modulate the 10.5-kc subcarriers in the SCO packages.

b. Development

The initial decision to use electronic solid-state commutators rather than mechanical devices was made on the basis of reliability. At that time, mechanical



NOTE:
UNLESS OTHERWISE SPECIFIED:
ALL RESISTOR VALUES ARE IN OHMS,
ALL CAPACITOR VALUES ARE IN UF.

Figure III-9. Schematic Diagram of the Ion-Beam-Probe Signal Conditioner

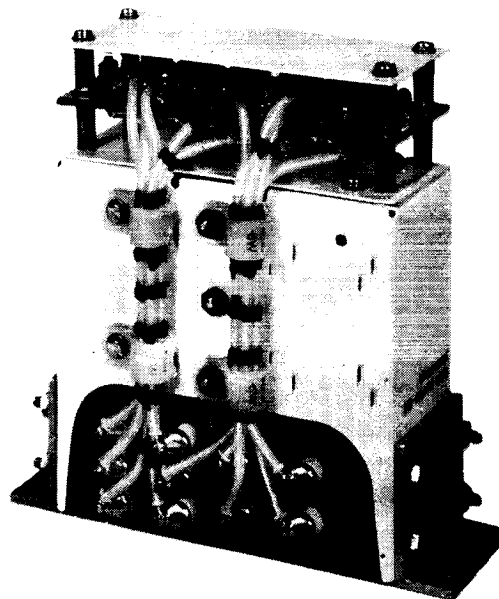


Figure III-10. Ion-Beam-Probe Signal Conditioner

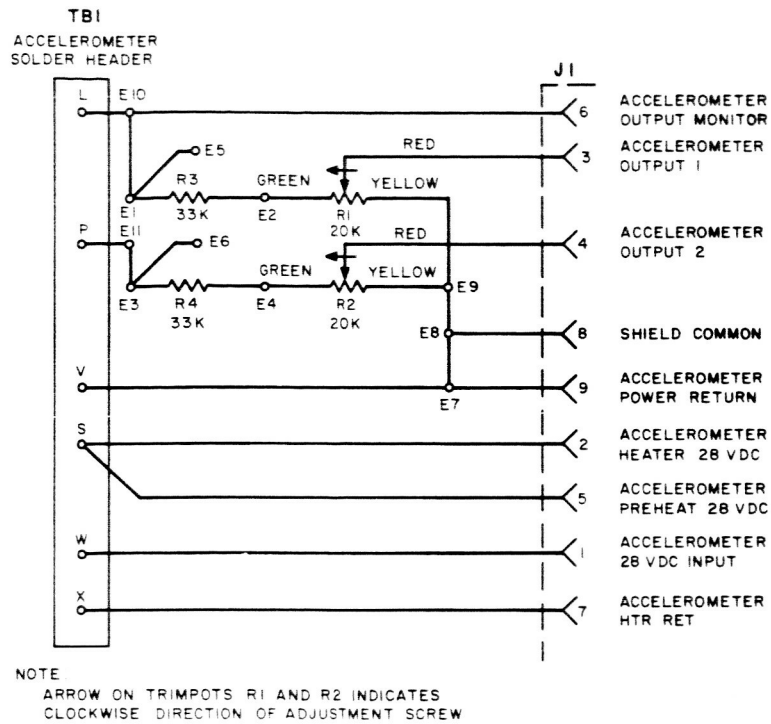


Figure III-11. Schematic Diagram of the Accelerometer Signal Conditioner

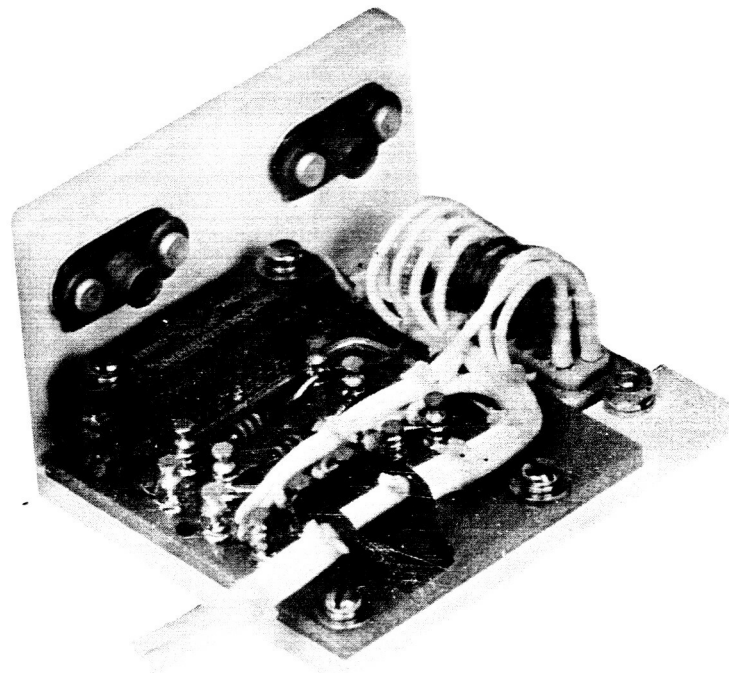


Figure III-12. Accelerometer Signal Conditioner

commutators had proven to be unreliable; rework was frequently necessary to correct the effects of wearout on mechanical parts. Subsequent developments (and improvements in the state-of-the-art) in the design of mechanical commutators occurred during the SERT program.

The electronic commutators were fully solid-state electronic devices which had a high input impedance, very high frame stability, internal pedestal and sync-pulse generation, and very high reliability for long term usage. The units passed all the qualification and acceptance testing before they were installed on the T-2 spacecraft (prototype).

During vacuum testing of the T-2 prototype at NASA, negative voltage spikes were detected at some of the commutator inputs. These spikes far exceeded the allowable amplitude of minus 10v to plus 25v, resulting in commutator failure. The spikes were induced into the telemetry-signal lines by transients resulting from high-voltage arcing at the ion engines. Complete protection of the two electronic commutators would have involved adding 83 separate low-pass filters at the channel inputs.

NASA directed that the solid-state commutators were to be replaced by mechanical commutators. The necessary pulse-train pedestal circuitry, spike filtering circuitry, and buffer circuitry were also added.

The first design included a dc-dc converter to supply a redundant negative dc source, Zener regulators, and voltage dividers to provide minus 1.25-volt pedestals for two commutators, low-pass RC filters for each SCO input and two buffer amplifiers to provide constant source impedances to the SCO's.

At NASA request, the buffer amplifier was eliminated and voltage-limiter diodes were added to each commutator output line. The voltage limiters are 1N645 diodes which are in a reverse-biased condition except when voltage spikes on the SCO input line exceed plus 6.2 or minus 2 volts. The diodes thus protect the SCO inputs from high voltage noise pulses arriving along the signal lines. The high-frequency components of these spikes are reduced by the low-pass filter ahead of the voltage limiters.

The new dc-dc converter is housed in a separate MU-metal shielded container to reduce interference. The bridge rectifier and filter for the converter are on the same circuit board as the low-pass filters and voltage limiters. This board also contains Zener-diode voltage regulators and resistive dividers which supply the minus 1.25-volt pedestal and plus 6.2-volt bias for the positive voltage limiters.

A commutator is mounted at each end of the signal conditioner (central unit). The mounting arrangement was designed utilizing two aluminum end bells which mate with the mounting holes that were used for the solid-state commutator. The bottom bell is large enough to house the commutator and dc-dc converter; the top bell is just large

enough inside to hold the other commutator. The two battery-current-monitor dc amplifiers mount externally on the flange alongside the upper bell.

The new circuitry required to supply pedestal voltages to the mechanical commutators and to protect the SCO inputs from high-voltage noise spikes was added. The transformer, switching transistors, and biasing resistors for the redundant negative voltage source are located in a MU-metal can mounted in the bottom end bell. This can reduces noise introduced by the switching spikes from the converter.

The protection circuits are in series with each commutator output line ahead of the SCO input. The low-pass filter is a simple RC network. The 3-db point for this filter is about 12 kc. Following this filter are two 1N645 diodes in parallel. One diode is returned to ground through a 6.2-volt source and the other through a minus 2-volt source. The diodes are connected so that they are in a reverse-biased condition unless the voltage on the SCO input line exceeds the bias voltage either in a positive or negative direction. The normal plus 5-volts or minus 1.25-volt telemetry signals will not cause the diodes to conduct. The bias voltage sources are of sufficiently low impedance to effectively short the SCO input in the presence of high-voltage noise spikes.

One minus 1.25-volt pedestal source is derived from the minus 23.7-vdc bus in the signal conditioner. The other minus 1.25-volt source is derived from the minus 15.5-vdc output of the new dc-dc converter by means of a resistive voltage divider. Both plus 6.2-volt bias sources for the positive voltage-limiter diodes are derived from the plus 28-vdc bus. One minus 2-vdc bias source is derived from the minus 23.7-vdc negative bus. The other minus 2-vdc bias is derived from the minus 15.5-vdc output of the new dc-dc converter by means of another divider network.

The dc-dc converter changes the plus 28-vdc from the spacecraft bus to minus 15.5-vdc to provide an additional negative voltage supply. The DC output at the filter capacitor is minus 18.3-vdc with plus 31-vdc at the converter input terminals. The minus 18-vdc is dropped to minus 15.5-vdc through a carbon resistor to a 1N695 Zener diode which regulates the output at minus 15.5 vdc.

Normal load current for the dc-dc converter is approximately 15 milliamperes; it has been tested successfully with a 40 milliamperes load.

One of the mechanical commutators was subjected to a complete SERT qualification level environmental test in accordance with Test Procedure SPO-46 (Reference III-6) and SERT Environmental Testing Specification, RCA Drawing No. 1175389 (Reference III-7).

The variation between pulses due to varying source impedances in the telemetry circuits was adjusted during system calibration and did not degrade overall system accuracy.

Reference III-5 describes this design and development effort in detail; references III-6 and III-12 describe the testing results.

5. Subcarrier-Oscillator (SCO) Package

a. General

Each SCO package (Figure III-13) provides the mixed fm signal which forms the input, or carrier modulation, to the fm transmitter. This signal is a mixture of the outputs of three independent fm subcarriers and the accelerometer signal conditioner (see Figure III-14). The SERT system utilizes two such packages in its semi-redundant telemetry subsystem design.

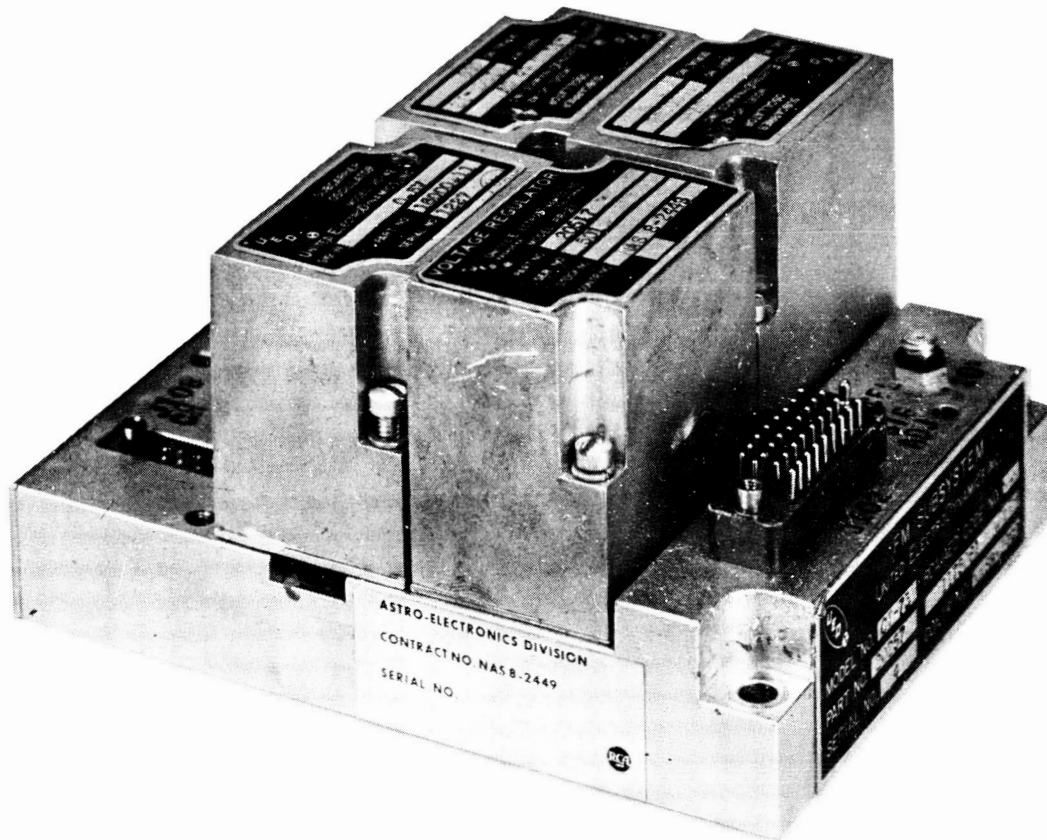


Figure III-13. Subcarrier-Oscillator Package

b. Description

Each SCO package consists of a plug-in reference voltage generator, three plug-in fm subcarrier oscillators with center frequencies of 1.7kc, 7.35kc, and 10.5kc, a passive mixing network, and a remote subcarrier input. The package will accommodate two additional plug-in fm subcarrier oscillators.

The reference voltage generator provides several reference voltages. Three of these voltages (0, 2.5, and 5) provide zero, mid-range, and full-scale calibration to one commutator; only zero and full-scale (5 volts) calibration voltages are provided to the other commutator.

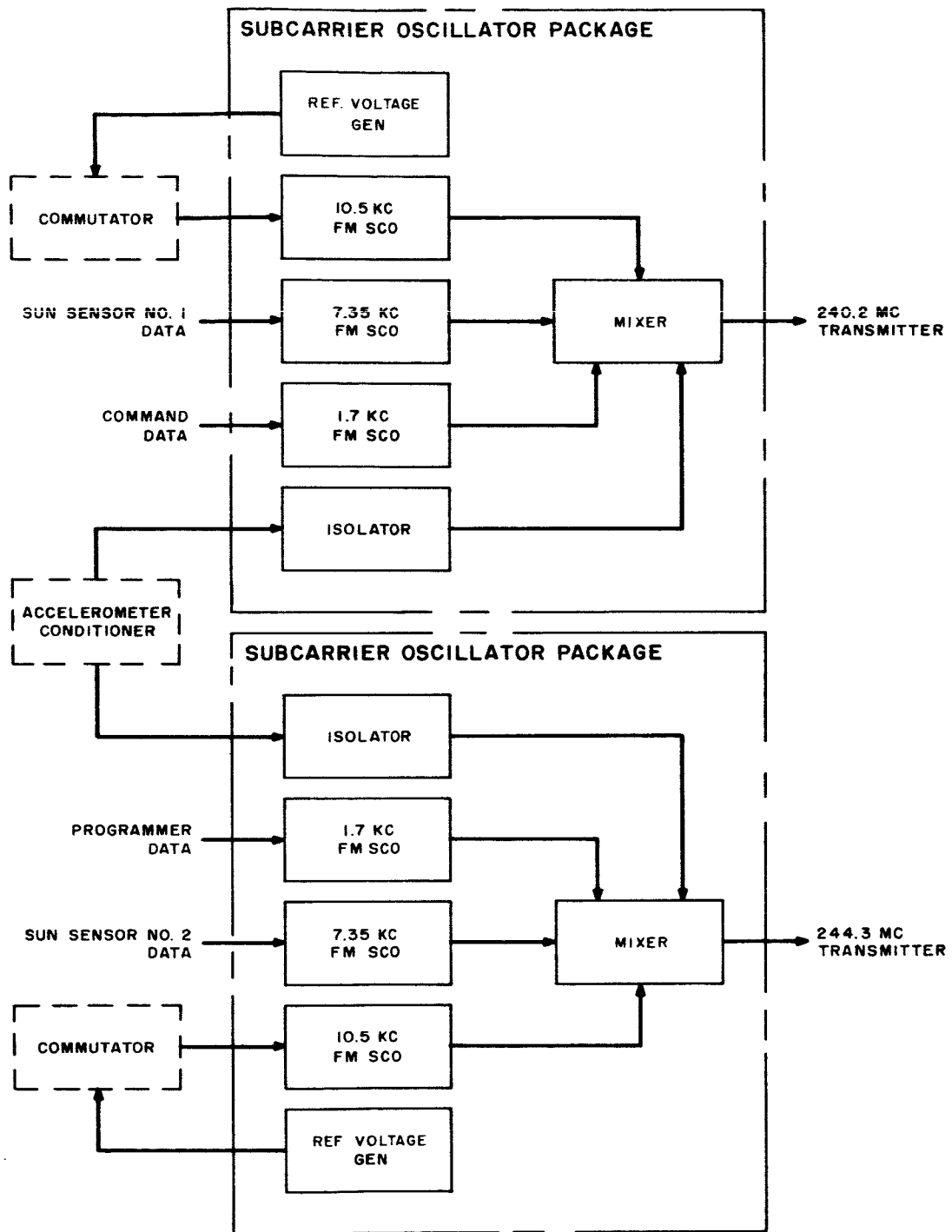


Figure III-14. Block Diagram of the Subcarrier-Oscillator Package

On-board-programmer milestone information and command-activate confirmation modulate the two 1.7-kc subcarriers, respectively.

The data consists of 0- to 5-volt staircase signals which frequency modulates the sub-carrier to the standard IRIG (Intra-Range Instrumentation Group) bandwidth of ± 7.5 percent. Sun sensor data similarly modulates the 7.35-kc subcarrier.

Ion-engine data and spacecraft housekeeping data in the form of the commutator wave trains modulate the 10.5-kc subcarriers. This oscillator is also designed to frequency modulate the SCO to the standard ± 7.5 -percent bandwidth with an input-signal range of minus 1.25 to plus 5.0 volts.

On-board accelerometer data is fed directly to the mixer package. Circuit isolation is provided by a 200 kilohm resistor.

The three fm subcarriers and the accelerometer signal are combined in a resistive, passive mixer to produce the signal which modulates the transmitter.

c. Development

The design and development of the SCO package was subcontracted. The original units selected showed poor performance and a questionable failure history in spite of concerted efforts toward improvement; this subject was fully covered in Reference III-8. The original SCO's were delivered for use on the T-2 spacecraft (the electrical prototype model). The SCO packages selected for the prototype and flight spacecraft met design specifications without difficulty.

During the program, mechanical commutators were substituted for electronic commutators (paragraph III-D.4. b). Because the output of the mechanical commutator was minus 1.25 to plus 5 volts rather than the 0 to 5 volts used for the electronic commutator, the 10.5-kc SCO's were replaced to accommodate the new input-signal range.

6. RF Transmission Equipment

a. General

The outputs of the SERT transmission equipment are two 10-watt fm-fm rf signals at frequencies of 240.2 and 244.3 megacycles. All spacecraft data is telemetered by way of these two channels with most of the critical data being redundant.

b. Functional Description

Two 10-watt tube-type power amplifiers, two 2-watt solid-state power-amplifier exciters, and two dc-dc input-power converters comprise the active rf

transmission equipment. (See Figures III-15 and III-16.) The subsystem receives its primary power from the spacecraft telemetry battery. The dc-dc converter converts an input 28vdc to 6.3 and 300 vdc regulated for power amplifier filament and B+ voltages, respectively. The component also has available a regulated 28vdc.

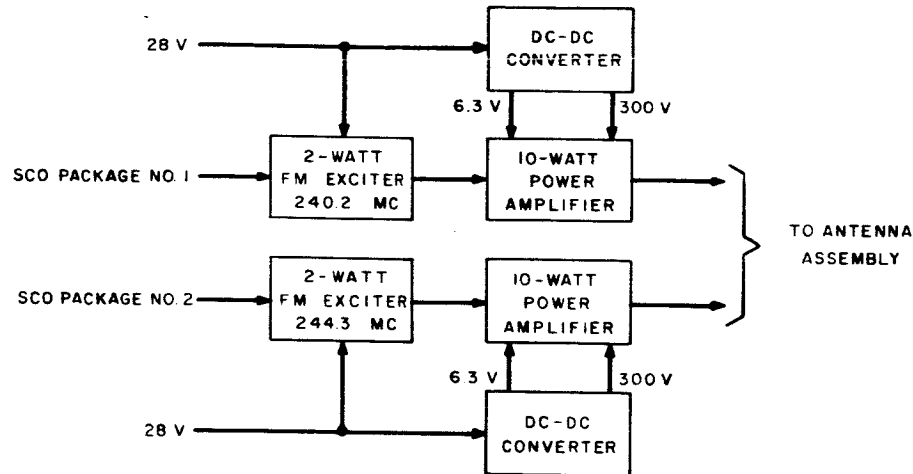


Figure III-15. Block Diagram of the RF Transmission Equipment

The fm exciter is a solid-state oscillator capable of a power output of two watts. The exciter is frequency modulated by the multiplexed signal from the SCO package. The modulation signal is adjusted for a carrier deviation ratio of 1.

The power amplifier is a tube-type unit which amplifies the two-watt rf signal to a power level of 10 watts (minimum). The power levels during testing were normally 12 to 12.5 watts. The two power-amplifier outputs are combined in diplexer (Figure III-17) to provide one 50-ohm output which feeds the antenna equipment.

c. Development

This subsystem, as designed, fit into the SERT system most acceptably. Only the dc-dc converter presented a potential problem. Because of its location on the spacecraft, a thermally-marginal condition was anticipated. To remedy this situation, the rf equipment was modified to eliminate the use of the 28-volt regulator in the dc-dc converter. The low-drift versus input-voltage characteristics of the fm exciter and the good battery self-regulation during the mission life made this modification possible.

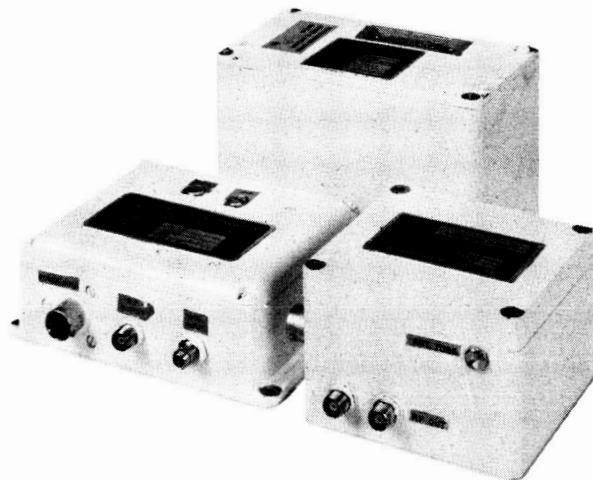


Figure III-16. RF Transmission Equipment

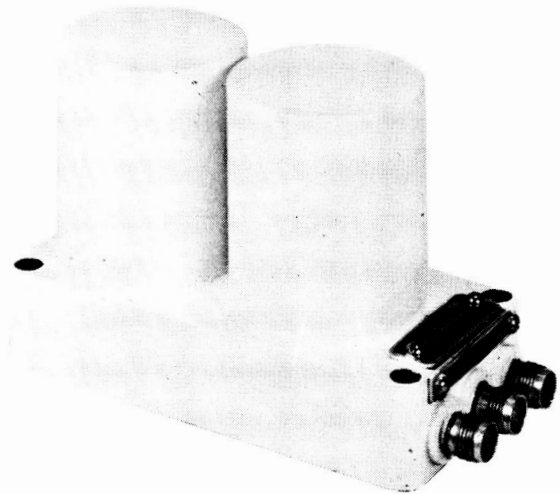


Figure III-17. Diplexer

Later in the program, the dc-dc converter was placed on the spacecraft in what was thought to be a better location; however, a marginal thermal condition was again detected. Rather than relocate the converter, the input voltage was reduced to 25vdc by adding a tap to the telemetry battery. This resulted in thermal compatibility again on the T-2 model.

On later spacecraft, the use of a 25-volt battery tap for the rf-subsystem power feed was eliminated and the use of 28 volts restored. This change was made to allow the use of the battery beyond its expected mission life during systems testing. In these later models, the converter was placed in a location which did not create a marginal thermal condition.

7. Antenna Equipment

a. General

The SERT antenna assembly radiates telemetry information on the 240.2- and 244.3-megacycle frequencies and receives command signals on 148.26 megacycles.

Both the transmitting and the receiving antenna assemblies were designed to fulfill the following three objectives:

- (1) To provide a circularly-polarized radiation pattern shaped in a 160 degree cone, centered at the spin axis and facing downward from the spacecraft. (See Figure III-18.) This pattern must be within ± 3 db of a hemispheric isotrope.
- (2) To provide a reasonably low VSWR on the two 50-ohm transmitter outputs and on the one 50-ohm receiver input.
- (3) To obtain maximum isolation between transmitter outputs and receiver inputs.

b. Description

(1) Transmitting

The transmitting portion of the antenna assembly consists of a diplexer, a 3-dbcoupler, a phasing-coupling network, and four antenna whips. (See Figure III-19.)

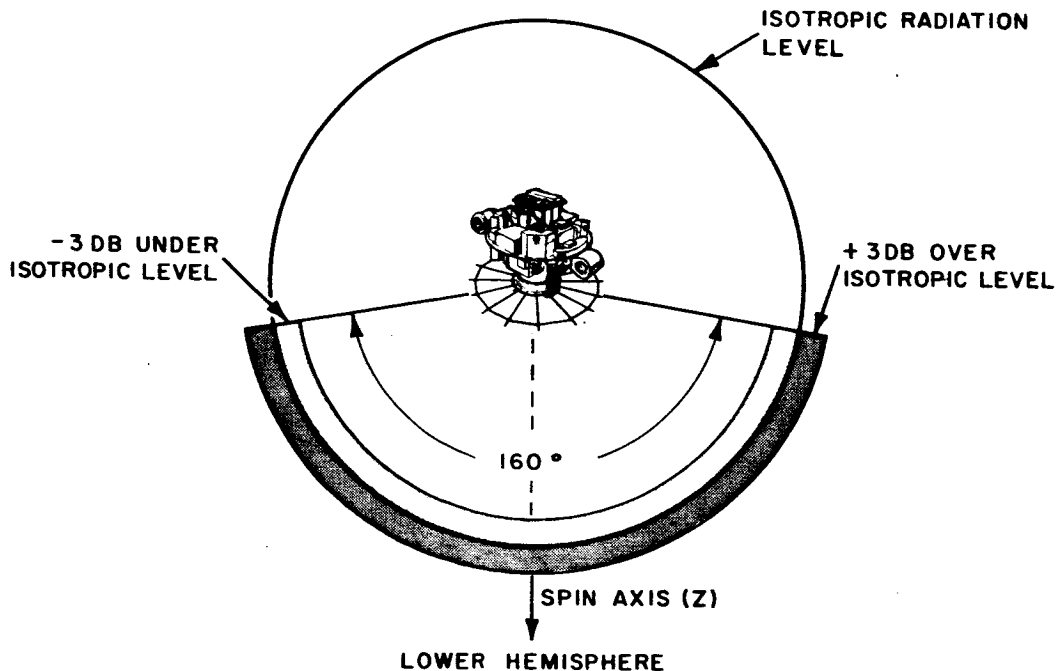


Figure III-18. Antenna-Pattern Requirements

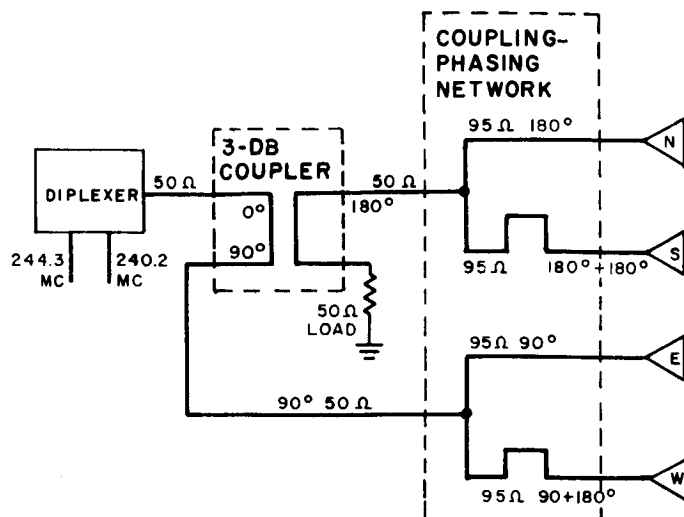


Figure III-19. Block Diagram of the Transmitting Antenna Equipment

The outputs of both power amplifiers (transmitters) are combined by a diplexer to allow simultaneous transmission into the 3-db coupler. The isolation between the input (transmitting) ports of the diplexer must be greater than 22 db. The VSWR at these ports must be less than 1.25:1 when the 3-db-coupler output is terminated by a 50-ohm resistive load. The diplexer is capable of carrying a total of 30 watts of transmitting power.

The 3-db coupler splits the transmitted power in two equal portions and provides a 90-degree phase-shift between these halves. The isolation between the diplexer and the phasing-coupling network is a minimum of 22 db with a VSWR less than 1.2:1.

The power is again split into two equal halves by the phasing-coupling network, providing an additional 180-degree phase shift between the antenna ports. The net result is that each of the four antenna whips is fed by equal power which is electrically 90 degrees out of phase with the power to the adjacent whip. The radiation produced is polarized left-hand circular.

(2) Receiving

The receiving portion of the antenna assembly consists of a rejection filter, a 3-db coupler, a phasing-coupling network, and four antenna whips. (See Figure III-20). The rejection filter attenuates the transmitting frequencies more than 40 db, while adding less than 0.8-db insertion loss to the receiving frequency. The 3-db coupler and phasing-coupling network serve the same purpose as in the transmitting portion of the antenna assembly described above. The system is designed to receive left-hand circularly-polarized radiation.

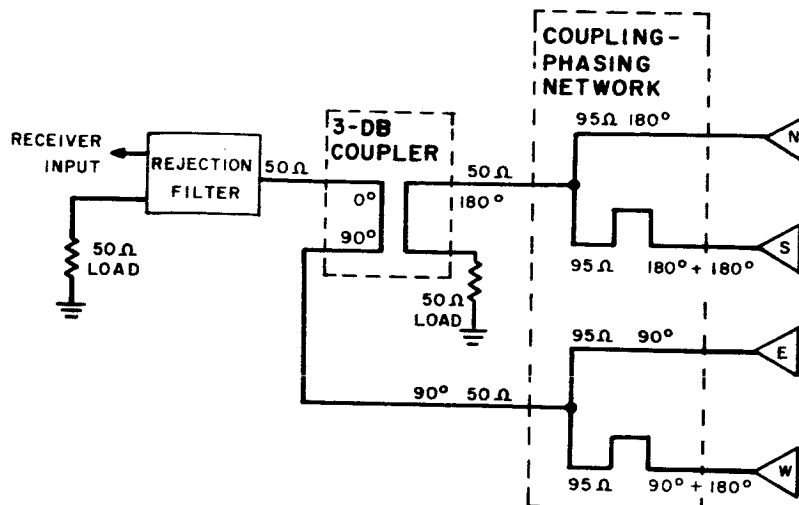


Figure III-20. Block Diagram of the Receiving Antenna Equipment

c. Development

The present antenna assembly is the result of three evolutions from that originally proposed. The basic requirements for the shape, gain, and polarization of the antenna patterns were unchanged; however, the transmitting and receiving frequencies were changed several times.

(1) Proposed Antenna Assembly

The originally proposed antennas were to operate on 215 mc and 400 mc. The 215-mc frequency was for command (receiving), and the 400-mc frequency was for telemetry (transmitting). These frequencies were changed subsequent to award of contract.

(2) Second Antenna Assembly

The second assembly was to operate at frequencies of 120 and 240 mc: the 120-mc frequency for command and the 240-mc frequency for telemetry tracking. The basic antenna consisted of four rods, one-quarter wavelength each at 120 mc, mounted around the 10-inch-diameter base ring beneath the spacecraft. These whips would be inclined at an angle of approximately 45 degrees from a perpendicular to the axis of the vehicle. For 240-mc transmission, the radiators would consist of sleeves concentric about the 120-mc radiators and located at the driven or ground end of the 120-mc radiators. The sleeves and rods were to be joined at the ground end providing a system resonant at both 120 and 240 mc. The radiators were to be insulated at their mountings and provided with appropriate co-axial fittings for subsystem connections.

A phasing-coupling network was designed (1) to provide quadrature feed to the four antennas, thus allowing circularly polarized radiation, (2) to match impedance from a 50-ohm source, and (3) to permit coupling of the two 240-mc transmitters and 120-mc receiver to the antennas with adequate isolation to prevent interference.

This antenna arrangement is feasible only when the frequencies have a harmonic relationship. When the final frequencies were decided upon, the arrangement was changed.

(3) Final Antenna Assembly

The final antenna assembly that evolved operates on two frequencies that are not harmonically related — 148 mc and 240 mc. The receiving or command antenna (148 mc) consists of four rods, one-quarter wavelength long at 148 mc, mounted to the 10-inch-diameter base ring on the underside of the spacecraft. These radiators are inclined at an angle of approximately 45 degrees away from the vehicle spin axis.

The transmitting or telemetry and tracking antennas (240 mc) consist of a separate set of rods, one-quarter wavelength at 240 mc, mounted to the base ring and interspersed with the command antennas. Each of these antennas is oriented as follows (See Figure III-21):

- (1) 45 degrees from the spin axis in a direction down and away from the base ring, as viewed edgewise to a plane containing the spin axis and the antenna mount; and
- (2) Tangent to the base ring at the antenna mount, pointing clockwise, as viewed from above.

A phasing-coupling network provides quadrature feed to the antennas for circularly polarized radiation along the spin axis. The radiation patterns are shaped in a 160-degree cone facing downward. The antenna gain is within ± 3 db of a hemispheric isotrope.

A large diameter ground plane (approximately one-half-wavelength in diameter at 148 mc) emanating from the base ring above the antennas, was necessary to provide two features. The first was to modify the pattern so it would be uni-directional, radiating most power in a downward direction from the spacecraft; the second was to provide isolation of the radiating antennas from the components on the upper side of the spacecraft.

During the development, many types of ground planes were tested. Some of these were unsuccessful because they provided insufficient isolation from the other end of the vehicle, others were too large physically, and others could not be properly folded and unfolded.

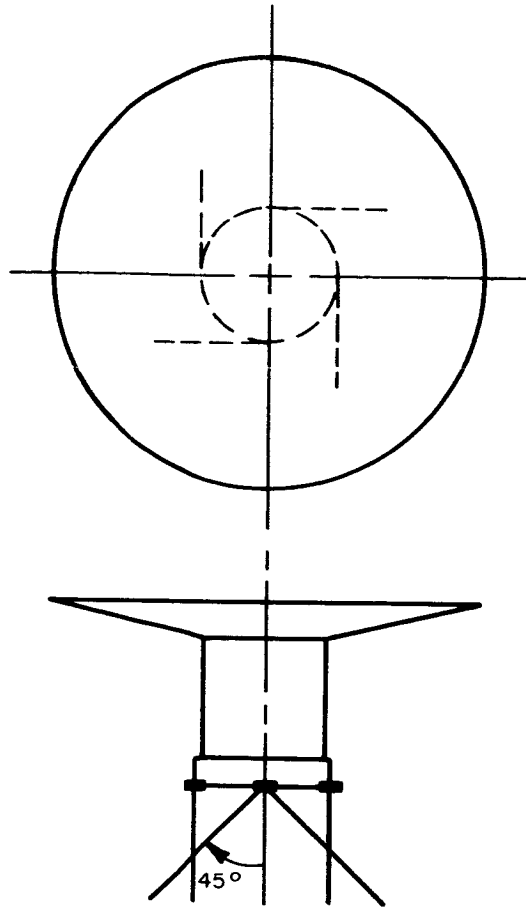


Figure III-21. Antenna Orientation

The final configuration, which has the appearance of a spoked wheel, provided suitable characteristics for the 240-mc frequency; however, much of the 148-mc received power was absorbed by the spacecraft. To correct this situation and to redirect the energy to the receiving antenna whips, two detuning loops were added to the spacecraft baseplate.

The specifications for the phasing-coupling network remained unchanged from the start except that two networks were now required (one for each frequency) and that a diplexer was added. This diplexer would couple the two transmitters to the phasing-coupling networks, allowing simultaneous operation of both transmitters.

The system operates on the frequencies specified below:

Reception	148.26 mc
Transmission # 1	240.2 mc
Transmission # 2	244.3 mc

The phasing-coupling networks, shown functionally in Figures III-19 and III-20, are mounted on two printed-circuit boards which are 1/8 inch thick by 8 inches in diameter. These networks weigh 2 pounds. The isolation from the transmitting (telemetry) output port to the receiving (command) input port is greater than 60 db, and loss from input to output does not exceed a maximum of 2.5 db at any of the above frequencies. This network provides an input impedance at each port of 50 ohms with a maximum VSWR of 1.2:1 and is capable of handling a maximum power of 30 watts. The 50-ohm load in the transmitting system is a special 15-watt rf resistor. Mounted beneath the spacecraft baseplate in a thermal sink, this load is used to absorb high reflected rf power occurring under the high VSWR conditions of launch.

During July, 1962, two complete sets of whip antennas (one prototype and one flight model) were assembled on a mock-up spacecraft and impedance-matched to a VSWR of 1.2:1, or less, measured at the antenna ports of the phasing-coupling networks. Several θ -variable patterns were taken in the following ϕ planes: $\phi = 0^\circ, 22.5^\circ, 45^\circ, 67.5^\circ, 90^\circ, 112.5^\circ, 135^\circ$ and 157.5° . (Refer to Figure III-22 which identifies the SERT antenna-pattern coordinate system.) For each ϕ angle, a pattern was taken using first a horizontal dipole and then a vertical dipole; these patterns were designated E_θ and E_ϕ , respectively.

The E_θ and E_ϕ components for each ϕ angle were superimposed on the same recording paper; a total of 48 patterns were recorded for each of the two antenna assemblies.

The isolation between the input port on the receiving phasing-coupling network and the output port of the transmit network was measured to be 76 to 80 db, depending on the transmitting frequency.

All final electrical data were taken with the receive whips tied out a specified distance to simulate the centripetal force due to the spin of the spacecraft. The transmitting whips, being much shorter in length, would not spin out significantly and were therefore tested in their static position.

Due to a decision to change the SERT spacecraft configuration from configuration A to configuration B (see paragraph I-E and Table I-5), the antenna testing was terminated after completing the impedance matching and electrical testing of two antenna systems. The electrical data and patterns were entered into two logbooks (references III-9 and III-10).

On January 14, 1963, RCA started testing three flight-model antenna assemblies. The task was to match three sets of whips and to take one complete set of θ -variable patterns. No design changes or modifications were to be made.

For testing purposes, a mock-up SERT vehicle was used. This model, designated as T-1C (representing configuration B), was fashioned in great detail out of balsa wood and represented all major changes made in the vehicle structure. The balsa wood was coated with a 10-mil thickness of aluminum using a hot-spray splatter process. The actual metal housing for the matching-coupling assembly was also utilized.

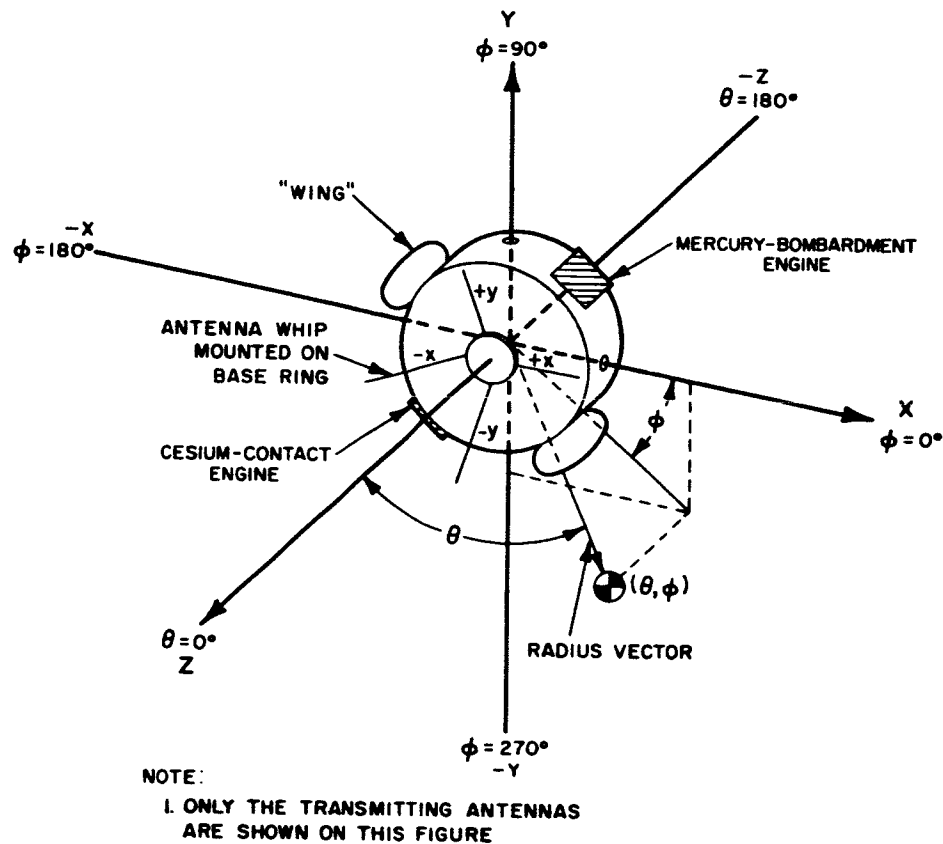


Figure III-22. Antenna-Pattern Coordinate System

For the first run, the antennas that were originally matched for the flight model tested in July 1962 were installed on the mock-up SERT vehicle to determine the magnitude of the changes in tuning.

Several significant changes had been made in the vehicle structure which affected the impedance match. The first one was the addition of four metal clamp-deflectors mounted near the antenna base mounts. An investigation showed that the brackets were adding significant capacity to the base impedance of the transmitter whips. Because these whips are extremely sensitive to changes in base impedance, retuning of the whips would have been a major effort; therefore, the metal deflectors were replaced with non-metal deflectors. After the metal clamp-deflectors were removed, the transmitter whips tuned easily to give a VSWR of 1.2:1, or less, at both diplexer input ports.

The receive whips, however, could not be tuned without making changes in the whip length and the base capacity. The changes made in the new vehicle components, even though they were made above the antenna ground plane, caused an impedance change in the receiving whip antennas. The limits set on the size and design of the radial-wire ground plane was, in large measure, the basis of this problem. The receive whips were successfully tuned by increasing the diameter of the capacity slug to 0.265 inches, decreasing the capacity dielectric to 0.0045 inch, and trimming the antenna length to 21.0 inches.

The very irregular shape of the E_{θ} and E_{ϕ} patterns at the receive frequency caused some concern. A thorough investigation showed that all the receiving whips were receiving equal power at the power-voltage phase; however, the axial ratio along the +Z axis (Figure III-22) was very poor. Further investigation, including rotating the antenna feeds and feeding one pair of whips at a time, showed that the inefficient ground plane and the irregular shape of the vehicle were definitely causing cross-polarized energy. It was shown that the axial ratio could be improved if the ground plane were made larger and made to look more "solid". However, since the vehicle will be receiving left-hand circularly polarized energy from the ground antenna, the poor axial ratio is of minor importance. Using a left-hand circular-polarized source antenna, the ϕ -variable cuts showed the patterns to be practically smooth circles for θ -angles from 0 to 45 degrees. As θ became greater than 45 degrees, the ϕ -variable patterns did have a somewhat four-lobed shape to them. However, this did not cause much concern since θ -angles greater than 45 degrees would be outside of the look area during flight. The cross-polarized energy, however, will cause approximately a 1-db decrease in gain. The transmit patterns were quite acceptable. The ground plane is much more effective at the higher frequency so that most of the transmitted energy is directed in the forward direction.

After all three antennas were tested, the six antenna patterns were examined to determine (1) whether they actually represented the radiation pattern of the spacecraft and (2) whether the measured patterns were compatible with system requirements. The following determinations were made:

- (1) Considering the ground plane on the command frequency (148.26 mc) it was found (as above for the first antenna tested) that the ground plane may be too small electrically to have the desired effect. Thus, spacecraft protrusions may cause a non-symmetrical radiation pattern with power-density minimums in the essential directions.
- (2) The telemetry antenna patterns seemed to be an accurate representation of the actual spacecraft radiation pattern.

- (3) The command-antenna patterns showed some non-symmetrical performance and a peculiar polarization tilt had also been noticed; therefore, it was decided to check the ellipticity of these patterns by utilizing an entirely new measurement technique. This technique involved (1) using several patterns to devise a composite antenna pattern and (2) using ϕ -plane data to determine θ -plane plots.

In May 1963, two sets of antennas were successfully matched to a VSWR less than 1.2:1, and one complete set of radiation patterns were taken with the detuning wings in the horizontal position. Field measurements at the command frequency were taken to determine the isotropic level; horizontal and vertical standard dipoles were used for this test. This measurement was then repeated using a circularly polarized signal source and rotating the spacecraft mock-up on its spin axis. The results of these tests demonstrated that the ellipticity of the circularly-polarized field was within specified limits (less than 1.5 db).

The matching of one set of whips was then checked and the following results were recorded:

<u>Frequency (mc)</u>	<u>Port</u>	<u>VSWR</u>
148.26	J2 Filter	1.06:1
240.20	J1 Coupler	1.20:1
244.30	J1 Coupler	1.06:1

Changes were then made in the spacecraft configuration (to configuration C). As a result, a new series of tests was necessary to check the radiation patterns and tuning of the antennas.

Specifically, the following tasks were required:

- (1) Rechecking the tuning of command and telemetry antennas,
- (2) Recording a set of command-antenna patterns using a left-hand circularly polarized probe (including gain measurements, primary-and-check θ -plane patterns, and primary-and-check ϕ -plane patterns), and
- (3) Repeating (2) above for the telemetry antenna patterns on both transmitting frequencies.

In order to prepare the modified SERT antenna-mock-up model, T-1C, for retuning, a double check of the prototype phasing-coupling network was necessary. Testing of this prototype network was completed on January 26, 1964; however, because of discrepancies found in the cables and connectors for this component, an actual flight-model network was also tested; the test results indicated general conformance with specifications.

The retuning was finally completed on March 5, 1964, and the equipment was delivered to the antenna range where the antenna patterns were to be taken.

During the above testing, some difficulty was encountered in inserting some of the straight cable connectors. To resolve this problem the straight cable connectors were replaced with right-angle connectors in certain transmitting antenna cables.

Before actually starting antenna-pattern measurements at the antenna site, VSWR tests were run. These tests had to be performed twice because the chevron ring, which is the upper portion of the separation mechanism and is attached to the spacecraft during flight, was not installed during the first test. The results from the second test (given below) include VSWR measurements taken with and without the chevron ring.

	<u>Frequency (mc)</u>	<u>VSWR</u>	
		<u>Without Chevron</u>	<u>With Chevron</u>
Port J1	240.2	1.23:1	1.36:1
	244.3	1.41:1	1.35:1
Port J2	240.2	1.43:1	1.8:1
	244.3	1.55:1	1.48:1
Port J3	148.26	1.165:1	1.18:1
Port J4	148.26	1.12:1	1.13:1

The only significant change measured was at port J2, but even this change did not result in a serious deterioration in VSWR readings. The chevron ring was left on the mock-up for the antenna pattern-measurements.

For these pattern measurements, a standard dipole, with a known 1.8-db gain over an isotropic source, provided the reference level. A 73-degree corner reflector, with 52-inch by 87.25-inch sides and 8.75-inch flatness at the vertex, and an adjustable half-wavelength dipole served as the transmitting antenna.

Analysis of the receiving frequency patterns in the θ plane showed that these patterns were reasonably symmetrical about the +Z (rotation) axis with the maximum power density in the $\theta = 0$ -degree direction. There was less than ± 3 db of power variation over the entire radiation pattern. As expected, the minimum power density was in the $\theta = 80$ -degree direction.

The minimum radiated power level was no more than minus 9 db below the maximum radiated power level. This represented a loss of 2 db compared with the model previously tested in April, 1963. This loss was due to changes in the geometrical configurations in the spacecraft and the alterations in the detuning wings.

The 240.2-mc transmitting antenna patterns presented no problems because the ϕ -plane primary patterns were very similar to the corresponding check patterns and the deviation was less than 3 db. See Figure III-23 for an example of the antenna pattern for the final configuration.

In general, the SERT antenna patterns, taken between March 23, 1964, and April 24, 1964, at the antenna range were representative of the new spacecraft configuration. Comparing the patterns taken using the new mock-up with those taken using the previous mock-up, only minor differences were found; that is, the command and transmitting frequency antenna radiation patterns remained basically the same even though the spacecraft geometry and the shape of the detuning wings were changed.

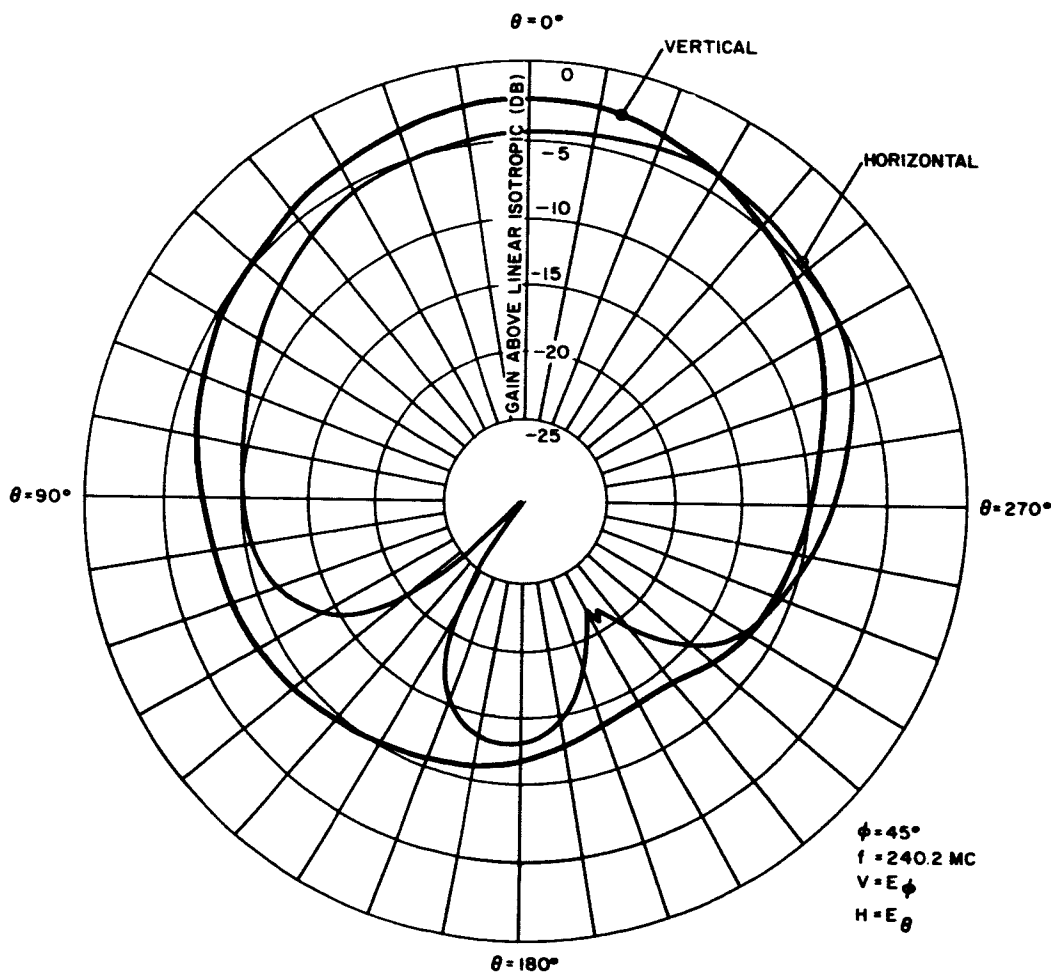


Figure III-23. Example of Antenna Patterns for the SERT Final Configuration

E. COMMAND AND CONTROL SUBSYSTEM

1. General

The command and control subsystem of the SERT spacecraft was designed to fulfill all in-flight control requirements.

In the original design concept, the spacecraft programmer was to be the only control element. A hard-line command through the umbilical (Payload Activate) was to be given a few seconds before lift-off to initiate the operation of the programmer. The programmer was then to be in absolute control of the flight sequence.

During the early development of the SERT program, an rf-link command subsystem was included as a back-up source to supplement the programmer in controlling the most critical functions of the flight sequence and to provide ground control in case of programmer failure.

In the final stages of the program, an auxiliary command unit was designed into the system to increase the flexibility of the command subsystem. With these refinements, ground control of all critical spacecraft functions was obtained, adding accessibility to control functions not before included in the programmer-controlled-flight sequence. The additional capability proved to be indispensable during system testing and later throughout the actual flight.

2. Subsystem Description

The command and control subsystem of the SERT spacecraft consisting of the command receiver, command decoder, auxiliary command unit, and the programmer provides full ground and in-flight control of the spacecraft operations. The receiver and command decoder are integrated in a single unit called the command subsystem.

The outputs of the programmer are signals (primarily in the form of relay closures) which activate functions within the power-switching unit (PSU) and the ion-engine subsystems.

Command and control functions which are independently controlled by either the command subsystem or the programmer are channeled directly via the spacecraft harness to their appropriate destinations.

A third control source which is to be used in the initial stages of the flight is contained within the spacecraft in the form of a barometric switch. This switch, added for range safety, will provide a squib-arming signal to the power switching unit at about 30,000 feet altitude. This function is backed-up by the command system.

Command acquisition by the spacecraft as well as programmed command execution confirmation are monitored at the ground control center through the spacecraft telemetry system.

A listing of the programmer times and events and description of a typical flight sequence is given in Table I-2.

3. Command Subsystem

a. General

The SERT command subsystem, consisting of the command receiver and command decoder, receives, processes, and decodes the rf command signals transmitted from the ground telemetry station to the SERT spacecraft; a 10-command capability is provided. The subsystem is designed to have a high immunity to noise and spurious signals; this characteristic is obtained through a combination of (1) use of combinations of discrete tones, (2) tone integration, and (3) prescribed tone sequencing. The receiver provides a demodulated subcarrier output which is fed into the decoder. The command decoder processes the subcarrier by means of digital-type logic. The decoder has a capability of processing ten commands by ten discrete relay closures. Upon receipt of a particular command signal, the decoder closes a DPDT-type relay which connects a particular control point to the 28-volt battery level and provides a discrete command-confirm signal which is transmitted back to the ground telemetry station via the telecommunications subsystem. Each of the 10 independent commands is activated by depressing the associated button in the ground station. Only one command may be transmitted at any one time.

As shown in Figure III-24, a command signal consists of two audio-tones of different frequencies sent in a real-time sequence. The following five tones are used to obtain the ten command signals described in Table III-1.

<u>Tone</u>	<u>Frequency (cps)</u>
A	400
B	560
C	730
D	1300
E	1700

b. Functional Description

(1) Command Receiver

As shown in the block diagram of Figure III-25, the 148.26-mc rf signal from the antenna network is fed to the rf amplifier of the command receiver. The amplifier feeds its output to a mixer which beats the incoming rf frequency with the local oscillator frequency of 128.26 mc and provides a 20-mc i.f. output signal. The i.f. amplifier consists of four 20-mc amplifier stages and a crystal filter which determines

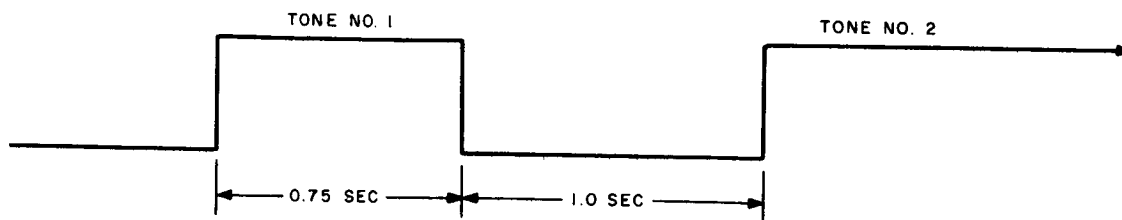


Figure III-24. Typical Command Signal Timing Sequence

the pass-band characteristics of the receiver. The bandwidth of each i. f. amplifier stage is sufficiently wide so that only the crystal filter determines the bandpass. This type of design eliminates the problem of change in i. f. bandwidth and center frequency with change in AGC voltage. The AGC voltage is supplied from a separate detector and is applied to the base of the transistor of the rf and i. f. amplifier stages to control the receiver gain. Originally, this receiver was developed for NASA under the TIROS program.

(2) Command Decoder

The command signal consisting of two audio tones in a fixed time sequence is applied to the five bandpass-filter channels of the command decoder. Each bandpass filter is tuned for one of the five audio-tone frequencies. A block diagram of the decoder logic is shown in Figure III-26.

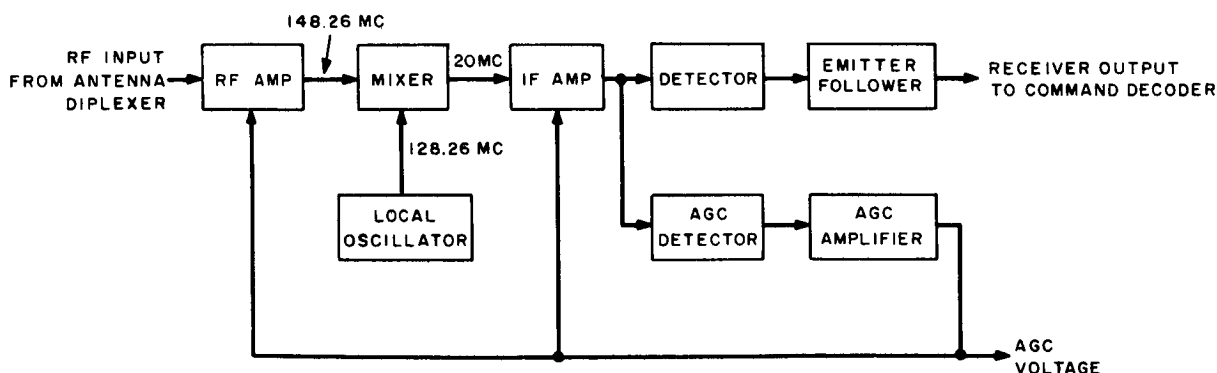


Figure III-25. Block Diagram of the Command Receiver

TABLE III-1. SERT I COMMANDS AND TONES

Command No.	Tone No. 1	Tone No. 2	Mode I Function	Mode II Function
1	A	B	Cesium-Contact-Engine Neutralizer Program Stop	-
2	A	C	Cesium-Contact-Engine Feed Valve Closed	-
3	A	D	Arm Squibs	Select Mode I
4	A	E	Separation and Damper Squibs	-
5	B	C	Unfold Squibs	Cesium-Contact Engine Off/ Mercury-Bombardment Engine On
6	B	D	Cesium-Contact-Engine Full Heat On	-
7	B	E	Select Mode II	-
			Cesium-Contact-Engine Pod Door Off	
			Cesium-Contact-Engine Boiler Off	
			Mercury-Bombardment-Engine Mag Field Interrupt	
8	C	D	Cesium-Contact-Engine DC On	
			Ground Plane Squibs	
			Cesium-Contact-Engine Boiler Off and Feed Valve Closed	
9	C	E	Programmer Advance (to Mercury-Bombardment-Engine Operation)	-
10	D	E	Programmer Reset (to Cesium-Contact-Engine Operation); Mercury-Bombardment-Engine Off/Cesium-Contact-Engine On	-

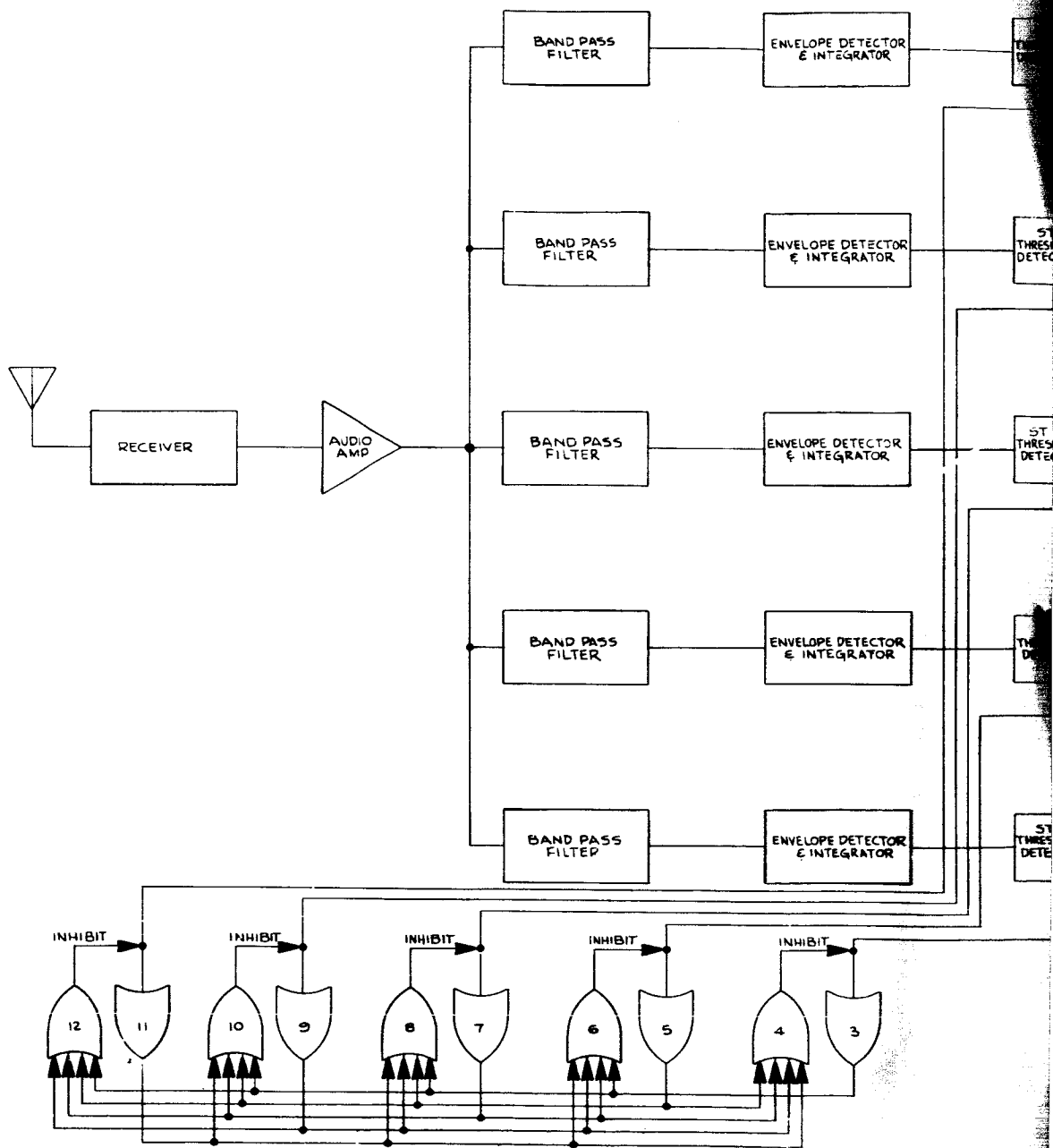
When a specific command is received, each audio tone of that command is selected by its respective filter. The envelop of the audio tone is detected and is integrated to set the Schmitt trigger associated with that particular audio-tone channel. When the Schmitt trigger for a particular channel is set, all other Schmitt trigger outputs are inhibited and the system will not recognize another tone. The Schmitt trigger also sets that channel flip-flop. A reset delay time is initiated when the flip-flop is set. If the second tone of the command is not received within three seconds, the flip-flop will be automatically reset and the system will return to the standby state. In addition, the AND-gate logic associated with the particular tone is placed in the ready state when the flip-flop is set. After 0.75 seconds, the first command tone is dropped and no tone is sent for one second. During this one-second period, the Schmitt trigger set by the first command tone returns to its normal state, and the inhibit on the other Schmitt triggers are removed. When the second tone arrives, it is processed in a manner similar to the first tone. The Schmitt trigger associated with the second command tone is set; all other Schmitt triggers are inhibited; the flip-flop associated with the active channel is set; and the AND-gate associated with the particular command is activated, energizing the associated relay. Any relay closure inhibits the flip-flop reset circuit from operating. The relay remains closed as long as the second command tone is present. When the second tone is removed, the Schmitt trigger resets after a delay, the relay opens, and the flip-flop reset operates. The decoder operation for all commands (No. 1 through No. 10) is processed in a similar manner utilizing the appropriate logic elements.

c. Development

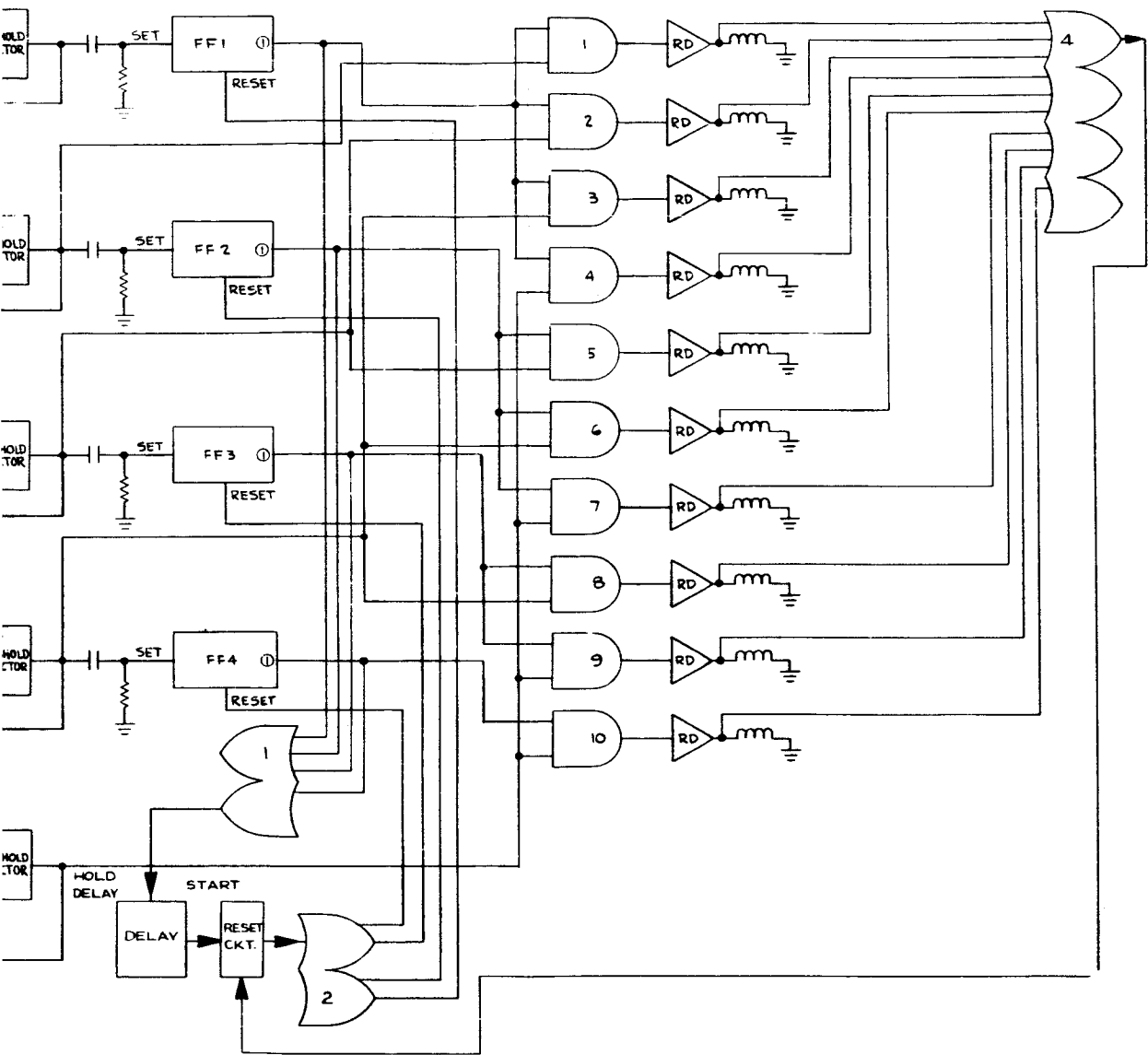
(1) Design Considerations

It was required that the SERT command subsystem operate in a noise environment expected to be on the order of 47 db/KTB. In this environment, it is necessary to insure that:

- (a) No command would occur due to a noise input alone.
- (b) A command can be obtained when desired, with an anticipated minimum signal input of 12 microvolts to the receiver.
- (c) No command would occur due to triggering from spurious radio broadcasts.



III-45



III - 46

Figure III-26. Logic Diagram
for the Command Decoder

The anticipated minimum carrier-to-noise ratio (C/N) at the receiver input was computed as follows:

Transmitter Power (2 KW)	33 dbw
Transmitter Antenna Gain	12 db
Path Loss for 4000 mi. Slant Range	-151 db
Receiving Antenna Gain	-3 db
Polarization Loss	-3 db
Network and Cabling Loss	<u>-3 db</u>
Received Power	-115 dbw
Receiver plus Antenna Noise*	-147 dbw
Receiver Input C/N	32 db

The worst-case input signal can be computed as follows:

$$\log \left(\frac{A}{1} \right) = -115 \text{ dbw}$$

$$\log \left(\frac{1}{A} \right) = 115 \text{ dbw}$$

$$\frac{1}{A} = 3.2 \times 10^{11}$$

$$P = \frac{V^2}{R}, V^2 = PR, R = 50 \Omega$$

$$V^2 = (3.1 \times 10^{-12}) (50) = 1.55 \times 10^{-10}$$

$$V = 12.5 \times 10^{-5} = 12.5 \mu \text{ volts}$$

This 12.5 microvolts level is sufficiently above the receiver sensitivity threshold of 1.0 microvolt.

A conservative design goal for operational capability in the presence of background noise which is 50 db above KTB noise was established. This requirement was to provide for the possibility of noise generated by the ion engines. Subsequent tests with specially designed and calibrated noise generators verified that the system would operate in a background noise environment of at least 47db above KTB noise. Based on these results, the maximum receiver plus antenna noise under which the unit will operate is -100 dbw. Under worst conditions, for which the system will still operate, the carrier-to-noise ratio is

$$C/N = (-115) - (-100) = -15 \text{ db.}$$

*For TIROS receiver, $T_{\text{eff}} = 3400 \text{ }^\circ\text{K}$ and $B = 40\text{kc.}$

Since a minimum carrier-to-noise ratio of +32 db is anticipated, a margin of at least 47 db should exist to satisfy unknown noise conditions. The system is actually tested for proper operation when the carrier-to-noise ratio is -12 db.

(2) Noise Immunity

The method of signal processing performed in the decoder provides a high degree of noise immunity. With an environmental noise level of 47 db above ambient, the carrier-to-noise ratio at the detector will be -15 db. From the Fubini and Johnson analysis (Reference III-11), the theoretical value for an a.m. detector can be obtained as follows.

For i. f. bandwidth (BI) of 40 kc, decoder post-detection filter bandwidth (BA) of 68 cps, and 100 percent modulation,

$$\frac{T}{N} = -26 + 10 \log \frac{BI}{2 \times BA} = -1.3 \text{ db}$$

where T/N is the tone-to-noise ratio, and -26 db is the post-detection S/N for input C/N = -15 db. By setting the integrator rise time to 0.5 seconds, the decoder post-detection bandwidth is reduced to 1 cps, and the theoretical T/N at the output at the integrator becomes +17 db.

After integration, it is assumed that the spectrum takes the form of a Rayleigh distribution. From the Rayleigh distribution curves, for a S/N of +17 db, the cumulative probability that a noise envelope will exceed 17 db and trigger the channel is less than 2×10^{-11} .

The measurement of the signal-to-noise ratio for a Rayleigh Distribution can be found in terms of known and measurable quantities. The signal-to-noise ratio required to satisfactorily operate the Schmitt trigger of an audio-tone channel is

$$S/N = 20 \log \frac{\Delta v}{EN_2},$$

where

Δv is the change in dc voltage on the integrator capacitor, and

EN_2 is the rms noise present after integration.

Since EN_2 cannot be measured directly, it is measured in terms of the following parameters:

$$EN_2 = \frac{EN_1}{\sqrt{\frac{BW}{B}}}$$

where

EN_1 is the rms noise at output of bandpass filter;

BW is the post-detection bandwidth of filter;

B is the bandwidth of integration = $\frac{0.5}{\tau}$; and

τ is the integration rise time.

$$\therefore S/N = 20 \log \frac{\left(\Delta v \sqrt{\frac{BW}{B}} \right)}{EN_1} \quad (\text{III-1})$$

Measurements were made on the prototype command subsystem. The following data was taken with 47 db/KTB noise and a minimum signal strength of 0.25 volts applied to the input:

$$EN_1 = 1.1 \text{ vrms}$$

$$BW = 68 \text{ cps}$$

$$B = 1$$

$$\Delta v = 0.95$$

The worst case occurs for the 1700-cps audio-tone channel (the maximum bandwidth filter). Applying equation III-1, the signal-to-noise ratio at the output of the band-pass filter is 17.2 db. From the Rayleigh curve shown in Figure III-27, this S/N corresponds to a probability of approximately 1×10^{-11} .

(3) Immunity to Spurious Signals

In addition to the protection provided by receiver limiting and filtering and integration of the subcarrier, the multiple-tone coding system is used. To execute a command, the system must receive two tones of different frequency in proper time sequence.

(4) Integration of Receiver and Decoder

Before integration with the command decoder, the receiver is thoroughly tested over its operating temperature range. When acceptable operation is demonstrated, the receiver is integrated with the decoder. At this time, the gain of the audio

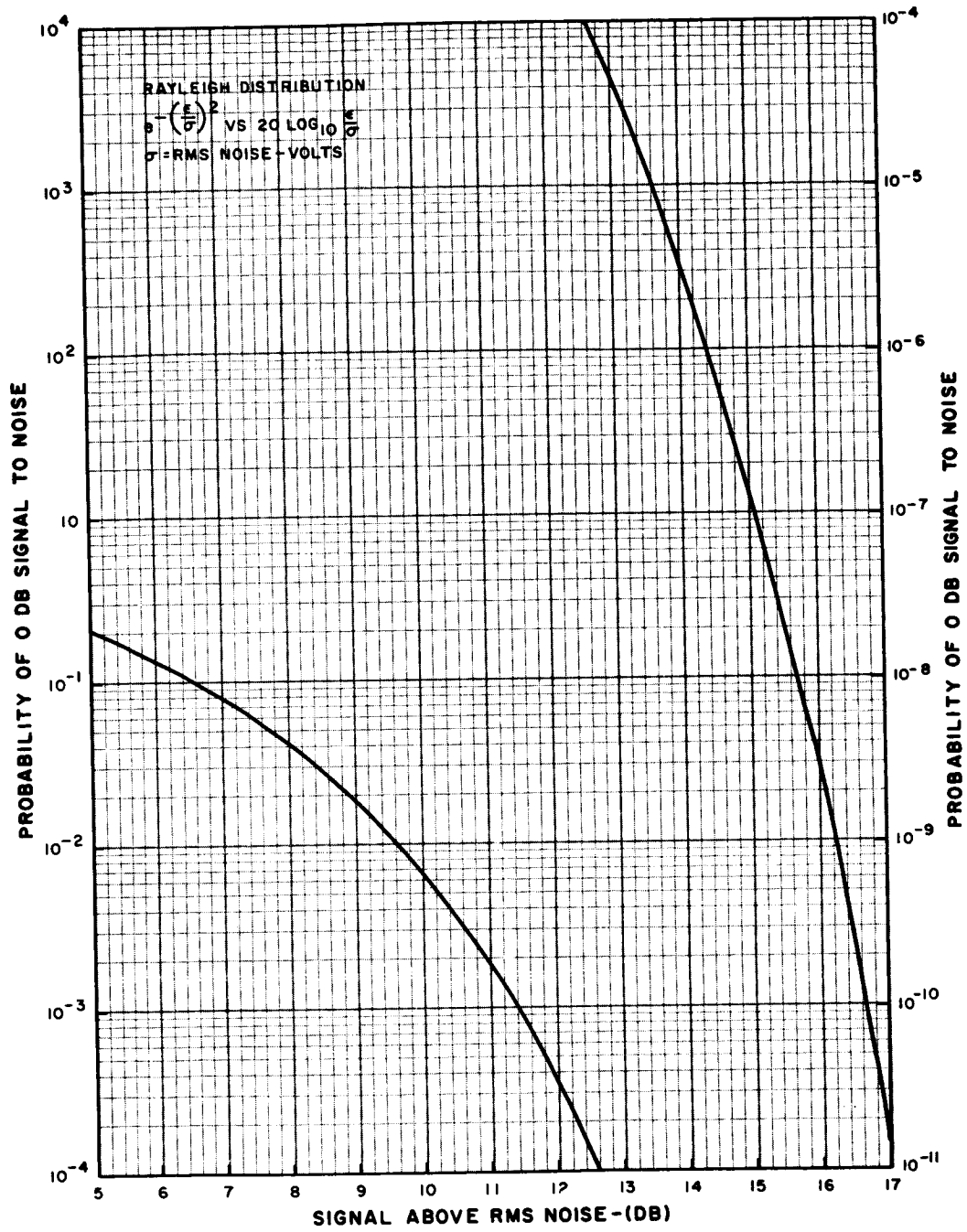


Figure III-27. Rayleigh Distribution Curve

amplifier in the decoder is established and timing and telemetry resistors are selected. Due to variations in maximum receiver output from unit to unit, receivers and decoders cannot be indiscriminately interchanged once a pair has been integrated. If it becomes necessary to replace a receiver, operation within specification must be verified over the temperature range and additional realignment performed if necessary.

4. Auxiliary Command Unit

a. General

The auxiliary command unit (ACU) was added to the SERT spacecraft as a result of the reliability study which was conducted for NASA (see Section VII) and the ion-engine development testing on spacecraft T-2. This unit (see Figure III-28) and the diode board were added to flight spacecraft T-3.

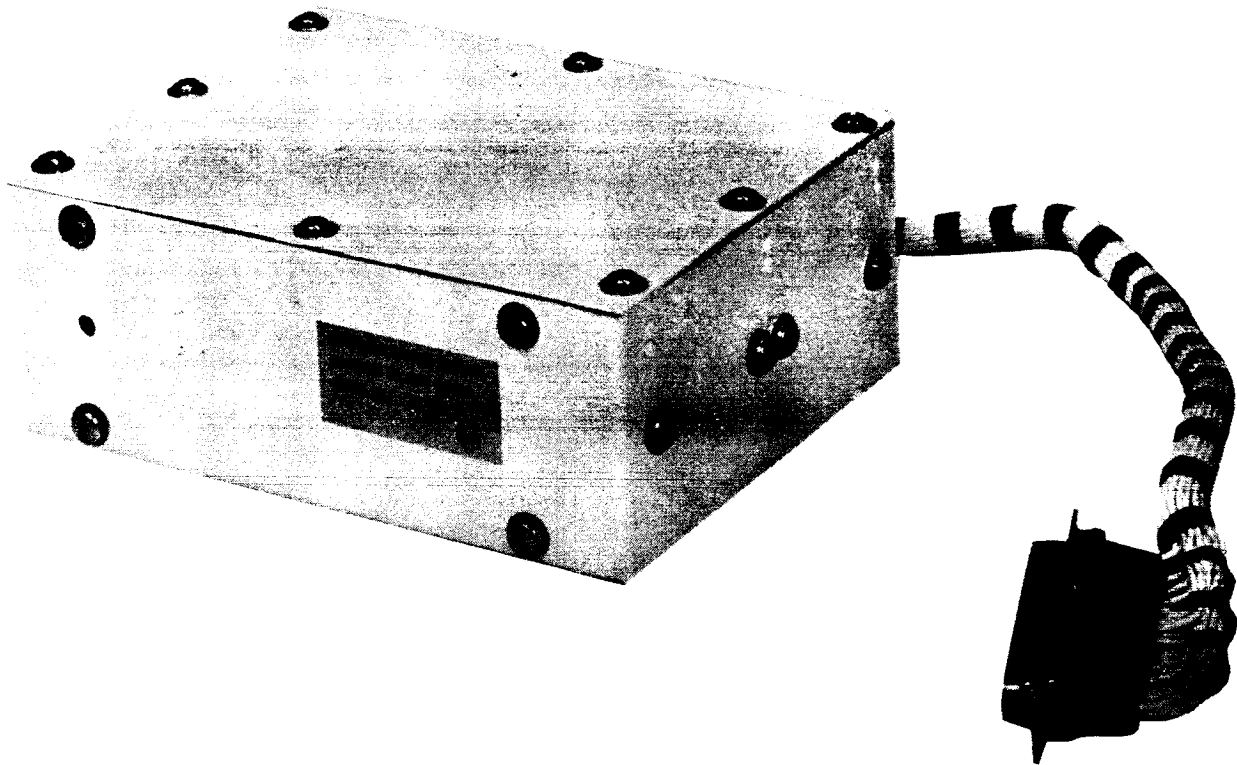


Figure III-28. Auxiliary Command Unit

b. Functional Description

The auxiliary command unit (Figure III-29) is functionally integrated into the SERT system between the command backup facilities and the spacecraft control equipment to provide additional ground control of the ion engines. The unit in conjunction with the diode board (Figure III-30) causes the system to perform the following additional functions when the following commands are given:

(1) Command No. 3

In addition to arming the spacecraft squibs, this command also enables reset to Mode I from Mode II.

(2) Command No. 5

In Mode I (original mode), this command performs its original function by firing the unfold squib. In Mode II (activated by Command No. 7), Command No. 5 turns off the cesium-contact-engine subsystem, turns on the mercury-bombardment-engine subsystem, and energizes and latches the neutralizer heater power of the mercury-bombardment engine.

(3) Command No. 7

In addition to the function of firing the cesium-contact-engine pod door it now interrupts the magnetic field power supply of the mercury-bombardment-engine, turns the boiler heater of the cesium-contact engine off, and selects Mode II.

(4) Command No. 4

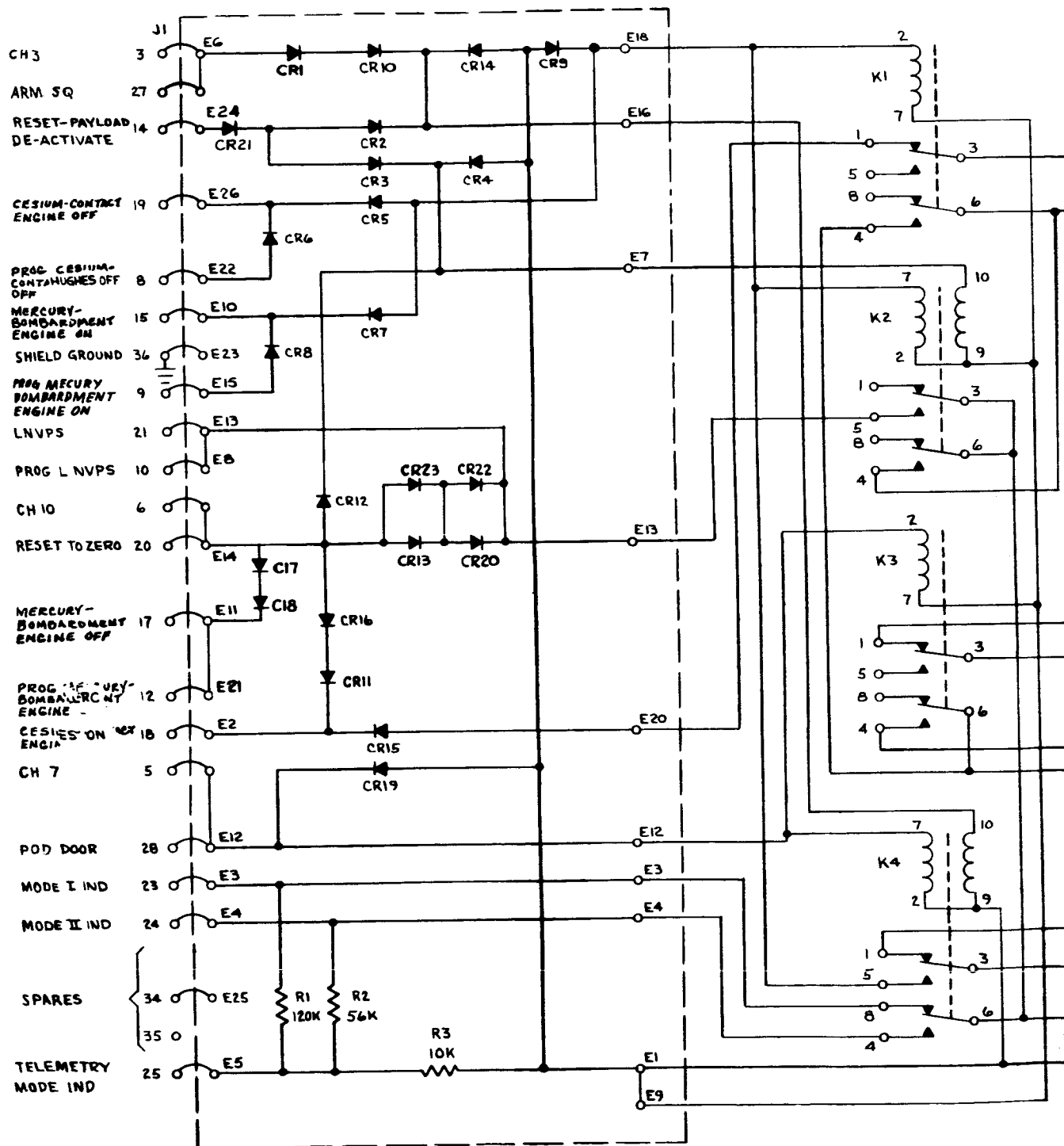
In addition to activating the dc voltages for the cesium-contact engine and firing the ground-plane squibs, this command now closes the cesium feed valve, and deactivates the boiler of the cesium-contact engine.

(5) Command No. 10

In addition to its normal function which is to reset the programmer to zero, it turns off the mercury-bombardment engine and energizes its neutralizer heater for the duration of the command, and turns on the cesium-contact engine.

The auxiliary command unit also has a coded output which corresponds to the setting of its internal mode relay. This signal is processed via the commutated telemetry.

A1



NOTES:

1. ALL DIODES ARE USAF1N645.
2. ALL RESISTORS ARE 1/4W, ±5%.
3. RELAYS K2 & K4 ARE SHOWN IN UNLATCHED POSITION.

III-53

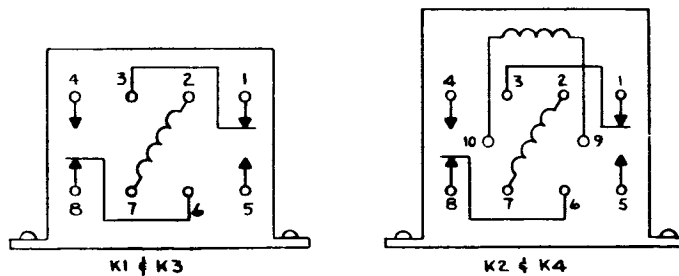
J1
 ○ 11 PROG CESIUM-CONTACT ENGINE
 ○ 30 TEST POINT

○ 7 }
 ○ 13 } SPARES
 ○ 22 }
 ○ 32 }

○ 16 PSU LMFPS
 ○ 29 MERCURY-BOMBARDMENT-ENGINE
 MAG FIELD PS

○ 33 TEST POINT
 ○ 31 TEST POINT
 ○ 37 CHASSIS GROUND

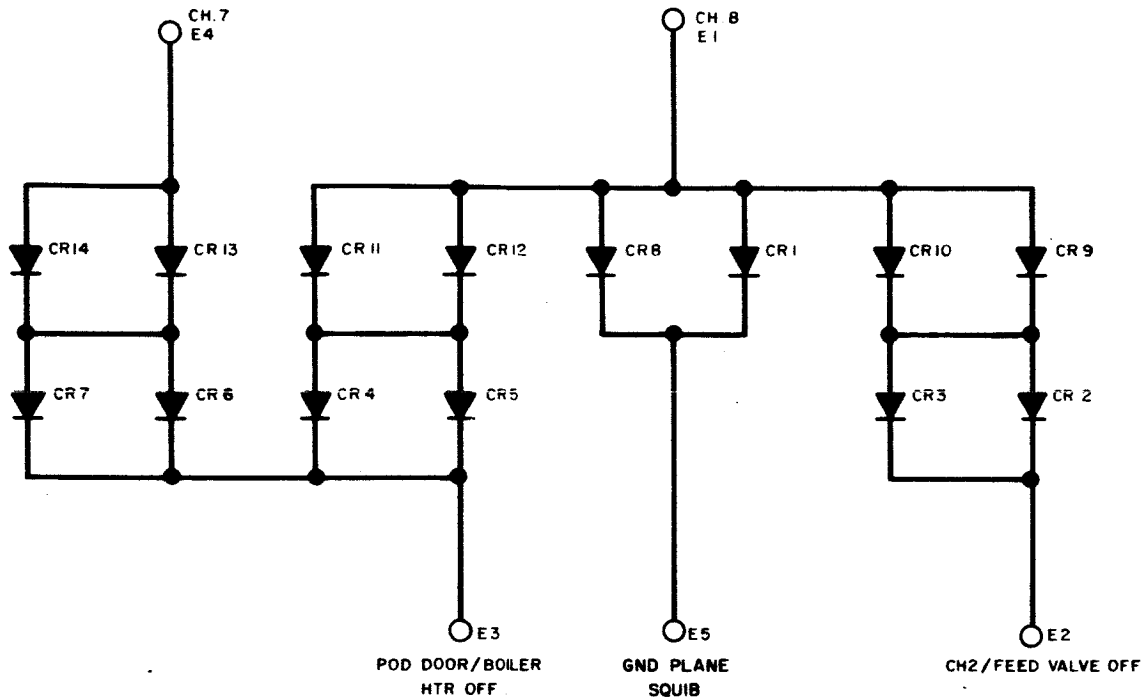
○ 26 UNFOLD SQ
 ○ 4 CH 5
 ○ 1 +28 VDC
 ○ 2 GROUND



TOP VIEW - PIN CONFIGURATION
NOT TO SCALE

III-54

Figure III-29. Schematic Diagram of the Auxiliary Command Unit



NOTE:
1. ALL DIODES ARE USAF IN645.

Figure III-30. Schematic Diagram of the Diode Board

c. Development

The development of the auxiliary command unit was accomplished without difficulty. The circuit logic of the auxiliary command unit was defined by the system requirements and the requirement for compatibility with existing units.

Relays, because of their relative simplicity and because of the potential effects of engine arcing on solid-state switches, were selected to accomplish the circuit switching. Diode quads were used where blocking diodes were required in circuits which were critical to the mission.

The auxiliary command unit was integrated into the SERT system with only one interface discrepancy. Here a sneak circuit latched the internal mode relay by way of the spacecraft pressure switch which arms the spacecraft squibs. The insertion of a blocking diode into the harness corrected the problem.

During the acceptance testing of the flight spacecraft, T-3, the diode board was added (at NASA request) to enable the simultaneous shut off of the cesium boiler heater and its feed valve while retaining the independent control of each. This was to be accomplished using command back-up facilities.

The board essentially became an additional auxiliary unit. It was designed using diode quads, fabricated, and installed by splicing it into the harness. It successfully passed all system tests.

5. Command Programmer

In-flight operation of the SERT spacecraft is controlled by the command programmer (GFE) developed by NASA Lewis Research Center in Cleveland, Ohio.

The programmer generates the controlling pulses to the various subsystems in accordance with the flight sequence. These pulses consist of relay closures feeding +28 vdc.

Timing within the programmer, which is started when the Payload Activate command is given 30 seconds before lift-off, is provided by a one-pulse-per-second generator.

The programmer also provides a series of coded voltages, representing a profile of the flight sequence, to the telecommunications subsystem for transmission to the ground receiving station, hence providing a real-time monitor of the flight sequence. A detailed description of the programmer functions is given in Table I-3.

F. POWER SUBSYSTEM

1. General

The power subsystem of the SERT spacecraft consists of two batteries (GFE) and the power-switching unit. The batteries have a combined power output capability of 2.0 kilowatts per hour. Power is supplied through the power-switching unit to all the spacecraft subsystems. All batteries are of the zinc-silver oxide primary type which are charged by the addition of electrolyte shortly before use.

2. Batteries

The main battery and the telemetry battery are the two primary power sources in the SERT spacecraft. The main battery, which consists of a set of two series-connected batteries, serves as the primary power source. It is used to power the engine subsystems. A separate battery is employed to supply power to the telecommunications and command and control subsystems in order to isolate these subsystems from the transients and noise associated with the high-power switching and high-voltage arc-overs inherent in the operation of the engine subsystems.

The two series-connected batteries continuously supply 56 volts to engine subsystems via the harness, fuse block, and power-switching unit. These batteries also supply 28 volts from their center tap to the control circuits of the engine subsystems. The momentary high currents which are required for activation of all the explosive devices within the spacecraft are also supplied by these batteries. The main battery supply is capable of providing 1.7 kilowatt-hours.

A 28-volt, 300-watt-hour battery is employed to power the command and control subsystems, the telecommunications subsystem, and the sensory subsystem. Again, all power switching is accomplished within the power-switching unit. The batteries were selected by NASA to meet total spacecraft requirements and were provided to RCA for integration.

3. Power-Switching Unit

a. General

The SERT power-switching unit was designed to serve as a central point on the SERT spacecraft for a number of basic electrical functions. These functions include the distribution of primary power, the sensing of primary power data, provisions for firing the spacecraft squibs, and provisions for the hardline interconnection of the spacecraft to the ground test station. A simplified block diagram of the power-switching unit is shown in Figure III-31.

b. Functional Description

The power-switching unit (PSU) operates on signals generated by the programmer, the command subsystem, and the ground-test-station control panel to perform a variety of functions which provide control of the SERT spacecraft. The unit serves four basic functions: power switching, battery monitoring, squib firing, and hardline ground control.

The PSU has six power-feed circuits, five of which are switched on and off by external commands; circuit No. 1 continuously feeds the main battery voltage of 56 vdc to the engine subsystems via the fuse block.

Circuits No. 2 (K1) and No. 3 (K2) switch the main battery voltage of 28 vdc to either of the engine subsystems upon either programmer, command-subsystem (via the auxiliary command unit), or umbilical command; this affects the on-off operation of either subsystem. Lockout circuitry prevents the simultaneous activation of both subsystems. Circuit No. 4 (K3) switches the main battery voltage of 28 vdc to the ion-beam-probe mechanism, the accelerometer heater, the neutralizer voltage control unit, and the cesium-contact-engine control box upon receipt of umbilical commands.

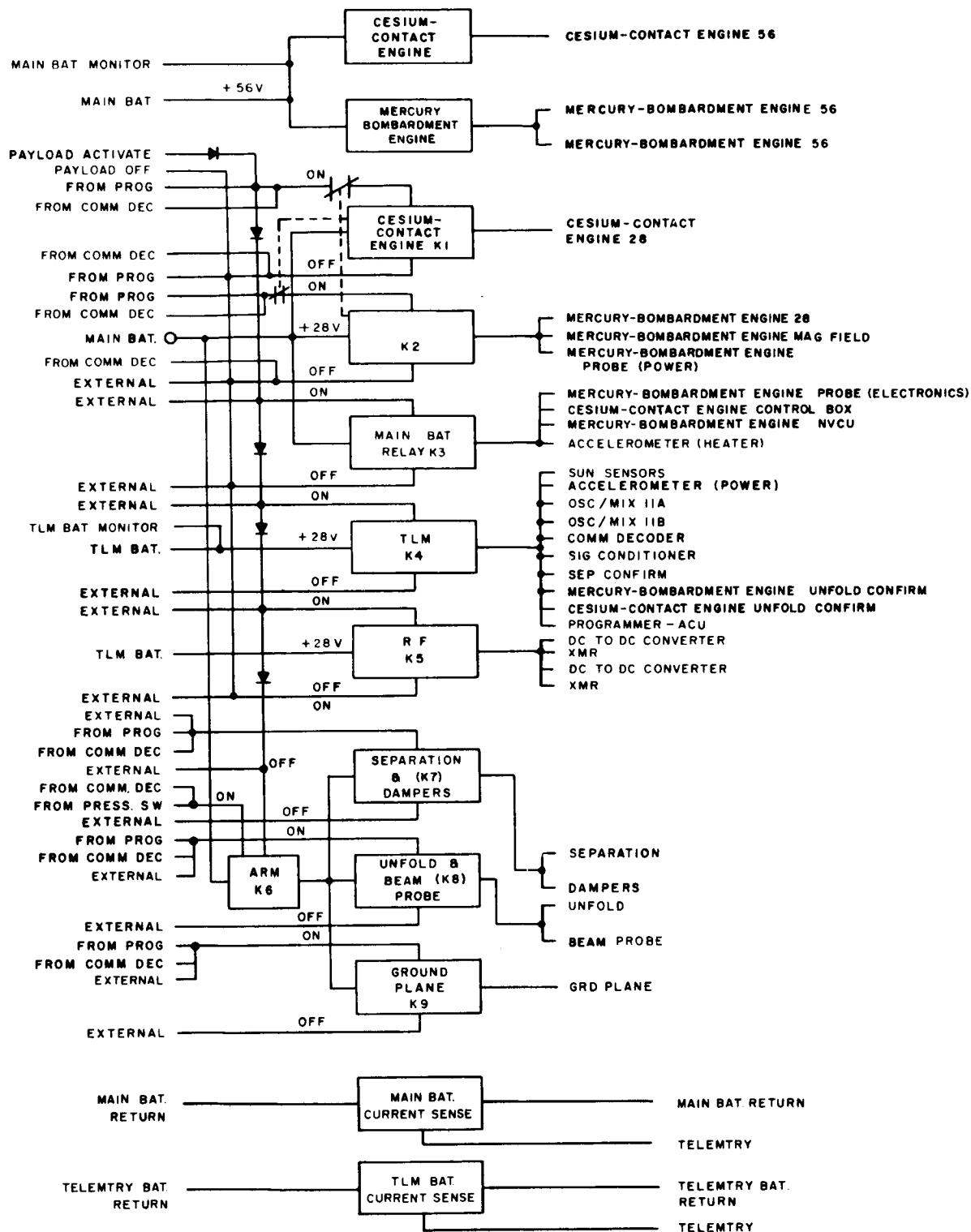


Figure III-31. Simplified Block Diagram of the Power-Switching Unit

Circuit No. 5 (K4) switches the telemetry battery voltage of 28 vdc to the telecommunications subsystem, the programmer, the auxiliary command unit, the command subsystem, the sun sensors, and the accelerometer electronics upon receipt of umbilical commands. Circuit No. 6 (K5) switches the telemetry battery voltage of 28 vdc to the rf subsystem upon receipt of umbilical commands.

The power-switching unit monitors the battery voltage levels and the current drain on the batteries and feeds the monitored information to the telecommunications subsystem.

The PSU has an arming circuit and three firing circuits which, upon command, activate the spacecraft squibs. Arming commands are derived either from a pressure switch or the command backup. Disarm commands are obtained via the umbilical. Each firing circuit is commanded either from the programmer, the command backup, or the umbilical. Firing circuit No. 1 (K7) simultaneously fires four damper and four spacecraft/vehicle separation squibs.

Circuit No. 2 (K8) fires four arm-release squibs, two for each engine-extension arm. Circuit No. 3 (K9) fires two ground-plane squibs.

Hardline ground control utilizes three umbilical cables: the primary power cable and the test cable which connect directly to the power-switching unit, and the flyaway cable which connects to the spacecraft harness.

The power supplied by the umbilical cable substitutes for the spacecraft battery power to provide external primary source inputs — one at 56 vdc and three at 28 vdc.

The power-switching unit, when operated with the test umbilical cable connection, allows independent ground control of its five subsystem switching circuits, control of squib arming and disarming, control of each firing circuit, monitoring of each firing circuit, and control of specific functions of the programmer. Among the programmer functions that can be controlled are start, stop, restart, reset, and test; the latter provides facilities to drive the programmer accumulator by using an external oscillator.

The PSU, when operated with the flyaway umbilical cable connection, permits further control of the spacecraft activity associated with launch countdown. A lead from the load side of each switching circuit is used either to supply external power to a particular subsystem, or to indicate the status of the switching circuit, i.e., closed or open.

The power-switching unit also performs a Payload Activate function and a Payload Off function when operated with the flyaway umbilical connection. Upon receiving a Payload Activate signal, circuitry within the PSU causes all of the spacecraft subsystems, except the mercury-bombardment engine subsystem, to turn on. This signal also pulses the disarm coil of the squib-arming relay to ensure "no fire" before the coil is armed by the altitude-sensing pressure switch. This Payload Activate signal is also fed via the harness to the programmer where it causes the initiation of the flight

count. The Payload Off signal causes all of the spacecraft subsystems to shut off and, via the harness, resets the programmer to zero.

c. Development

(1) Power Switching

Primary power switching to the five major spacecraft subsystems had to be accomplished before and during flight operation. A voltage level of 28 vdc at currents up to 10 amperes had to be switched to the rf equipment, the telemetry equipment, and the programmer. Voltage levels of 28 vdc at 3.5 amperes and 56 vdc at currents up to 30 amperes had to be switched to the cesium-contact and mercury-bombardment-engine subsystems.

Relays and solid-state devices were two methods of power switching that were investigated during the course of the study and design. Relays offer a distinct advantage in their circuit simplicity and their proven usage in satellite hardware. For this particular application, however, certain disadvantages are evident. First, the high currents associated with the 56-vdc power necessitate rather large contact masses and coil powers, hence rather large and heavy relays. Second, contact closure had to be maintained at high-current levels throughout the high vibration period experienced during launch and still be operable during flight.

Solid-state devices such as silicon controlled rectifiers with no moving parts offer advantages in their great immunity to vibration and their high current carrying capacity (a condition of prime importance in this application). Other advantages include their small size and weight. The disadvantages of the solid-state devices were also considered. Circuit design is complicated, especially for shut-off. High power losses are encountered by relatively high junction impedances, thus necessitating large heat sinks and special mounting techniques. The possibility of false firing due to noise was also considered a disadvantage. Turn-off requires application of output voltage in excess of nominal values.

It was concluded that, due to their high current-carrying capacity and high immunity to vibration, silicon controlled rectifiers best enabled reliable operation in the unusual SERT spacecraft switching operations.

A simplified diagram of the circuit used for switching power to the telecommunications subsystem and programmer is shown in Figure III-32. A similar diagram for the engine subsystems is shown in Figure III-33.

After qualification of the SCR-operated unit at the component level and during preliminary spacecraft testing, it was discovered that the cesium-contact-engine subsystem was adversely affected by the overvoltage produced by the shut-off pulse in

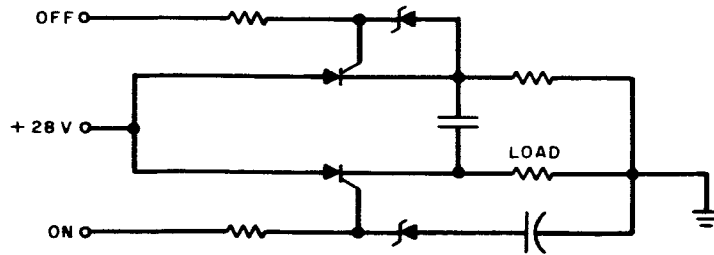


Figure III-32. Schematic Diagram of the Power-Switching Circuit for the Telecommunications Subsystem and Programmer

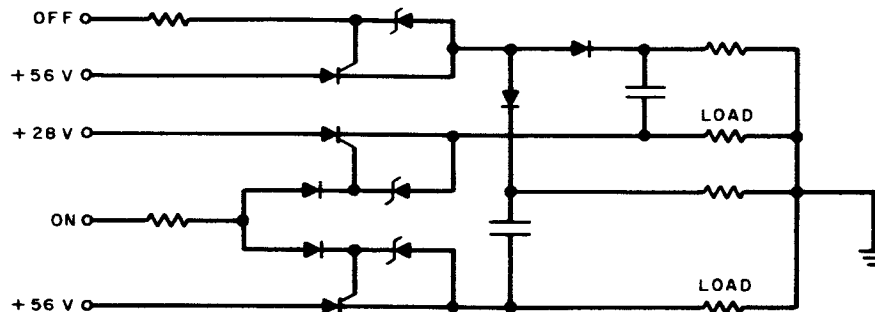


Figure III-33. Schematic Diagram of the Power-Switching Circuit for the Engine Subsystems

the 56-volt line. It was further established by NASA that cesium-contact-engine subsystem could not tolerate such overvoltage, inherently required for the operation of the SCR. Such limitation made the use of SCR's incompatible with the design of the cesium-contact-engine subsystem.

The final design of the power-switching unit evolved as a result of a series of discussions between NASA and RCA. This design utilized relays in place of all SCR's in the 28-volt circuits; the switching requirement in the 56-volt circuits was deleted. This deletion was made possible because the existing ion-engine power supply circuitry could perform the switching functions. In all other respects, the redesigned unit was electrically identical to the SCR model. Only minor modifications were required to the mechanical configuration.

The redesign of the unit was greatly simplified by the removal of the switching requirements for the 56-volt lines. Latching relays with contact-current-carrying capacities of 10 amperes were substituted in place of the SCR's in the 28-volt-circuits for the engine subsystems, the telecommunications subsystem, and the programmer.

Load switching with the relays was accomplished in much the same manner as with the SCR's. The "on" pulse was fed to the set coil of the relay instead of the gate of the "on SCR." The "off" pulse was fed to the reset coil instead of the gate of the "off SCR." Here again, the design was simplified since one relay substituted for two

SCR's and eight other components, including Zener diodes, capacitors, and resistors. Isolation diodes for multi-channel operation were preserved wherever required.

Simultaneous operation of the 28-volt lines to the engines was eliminated by positively disabling one system at the activation of the other by means of relay contact openings.

(2) Squib Firing.

Basically there are two types of squibs to be fired in the SERT spacecraft. The separation squibs which require four-amperes firing current and the unfold damper squibs which require two amperes. Adequate protection against false firing had to be included in the design of their firing circuitry. The squib firing circuitry is composed of an arming relay, three firing relays, and current limiting resistors. The arming relay is controlled by a spacecraft pressure switch which prevents false actuation of the firing circuitry on the ground. The arming relay is disarmed by the Payload Activate command to prevent false firing during launch. In addition, the unit has the ability to monitor the Disarm state of the firing circuitry and indicate its status to the ground station. The normally closed contacts of the firing relays ground the squibs through the low-resistance limit resistors to prevent noise firing of the squibs. The limit resistors prevent relay contact burnout and excessive battery drainage during firing. In addition, the circuits are electrically isolated to prevent the loss of firing current to parallel squibs in the event of a squib short after firing, a condition known to occasionally occur. A simplified circuit diagram is shown in Figure III-34.

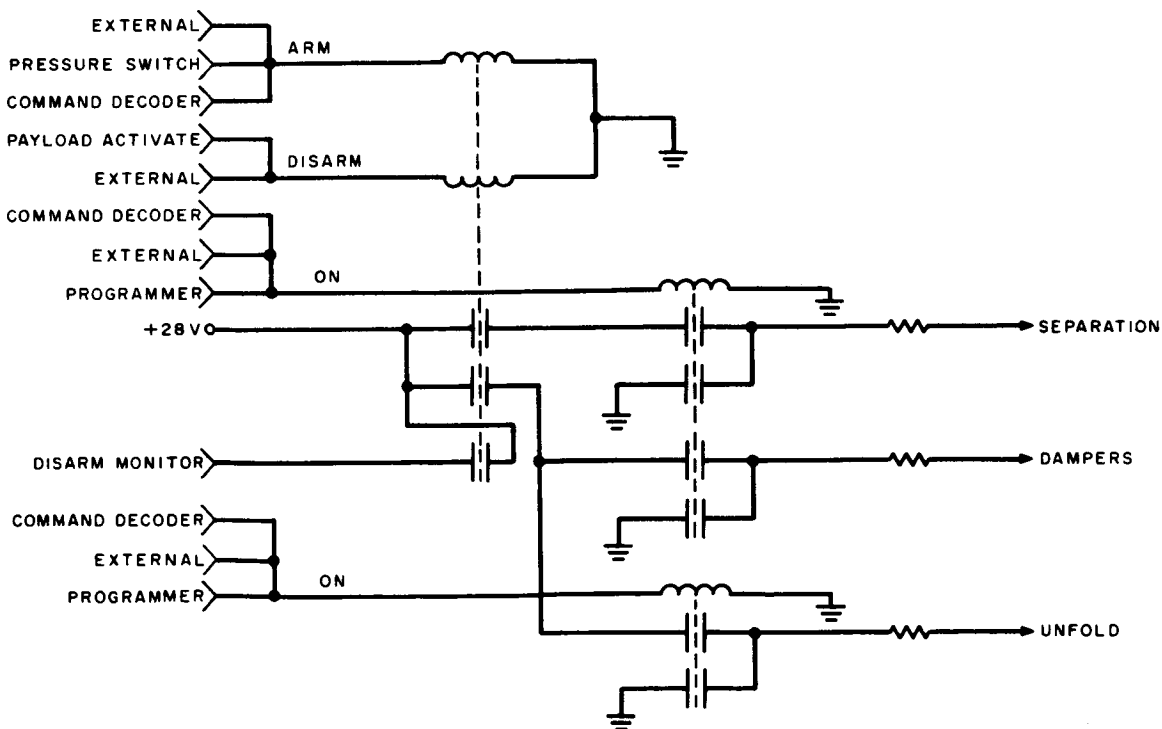


Figure III-34. Schematic Diagram of the Squib-Firing Circuitry

(3) Power Monitoring.

In addition to its principal function of switching power "on" and "off" to the various subsystems, in response to the programmer or ground station commands, the power-switching unit provides an accurate measurement of the current being supplied to any of the major subsystems.

Current supplied by the main battery is measured by a 30-ampere, 50-millivolt shunt located in its return line. Similarly a 10-ampere 50-millivolt shunt, located in the return line of the telemetry battery, is used to measure the current supplied by this battery. The voltage developed at each of the shunts is connected to the telecommunications subsystem for monitoring.

When external power is used, the main battery shunt senses the current at the 56-volt loads, while the telemetry battery shunt senses the current in the 28-volt loads.

(4) Voltage Monitoring.

The power-switching unit senses the voltages at the main and telemetry batteries; these voltages are monitored at the telecommunications subsystem.

(5) Hardline Ground Control.

During flight, the power-switching unit distributes power to the various subsystems in response to the commands of the programmer. However, for system testing and pre-flight checkout purposes, the power-switching unit, through a test umbilical, makes all of its channels available to the ground station. It is in this manner that any subsystem or combination of subsystems, including the programmer, can be individually tested.

(6) Detailed Mechanical Description.

The case of the power-switching unit (Figure III-35) is a $3 \frac{7}{8}$ -inch by $4 \frac{1}{4}$ -inch by $10 \frac{1}{4}$ -inch machined casting with a removable faceplate cover. Connectors are located on two faces of the casting. Lugs on the $3 \frac{7}{8}$ -inch by $4 \frac{1}{4}$ -inch face are used to mount the PSU to the spacecraft baseplate. Other faces are used to mount the electrical components inside the package.

The electrical components within the PSU are mounted with their most sensitive axes perpendicular to the axis of thrust of the spacecraft.

Mounting is accomplished by bolting the base of the package to the spacecraft baseplate and locking the package mounting studs to the spacecraft distributor frame.

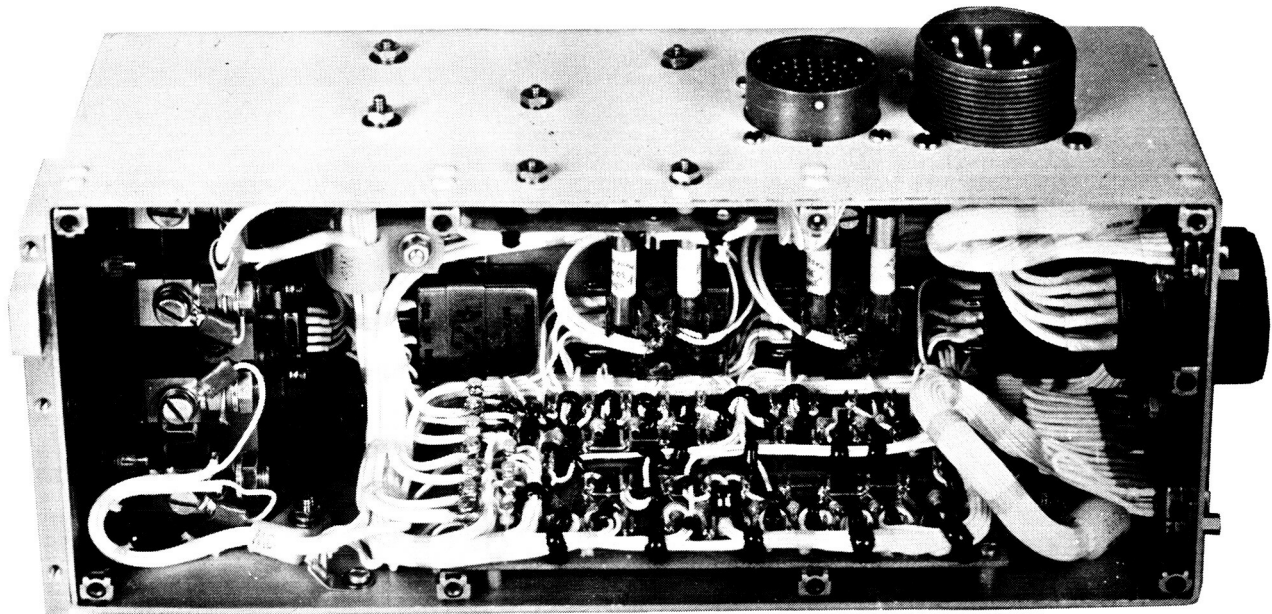


Figure III-35. Power-Switching Unit

Connectors are located such that external power and test connections are made in a vertical plane to one side of the package, and spacecraft connections are made to the top of the package.

G. SENSORY SUBSYSTEM

1. General

The sensory subsystem constitutes basic elements of the SERT spacecraft which perform some of the critical measurements of the SERT mission.

Included in the sensory subsystem are the sun sensors and radial accelerometer, which detect the spin rate of the spacecraft, and the ion-beam probe, which measures the energy characteristics of the beam exhausted by the mercury-bombardment engine.

Monitoring of the radial accelerometer output and the mercury-bombardment-engine beam are performed through the telecommunications subsystem. The outputs of the sun sensors are monitored by a set of two subcarrier oscillators allocated to this purpose.

2. Sun Sensors

a. General

The sun sensor provides the means of accurately determining spacecraft spin rate by sensing the passage of the sun once each rotation of the spacecraft. The SERT program utilizes this measurement in the computation of ion-engine thrust.

b. Functional Description

The sun sensor subsystem (see Figure III-36) is a totally redundant system in that it includes two independent sets of light detection, pulse shaping, power regulation, and telemetering equipment. Each set of equipment consists of a light-sensing element located on the outer rim of the spacecraft in such a manner that a restricted look angle is available for solar detection. The cell excitation is amplified and shaped with a one-shot multivibrator to modulate a 7.35-kc subcarrier oscillator and; hence, telemeter an accurate pulse-to-pulse time determination to the ground. A schematic diagram of the sun sensor is given in Figure III-37; a photo is shown in Figure III-38.

Since the parameter of interest is the time between pulses, the only system requirement is that the waveshape of the pulses arriving at the ground station be consistent. If the same point on the slope of the rise time is used to measure the interval each time, resolution in time is not dependent upon a fast-rise-time pulse. This method of interval measurement depends on the short-term consistency of circuit operation

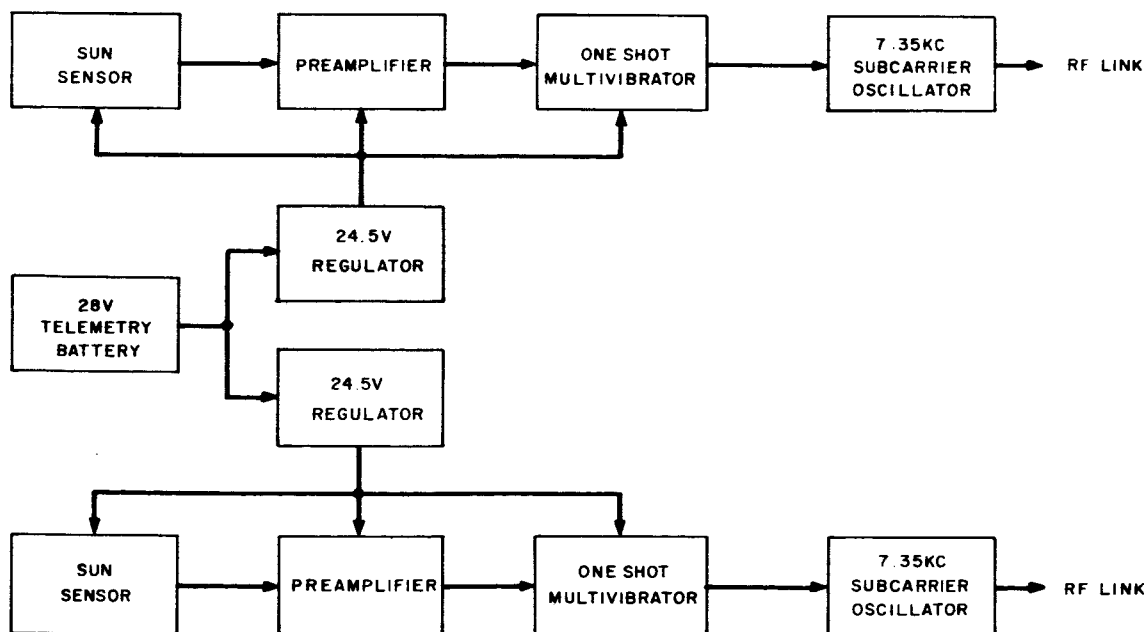


Figure III-36. Block Diagram Showing the Sun Sensor Link

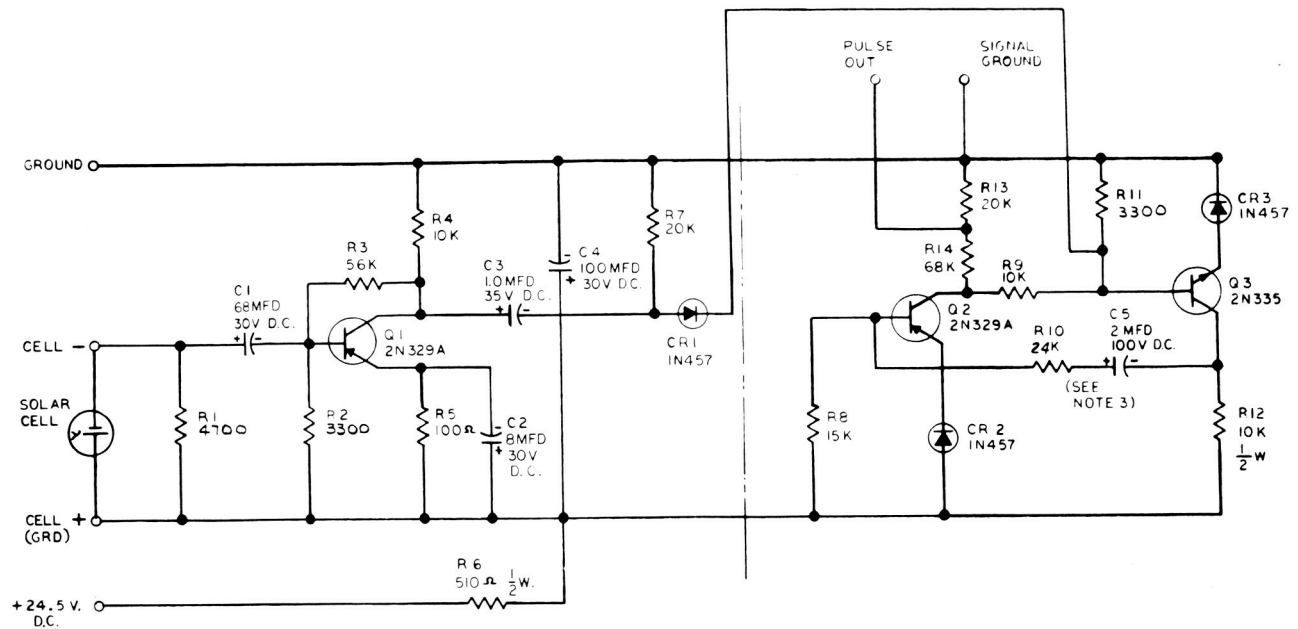


Figure III-37. Schematic Diagram of the Sun-Sensor Circuit

in the spacecraft and on the ground. System error or jitter is contributed by the sensor electronics, the telemetry and rf link, the ground station data presentation equipment, and spacecraft nutation. A system description and error analysis is given in Paragraph IV-B.

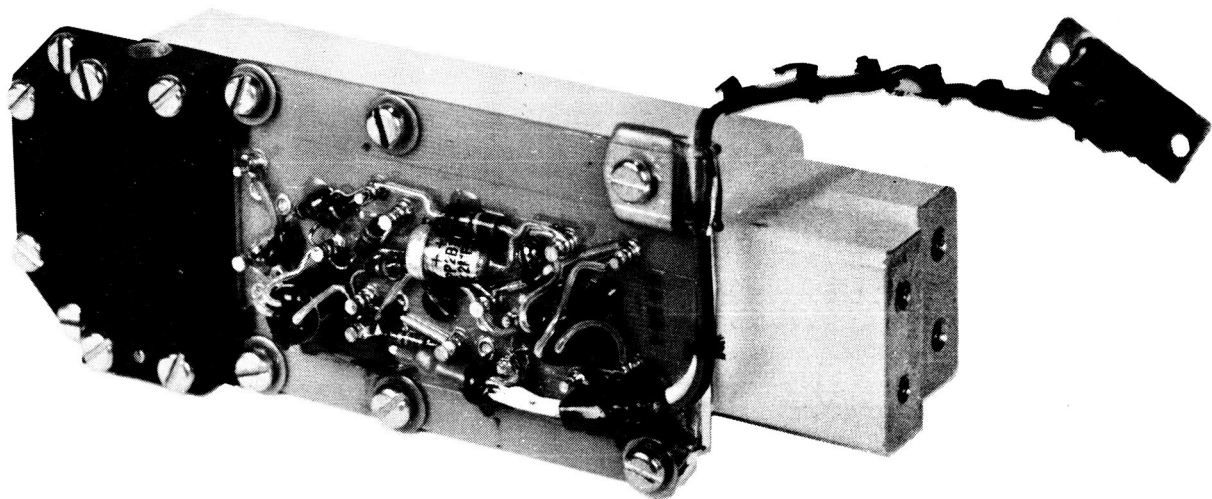


Figure III-38. Sun Sensor

3. Radial Accelerometer

A radial accelerometer was used on the SERT spacecraft to provide a measure of the spacecraft rate of change of radial acceleration during the flight operations. Special conditioning circuitry was designed to process the accelerometer output for transmission to the ground control station. Since the accelerometer was provided by NASA, a detailed description is not given in this report.

4. Ion-Beam Probe

a. General

The ion-beam probe, developed by the NASA Lewis Research Center, was designed to measure the density characteristics of the ion-beam exhaust produced by the mercury-bombardment-engine.

Five temperature-sensitive probe elements are located on a movable arm which swings out to intercept the neutralized beam of mercury ions being expelled by the mercury-bombardment engine. The probe actuator system developed by RCA provides the mechanism by which the probe is swung into position. Since the probe sensing elements are isolated from ground, signal conditioner circuitry was developed to de-couple and process the signals through the telecommunications subsystem.

b. Ion-Beam Probe Actuator

(1) General

The probe actuator (shown in Figure III-39) consists of a single housing and cover which contain all the mechanical and electrical items that make up the system. The assembly which mounts on the mercury-bombardment-engine arm is pivoted on a bracket which is fastened to the baseplate. The position of the probe actuator system relative to the engine is, therefore, fixed; both swing from the stowed to the extended position together when the engine is released. The unit is sealed by O-rings and a gasket so that it will retain a positive pressure during operation. The major components contained in the housing and cover are a motor, gear train, slip clutch (to prevent accidental overloading of the motor and gear train during assembly and testing of the actuator system), potentiometer, relay, probe output shaft, and electrical circuitry. All external materials are either aluminum alloy or stainless steel.

The electrical circuitry supplies power to the motor and performs the switching required to move the ion-beam probe through the ion beam and then return it to the starting position. The second circuit is used for the potentiometer output signal.

The "hot" wires of the probe travel in a plane perpendicular to the ion beam at a distance of approximately 6-1/2 inches from the engine exhausts.

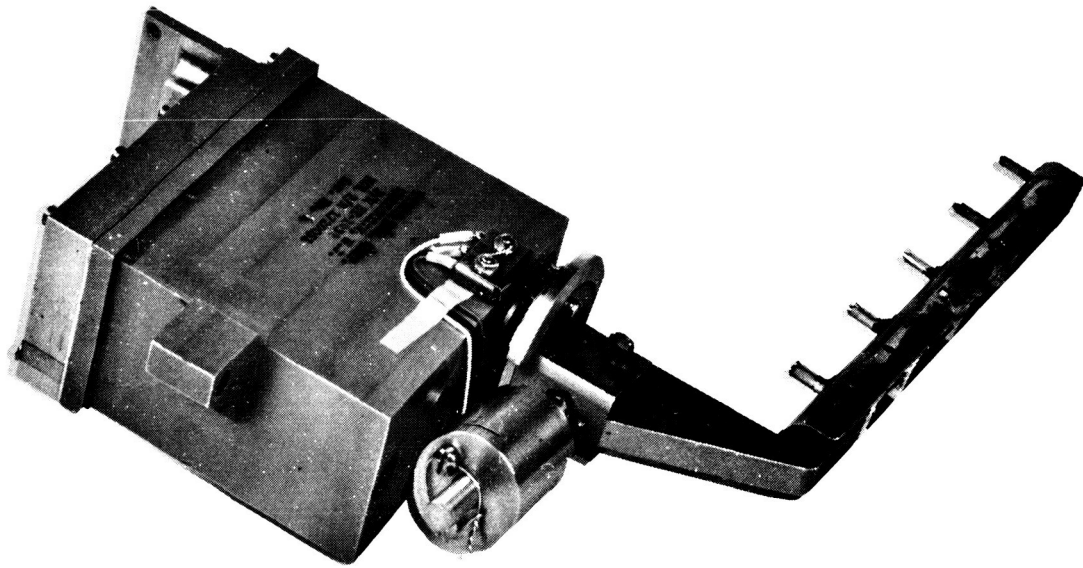


Figure III-39. Ion-Beam Probe and Actuator

(2) Functional Description

The permanent-magnet dc gear motor operates at 6400 revolutions per minute. The motor is attached to an integral gear box which reduces the motor output shaft speed to 8 revolutions per minute. The output shaft, upon which the ion-beam probe is mounted, is driven through an arc of approximately 80 degrees at a speed reduced to approximately 0.5 revolutions per minute by the gear train. The probe is counterbalanced to minimize motor and gear train loading caused by centrifugal forces of the spinning vehicle. The counter-balanced load and a slip clutch setting of 40 to 50 inch-ounces minimized the problem of selecting a motor. The history of the motor chosen indicated that the life of the motor under extreme vacuum conditions far exceeded the requirements of this application. The probe actuator system is sealed at assembly providing the motor with a positive ambient pressure which tends to increase the life and reliability of the motor. The motor produces a minimum output torque of 15 inch-ounces at an input voltage of 28 ± 2.8 vdc. A theoretical torque reduction of 3.8:1 between the slip clutch and the motor output shaft insures the motor against overload.

A short duration signal from the spacecraft programmer starts the probe cycle by causing the relay to latch. While the relay is in the latched position, power at 28 vdc drives the motor causing the probe to traverse the ion beam. The microswitches (S1 and S2) shown in Figure III-40 are in the Ready position at a time before the cycle begins. When the probe traverse starts, the position of switch S2 changes from that shown in Figure III-40. At the end of the first half of the cycle, switch S1 is actuated. This causes the relay coil to become de-energized, which in turn causes the direction of the power to the motor to be reversed. The probe then traverses the ion beam in the opposite direction returning to its original position. When the probe

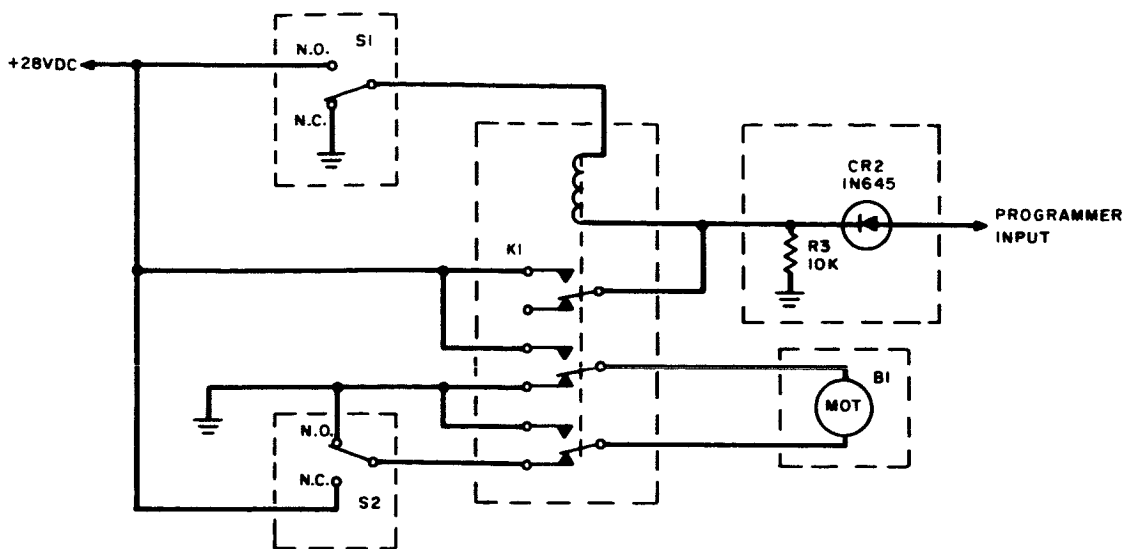


Figure III-40. Simplified Schematic Diagram of the Beam-Probe Actuator System

arrives at this position, switch S2 is actuated, interrupting the power to the motor and completing the cycle; the probe-actuator system is then returned to the Ready position.

The relay was selected because of its miniature size and rugged construction. The relay specifications indicated that it could operate under vibration and shock conditions exceeding those required during environmental testing of the probe actuator system even though the relay does not operate during these conditions of the actual mission.

A single-turn potentiometer having a linearity tolerance of ± 0.5 percent produces a signal indicating the position of the probe at any time during the survey. It is mounted directly to the output shaft so that no relative motion between the probe and the potentiometer is possible. The potentiometer circuit is designed so that a 28-vdc input signal results in a 5-volt output for the full travel (80 degrees) of the probe. The potentiometer is mechanically positioned so that the lower limit of the voltage range occurs at zero volts.

(3) Development

The basic design of the probe actuator system was qualified at the component level without difficulty. However, a redesign of the probe by NASA subsequent to qualification of the actuator system resulted in a threefold increase in the weight of the probe and its counterweight. The output shaft upon which the probe and counterweight are cantilevered failed during the full-level-prototype spacecraft vibration test. The output shaft was redesigned, eliminating sections having extreme stress concentrations and using a material having an ultimate stress three times greater than the original shaft material. The probe actuator system was then successfully requalified.

H. ELECTRICAL INTEGRATION

1. Wiring and Cabling

a. General

The spacecraft wiring and cabling provides all the necessary electrical interconnections between the various subsystems. The SERT cabling carries currents ranging from microampere telemetry signals to 40-ampere power, at potentials from negative 2000 to positive 5600 volts.

b. Description

The SERT harness consists of three individual harnesses which are separated to minimize electromagnetic and capacitive coupling. The largest harness carries the signal functions and distributes the low-level power. A second harness carries the high-current functions, and a third carries the high voltage.

The harnesses are made from teflon-insulated wire. Conductor sizes range from No. 22 to No. 12. A special teflon-insulated cable is also used for the high-voltage applications. High-temperature cable is used for coaxial applications.

Connectors are used in the harness for most cable terminations. In some cases, terminal studs are used as the termination; in other cases, solder terminals are used. Special potted terminations are used for the high voltage applications.

The harness also includes a number of small component boards which are permanently wired in. These include a high-current junction on a 1-inch by 2-inch board which serves as the series tie point of the main 28-volt batteries. A 2-inch by 2-inch board also is included which serves as a low-level power distribution point. A 2-inch by 3-inch silver-plated copper plate with many terminals serves as a system ground point. A 2.5-inch by 2.5-inch board containing 14 diodes serves as a special command back-up auxiliary board. A bracket holds three stud-type high-current diodes. Also permanently wired in is a simple resistor-Zener-diode regulator on a 1-inch by 2-inch board.

c. Development

Early in the SERT program, as the mechanical layout of the spacecraft was being developed, the basic concept of the harness was established (see Figure III-41). Harness cabling extends out from a centrally located 10-inch by 14-inch horizontal rectangle which is located about 12 inches above the center of the baseplate atop the distributor frame. As shown in Figure III-42, cables which extend from the topside of the baseplate to the underside pass by way of grooves at the outer edge of the baseplate. This basic configuration was held throughout the program.

Another requirement which was studied early in the development program involved wire size versus current-carrying capacity. An analysis was made of wire temperature as a function of current loading and wire gauge. Computations were made for a wire placed in an enclosure at several sink temperatures and were repeated for a wire exposed to free space. This computation was then repeated for a wire enclosed in a bundle of wires.

Another important program decision was to use connector interfaces in the wiring between components. This decision was based primarily on the convenience offered in testing and replacement of spacecraft components.

The type of wire insulation material was an additional development requirement that was studied. The thermal data indicated that an insulation which could withstand temperatures generally over 100°C should be used. Preliminary information from the ion-engine designers indicated operation of the engines in the vicinity of 200°C or more. Also, the insulation should be of a low-outgassing material which would not contaminate the vacuum in the vicinity of the spacecraft, allowing high-voltage breakdown paths. The material must also be a good high-voltage insulator with special consideration to corona.

In selecting the insulation material, special consideration had to be given to flexibility, low-outgassing properties, adhesion between insulator and conductor to minimize the outgassing of entrapped air, operation at relatively high temperatures, and,

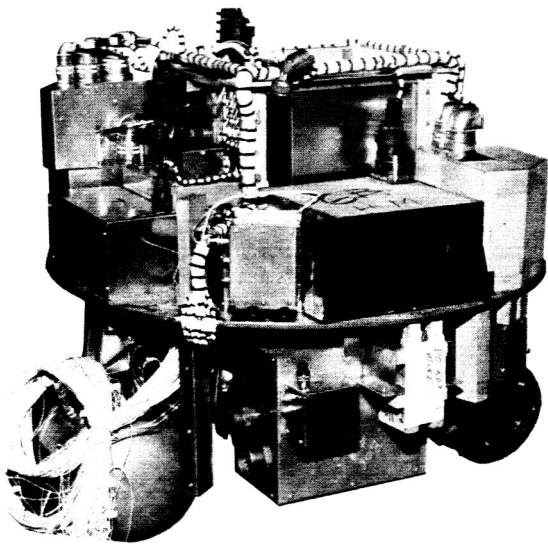


Figure III-41. SERT Harness During Fabrication on Harness Dummy

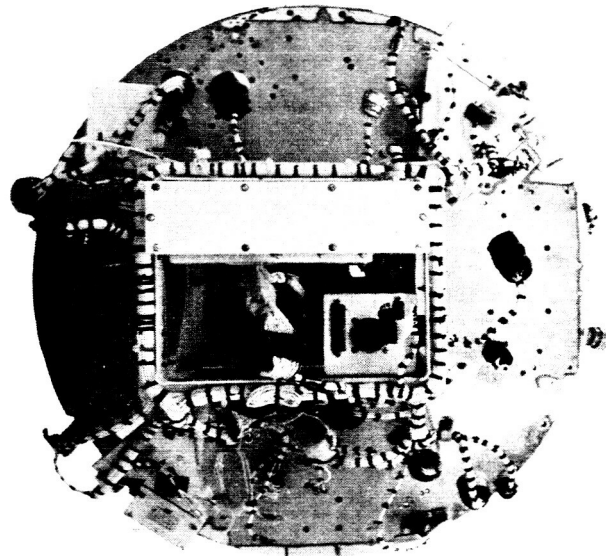


Figure III-42. Top View of Prototype SERT Spacecraft, T-1B-3

in high voltage applications, good insulation and corona characteristics. These considerations limited the insulation material selection to polyethylene, teflon, and silicone rubber.

Polyethylene insulation has excellent adhesion, low material outgassing, and good corona and high-voltage insulation properties. The insulated wire, however, would be fairly stiff when compared to teflon and silicone rubber. Further, its operation is limited to 110 °F and many of the spacecraft applications appear to be at a greater temperature.

Teflon insulation has excellent adhesion, non-measurable material outgassing, medium flexibility, good voltage insulation properties, and operation at temperatures up to 200 °C. The insulated wire, however, would have a cold flow problem at room temperature and poor corona characteristics. The corona problem, however, would only exist up to 100,000 feet.

Silicone rubber insulation has excellent flexibility, operation in temperatures up to 150 °C, and good high-voltage insulation and good corona characteristics. It would, however, have medium material outgassing and poor adhesion thus presenting outgassing problems.

Because the high voltages would be off until the spacecraft reached hard vacuum, corona would not be a problem. Teflon, being superior in the other areas of comparison, was therefore selected as the insulation material. Stranded wire insulated with polytetrafluorethylene (PTFE) resin conforming to type E in the Military Specification MIL-W-16878D (NAVY) is used for the low-voltage applications.

The special wire for the high-voltage applications is stranded wire with the identical teflon insulation as the low-voltage wire except that the wall thickness was increased to 43 mils. The test requirements of the military specification were changed to those of a wire having a dc voltage rating of 10,000 vdc rather than type E (600 vdc).

The selection of a grounding technique was another early consideration. The signals carried in the harness ranged from the microampere-range AGC telemetry current to the 30-ampere load current of the main batteries. In addition, many of the lines were subject to rather drastic pulsing from ion-engine arcing. In order to help in the reduction of coupling between wires and in order to minimize loops, a single-point grounding system was specified. Even test equipment such as the external power supplies obtained their circuit ground at the spacecraft system ground point.

The wiring specifications which were drawn up in the initial stages of the program, except for a few minor items, were still valid at the termination of the program.

The most significant change in the basic harness configuration occurred after the completion of ion-engine development testing with the T-2 spacecraft at the NASA Lewis Research Center. The ion engines in operation sometimes produced a good deal

of plasma arc-over to unpredictable points on the spacecraft. Engine arc-over also produced high-current surges in the feed lines. As a result of the knowledge gained in the engine testing, the harness and other areas of the spacecraft were modified to minimize the undesirable effects of the arcing.

The harness was split into three separate harnesses: the signal harness, the high-voltage harness, and the high-current harness. The high-voltage harness contained all of the interconnections which were at voltage levels greater than 100 volts. The high-current harness contained all of the interconnections which normally carried heavy currents and were subject to current surges when either engine arced. The signal harness contained all of the functions which were not included in the other two harnesses. The harnesses were routed as far apart as possible, parallel runs were kept to a minimum, and crossovers were made at right angles in order to minimize electromagnetic coupling.

During the program, a number of small component boards were included as part of the harness. Early in the program, the need for a high-current tie point to connect the two main batteries in series was satisfied with a simple copper bar which interconnected three solder terminals. This was mounted on a fiber-glass board which used a space of 1/2 inch by 1 1/2 inches on the distributor frame.

A silver-plated copper plate containing solder terminals and occupying a space of approximately 2 inches by 3 inches is utilized as a system grounding point when bolted to the spacecraft. It contains provisions for terminating about 54 wires.

A fiber-glass board occupying a space of approximately 1 1/2 inches by 2 inches serves as a low-level-power distribution point and, as such, becomes a convenient test point.

A simple resistor and Zener diode voltage regulator occupies a space of approximately 1 inch by 2 inches on one of the baseplate ribs. This board provides power for one of the sun sensors to make the two sun sensors truly redundant.

Three high-current stud-type diodes are mounted on a bracket which bolts to the distributor frame. They were added to block sneak paths which were detected during systems testing.

A space of approximately 2 inches by 2 inches contains a fiber-glass board of 14 diodes. This circuitry was spliced into the harness late in the development program to provide additional command backup control of the operation of the cesium-contact engine.

Late in the program, a major problem developed in the high-voltage harness. The connectors which carry the high-voltages arced pin-to-shell across the mating plug and receptacle face when the spacecraft was subjected to its fast-pumpdown vacuum qualification tests. This first occurred on prototype spacecraft T-1B-3.

A combined NASA and RCA team effort solved the problem. All of the insulation material was cleaned out of a harness plug; the plug was mated to the box receptacle; and the

connection was potted. A total of eight connectors, including three on the mercury-bombardment engine power supplies, one on the neutralizer voltage control unit, and two on the cesium-contact engine power supplies were potted with Stycast 2651-7%, catalyst No. 9. Because of their extremely high operating temperatures, the two connectors of the cesium-contact-engine subsystem were potted with Stycast 2662-7%, catalyst No. 9.

The connections were potted off the spacecraft, thus presenting a pigtail wire to be mated to the appropriate harness wire. This was accomplished using special techniques which converted AMP "helicon" disconnects and "window" splices to special high-voltage splices.

The prototype spacecraft T-1B-3 then qualified when subjected not only to a fast-pump-down vacuum test but also to a "quick dump" vacuum test. The potting and splicing techniques looked promising, but had not been proven for flight environments other than short duration vacuum. A program to evaluate both the splicing and the potting techniques was immediately initiated.

The evaluation program was successful in developing good, quality techniques to enable the field splicing of wires which are at high potentials and are required to operate in the SERT flight environment. The splices proved, with a limited number of test samples, the capability of operating at a level of 10 kilovolts at sea level, in vacuum, and at all levels in between including critical pressures.

The evaluation program, however, was marginal in developing a qualified technique for potting the harness to the high-voltage receptacles. Under stringent repetitive thermal cycling, failures occurred involving the separation, due to differential thermal expansion, of the potting from the glass seal at the base of the connector receptacle.

Arcing then occurred through residual air, at partial pressure, which flowed into the resulting void. The three most promising room-temperature curing materials tested were Stycast 2651, Scotchcast 9, and RTV-60 silicone rubber.

RCA did design an open-connector configuration termination which allows a fast escape path for air and is operable at sea level and in vacuum but not during the short flight transition period. An engineering model of this configuration was successfully built and vibration tested.

A complete report of the evaluation program is given in RCA Technical Memorandum TM-1602, "Evaluation of SERT High-Voltage Terminations and Interconnections" (Reference III-13).

A further change of note involved the addition of a spring-loaded cover over the "fly-away" umbilical connection to guard against the possibility, during test or in flight, of the ion-engine arcing through the plasma to the exposed connector pins.

2. Fuse Block

a. General

The development of the SERT fuse block was initiated as a result of the burn-out of a power-switching unit which was being used in ion-engine development testing at the NASA Lewis Research Center. The burn-out of the unit occurred due to short circuits which were created when internal test fuses exploded under vacuum conditions and scattered metallic debris throughout the PSU.

The fuses are used in the SERT system to prevent the loss of the mission due to the drain of the batteries from a short in either of the two ion engine subsystems.

b. Functional Description

Two fuses are connected in parallel in the line which feeds 56 vdc to the mercury-bombardment engine subsystem. Two fuses are similarly connected in the 56-vdc feed line to the cesium-contact engine subsystem. The fuses are selected so neither steady state nor current surges emanating from ion-engine arcs will cause the fuses to blow. A permanent short, however, will blow the fuses within 10 seconds. The fuses are housed in separate compartments within a completely closed fiber-glass block (Figure III-44) in order to prevent the contamination of the spacecraft in the event of blown fuses.

c. Development

Standard ceramic 30-ampere aircraft fuses were being used in the power switching unit at the time of the fuse explosion. These fuses were intended for use during electrical testing only and would have been removed before flight. The evidence showed that the metallic parts had been heated, possibly even to a vapor, when the debris was scattered throughout the component. Judging from the type of debris, the cause of the explosion was thought to be from an overvoltage condition rather than the normal blowing of the fuse. In support of this, the fuse vendor insisted that the fuses would explode in vacuum only under over-voltage conditions. The aircraft-type fuse was therefore considered to be unsuitable for use in this application.

A survey of the market failed to turn up a space-proven fuse; one that would not only meet the rigors of space in normal operation but also would not explode in vacuum whether due to overcurrent or overvoltage or both. Low current fuses, using Pyrofuze wire encased in a fiber-glass block, had been developed by RCA for use in the Ranger program*. The Ranger fuses encouraged further development in this area.

*The Ranger TV Subsystem was designed and built by the Astro-Electronics Division of RCA for the Jet Propulsion Laboratories of the California Institute of Technology under NASA Contract No. NAS 7-100 (JPL Contract No 950137).

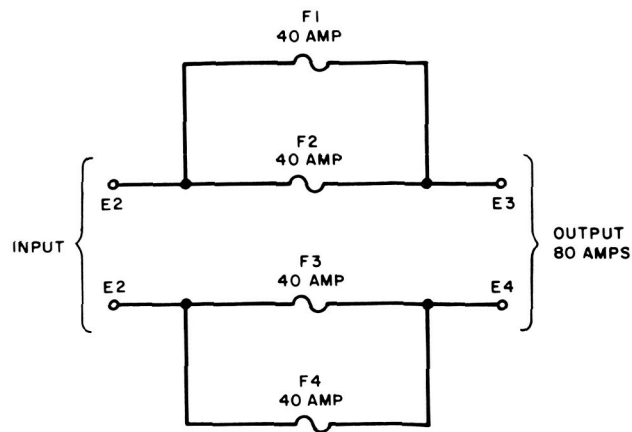


Figure III-43. Schematic Diagram of the Fuse Block

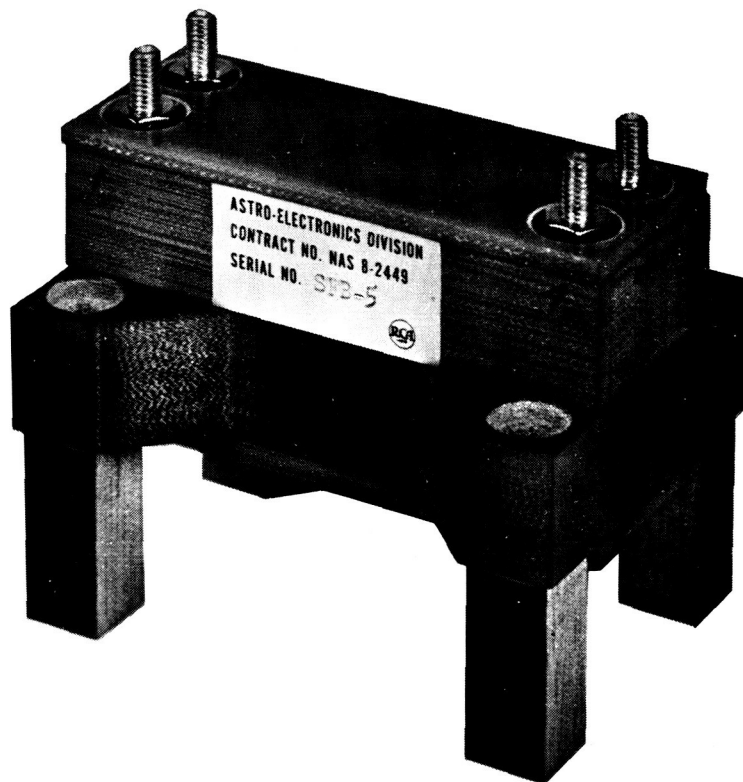


Figure III-44. Fuse Block

Pyrofuze wire is a proprietary composite wire having a core of aluminum and a sheath of palladium in the ratio of 1.25 to 1 by weight, respectively. When heated to 680°C, an exothermic chemical reaction, deflagration, is initiated which propagates along the wire without the need for external power or oxidizer. The wire melts, since temperatures up to 2800°C are generated, opening the circuit positively and rapidly.

The fuse specifications were jointly drawn up by NASA and RCA such that each fuse would be capable of carrying a current of 60 amperes continuously for 5 hours at 50° C in vacuum, while 80 amperes will blow the fuses within 90 seconds at 10° C.

Samples of the Pyrofuze wire of various diameters were made. These samples were designed to operate to the specifications. These were tested at RCA, and resulted in a fuse which consisted of a two-inch active length of LoR (a 0.050-inch diameter Pyrofuze wire when used with particularly-sized end studs).

The end studs were designed to minimize the effects of the thermal environment and the current-carrying losses of the connecting wire and the studs themselves, such that the active length of Pyrofuze wire was only sensitive to its current-carrying losses. The end studs were also designed to withstand the extreme temperatures which develop when a fuse blows.

Each fuse is positioned within an alumina tube to contain the deflagration products. In addition, each fuse is housed in a separate chamber in a fiber-glass block to isolate any outgassing material. The fiber-glass block also provides high-voltage isolation of the circuitry from ground.

In addition to the qualification testing of the prototype model and acceptance testing of the flight models (both of which are non-destructive), one of the flight model units was selected at random and successfully subjected to the destructive test.

REFERENCES

- III-1 RCA Technical Memorandum TM-1104, "Effect of Ion Engine Exhaust on SERT Communication," Contract NAS-8-2449, Mar 4, 1963.
- III-2 RCA Technical Memorandum TM-1105, "SERT Signal Conditioner Data," Contract NAS-8-2449, Apr 1, 1963.
- III-3 RCA Technical Memorandum TM-1103, "Technical Report - SERT Signal Conditioner," Contract NAS-8-2449, Oct 5, 1962, revised Dec 30, 1963.
- III-4 RCA Document SPO-11, "SERT Signal Conditioner Scale Factors," Contract NAS-8-2449, Oct 22, 1962.
- III-5 RCA Technical Memorandum TM-1106, "Report of a Study of the Addition of Mechanical Commutators to the SERT Telemetry Subsystem," Contract NAS-8-2449, Jan 27, 1964.
- III-6 RCA Document SPO-46, "Mechanical Commutator Qualification Electrical Test Procedure," Contract NAS-8-2449, Oct 12, 1963.

- III-7 RCA Specification 1175389, "SERT Environmental Testing Specification."
- III-8 RCA Document SPO-18, "Documentation of Test and Failure History of Vector Subcarrier Oscillator Packages," Contract NAS-8-2449, Jan 23, 1963.
- III-9 SERT Logbook for Prototype No. 1 Antenna System, NAS-8-2449.
- III-10 SERT Logbook for Prototype No. 2 Antenna System, NAS-8-2449.
- III-11 Fubini and Johnson, "Proceedings of the IRE," (36: 1461) 1948.
- III-12 RCA Document SIM-46, "SERT Mechanical Commutator Operation Report," NAS-8-2449.
- III-13 RCA Technical Memorandum TM-1602, "Evaluation of SERT High-Voltage Terminations and Interconnections," NAS-8-2449.

SECTION IV

SPACECRAFT DYNAMICS

A. INTRODUCTION

The SERT spacecraft must be stabilized to provide a frame of reference against which the thrust of the ion engines can be measured. For reasons which shall be discussed in this section, spin-stabilization was chosen. The spin, at a rate of approximately 100 rpm, is imparted to the spacecraft before booster separation by spin-up rockets attached to the Scout fourth stage. After separation, the increase in spin-axis moment of inertia resulting from the extension of the ion engines causes a decrease in the spin rate of approximately 15 percent.

Disturbance torques such as those introduced by separation forces or by extension of the engines may create an angular velocity about an axis other than the original spin axis. As a result, the spacecraft nutates or wobbles in a conical pattern about the angular momentum vector of the spacecraft. To reduce the nutation to a low value (less than 1 degree) so that its effect on spin-rate determination is minimized, tuned energy-absorption mass (TEAM) precession dampers are mounted on SERT.

Spin-stabilization was particularly desirable for SERT because the method offers advantages not otherwise achievable in as simple a fashion. The advantages are:

- (1) A simple approach to the measurement of engine thrust through change of spin rate is established. Alternate approaches would involve the use of a stabilized platform or an active attitude-control system, which would greatly increase complexity and weight.
- (2) The orientation control of the spin axis thus achieved permits the measurement of spin rate, and hence the determination of engine thrust with simple instrumentation (sun sensors).
- (3) The attitude control afforded by spin stabilization permits the rf energy to be concentrated in the lower hemisphere beneath the spacecraft baseplate, reducing the rf power requirement below that needed for isotropic radiation. During flight, all of the ground stations are in this lower hemisphere.
- (4) Spin provides the centrifugal force necessary to extend the ion engines.

- (5) The angular momentum of the spinning vehicle provides a buffer against unwanted torques, including those generated by the engine thrust about axes transverse to the spin axis.

The ratio of engines-extended to engines-folded spin rate is given by the relationship

$$\frac{N_{\text{ext}}}{N_{\text{folded}}} = \frac{I_{\text{sp(folded)}}}{I_{\text{sp(ext)}}} = 0.826$$

where

N is the spin rate in rpm and

I_{sp} is the spin-axis moment of inertia in slug-ft².

Thus, an engines-extended spin rate of 82.6 rpm would result from an initial rate of 100 rpm.

B. MEASUREMENT OF ENGINE THRUST

1. General

During flight, the SERT ion engines are positioned such that their thrust axes are normal to the spacecraft spin-axis. This condition permits the thrust of the engines to be measured by its effect on spacecraft spin rate. Extension of the engines places the thrust axes at an extended moment arm providing increased sensitivity of the spacecraft spin rate to engine thrust.

The geometry necessary to determine the relationships between spin rate change and thrust are shown in Figure IV-1. The equation for spin-rate change is

$$\dot{\omega} = \frac{F Y_{\text{eng}}}{I}$$

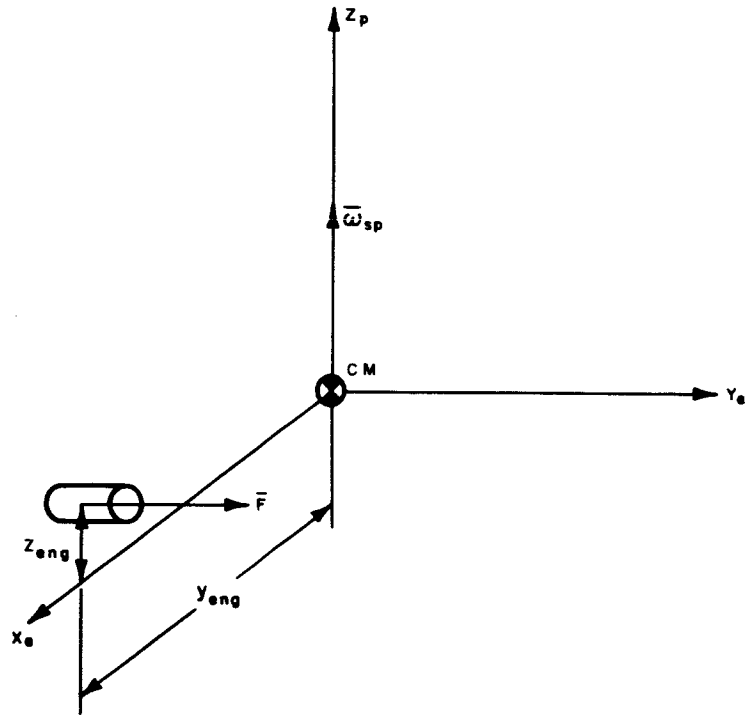
where

$\dot{\omega}$ is the spin rate;

F is the engine thrust;

Y_{eng} is the thrust moment arm; and

I is the spin-axis moment of inertia (engines extended).



X_e is the engine reference axis (\perp to \bar{F});

Y_e is the engine reference axis (\parallel to \bar{F});

Z_p is the spin axis (principal axis);

$\bar{\omega}_{sp}$ is the spin vector;

\bar{F} is the engine thrust vector; and

Y_{eng}, Z_{eng} are coordinates of the engine force vector.

Figure IV-1. Spin-Rate and Engine-Thrust Geometry

The relationship between spin-period change and thrust is given by the equation*

$$F = \frac{\pi I N^2}{1.80 \times 10^6 Y_{\text{eng}}} \left| \frac{\Delta T}{\Delta t} \right|,$$

where

F is thrust in millipounds;

Y_{eng} is thrust moment arm in feet;

I is spin axis moment of inertia in slug ft²;

N is spin rate in rpm;

ΔT is change in spin period in microseconds; and

Δt is time increment in seconds.

Anticipated values of period rate of change for the SERT I flight are, for $I = 10.5$ slug ft² and $N = 90$ rpm:

<u>Engine</u>	<u>Thrust (millipounds)</u>	<u>Moment Arm (inches)</u>	<u>Spin-Period Rate of Change (μ sec/sec)</u>
Cesium-contact	1.6	21.75	19.6
Mercury-bombardment	6.0	22.0	74.0

The relationship between rate of change of spin period and engine thrust for a 22-inch moment arm is plotted in Figure IV-2.

*See Appendix E for the development of the equation

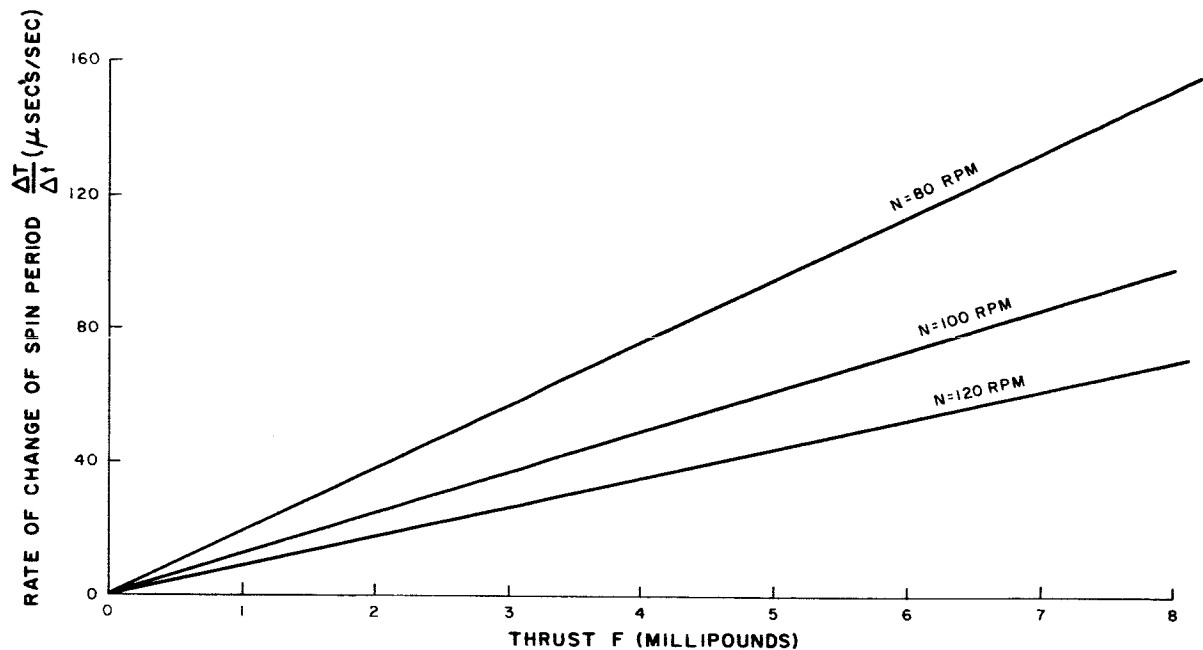


Figure IV-2. Spin-Period Change Versus Engine Thrust for a 22-inch Moment Arm

2. Thrust Measurement Systems

Spin rate may be determined to varying degrees of accuracy by any one of the following techniques incorporated in the SERT I system:

a. Sun Sensor System

This system for detecting spin rate employs, as its basic instrument, the sun sensor, which is designed to detect the passage of the sun once each revolution of the spacecraft. The train of pulses generated at successive sun crossings is telemetered to the ground station where it activates a set of counters to obtain continuous readings of spacecraft spin period.

b. Radial Accelerometer System

This system employs a highly-accurate accelerometer to detect spacecraft centrifugal acceleration. The frequency or digital output of the accelerometer directly modulates the rf carrier and is transmitted to the ground where special data handling equipment converts this signal to analog spin-rate information.

c. Ground Receiver AGC

This technique, intended as a back-up in the event of failure of the other systems, takes advantage of the fluctuation in the ground receiver AGC (automatic gain control) voltage created by the asymmetry of the spacecraft antenna pattern. Values of spin rate accurate to several percent may be obtained with this approach after several minutes of data smoothing; further treatment and longer integration of the data will provide increased accuracy.

Further discussion of the sun sensor system is presented below. The radial accelerometer is not discussed further since it is outside the area of RCA responsibility; however, for completeness, let it suffice to say that the input axis of the instrument is aligned along a radial from the spacecraft center of mass (c.m.) in order to detect the largest component of centrifugal acceleration while minimizing inputs due to spin-axis nutation.

A block diagram of the sun sensor system is shown in Figure IV-3. The part of the system lying within the spacecraft is redundant in all active electronics, with the antenna and its diplexing networks being completely passive elements. Redundancy is also provided through the ground receiving and discriminating system, although audio signal recording must be depended upon to provide back-up in the event of ground equipment failure.

The sun sensor, described in detail in Paragraph III-1 G.2, consists of a silicon solar cell placed behind a narrow (1 degree wide) slit aligned parallel to the spacecraft spin axis. A sketch of the sun sensor's geometric relationship is given in Figure IV-4. Once during every revolution of the spacecraft, the sun's rays impinging on the cell produce a voltage which triggers a one-shot multivibrator. The rectangular pulse output of this circuit is highly reproducible both in shape and magnitude; hence, time measurements between successive pulses provide an excellent measure of the spacecraft spin rate.

The sun-sensor slit subtends an angle in the plane of the spin axis between approximately 75 degrees above and 30 degrees below the baseplate plane (normal to the spin axis). The sun sensor system will, therefore, operate whenever the sun lies within this angular range. The launch trajectory and time of launch must be selected so that, after separation, the angle between the inertially-fixed spin axis and the line to the sun meets the specified requirements. The trajectory and launch "window" may be selected to meet tighter requirements to reduce the cyclic modulation of spin period which arises from spin-axis nutation.

The sun-sensor output pulse is fed to a voltage-controlled subcarrier oscillator, whose output is summed with other telemetry signals before modulating the transmitter. As shown in Figure IV-3, the rf signals are transmitted to the ground station, where the discriminated subcarrier signals are fed to the spin-rate rack. A switch is provided so that the signal from either of the two redundant sun sensors may be selected.

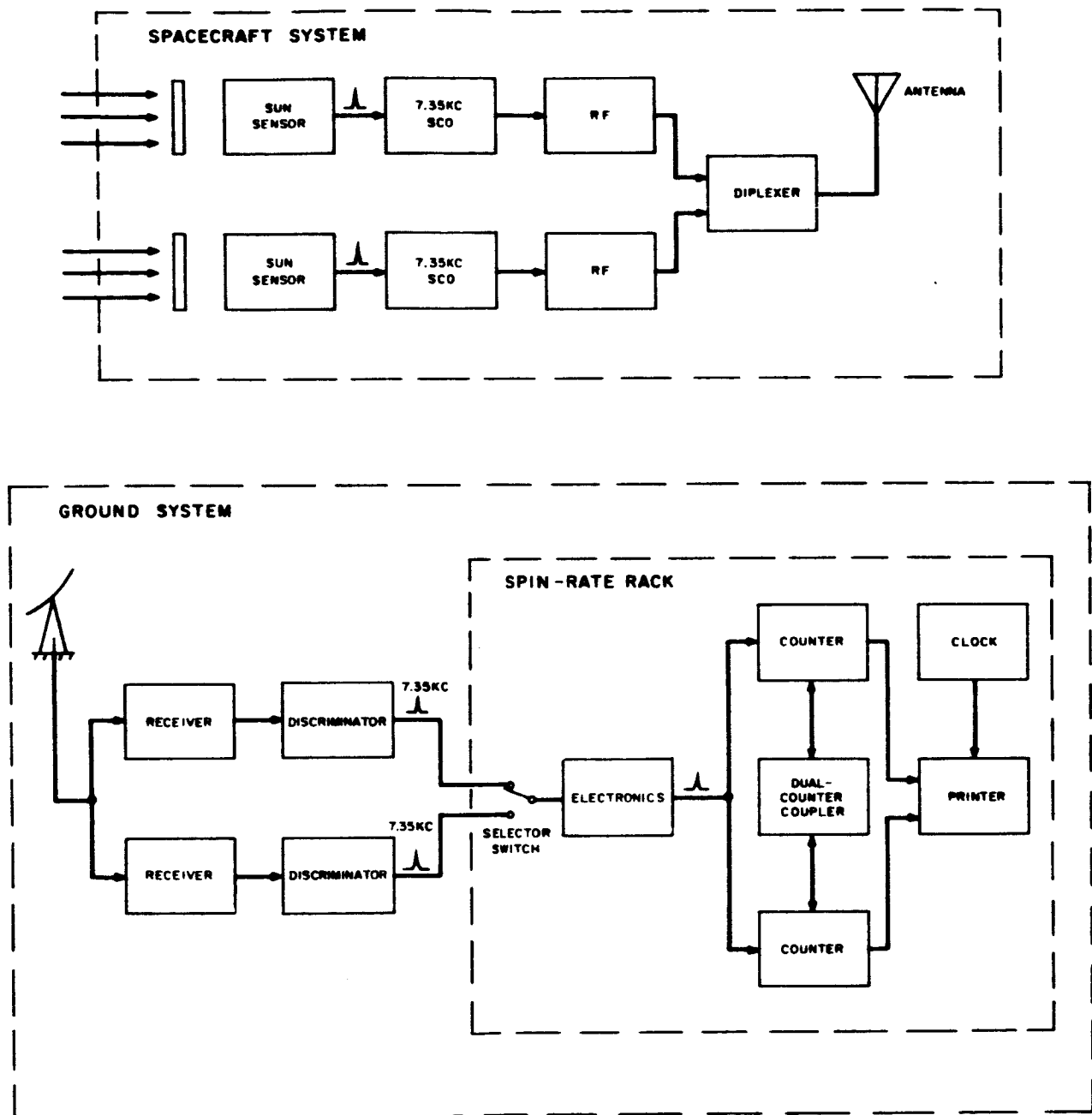


Figure IV-3. Block Diagram of Sun-Sensor System for Spin-Rate Detection

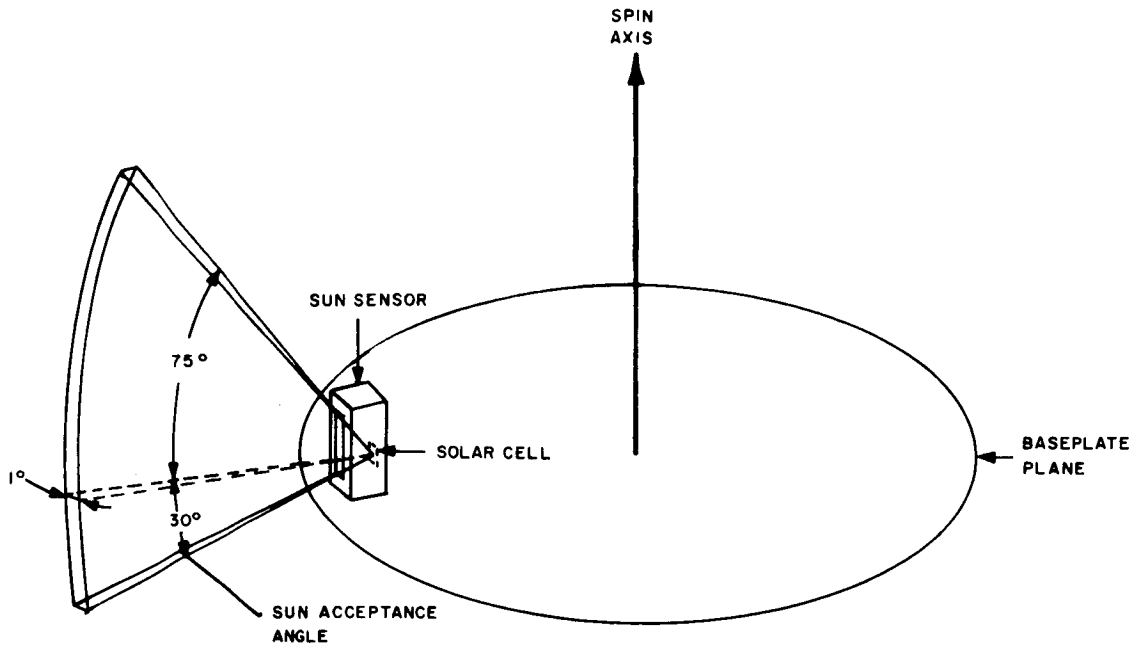


Figure IV-4. Sun-Sensor Geometric Relationships

The operation of the spin-rate rack is fully covered in Section V-D. Briefly, this equipment consists of an electronics board, two counters, a dual counter coupler, a printer, and a timing clock. The electronics contains a Schmitt trigger and flip-flop circuitry for a divide-by-ten function (optional). The two counters and coupler are arranged so that each pulse starts one counter while stopping the other. The duration count of each counter, alternately, is recorded on the printer along with running-time from the clock, thus providing a continuous record of successive spin periods. The spin-rate rack is arranged to record to the nearest microsecond.

3. Thrust Measurement Errors

Errors in the spin-period measurement arise either within the system itself or from the dynamics of the spinning spacecraft. System errors may be seen as developing within the sun sensor electronics, communications link, and spin-rate rack. An experimental study to measure system error was conducted on an analog system consisting of a light source, sun sensor, subcarrier oscillator, discriminator, counter, and printer (refer to Appendix F). With the transmitter-to-receiver error derived analytically, a total 3-sigma error in period is broken down as follows:

Sun Sensor	9 microseconds
SCO - Discriminator	7 microseconds
Communications path	1 microsecond
<u>Spin Rate Rack</u>	<u>20 microseconds</u>
Total (root square sum)	23 microseconds

This uncertainty over one period would cause an acceleration measurement error, greater than that expected for the cesium-contact engine, of 19.6 usec/sec. When handled statistically over a large number of cycles, however, the error will reduce quite rapidly, as expressed by the following equation (refer to Appendix K):

$$\sigma (T) = \frac{6 \sqrt{S} \sigma (T)}{\sqrt{N^2 - 1} \sqrt{N^2 - 4} \sqrt{N} T}$$

The error after 10 cycles of mean-square fit would then be 0.25 usec/sec at 90 rpm, or one percent of the acceleration expected due to cesium-contact-engine thrust.

Errors in thrust measurement related to the dynamics of the spinning vehicle may arise from a number of sources (refer to Appendixes G and H). Briefly, the major errors investigated are:

- a. Thrust-axis misalignment,
- b. Thrust-axis offset,
- c. Moment-of-inertia change due to thermal expansion, and
- d. Nutation.

From past experience it was decided that effects of micrometeorite impacts, magnetic field interactions, and differential gravity torques were too small to consider.

The largest source of error in spin-period measurement is spin-axis nutation. For SERT, the maximum period-error per cycle can be as large as 350 usec at steady-state nutation, a sun-spin axis angle of 70 degrees, and a spin rate of 90 rpm (refer to Appendix J). As discussed in Appendix K, this data can also be handled statistically, although after one minute of simple averaging the error in acceleration measurement would rapidly fall below one percent of that expected due to the thrust of the cesium-contact engine.

The largest steady-state error determined analytically was 2.25 percent of the expected thrust (1.6 millipounds) of the cesium-contact engine. This value was the result of spacecraft expansion due to an assumed 50° C temperature rise. However, since this effect is not random, and temperature distribution data is available, the thrust uncertainty can be reduced to less than 1/2 percent of the expected cesium-contact-engine thrust after a correction is applied. Large bias errors can also be anticipated during nutation damping, but these are limited to the first several minutes after separation and engine extension.

An additional error of great significance is that caused by the moment arm itself. While center-of-gravity, spin axis, and geometrical measurements can be made which provide moment arm accuracies within several tenths of a percent, the greatest uncertainty is in the position of the total thrust vector within the ion beam. It is hard to conceive of this error exceeding 5 percent, although estimates could best be provided by the ion-engine developers.

C. THE PRECESSION DAMPER

1. General

The SERT spacecraft design included two (for redundancy) tuned energy-absorption mass (TEAM) precession dampers to remove excess nutational motion from the spinning vehicle. The TEAM precession dampers were developed for NASA as part of the TIROS satellite* program (Reference IV-1). In TEAM, the absorbing mass does not itself absorb energy, but by its motion it produces friction which dissipates energy in the form of heat. Since the motion of the TEAM mass is due to the motion of the spacecraft, a one-way energy flow occurs (conversion of kinetic energy to heat). This energy conversion process continues until no more precession is present and the body spins about its maximum moment of inertia.

2. Functional Description

The TEAM precession damper, shown in Figure IV-5, consists of an enclosed mechanism, which is mounted parallel to the spin axis at the maximum possible radial distance.

The mechanism consists of a supporting structure housing a moving mass. The mass is confined to roll (on bearings) along a curved track or rod. A means of varying the curvature of the rod is provided in order that the natural frequency of oscillation of the mass can be tuned to the forcing frequency encountered during nutation of the vehicle, as the mass moves back and forth along the rod. Since an unfavorable inertia ratio (which augments the build-up of nutation) exists during the boost period, the precession damper mechanism is provided with a metallic pin to cage the mass during launch. At separation of the spacecraft from the launch vehicle, squibs are fired which release the caging pin, allowing the sliding mass to move back and forth along the rod. Firing of the squibs by ground command is provided as back-up to the programmed operation.

An oscillating acceleration field, set up by any major nutation of the vehicle, causes the sliding mass to traverse back and forth on the curved rod. This motion produces friction, which dissipates mechanical energy in the form of heat. Since the conversion

*The TIROS satellite was designed and built by the Astro-Electronics Division of RCA for NASA under contract No. NAS 5-3173.

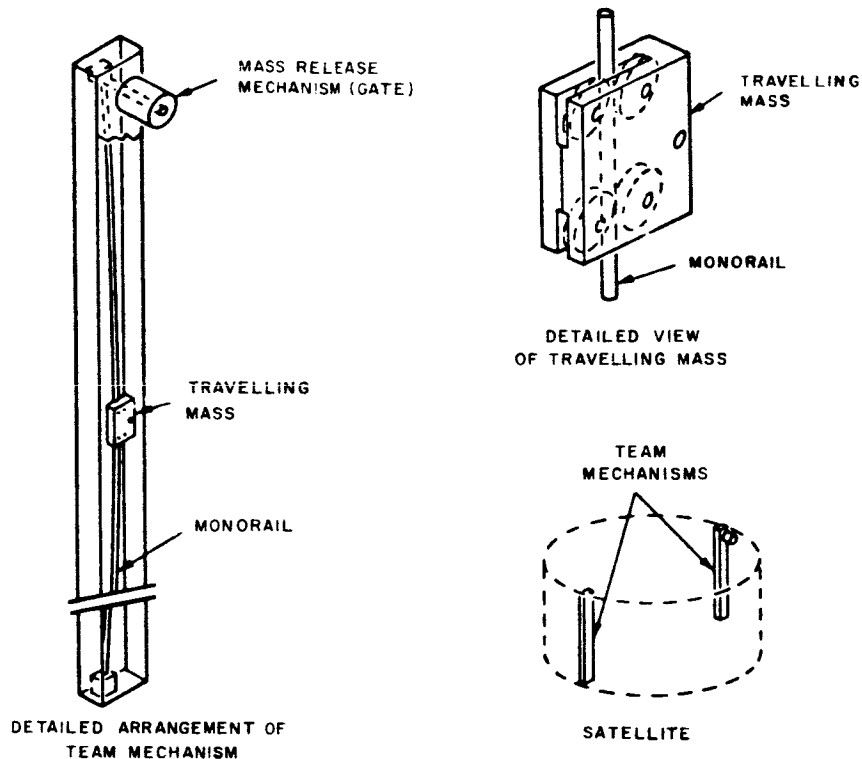


Figure IV-5. Precession-Damping Mechanism

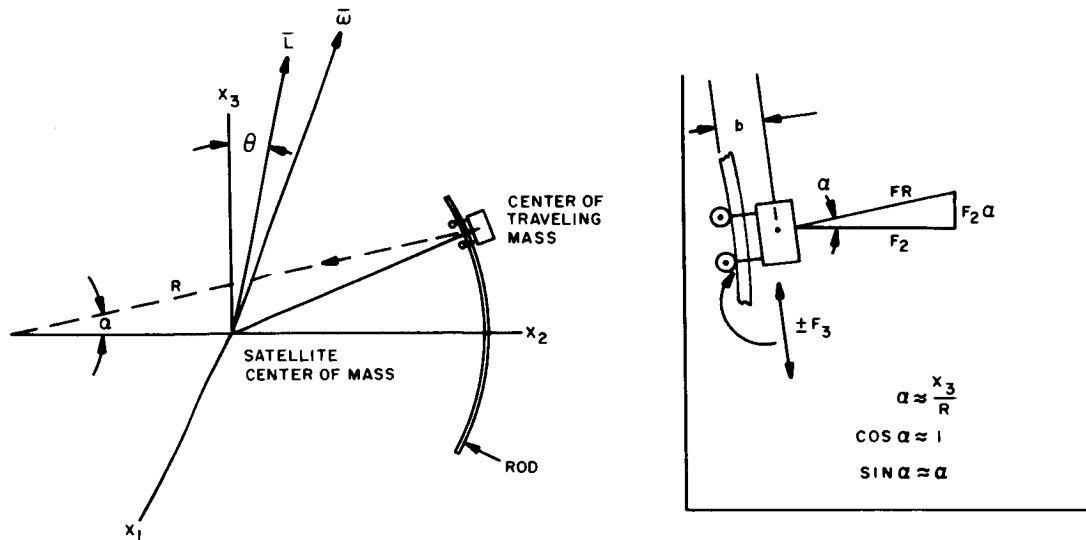
of kinetic energy to heat is a one-way energy flow, the energy associated with the nutation is continuously dissipated until the response threshold of the damper is reached. The sliding mass then ceases to move and the dissipation of nutation, now dependent upon flexure of the structure alone, will continue at a much lower rate.

Ultimately, the spacecraft reaches a state of nearly uniform spin about its axis of maximum moment of inertia, with the sliding mass at rest at, or near, the center of the monorail.

3. Design Analysis

This design analysis section contains a brief analytical background of the TEAM precession damper. To make the equations amenable to simple solution, it is assumed that the moments of inertia about the principal axes transverse to the spin axis are equivalent.

The geometry shown in Figure IV-6 (a coordinate system X_1, X_2, X_3 , fixed to the spacecraft) was used in the method summarized here. Assume rotation about one axis (X_3) fixed to the spacecraft while the entire spacecraft coordinate system rotates about a line fixed in space. This line is in the direction of the total angular momentum of the spacecraft at the instant of release from the final stage. These two rotations may be combined into one angular velocity which does not coincide with either the angular momentum vector or the spacecraft spin axis.



\bar{L} AND ω HAVE COMPONENTS IN x_1, x_2, x_3 DIRECTIONS
 ROD LIES IN x_3-x_2 PLANE
 x_1, x_2, x_3 ARE FIXED TO SATELLITE

Figure IV-6. Coordinate System for TEAM Precession-Damping Mechanism

Before engine thrust can be measured, it is necessary to reduce the angle between the instantaneous velocity vector (ω) and the spacecraft spin axis (X_3) to a small value. If energy is removed from the system while a constant momentum is maintained, the desired alignment of the spacecraft spin axis and instantaneous angular velocity will take place.

The following equations were used for determining the size of a TEAM precession damper and its limitations:

The forcing frequency to which the TEAM is tuned is

$$\dot{\psi} \approx K |\omega_3| = \sqrt{\frac{(I_3 - I_1)(I_3 - I_2)}{I_1 I_2}} |\omega_3| \quad (IV-1)$$

where

ω is the forcing frequency in radians/sec;

$\omega_1, \omega_2, \omega_3$ are the components of the spacecraft's instantaneous velocity vectors resolved into the spacecraft fixed coordinates in radians/sec; and

I_1, I_2, I_3 are the principal moments of inertia of the spacecraft.

The natural frequency of TEAM is

$$\omega_n = \omega_3 \sqrt{\frac{r}{R}} \quad (\text{IV-2})$$

where r is the distance of rod from the center of mass of the spacecraft, and R is the radius of rod, from which tuning is achieved when

$$\frac{r}{R} = K^2. \quad (\text{IV-3})$$

The energy which must be dissipated to make the spacecraft reduce its precession angle from θ_1 to θ_2 is

$$\Delta T \approx \frac{1}{2} \frac{I_p}{I_3} \left[\frac{1}{p} - 1 \right] (\omega_3)^2 \left[(\theta_1)^2 - (\theta_2)^2 \right] \quad (\text{IV-4})$$

where

ΔT is the change in energy of the spacecraft required to produce a change of precession angle from θ_1 to θ_2 ;

θ_1, θ_2 are the maximum and minimum angle in radians that the X_3 axis, fixed in the spacecraft, makes with the total angular-momentum vector \bar{L} ;

\bar{L} is the total angular momentum vector fixed in inertia space; and

$$I_p \approx \sqrt{I_1 I_2}.$$

For nearly perfect tuning, the loss of energy per cycle is

$$4f (X_3)_{\max}. \quad (\text{IV-5})$$

where

f is the friction force acting on damper traveling mass, in pounds, and

$(X_3)_{\max}$ is the half amplitude of motion, in inches.

This rate of energy loss is assumed to hold until the amplitude of precession, θ , reduces to a value such that

$$\theta = \frac{\mu}{(1-K^2)} \quad (\text{IV-6})$$

where

θ is the angle in radians that the X_3 axis, fixed in the spacecraft, makes with the total angular momentum vector, \bar{L} , and

u is the coefficient of friction (rolling).

Equations (IV-1) through (IV-6) are enough to establish design parameters and allow estimation of the time-to-damp precession to a value specified by Equation (IV-6). This equation is a relation involving Equations (IV-1), (IV-4), and (IV-5). It is sufficient for many applications in which the angle of precession is several times larger than the threshold value of the damper.

4. SERT T-3 Nutation Damping Characteristics

Tuning of the precession dampers for the T-3 spacecraft was calculated from Equation (IV-3)

$$R = \frac{r}{K^2} = \frac{12.8}{0.1068} = 120 \text{ inches.}$$

This radius of curvature is obtained by tuning the damper in a 1-g field for which the period of oscillation is given by

$$P = \sqrt{\frac{R}{9.80}} = 3.50 \text{ secs.}$$

The time-to-damp characteristics are expressed in Figure IV-4.

The rolling-friction threshold-nutation angle is obtained from Equation (IV-6):

$$\theta_{\text{roll}} = \frac{.0025}{(1-K^2)} \approx 0.16 \text{ degrees,}$$

and the static friction threshold, which determines the angle at which the damper will again operate after having been stopped, is

$$\theta_{\text{st}} = 0.32 \text{ degrees (twice } \theta_{\text{roll}} \text{)}.$$

The friction coefficients, u , were obtained from experiments performed under the TIROS program.

REFERENCE

- IV-1 TIROS I Meteorological Satellite System, Final Comprehensive Technical Report, (Volume II) Prepared for the U.S. Army Research and Development Laboratories and NASA by the Astro-Electronics Division of RCA, Jul. 1, 1961

SECTION V

GROUND EQUIPMENT DESIGN AND DEVELOPMENT

A. GENERAL

The SERT ground equipment consists of three basic complexes of electronic equipment which control and monitor the operation of the SERT spacecraft during all phases of its testing and its flight performance. The ground equipment complexes include (1) the RCA Laboratory Test Station used in the electrical operation of the spacecraft at AED, (2) the Wallops Island Launch Checkout Equipment used in the electrical operation of the spacecraft during prelaunch testing at the NASA Lewis Research Center and at the Wallops Island launch site, and (3) the Flight Monitoring and Control Equipment used for monitoring and control of the spacecraft during launch and flight operations at Wallops Island and the Bermuda tracking station. The RCA Laboratory Test Station served as a model for the SERT Electronics Van, which is a part of the Wallops Island Launch Checkout Equipment.

The following paragraphs provide a description of the basic functional and physical characteristics of the SERT ground equipment and a history of its design and development.

B. RCA LABORATORY TEST STATION

1. Description

The RCA Laboratory Test Station consists of a semi-permanent electronics installation in the clean-room facility at AED. The installation consists of nine racks of equipment, portable test equipment, and cabling that connects the clean-room area with the AED environmental test area. Detailed photographs of the major special equipment are presented in Figures V-1, V-2, and V-3. The nine racks of equipment can be grouped into the following functional categories:

- a. Checkout Control Equipment Rack (1 rack—Rack 1, Figure V-1)
- b. Telemetry Receiving and Decommutation Equipment Racks (3 racks—Racks 4, 5, and 6, Figures V-2 and V-3)
- c. Data Presentation and Recording Equipment Racks (4 racks—Rack 2 shown in Figure V-1 and Rack 7 in Figure V-8; the other two racks consist mainly of standard commercial equipment.)
- d. Command Test Equipment Rack (1 rack—Rack 5, Figure V-2)

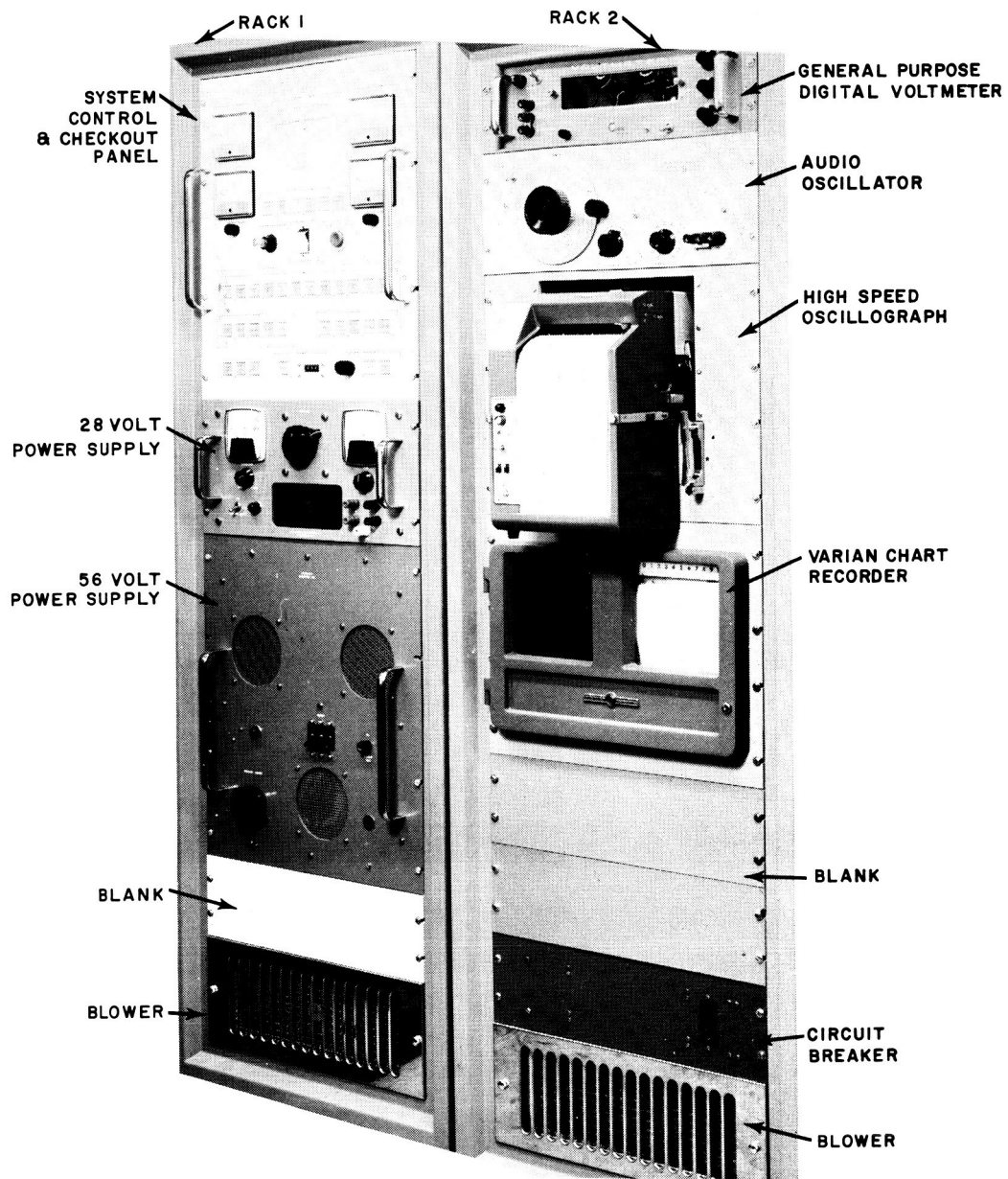


Figure V-1. Laboratory Test and Control Equipment, Racks 1 and 2

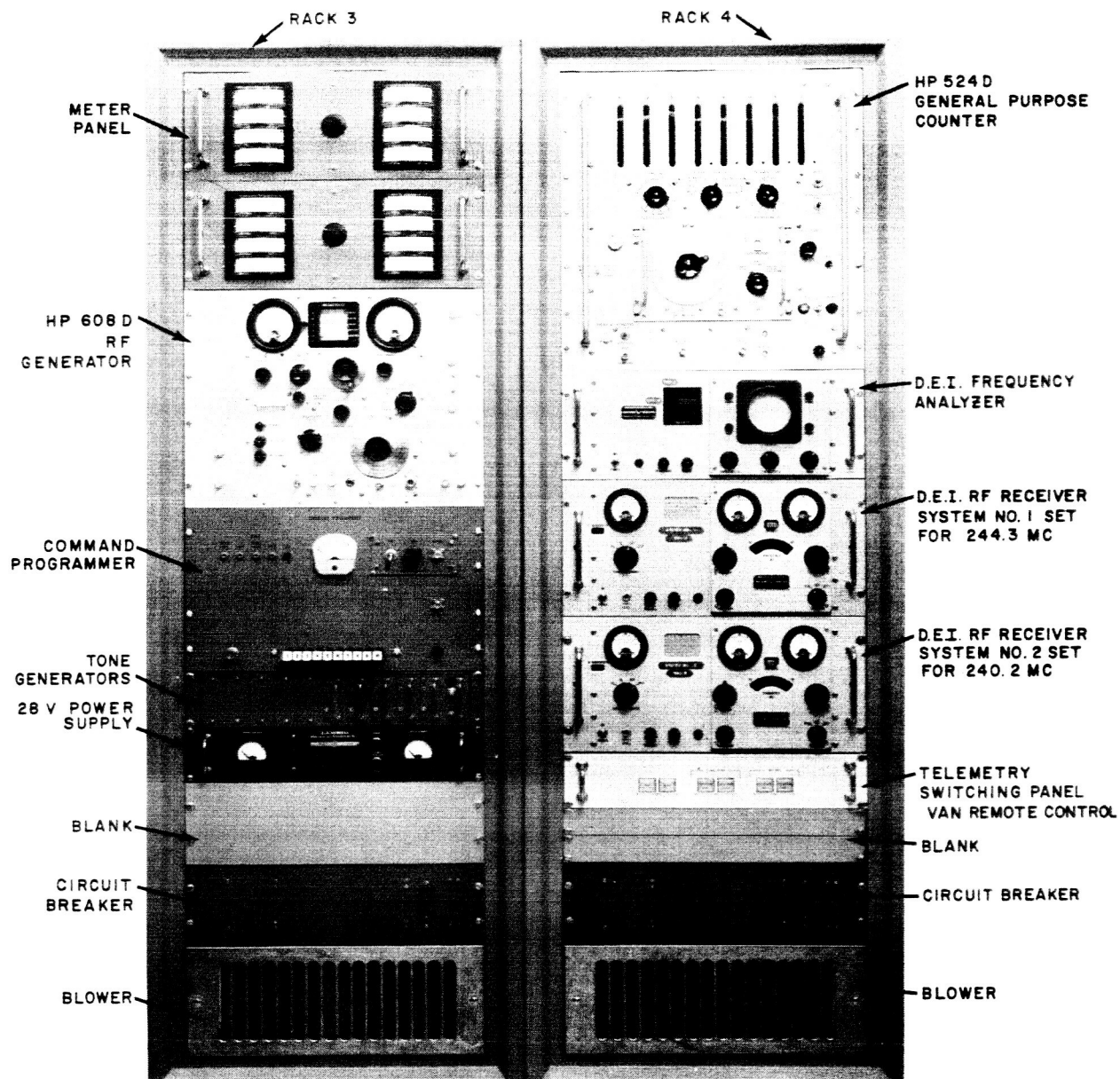


Figure V-2. Laboratory Test and Control Equipment, Racks 3 and 4

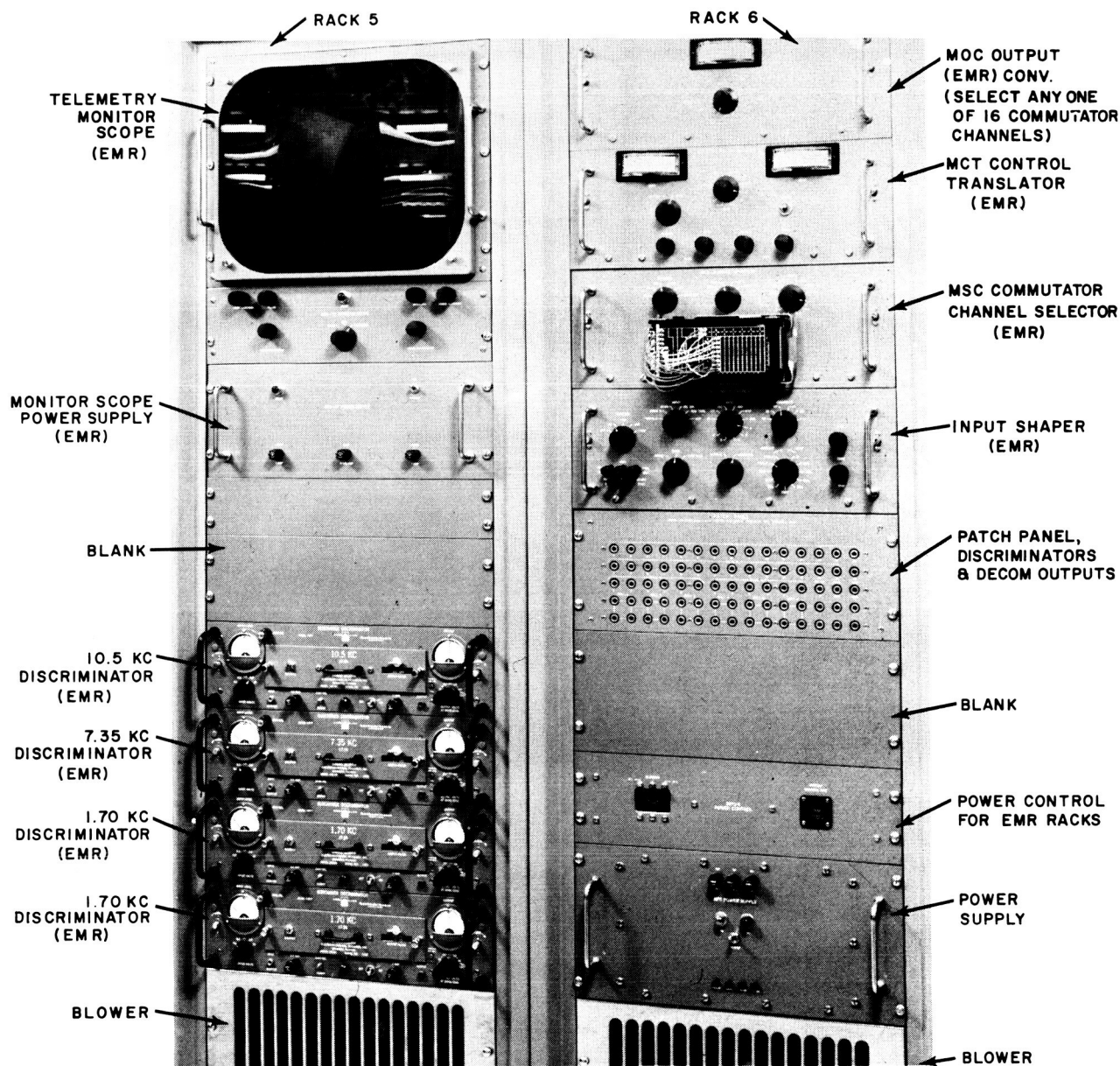


Figure V-3. Laboratory Test and Control Equipment, Racks 5 and 6

Table V-1 lists the equipment contained in the RCA Laboratory Test Station. The test station is used to energize and control the operation of the SERT spacecraft and monitor its performance during electrical debugging operations and during all phases of qualification and acceptance testing at AED.

Electrical debugging of the spacecraft is performed within a fence enclosure in the clean-room area. The electrically-interlocked fence protects the test personnel from the spacecraft high voltages which exist during testing. Adjacent to the fence enclosure are the racks of equipment and special portable test devices employed in the test operation.

Environmental qualification and acceptance testing of the SERT spacecraft is conducted at facilities remote from the clean-room area. Operation of the spacecraft at the remote environmental test location is accomplished using the test equipment located in the clean-room area. Cabling connects the clean-room area with the AED environmental test area.

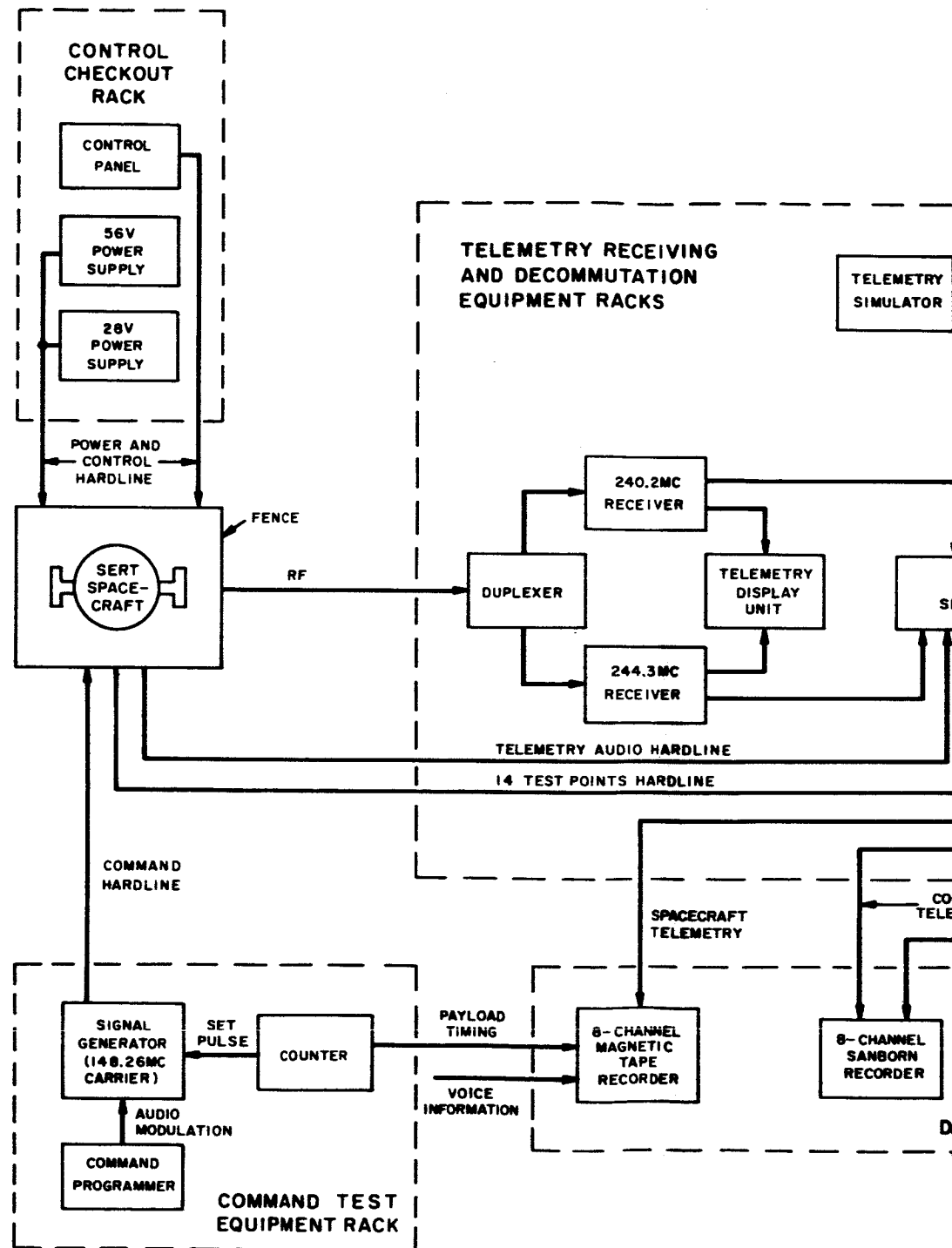
2. Development

The final configuration of the RCA Test Station closely resembles its original design concept. During the development of the station a number of improvements were made to facilitate its use. One major improvement was the addition of a magnetic tape recorder and two 8-channel Sanborn recorders to the data presentation and recording equipment. This addition provided the equipment with the capability to store test data on tape and to provide a continuous display of decommutated data. Two other changes made to the test station included replacement of the sound-powered phone intercom system with an audio system capable of driving the newly-acquired magnetic tape recorder so that voice observations could be recorded and addition of a subcarrier oscillator calibration box to test and calibrate the fm subcarrier oscillators. Other minor pieces of equipment were added to facilitate (1) measurement of the rf transmitted power, (2) performance of tests on the neutralizer voltage control unit with the unit mounted on the spacecraft, and (3) performance of the squib-firing tests. The soundness of the basic design of the test station (and the changes that were made to it) was verified by extended use of the station throughout the 2 1/2-year SERT program.

The test station equipment racks are described in detail in the following paragraphs. A block diagram of the RCA Laboratory Test Station is shown in Figure V-4.

TABLE V-1. RCA LABORATORY TEST STATION EQUIPMENT RACKS

Unit	No. of Units
Checkout Control Equipment Rack	
Control Panel	1
56 V Power Supply	1
28 V Power Supply	1
Telemetry Receiving and Decommutation Equipment Racks	
Telemetry Monitor Scope	1
Monitor Scope Power Supply	1
VHF Telemetry Receivers	2
Telemetry Display Unit	1
Telemetry Selection Panel	1
Precision Subcarrier Discriminators	4
Channel Selector	4
MOC Output Converter	1
MCT Control Translator	1
MCS Commutator Channel Selector	1
MIS Input Shaper	1
Patch Panel	1
MPC Power Control	1
MPS Power Supply	1
Telemetry Simulator	1
Data Presentation and Recording Equipment Racks	
Magnetic Tape Recorder	1
18-Channel Recorders	2
Chart Recorder	1
High Speed Oscillograph	1
MMU Meters	
Command Test Equipment Rack	
VHF Signal Generator	1
Electronic Counter	1
Frequency Counter	1
Time Interval Unit	1
Command Programmer	1



V-7

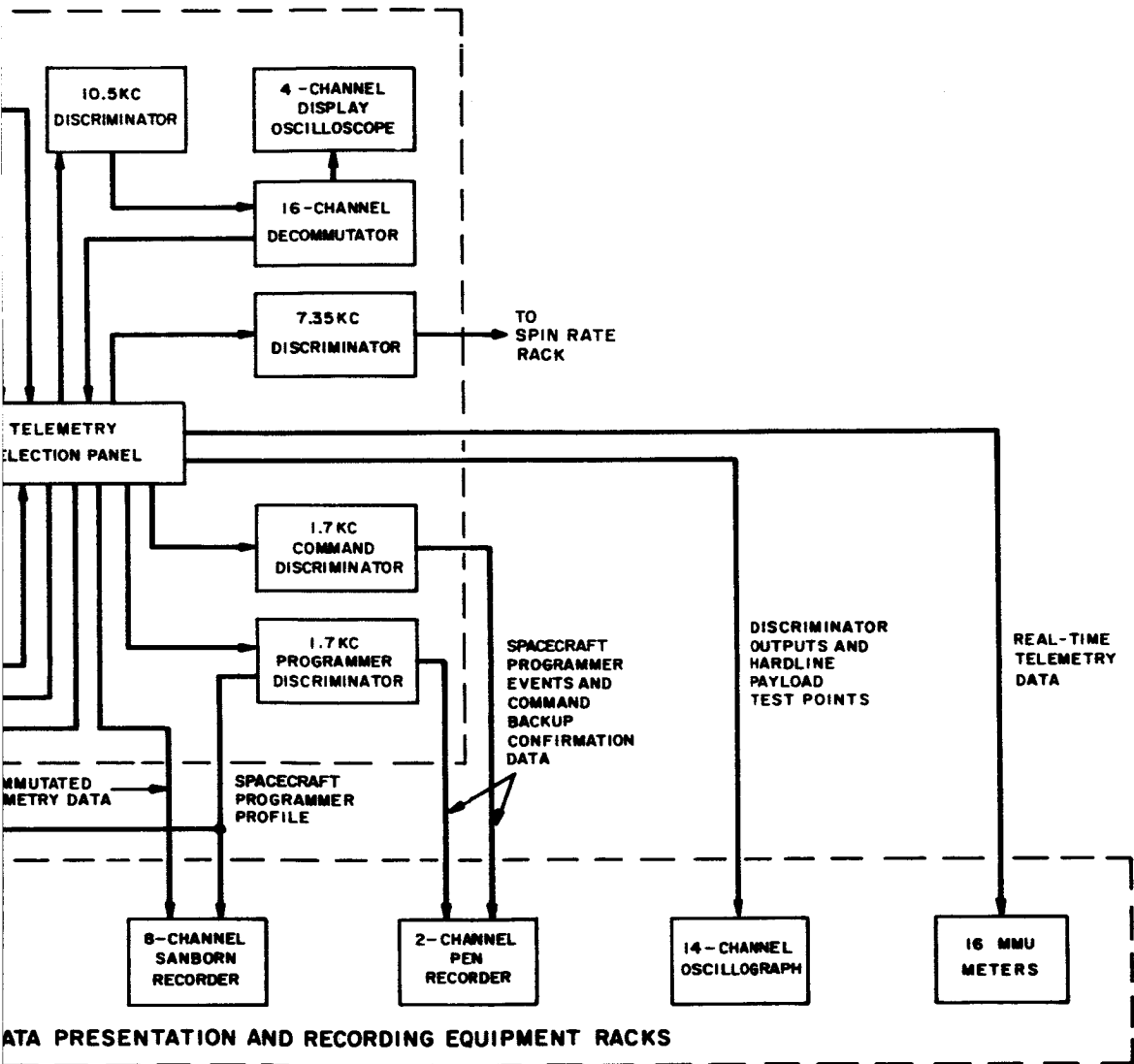


Figure V-4. Block Diagram of the RCA Laboratory Test Station

V-8

3. Checkout Control Equipment Rack

a. General

The SERT checkout control unit was designed to simulate the spacecraft battery power source and to provide a facility for hardline control of the spacecraft operation and hardline monitoring of performance during testing. The checkout control unit consists of a control panel and two power supplies installed in a standard six-foot by nineteen-inch electronics rack. All the hardline interconnections between the spacecraft and the control panel are listed in RCA Document S-19 "SERT Umbilical Requirements" (Reference V-1).

b. Control Panel

The control panel provides the facility for energizing and de-energizing all of the spacecraft subsystems and for direct monitoring of the operation of each of the subsystems by means of hardwire connections. It controls and monitors the external spacecraft power, the telemetry equipment, the rf transmission equipment, miscellaneous components, and the two independent ion engine subsystems.

The control panel also arms and fires all spacecraft squibs, enables stepper control of the neutralizer voltage control unit, externally drives the programmer at a rate which is adjustable by panel control, provides information on the mode of the auxiliary command unit, tracks the programmer with a counter and accomplishes various other testing operations. An output pulse every ten counts of the programmer is also provided for data recording use.

The control panel has the facility to duplicate the function of the launch control panel which enables it to simulate the launch mode of spacecraft operation during testing. The operation of the control panel in the external mode enables it to supply complete power to the external spacecraft and to monitor and control specific spacecraft functions.

c. Power Supplies

The external power is supplied by two power supply units in the checkout control rack. Both units have a power capability exceeding the anticipated demand. This is done to overcome the considerable line drop that develops during remote-location testing. The unit which is normally used to supply up to 26 amperes to the spacecraft at 56 vdc has the capability of supplying 30 amperes at 80 vdc; the other unit which is used to supply up to 13 amperes at 28 vdc has the capability of supplying 15 amperes at 36 vdc. Remote sensing is used to provide the required load regulation. The 28-volt power supply also provides power for the control panel.

4. Telemetry Receiving and Decommuration Equipment Racks

a. General

The telemetry receiving and decommuration equipment receives the telemetry signals from SERT and prepares them for visual presentation. This equipment, which consists of telemetry receivers, discriminators, and a decommurator, is installed in three 6-foot by 19-inch electronics racks.

b. Telemetry Receiving Equipment

The telemetry receiving equipment consists of two standard fm telemetry receivers with plug-in crystals for optimal local-oscillator frequency control, a telemetry display unit, and a telemetry selection panel. The multiplexed rf output from the spacecraft is fed to the two receivers. The telemetry display unit displays each carrier and its associated deviation on a CRT. The receivers provide a mixed audio output to the telemetry selection panel; the outputs are also recorded on a magnetic tape recorder.

c. Telemetry Discriminators

The mixed telemetry signals are demodulated by four precision subcarrier discriminators. The particular type of discriminator employed permits selection of the frequency to be demodulated by use of a plug-in unit. The four discriminators with plug-in units, to IRIG standards, provide demodulation of the SERT telemetry subcarriers; one at 10.5 kc, one at 7.35 kc, and two at 1.7 kc. The discriminators are connected into the test station as shown in Figure V-4.

d. Telemetry Decommurators

The decommuration of the SERT PAM pulse train is accomplished by a decommuration complex mounted in two 6-foot by 19-inch electronics racks. The complex provides decommuration of any 16 of the 43 data channels of the SERT pulse train by use of a snap-in patchboard. In normal operation, channel selection is accomplished by use of pre-assembled patchboards. The display oscilloscope used in the decommurator complex presents a bar display of the commutated PAM pulse train on the selected telemetry channel which is being decommurated. The decommuration system has a memory circuit which allows the loss of up to eight channels without a loss in sync. The telemetry simulator included in the complex provides a calibrated mixed signal equivalent to the output of the spacecraft telemetry mixers. Accelerometer telemetry is not included in this signal.

The telemetry selection panel selects the data that will be shown on the data presentation equipment. The panel provides selection of either the mixed audio telemetry signal from the receivers or the corresponding signal from the spacecraft telemetry mixers via the hardline. The telemetry signal which is selected is further processed by independent selectors to discriminate between the commutated data, (10.5 kc) and the spin-rate data (7.35 kc) of either of the two rf systems. The 1.7 kc data of both rf systems is processed straight through for discrimination.

5. Data Presentation and Recording Equipment Racks

The presentation and recording of the SERT telemetry data is accomplished with an electronics complex which includes a 14-channel magnetic-tape recorder, two 8-channel Sanborn recorders, a pen recorder, a 14-channel oscillograph, and 16 MMU meters. This equipment is mounted in four six-foot by nineteen-inch electronics racks.

a. Magnetic Tape Recorder

The magnetic tape recorder was provided as GFE to the RCA test station by NASA Lewis Research Center. The tape recorder has been used throughout the program to record spacecraft telemetry, timing, and the voice comments of the test personnel.

The telemetry information taken from the hardline output taps of each telemetry mixer and the outputs of each test station receiver is recorded on four channels of the tape recorder. The test station has the provision for playing back the recorded telemetry through the discrimination and decommutation equipment.

The recorded voice information consists of all comments which are made by the test personnel from the various intercom stations. The test station is setup to play back this channel into a speaker.

The magnetic tape recorder was not included in the original test station. During the integration of spacecraft T-2 (the electrical model) it was found that a recording system of greater capability and capacity than the 14-channel oscillograph would greatly facilitate the testing operation.

b. Strip-Chart Recorders

The Strip-Chart recorders are used to present a continuous graphical display of the commutated telemetry data and the spacecraft programmer profile; the latter is used as a timing reference. Seven of the 8 channels of each recorder are used for data and one for programmer profile. Thus, at least 14 channels of real-time decommutated data

are continuously presented during spacecraft testing. A continuous graphical presentation of all of the commutated data is presented by playing back the taped telemetry through the decommutation equipment.

These recorders were not included in the original test station. They were later supplied from the RCA capital equipment pool in order to facilitate post-test data playback and analysis.

c. Pen Recorder

A two-channel pen recorder is used to present a continuous track of the spacecraft programmer event profile, and the command backup confirmation profile both in real time and from telemetry playback. One of the two timing pens of the recorder was modified to accept a signal every tenth pulse of the spacecraft programmer.

This unit was part of the original test station and was used frequently in the early part of the program. It, however, had to be redesigned by RCA in order to eliminate the frequent occurrence of gears stripping. It was also found that if the unit was not used every day, maintenance was necessary to keep the pens from clogging. The unit was used very little in the latter stages of the SERT program.

d. Oscillograph

The 14-channel oscillograph is used to record any data which is desired in real time. The test station is wired such that all the telemetry from discriminator outputs, decommutated channels, and hardline spacecraft test points can be presented.

e. MMU Meters

The 16 MMU meters (located in the command test equipment rack) are principally used to provide a real-time presentation of the telemetry channels which have been selected for real-time decommutation. The meters are also used for the calibration of the spacecraft telemetry signal conditioner.

Throughout the SERT program, the MMU meters proved to be a valuable real-time data tool in the electrical integration of the SERT spacecraft.

6. Command Test Equipment Rack

The command test equipment is used during all phases of electrical integration to check out the command and control subsystem. The command test equipment consists

of a VHF signal generator, a command programmer, and a counter mounted in a six-foot by nineteen-inch electronics rack. The VHF signal generator serves as the 148.26-megacycle carrier generator; the counter is used to set the carrier; and the command programmer is used to modulate the signal generator output. The command programmer generates the coded audio commands required for command subsystem operation in response to individual push-button switches. The programmer also has facilities for the generation of noise in place of, or in addition to, the coded modulation.

The command test equipment has performed satisfactorily throughout the SERT program.

7. General Test and Checkout Equipment

a. General

During the three-year SERT program, a number of pieces of portable test equipment have been used to supplement the function of rack-mounted test equipment. This equipment was either obtained from the test-equipment pool, purchased, provided as GFE, or designed and built by the integration personnel.

The equipment includes telemetry calibration boxes, ion-engine dummy loads, a mercury-bombardment-engine neutralization simulator, battery-charger and burn-off box, squib-firing dummy loads, an rf dummy load box, rf measuring equipment, oscilloscopes, multimeters, and many other portable pieces. In addition, many pieces of test station intercabling were made.

b. Telemetry Calibration Equipment

The entire telemetry system is tested using highly accurate signals supplied by a telemetry signal simulator and a subcarrier oscillator calibration (SCO CAL) box. The telemetry signal simulator is physically mounted in a small suitcase. It plugs into the spacecraft signal conditioner and provides a full range of voltages to each of the 90 commutated telemetry channels. The signals are processed through the spacecraft communications telemetry subsystems and sent to the ground test station where they are decommutated to calibrate each of the commutated telemetry channels.

The SCO CAL box which is designed to plug into the spacecraft telemetry mixers provides calibration voltages corresponding to center-frequency and band-edge modulation of each of the three fm subcarrier oscillators. The signals are processed through the spacecraft telecommunications subsystems. The telemetry subcarrier signals are then demodulated, discriminated, and the frequencies read on a counter.

c. Ion Engine Dummy Loads

Since the ion engines are operable only in a vacuum, substitute dummy loads were required during all non-vacuum testing. These loads which were supplied as GFE performed quite adequately during testing. It is noteworthy to mention that the function-monitoring meters on the mercury-bombardment-engine load proved to be very helpful in the integration of the ion-engine subsystem.

The telemetry-data outputs of the ion engine subsystems were monitored with a dummy signal conditioner in order to establish their intercompatibility before system integration. This box was very useful early in the program when interface problems were being solved.

d. Mercury-Bombardment-Engine Neutralization Simulator

This equipment was designed to simulate the neutralization of the mercury-bombardment engine, a condition which is necessary in order to systems integrate the neutralizer voltage control unit (NVCU). The load current is regulated while the NVCU switches in loads which vary the load voltage from 0 to 1200 vdc by the use of a 5000-volt power supply and high-power series resistance network. A spark gap protects the spacecraft from overvoltage.

e. RF Dummy Load Box

An rf dummy load was designed to substitute for the spacecraft transmission antennas during system testing. It consists of a separate load circuit for each antenna. Each load circuit consists of a one-quarter wavelength impedance transformation line to match 95 and 50 ohms, an rf signal sampler, and a 5-watt 50-ohm load. These matched loads were substituted for the four antennas during much of the spacecraft system testing. Sampling ports were provided to permit rf power measurement.

f. Squib Dummy Load Box

A box was designed and fabricated to simulate loads for the spacecraft squib firing circuits, to provide lights for visual confirmation of firings, and to provide outputs for recording of firings. The simulated squib loads are fuses. Indicators on the squib dummy load box light upon the burn out of the fuse and stay on during the one-second firing time. The recorder outputs were used during spacecraft vibration testing to monitor possible firing relay closures.

C. WALLOPS ISLAND LAUNCH CHECKOUT EQUIPMENT

1. General

The Wallops Island launch checkout equipment is used to operate and evaluate the SERT spacecraft during the four-week preparation period before launch and during launch countdown. The equipment consists of an electronics van and sets of rack-mounted equipment installed in the blockhouse, the launch tower terminal building, and the top of the launch tower. See Figure V-5 for a functional block diagram of the launch checkout equipment.

2. Electronics Van

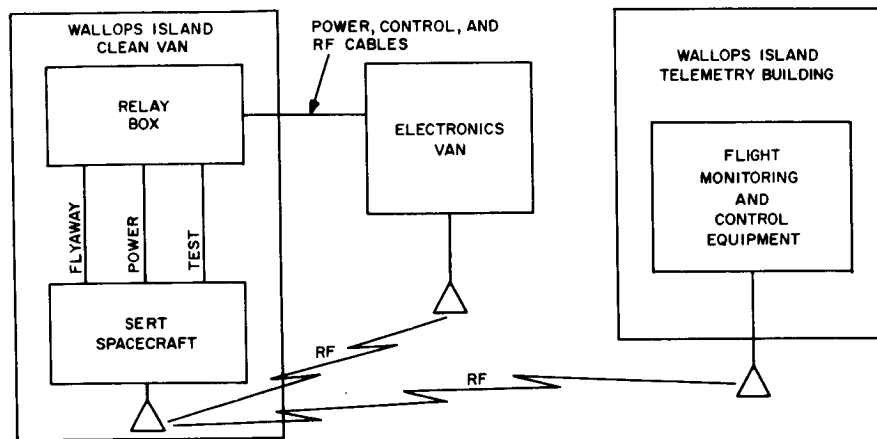
The electronics van is a mobile systems test station which is capable of operating SERT at any physical test location. Figure V-6 illustrates the physical layout of equipment in the van. The van, converted from its previous radar application by NASA Lewis Research Center, was supplied to RCA as GFE for employment in the SERT program. RCA equipped it with light and power facilities, electronic equipment, electronic maintenance facilities, and remote cabling.

The van was equipped with eight racks of electronic equipment identical to the racks of equipment of the RCA test station as it was originally conceived. The van equipment consists of a checkout control unit (Paragraph V-B.3), telemetry receiving and demodulation equipment (Paragraph V-B.4), and such ancillary electronic test equipment as an oscilloscope, VTVM, multimeters, etc. To provide single interface connection with the remotely-located spacecraft, the equipment was wired to a multi-connector panel located at one end of the van. The van supplied power via a circuit breaker panel to all of the electronics racks, a fluorescent and an incandescent lighting system, and two 6-foot maintenance benches with power and lighting fixtures.

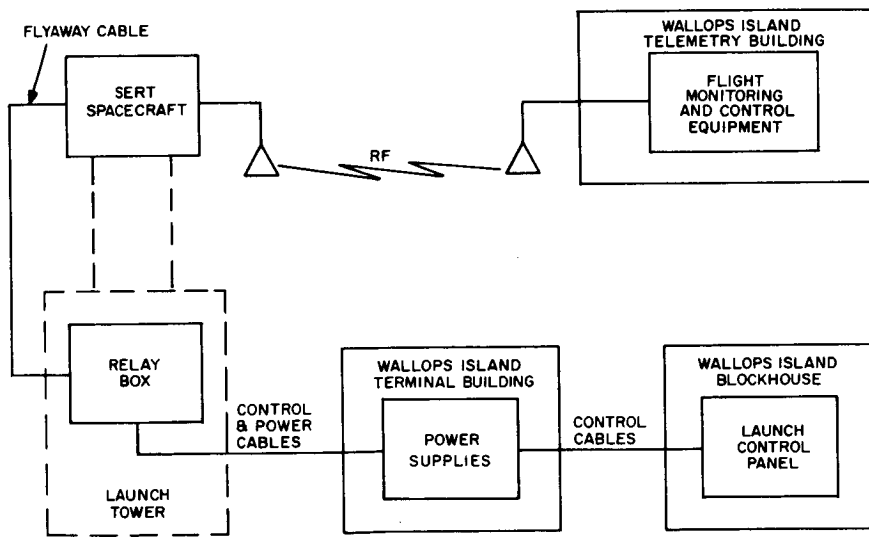
The van was successfully checked out with the SERT T-2 spacecraft and delivered to NASA with the T-2 spacecraft in December 1962. The van remained in operation throughout the remainder of the SERT program. For more than 1-1/2 years, NASA personnel used it in the development of ion-engine flight systems at the Lewis Research Center. It also was used as the prime spacecraft checkout station in the successful SERT I launch from Wallops Island in July 1964.

3. Blockhouse and Terminal Building Equipment

The electronic equipment installed in the blockhouse and launch tower complex was designed to function, in conjunction with the flight monitoring equipment in the Wallops Island Telemetry Building, during the vehicle launch operations. The equipment consists of a rack of remotely-controlled power supplies which are located in the terminal building, a relay box located on the launch tower, and a control panel which is located in the blockhouse.

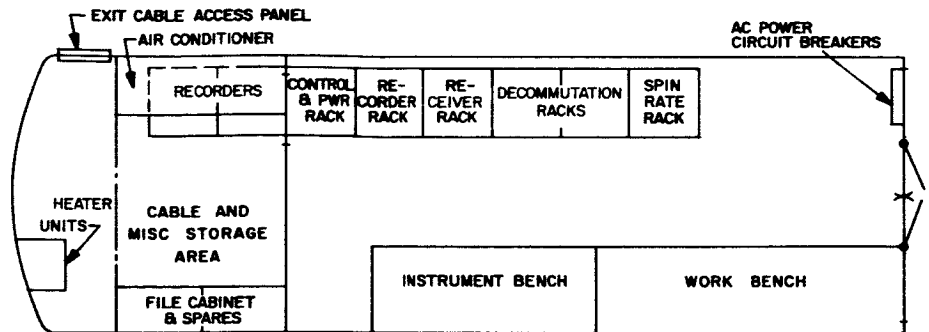


a. PRELAUNCH CONFIGURATION

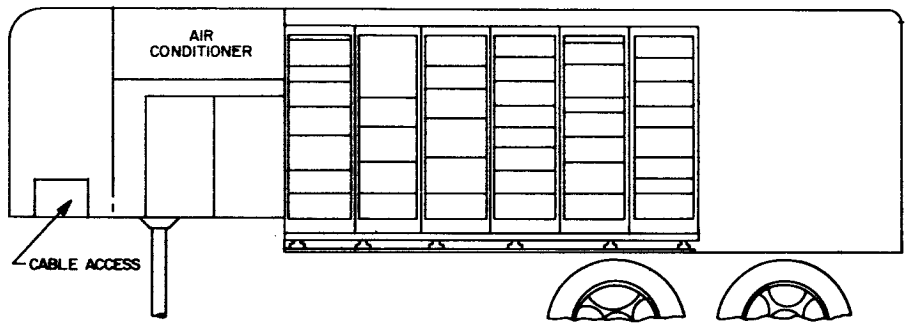


b. LAUNCH CONFIGURATION

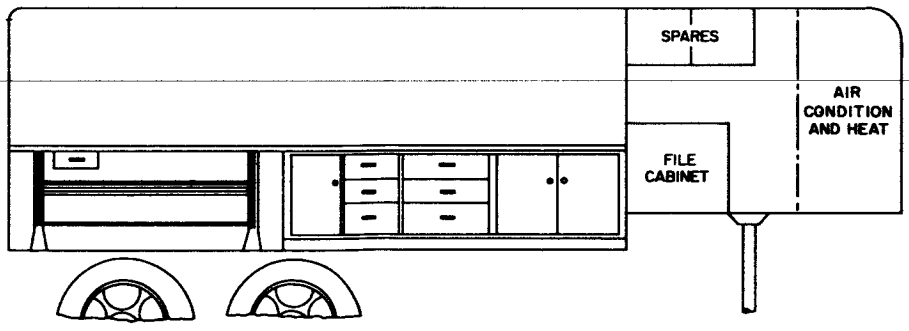
Figure V-5. Block Diagram of the Launch Checkout Equipment



(a) PLAN VIEW



(b) ROADSIDE ELEVATION



(c) CURBSIDE ELEVATION

Figure V-6. Equipment Arrangement in the Electronics Van

a. Terminal Building Power Supplies

The two power supplies located in the terminal building provide the source of external power for the spacecraft when it is in a launch configuration. One unit is capable of supplying 80 vdc at 30 amperes; the other unit is capable of supplying 36 vdc at 15 amperes. Both units supply power to the remotely located relay box in the tower approximately 150 feet away. Remote sensing enables regulation at the load.

b. Tower Relay Box

The tower relay box is a local control device which responds to remote commands from the blockhouse control station to switch external power to selected spacecraft subsystems, to activate and monitor the performance of the spacecraft during operation on its batteries, to provide battery charging power, and to shut down the spacecraft. The relay box also amplifies the hardline output signals from the spacecraft telemetry mixers.

The first of two relay boxes was delivered to NASA LeRC with the van very early in the SERT program. This relay box was subjected to considerable modification during the 1-1/2 years it was used at NASA LeRC. Consequently, the second relay box which incorporated the modifications made to the first box was built late in the SERT program and was somewhat larger than the first box. It performed without failure during the SERT I launch operation.

c. Blockhouse Payload Control Panel

The blockhouse payload control panel (Figure V-7) controls the operation of the spacecraft during the launch countdown. It performs this task in conjunction with the terminal building power supplies and the launch tower relay box. The panel is designed to control the operation of the spacecraft while it is powered by either the external terminal building source or the internal battery. Specific spacecraft subsystems can be activated by command from the control panel. These include the telemetry subsystem, rf subsystem, the cesium-contact-engine subsystem, and the accelerometer. By using the external power source rather than the internal batteries for the operation of the spacecraft subsystems during countdown, spacecraft battery power can be conserved.

During power operation using the external source, the power supply voltages and currents drawn are continuously displayed on meters. Voltage levels are adjustable by the operator. The control panel has test points available which monitor the spacecraft voltages. It is intended that these voltages be monitored on a digital voltmeter.

The operation of the spacecraft on internal power is initiated at the control panel by pressing the ACTIVATE PAYLOAD pushbutton. Activation of this button starts the predetermined flight program. The signal which is activated by this button is carried by hardline to the power-switching unit where it is processed and turns on battery power to all of the equipment except the mercury-bombardment engine subsystem. It also starts the count of the on-board programmer.

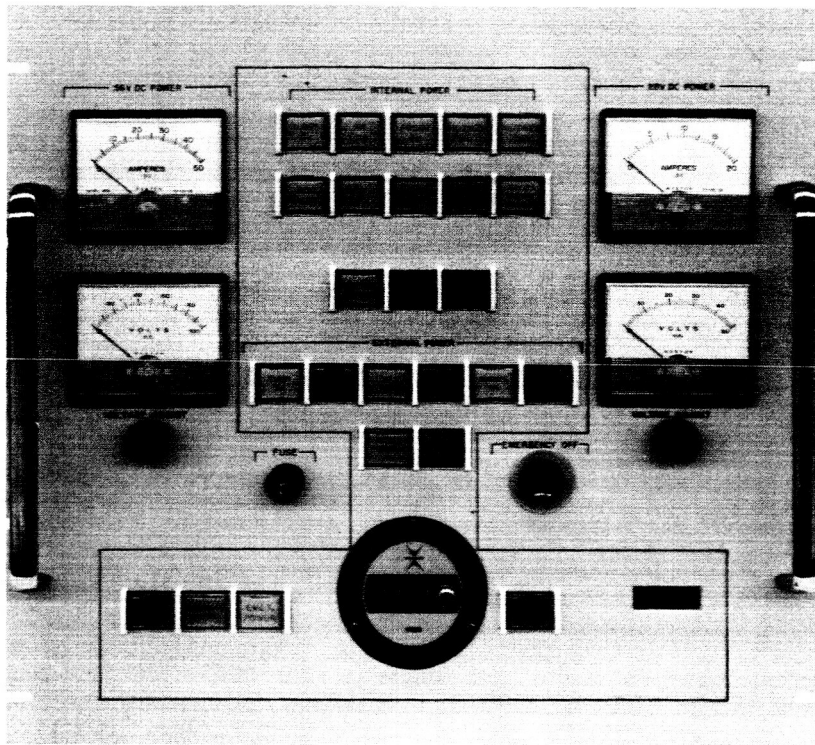


Figure V-7. Blockhouse Control Panel

The ACTIVATE PAYLOAD signal is initiated about 30 seconds before to vehicle liftoff. It is not, however, irreversible as long as the flyaway cable to the spacecraft remains plugged-in. With this connection still intact, either PAYLOAD OFF, EMERGENCY OFF, or a count of 300 on the control panel counter will shut down the spacecraft and reset the on-board programmer.

The 30-second period between the time the spacecraft is activated and the time the vehicle lifts-off allows only a short period of time in which to confirm proper operational status of the spacecraft. Because of this rather limited time period, the control panel is designed with a fail-safe system which monitors all the critical parameters via a hardline and provides a green/red indicator display. The appearance of a red indicator at any time before the separation of the flyaway cable means "hold." The appearance of all green indicators signifies "go."

This hardline monitoring system is intended to complement, not replace, the function of the spacecraft telemetry which is being received in the Wallops Island telemetry building.

The control panel has special functions, these include a BATT BURN-OFF pushbutton which causes burn-off of the main battery peaks, a LERC NEUT pushbutton which enables the stepping switch in the neutralizer voltage control unit (NVCU) to advance to its zero position, and an indicator which detects the switch position at zero. Other

functions include an indicator which denotes the mode of the auxiliary command unit, an indicator which confirms the disarming of the spacecraft squibs, and a pushbutton, which, via spacecraft interlocking circuitry, resets the panel counter if the on-board programmer is at zero. The panel also has potentiometers which allow the remote adjustment of the ionizer and the boiler of the cesium-contact-engine subsystem. The output of the 56-volt power supply can be controlled from this panel. This allows simultaneous battery charge and power feed to the cesium-contact-engine subsystem. The control panel has local functions which include a lamp-test circuit and a switch-over circuit which change the power for the panel from a power supply to a battery pack in the event of any loss of primary power. A timer also is included to keep track of spacecraft battery-drain time.

The control panel was designed and fabricated early in the SERT program. During the 1-1/2 years before its use in the launch of SERT I, it was modified several times. Some panel changes were made a relatively short time before the launch. The basic panel layout and electrical design proved to be readily adaptable to the rework which was necessary.

D. FLIGHT MONITORING AND CONTROL EQUIPMENT

1. General

The flight monitoring and control equipment consists of a spin-rate equipment rack, command programmer equipment rack and meter panel which, in conjunction with the communications facilities at the Wallops Island station, is used to monitor and control the flight of the SERT spacecraft. The equipment, racked and dolly-mounted for ease of handling, is located in the telemetry building.

2. Spin-Rate Equipment Rack

The spin-rate equipment provides for processing and display of the real-time spin information of the SERT spacecraft. The equipment consists of a pulse shaper, input selector, and divider unit, two digital counters, a counter coupler, a digital printer and a digital clock with visual time display. A block diagram is shown in Figure V-8, and a photograph of the equipment rack in Figure V-9.

The received spacecraft sun-sensor pulses are obtained from the Wallops Island 7.35-kc discriminator outputs and fed to the spin-rate rack. The selector switch couples one of the outputs from the two 7.35-kc discriminator channels to the pulse shaper. The train of shaped pulses is then fed to an optional divide-by-ten scaler and then to the dual-counter coupler. The counter coupler gates the pulses such that

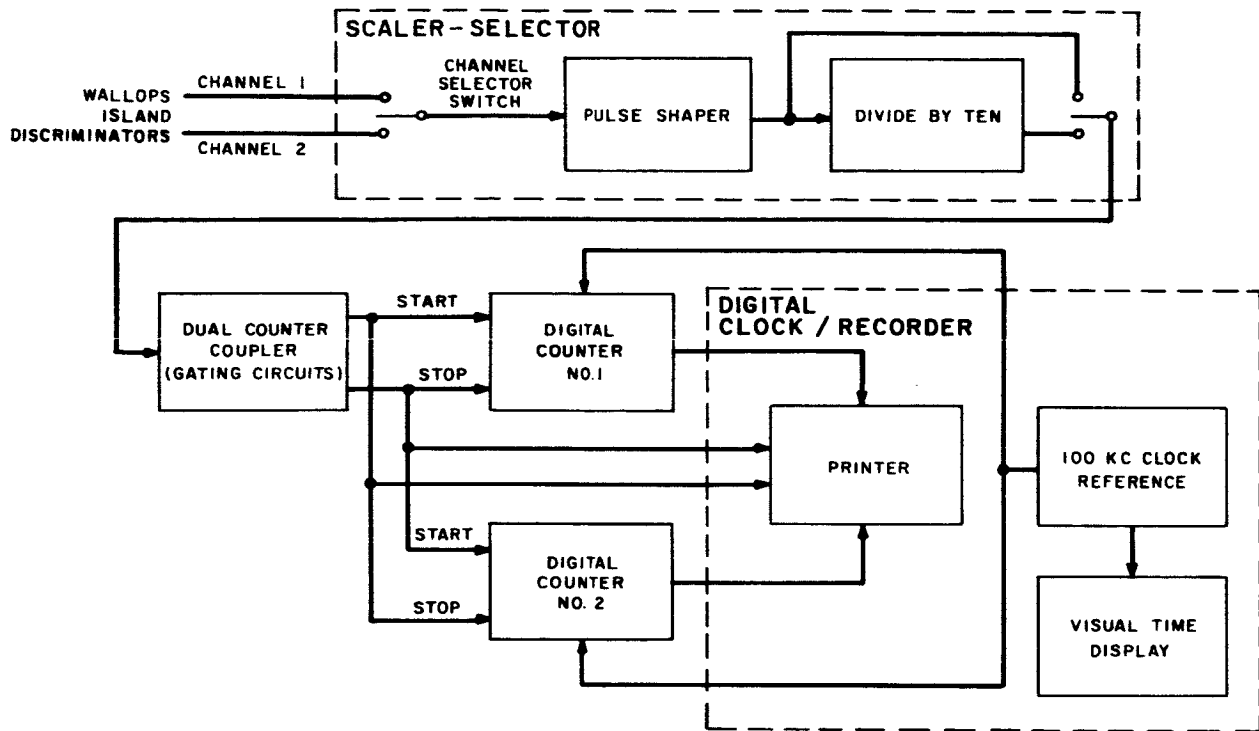


Figure V-8. Block Diagram of the Spin-Rate Rack

alternate pulses start and stop the two counters sequentially. During the period between spin-rate pulses, the activated counter accumulates the output of a standard 100-kc clock reference and the deactivated (stopped) counter is read and printed out. The use of two counters alternately provides continuous monitoring of the spin rate periods. The divide-by-ten scaler was designed to provide the capability for recording spin performance throughout the flight within the capacity of the printer recording paper.

A visual time display was also provided and slaved to the 100-kc reference clock. In addition, an analog voltage output of a selected number of significant figures of the counter was provided.

3. Command Programmer Equipment Rack

The command programmer equipment generates the coded audio tones for modulation of the rf carrier; these tones are used for command transmission to SERT via the Wallops Island transmitter. The equipment, which consists of a tone-generator unit and a command programmer unit is mounted in a standard electronics rack. The equipment is identical to that used in the RCA test station (see section V-B. 6) except that the noise generator is omitted.

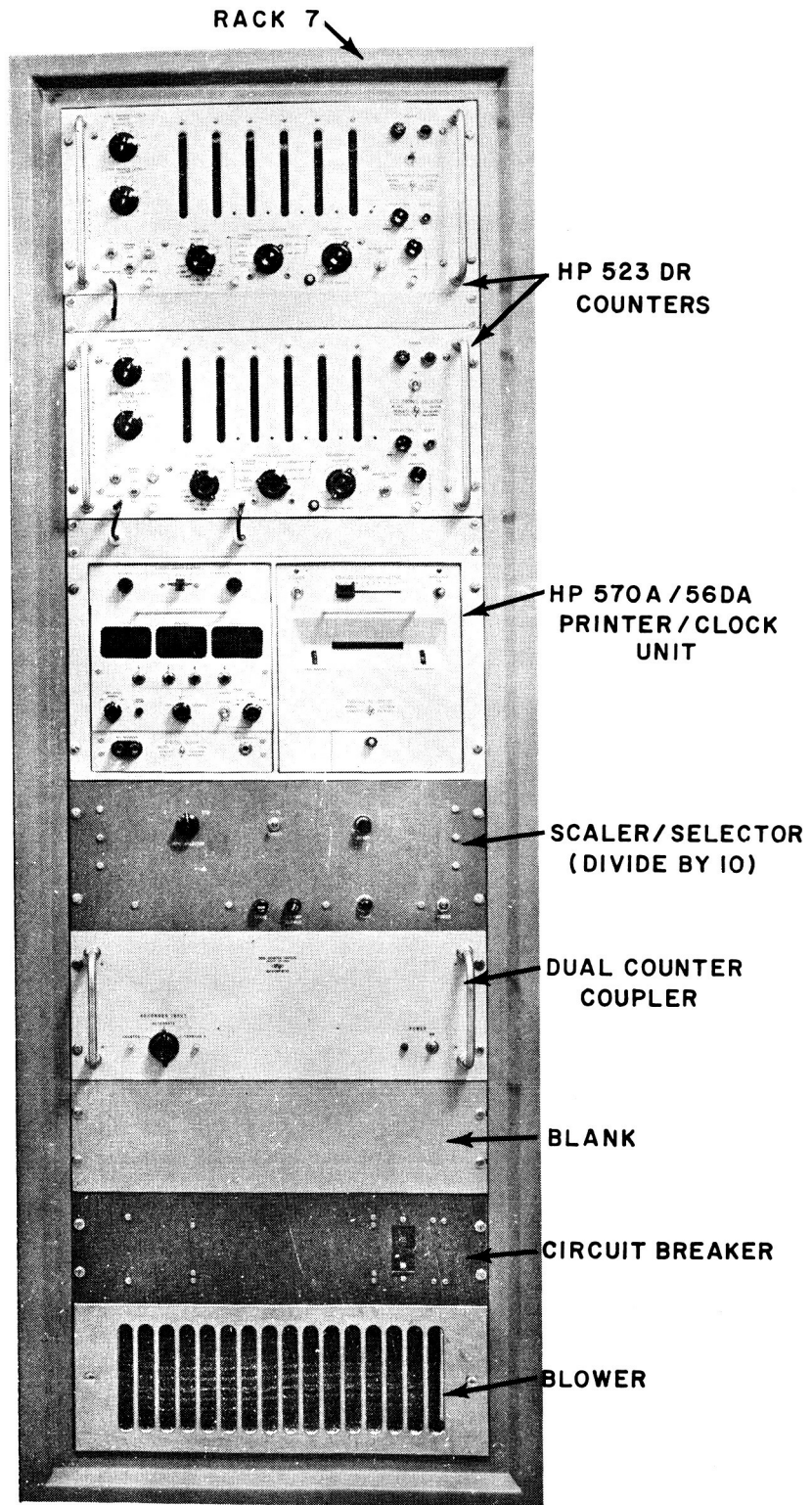


Figure V-9. Spin-Rate Rack (Rack 7 of AED Test Station)

A command is generated by the activation of any one of the ten command selector controls located on the front of the operator panel. A command selector control is used to initiate the automatic selection and time sequence of a coded pair of audio tones required for the transmission of a particular command.

A single front panel control selects and generates for transmission an address tone for 0.75 second, followed by a 1.0 second delay, and then followed by a continuous tone for as long as the control is actuated. The digital decoding circuitry of the spacecraft command subsystem is enabled by the first tone and executes the command upon reception of the second tone.

The tone generators consist of a set of five standard IRIG audio-frequency oscillators which modulate the transmitter rf carrier when selected by the command programmer.

The TIROS a. m. transmitter at Wallops Island, which is used to command the spacecraft, is operated at the carrier frequency of SERT and is modulated by the SERT audio command tones. The transmission link is completed by using the TIROS high-gain antenna.

4. Meter Panel

A set of 16 MMU meters which are described in Paragraph V-B.5 of this section is used for real-time flight monitoring of selected spacecraft parameters. The meter panel is integrated into the command programmer equipment rack.

REFERENCES

V-1. RCA Document S-19, "SERT Umbilical Requirements," NAS-8-2449.

SECTION VI

TESTING PROGRAM

A. INTRODUCTION

The SERT test program was designed to demonstrate, with a high degree of confidence, that the spacecraft will fulfill the mission requirements. To this end, a qualification and acceptance test philosophy was adopted which would allow the systematic failures to be exposed (and designed out) and to demonstrate a random failure rate that is conducive with a high probability of mission success. * This test philosophy has been applied to both component and complete spacecraft levels. Supporting the qualification and acceptance test programs are the development, design-criteria, and special-parts-evaluation test programs. This testing, coupled with the subsequent reliability analyses, has established the aforementioned confidence level.

The qualification test program consists of subjecting one flight-standard model to levels of environmental stress above operational level. Under these conditions of overstress, the equipment is required to operate within specification in accordance with the mission profile. One unit shall successfully complete this test phase without a systematic failure.

In consideration of the length of the mission (less than 1 hour), sufficient accumulated test time exists to make life testing or endurance testing unnecessary. For components, a level of overstress was selected to provide a high confidence level for each unit in spite of the absence of definition, at the outset of the program, of its location in the spacecraft. In the vibration environment, for example, the various amplifications or resonant frequencies were not known with respect to the mounting of the various components. Therefore, random-vibration-spectra testing was adopted, with the level established by experience gained under the TIROS program. Again, in the thermal-vacuum environment, the ranges of temperature were not known with respect to component mounting positions. In thermal-vacuum testing, temperature ranges exceeding those anticipated were adopted. All electrical and active mechanical components were subjected to this type of testing; passive mechanical components were not (No stress testing on the baseplate, mounting brackets, etc.). For the integrated spacecraft, environmental levels and exposures were selected to subject the complete spacecraft

*A systematic failure can be assigned a definite cause and, hence, can be analyzed and rectified; usually, these failures occur independent of time and are a function of stress. Random failures have no particular pattern and no assignable cause; the time between such failures can usually be estimated.

to overstress conditions. As the thermal-vacuum testing was performed at NASA, the main area of concern at RCA was vibration. The spacecraft vibration test specification was based upon Scout program recommendations.

The acceptance test program was designed to prove that the equipment conforms to the applicable drawings and specifications without subjecting the units to a degree of fatigue which would impair their mission performance or reliability. All flight production models were subjected to this testing before delivery or installation on the spacecraft. At the integrated spacecraft level, testing at RCA was limited to vibration and electrical performance testing. As for the qualification tests, thermal-vacuum tests with operating ion engines were conducted at the Lewis Research Center.

B. COMPONENT TESTING

1. General

Each component of the SERT spacecraft was subjected to a series of tests designed to ensure the proper performance of the equipment in its service environment prior to the integration of the component into the system. The environmental tests for prototype qualification and the flight model acceptance tests were in conformance with the test specifications detailed in RCA Drawing 1175389. Table VI-1 summarizes these environmental tests.

The testing program for each component was tailored, insofar as possible, to its operational and environmental profile. In general, testing was initiated by a complete performance verification of the component at ambient conditions to establish a standard of reference. Measurements taken during environmental exposure were related to performance requirements in the environment. In some cases, performance checks were also conducted after exposure to determine performance trends. A complete performance test was always performed at the end of the environmental test program. In a number of cases, certain tests were omitted at the component and subsystem level when the test requirements were considered to be excessive and the level of confidence in the component was high.

Table VI-2 presents a brief description of the test program for each of the SERT components and subsystems. The performance measurements for each are described in the following paragraphs.

2. Performance Measurements

A general description of the performance test operation, a list of the measurements which were made, and the reference to the detailed test procedure for each component is compiled here. Specific details (voltage levels, test set-up and problems)

TABLE VI-1. SUMMARY OF ENVIRONMENTAL TESTS

VIBRATION					
	Direction	Frequency Range	Acceleration Density	Duration	
Prototype	Thrust Axis	15-2000 cps	0.329 g ² /cps	5 min	
	Transverse Axes	15-2000 cps	0.120 g ² /cps	5 min	
Flight	Thrust Axis	15-2000 cps	0.050 g ² /cps	1 min	
	Transverse Axes	15-2000 cps	0.050 g ² /cps	1 min	
ACCELERATION					
	Direction	Acceleration Level	Duration		
Prototype	Thrust Axis	25 g	5 min		
	Transverse Axes	15 g	5 min		
SHOCK					
	Direction	Severity	No. of Shocks		
Prototype	Thrust Axis	50 g	5		
THERMAL VACUUM					
	Temperatures			Test Duration	Cycles
	min	nom	max		
Prototype	-10° C	25° C	75° C	2 hr ea temp	2
Flight	0° C	25° C	65° C	2 hr ea temp	2

TABLE VI-2. SERT COMPONENT TEST PROGRAM

Component	Performance Test	Environmental Exposure						Notes
		Vibration	Shock	Acceleration	Thermal-Vacuum	Spin		
Neutralizer Voltage Control Unit	Electrical	N	P	P	O			
Signal Conditioner	Electrical	O	P	P	O			
DC Amplifiers	Electrical	O	P	P	O			
Ion-Beam Probe Signal Conditioner	Electrical	N	P	P	O			
Commutator	Electrical	O	P	P	O		Vibrated with Signal Conditioner during Qualification Program	
SCO Package	Electrical	O	P	P	O			
RF Equipment	Electrical	O	P	P	O			
Diplexer	Electrical	O	P	P	O			
Antenna Coupling Network	Electrical	O	P	P	See Notes		Critical-pressure breakdown test	
Command Subsystem	Electrical	O	P	P	O		Outputs monitored during vibration	
Auxiliary Command Unit	Electrical	O	P	P	O		Outputs monitored during vibration	
Power Switching Unit	Electrical	O	P	P	O		Outputs monitored during vibration	
Sun Sensor	Electrical	O	P	P	O			
Ion-Beam Probe Mechanism	Electro-Mechanical	N	P	P	O			
Fuse Block	Electrical	O	P	P	O		Qualified for rated "blow" current in vacuum	
Engine Extension Subsystem	Mechanical				N		Vibration simulation only on spacecraft; shock and acceleration specs exceeded during spin	
Antenna Ground Plane	Mechanical						Only significant environmental condition	
Precession Damper	Mechanical	N					Only significant condition; qualified under TIROS program	

NOTES: N Non-operating during exposure

P Prototype exposure only

O Operating during exposure

may be found in the log book for each component. Each electrical component of the SERT I spacecraft was operated from specially designed control panels during the environmental qualification and acceptance tests. Measurements were made using standard test equipment which assured performance within the specifications of the component.

a. Neutralizer Voltage Control Unit (Mercury-Bombardment Engine Subsystem)

Description: A calibrated current of 0.3 amperes simulating the neutralization current was applied to the input from a test source. The source maintained the current at an essentially constant level while the component was activated to switch in its potential-producing resistors.

Measurements:

1. Telemetry current monitor calibration
2. Telemetry voltage monitor calibration
3. Flight sequence performance

Procedure: SPO-8 "Neutralizer Voltage Control Unit Test Specification" (Reference VI-1)

b. Signal Conditioner, Central Unit, (Telecommunications Subsystem)

Description: Accurately known signals corresponding to the low end and the high end of the channel range were applied to each channel input. This was compared to the channel output to obtain a two-point calibration of each channel over its range of operation.

Measurements:

1. Channel full-range calibration
2. Pulse-train noise and channel drop-out during vibration. For this test, the signal conditioner was integrated with the commutators.

Procedures: SPO-66 "Signal Conditioner Qualification Test Procedure" (Reference VI-2)

SPO-67 "Signal Conditioner Acceptance Test Procedure" (Reference VI-3)

c. DC Amplifiers (Signal Conditioner)

Description: Accurately known input signals were used to drive the amplifier over its range of operation while the output was monitored.

- Measurements:
1. Amplifier gain
 2. Amplifier drift
 3. Amplifier linearity
 4. Amplifier B+ stability

Procedure: SPO-55 "Test Procedure for Sonex DC Amplifier" (Reference VI-4)

d. Ion-Beam Probe Signal Conditioner

Description: Resistances simulating the sensors were varied over the operation range, and each amplifier output was monitored.

- Measurements:
1. B+ stability
 2. Amplifier output calibration vs input
 3. High potential test

Procedure: SPO-77 "SERT Lewis Probe Amplifier Test Procedure" (Reference VI-5)

e. Commutator (Telecommunications Subsystem)

Description: The channel segments and pedestal segments were activated with accurately known test signals. The measurements were made at the output terminals.

- Measurements:
1. Contact resistance
 2. Duty cycle
 3. Edge noise

4. Contact noise
5. Speed control
6. Input power

Procedures: SPO-46 "Mechanical Commutator Qualification Electrical Test Procedure" (Reference VI-6)

SPO-47 "Mechanical Commutator Acceptance Test Procedure" (Reference VI-7)

f. Subcarrier Oscillator Package (Telecommunications Subsystem)

Description: A special test fixture enabled the application of accurately known, independent subcarrier modulation signals to each subcarrier. Measurements were made at the subcarrier output mixing point.

- Measurements:**
1. Input power
 2. Frequency stability
 3. Amplitude modulation
 4. Linearity
 5. Sensitivity
 6. Distortion

Procedure: SPO-71 "Test Specification for the SCO Package" (Reference VI-8)

g. Special 10.5-kc Subcarrier Oscillator (Telecommunications Subsystem)

Description: A special test fixture enabled the application of accurately known subcarrier modulation signals to the oscillator. Measurements were made at the output.

- Measurements:
1. Linearity
 2. Sensitivity
 3. Distortion
 4. Amplitude modulation
 5. Frequency stability

Procedure: SPO-56 "Test Specification for 10.5-kc SCO" (Reference VI-9)

h. RF Transmission Equipment

Description: The transmitter, TR-16, was initially tested to obtain its characteristics vs. temperature data. The transmitter was then integrated with the power converter, PC-31, and power amplifier, PA-19, to form a complete set comprising transmitter, power amplifier, and power converter. The complete set was then subjected to the acceptance tests as a unit.

- Measurements:
- (1) Transmitter TR-16
 - (a) Input power
 - (b) Output power
 - (c) B+ stability
 - (d) Frequency stability
 - (e) Modulation carrier deviation
 - (f) Modulation distortion
 - (2) Transmitter, Power Amplifier, and Converter
 - (a) Input power
 - (b) Output power

- (c) Frequency stability
- (d) Modulation carrier deviation
- (e) Modulation distortion

Procedure: SL-12, -13, -14, -15, -18, -19, "Log Book Transmitter System," and SL-134, "Log Book RF Subsystem TR-16 S/N 507 (Reference VI-10)

i. Diplexer

Description: Each input was driven by rf signals corresponding to the system power and frequency requirements. Measurements were taken at each of the diplexer ports using calibrated standard test equipment.

- Measurements:
1. Insertion Loss
 2. Interchannel rejection
 3. VSWR

j. Antenna Coupling Network

Description: The unit was tested with standard test equipment supported by special one-quarter wavelength matching transformers at each antenna port.

- Measurements:
1. Transmission and Receiving Insertion Losses
 2. Reflected power to transmitting and receiving ballast ports
 3. Power output balance between antenna load ports (transmitting and receiving)
 4. Transmission and reception VSWR
 5. Transmission/reception section isolation

Procedures: SPO-91 "Acceptance Test Procedure for Antenna Complex Assembly," (Reference VI-11)

SPO-92 "Transmitter Coupler and Balun Qualification Test Procedure for Critical Pressure Voltage Breakdown" (Reference VI-12)

k. RF Diplexer Ballast Load

Description: The load was subjected to qualification and acceptance testing using standard test equipment

Measurements: 1. Resistance
2. VSWR
3. Power dissipation
4. Thermal

Procedure: SPO-90 "RF Diplexer Ballast Load Qualification Specification and Acceptance Specification" (Reference VI-13)

l. Command Subsystem (Command and Control Subsystem)

Description: The command subsystem, composed of the receiver and command decoder unit, was tested in two phases. The receiver was fully tested as an independent unit; the command decoder was then integrated with the receiver and the two units were tested as a subsystem.

Receiver Test Description: The receiver was exercised with an amplitude-modulated calibrated rf carrier source. Measurements were taken at the receiver output and the receiver characteristics were determined over the entire operating range.

Measurements: 1. Noise figure
2. IF bandwidth
3. AGC calibration curve

4. AGC telemetry output
5. Audio output level
6. Audio output bandwidth
7. Sensitivity curve (rf input vs audio output without AGC)
8. Oscillator stability

Subsystem Test Description: During the subsystem test, a special command subsystem test set provided the audio tones and tone combinations to modulate the rf generator used in the testing of the entire command sequence. A test panel monitored the relay closures at the command decoder as the commands were exercised. During the vibration test, high-speed recording equipment was employed to detect any relay contact crossovers.

- Measurements:**
1. Audio amplifier gain
 2. Command verification as a function of:
 - (a) Minimum input signal to receiver
 - (b) Strong signal (saturated receiver)
 - (c) Steps (a) and (b) in noise environment
 - (d) Noise input only
 3. Command reset
 4. Command lock-out function
 5. Output relay crossovers (vibration test only)

Procedure: "SERT Command Subsystem Test Procedure" (Reference VI-14)

m. Auxiliary Command Unit (Command and Control Subsystem)

Description: All tests of this component were conducted using a specially designed test panel. During the vibration environment qualification and acceptance tests, the command outputs were monitored to detect possible false commands, particularly those which might be caused by very short duration closures of a relay.

Measurements: 1. Telemetry mode indication calibration
2. Flight operation
3. Detailed monitor of command outputs to detect any evidence of false commands during vibration environment

Procedure: SPO-52 "SERT Qualification Procedure for Auxiliary Command Unit" (Reference VI-15)

n. Power-Switching Unit (Power Subsystem)

Description: All tests of this component were conducted using a specially designed test panel. During vibration environment qualification testing, the relay-controlled outputs were monitored to detect any relay contact crossover.

Measurements: 1. Flight operation
2. Detailed monitor of relay-controlled outputs to detect any evidence of relay contact crossover

Procedure: SPO-2 "Qualification Procedure for Power-Switching Unit" (Reference VI-16)

o. Sun Sensors (Sensory Subsystem)

Description: The unit was tested by activating the sensing element with a strobotac and measuring the resultant output pulse.

- Measurements:**
1. Input power
 2. Pulse amplitude
 3. Pulse width
 4. Pulse rise time
 5. Pulse droop
 6. Pulse fall time

Procedure: SPO-93 "SERT Sun Sensor Electrical Test Specification"
(Reference VI-17)

p. Ion-Beam Probe Mechanism (Sensory Subsystem)

Description: The unit was tested with a special calibration fixture which provided a precise determination of the angular position of the probe vs. the probe-position-telemetry output. An initial calibration of the device established the reference for all the subsequent tests.

- Measurements:**
1. Start signal operation
 2. Probe sweep time
 3. Calibration of angular probe position vs. telemetry output
 4. B+ stability
 5. Flight operation

Procedure: SPO-48 "SERT Test Specification of the LeRC-Probe Mechanism" (Reference VI-18)

q. Fuse Block (Electrical Integration)

Description: The fuse block was tested using a test circuit which provided the rated current of the fuses. Calibrated meters were used to monitor the current through, and the voltage across the

fuses before, during, and at the conclusion of each test. During the qualification testing, the fuse block was tested for rated blow current under environmental conditions.

- Measurements:
1. Current
 2. Voltage
 3. Resistance

- Procedures:
- SPO-68 "Acceptance Electrical Test Procedure for Payload Fuse Block" (Reference VI-19)
- SPO-70 "Qualification Electrical Test Procedure for Payload Fuse Block (Reference VI-20)

r. Engine Extension Subsystem

Test Set-Up Description: The functional tests on the engine-extension subsystem were performed on a spin-test rig designed and built for this particular purpose. The basic elements of the device are a variable speed drive, a speed reduction gear box, and a rotating gimbaled platform. A simulated center column assembly containing dummy damper-lock brackets is mounted on the platform. Four equally spaced dead weights and four equally spaced adjustable threaded rods, upon which adjustable weights are mounted, extend radially from the column assembly in order to closely duplicate the moment of inertia of the total SERT spacecraft. Two slip-ring assemblies are available for electrical signals to the rotating platform.

The engine extension subsystem, dummy engines, and all related engine mounting brackets were installed on the spin rig. The assembly was positioned so that, upon release, the extension of the subsystem was aided by a one-g field. Since the engines swing downward, they provide a conservative test of (1) the damper system which must operate against the forces created by the one-g field and (2) the force required to fully extend the engines. A photograph of the test arrangement is shown in Figure VI-1.

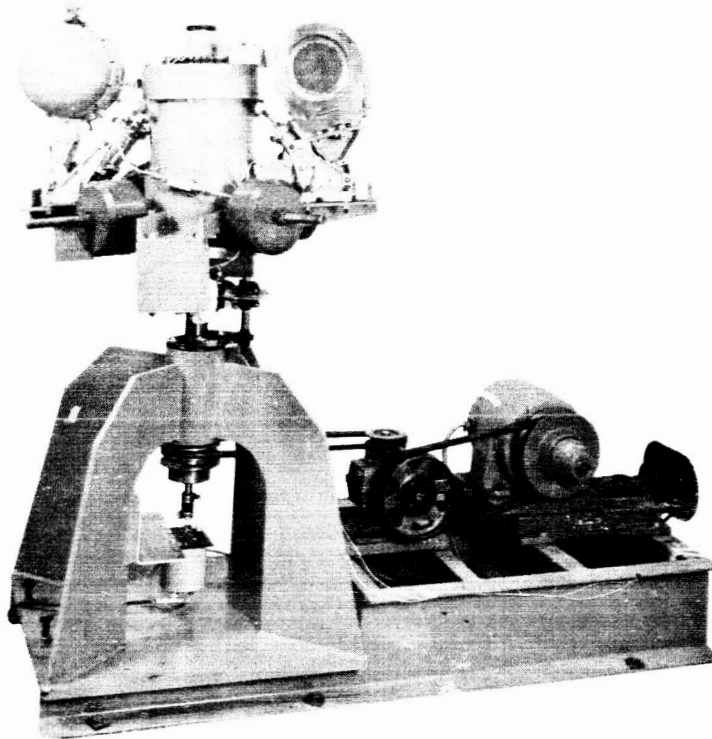


Figure VI-1. Spin-Test Setup

Measurements: The speed at which the tested items rotated was carefully adjusted and recorded. However, the most critical requirement was to make observations of the test progress, as well as to analyze the test results. Significant observations made during the test progress were (1) the approximate length of time taken for the engines to unfold and (2) the synchronization of the unfolding of the two engines. At the conclusion of the test, observations were made relative to amount of fluid leakage, abnormal marks and stiffness of the hydraulic system.

Procedures: SPO-88 "Flight Test Specification of the Hydraulic Damper System" (Reference VI-21)

SL- 36 Log Book (Reference VI-22)

SL-150 Log Book (Reference VI-23)

SL-168 Log Book (Reference VI-24)

s. Antenna Ground-Plane

Test Set-Up Description: The test set-up for the antenna ground-plane spin test was essentially the same as for the engine-extension subsystem test. However, the entire gimballed platform and center column was removed from the spin rig. The lower ring and ground plane assembly was then fastened to the flange of the rotating spin shaft.

- Measurements:**
1. Spin-rig speed
 2. Observation of the physical pattern of the ground-plane wires while spinning after wires had extended
 3. Visual inspection for damage subsequent to the spin test

References: SPO-89, "SERT Flight Test Specification for the Ring and Ground Plane Assembly" (Reference VI-25)

SL-48 Log Book and SL-165 Log Book
(Reference VI-26)

t. Precession Damper

Test Set-Up Description: A precession damper was set up on blocks so that the curved rod lay in a vertical plane with the center of the rod below its ends.

- Measurements:**
1. Friction level - measured by counting the number of oscillations of the cart on the curved rod when the cart is released at one end of the rod.
 2. Period - The average period was determined by measuring the time taken by the cart to complete three cycles and dividing by three.

Procedures: SL-145 Log Book, SL-163 Log Book,
and SL-164 Log Book (Reference VI-27)

C. SYSTEMS DEVELOPMENT TESTING

1. General

The systems development testing for the SERT I program was instituted to test the design and interface compatibility between subsystems, and between the spacecraft and the test station. The tests also included the checkout of the interface between the spacecraft and the electronics van which was to be used during launch operations. The development testing also afforded the opportunity to establish an orderly sequence of procedural testing methods. In addition, the program was used to evaluate the performance at the subsystem and system level in accordance with the respective design specifications and test procedures. Finally, the program included a survey of the system operation with the systems exposed to the mission temperature profile.

2. Nutation Test

a. Test Set Up

This test was performed using the spin-test rig described in paragraph VI-B.2.r of the engine-extension subsystem tests. Since the dummy spacecraft was gimbal-mounted to the spin-rig drive mechanism shaft, a "floating action" was created. This permitted the study of the precession characteristics of the spacecraft during the unfolding of the engines. A light focussed through an optical lens was attached to the center of the dummy column at the top and was pointed vertically upwards. A mirror, suspended above the spin rig, reflected the focussed light rays onto a screen placed at a given distance from the mirror.

b. Measurements

The amount of precession was determined by measuring the size of the circumscribed circle made by the focussed light rays on the screen. Clay was added at appropriate locations of the dummy spacecraft until dynamic balance was obtained at which time the projected light appeared as a point on the screen. While the engines were unfolding, marks were made on the screen at the circumference of the largest circle projected by the light. Since the distances from the light source to the mirror and from the mirror to the screen were known, the amount of precession could be determined. Test results showed the precession induced to be on the order of 1 degree. Values as large as 5 degrees, although undesirable, could have been tolerated.

3. Systems Electrical Development Tests

Systems electrical development testing was conducted on the T-2 spacecraft during the early part of the program. The tests were conducted in four major phases:

- Subsystem Testing,
- System Testing,
- Electronics-Van Testing, and
- Thermal Testing.

a. Subsystem Testing

Each subsystem in the spacecraft was independently tested. This testing included:

- (1) Verification of harness design and fabrication and power-switching unit operation by power and signal checks at the harness outputs;
- (2) Checkout of all spacecraft control functions in accordance with the programmer profile;
- (3) Testing and calibrating of the telecommunications subsystem (This test was performed in steps which consisted of testing and calibrating each component in the subsystem prior to overall subsystem testing.);
- (4) Checkout of the command subsystem;
- (5) Testing both engine subsystems using dummy-engine loads; and
- (6) Testing of the sensory subsystems.

b. System Testing

After subsystems testing, the fully integrated spacecraft was tested at ambient conditions. The test consisted of activating the spacecraft in a simulated flight sequence. Dummy loads were used in place of the ion engines.

c. Electronics Van Test

A test was conducted to verify the interface compatibility between the spacecraft and the electronics van. This test consisted of verifying all of the spacecraft operations that are controlled and monitored at the van.

d. Thermal Test

The T-2 spacecraft was subjected to a thermal test in order to verify (1) the capability of the system to operate over the temperature range and (2) the specification performance of the telecommunications system (telemetry accuracy). The spacecraft was installed in the 14-ft thermal-humidity chamber at AED. For the telecommunications test, calibrated inputs were provided to the signal conditioner by the Telemetry Signal Simulator. System outputs were connected to the RCA Laboratory Test Station by hardline, and the decommutated outputs were recorded. The test was performed at each of three separate temperatures (0 °C, + 25 °C, and + 50 °C).

System operation was then checked by the performance of a complete flight sequence, on spacecraft battery power, in the thermal-humidity chamber.

e. Results

The systems electrical development testing served to uncover, and subsequently verify solution of, a number of subsystem and system interface problems. Furthermore, the final configuration of the RCA system was shown (with few exceptions*) to be capable of meeting design requirements.

For the subsystem and system tests, the following significant results and accomplishments can be cited:

- (1) Proper integration of the subsystems into the system was demonstrated.
- (2) As a result of interface incompatibility between the power-switching unit and the cesium-contact-engine subsystem, and the determination by NASA that the high-current switching could be accomplished within the ion-engine subsystems, solid-state switching in the power-switching unit was replaced with relays (Refer to Paragraph III. F. 3).
- (3) The incompatibilities between the laboratory test station and the spacecraft were removed from the system. These consisted primarily of "backdoor" circuits which were removed through minor wiring changes in the test station.

*Electronic commutator failures due to inputs outside of specification limits were uncovered later during T-2 testing with operating ion engines at Lewis Research Center. The units were replaced with mechanical counterparts. (See Paragraph III-D. 4)

In the electronics van test, minor interface problems were solved, and more important, operational improvements were developed.

The thermal test served two major purposes:

- (1) The capability of the telecommunications subsystem to operate well within specifications over the temperature range without the need for temperature calibration was demonstrated.
- (2) All RCA subsystems operated satisfactorily during the flight sequence test, although difficulty was experienced with one of the ion-engine subsystems. Component thermal behavior was within specifications during the test.

After the system development tests had been completed, the electrical prototype model, T-2, and the electronics van were delivered to NASA LeRC for live ion-engine integration testing at the NASA vacuum facility.

4. Thermal-Vacuum Tests

All thermal-vacuum development testing for the SERT I program was performed by NASA at Lewis Research Center, with the technical cooperation of both the Hughes Aircraft Co. and RCA.

For information pertaining to this phase of the testing program (details about problems associated with plasma and high-voltage arc-overs, their effect on spacecraft performance, and their ultimate solution) the reader is referred to the Lewis Research Center, Cleveland, Ohio.

5. Qualification Vibration Testing, Model T-1B-1

a. General

Since the final location of components and the vibration environment to be found at these locations were not fully known, a random-noise vibration profile was used for qualification and acceptance testing of all components (see Paragraph VI-B. 1.). Midway in the program, and before the integration of the final configuration, it was felt that exposure of components to the real vibration environment existing on the spacecraft structure would be desirable in order to isolate any problem area and to enable RCA to solve these problems with a minimum of compromise to the program. Consequently, shortly after the successful completion of the T-1B (Configuration B) vibration survey testing (see Section II-B. 2.), a complete structure together with a majority of the system components was assembled and identified as T-1B-1. The T-1B-1 model integrated to the Scout separation mechanism is depicted in

Figure VI-2. The model was wired only as necessary to provide power to, and performance monitoring of, those components operational during launch. Acceleration instrumentation was also provided at selected locations. As a compromise to the degree of harnessing required and the complexity of the test, power was not applied to the cesium-contact engine subsystem. The model was subjected to a complete prototype vibration test, with individual performance testing of the components taking place before and after the vibration test. Detailed discussions of the testing and its results will be found in References VI-28, VI-29, and VI-30.

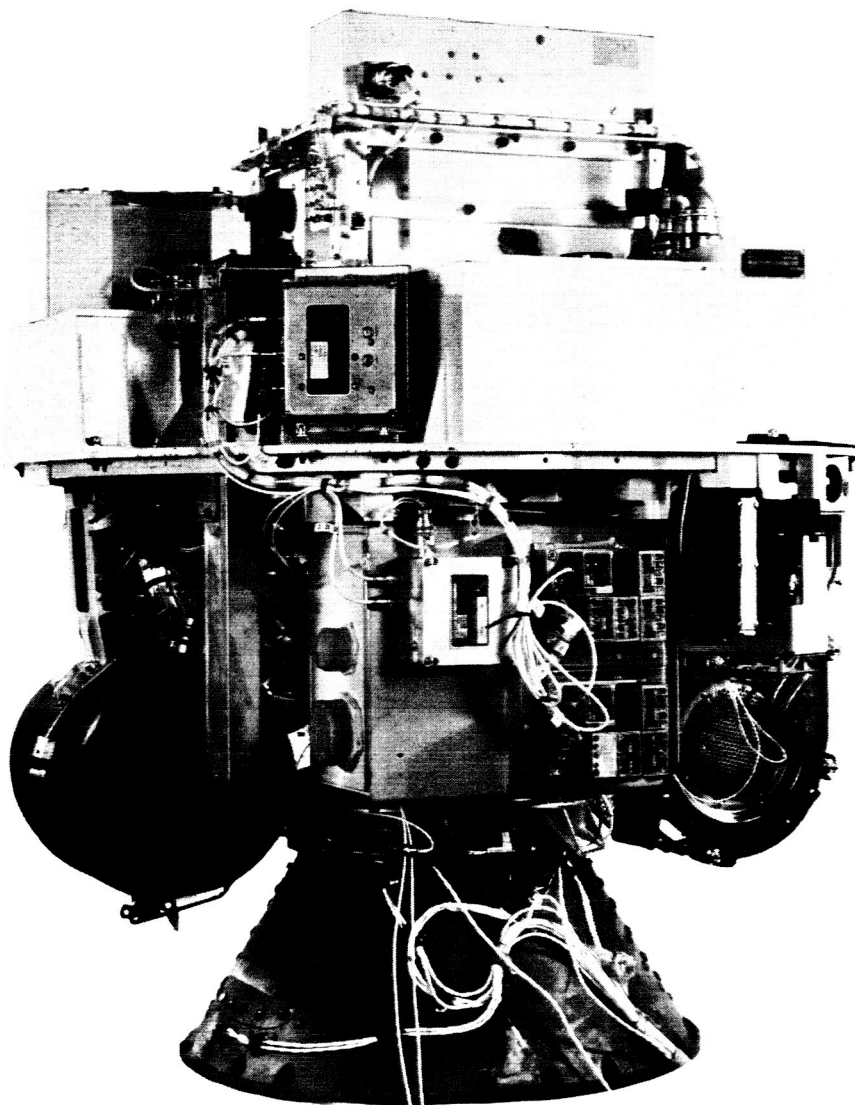


Figure VI-2. SERT Vibration Survey Model (T-1B-1)

b. Test Setup

The spacecraft model and the Scout separation mechanism were mounted on the AED 28,000-lb vibration table. The spacecraft electrical operations were controlled through the system control panel. The laboratory test station was used to monitor all operational parameters via hardlines and special cables, which were installed for this purpose. The subsystems that were interconnected by the special harness and activated during test operation included:

(1) **Power Subsystem:** Although activated batteries were installed in the spacecraft, power supplies in the system control panel were used to provide all the vehicle power. Switching was performed by the power-switching unit. All relays within the power-switching unit, including those in the squib-firing circuits, were monitored with special high-speed recording equipment to detect any contact crossovers.

(2) **Telecommunications Subsystem:** The telemetry signal simulator was used to provide calibrated inputs to the signal conditioner. The non-commutated data telemetry equipment was activated by the normal system signal inputs. The rf outputs were cabled to the laboratory test station for monitoring and recording.

(3) **Command and Control Subsystem:** During the vibration test, primary power only was applied to the programmer. Although the command and control subsystem was in full operation, its output commands were not used. Command subsystem outputs were monitored and recorded to determine the presence of contact crossover.

(4) **Sensory Subsystem:** During the vibration test, primary power was applied to the sun sensors and ion-beam probe signal conditioner but not to the ion-beam probe mechanism.

c. Test Description

The vibration survey consisted of a sequence of tests in which the spacecraft was exposed to sinusoidal and random excitation in its thrust (Z), lateral (X), and lateral (Y) axes.

The test was initiated by activating the spacecraft and applying the vibration stresses. The electrical subsystems that were activated remained energized throughout the duration of the test.

Spacecraft operation was monitored throughout the entire test. Test sequence, stress levels, etc., are delineated in Table VI-3.

TABLE VI-3. PROTOTYPE-MODEL VIBRATION TEST SEQUENCE

Run No.	Axis	Excitation Mode	Frequency Range (cps)	PSD* g ² /cps	Acceleration g-0 to peak (inches D. A.)	Acceleration g - RMS (approx.)	Duration (Minutes)
1	Thrust (Z-Z)	Sinusoidal	5 - 10		0.4		0.5
			10 - 50		2.3		1.16
2	Thrust (Z-Z)	Combustion Resonance Dwell	50 - 500		6.0		1.66
			500 - 2000		20.0		1.00
			525 - 625		45.0		0.5
3	Thrust (Z-Z)	Random	20 - 2000	0.07		11.8	4.0
4	Lateral (X-X)	Sinusoidal	5 - 10		0.2		0.50
			10 - 40		1.0		1.00
			40 - 500		2.0		1.82
			500 - 2000		4.0		1.00
5	Lateral (X-X)	Random	20 - 2000	0.02		6.3	4.0
6	Lateral (Y-Y)	Sinusoidal	Same as Run 4				
7	Lateral (Y-Y)	Random	Same as Run 5				

Notes:

- Sinusoidal vibration was applied at a constant-octave sweep rate of 2 octaves per minute.
- The random noise equalization was within ± 3 db.

*PSD: Power Spectral Density

After all vibrations tests were completed, each component was removed from the spacecraft, inspected, and tested for conformance to the corresponding design specifications.

d. Results

The T-1B-1 vibration test program proved extremely valuable in that it (1) showed most components to be capable of withstanding the vibration environment, (2) directed attention to a few problem areas, and (3) supported conclusions from previous tests, which were performed with dummy components to show that the structure would provide a suitable vibration environment.

In the areas of RCA responsibility, the command subsystem and ion-beam probe mechanism were revealed as problem areas. Problems were encountered with the engine-extension subsystem, the diplexer, and the neutralizer voltage control unit. Subsequent analysis and design modifications eliminated these problems.

D. SYSTEM TEST PROGRAM

1. General

The SERT system-test program was conducted in two phases;

- Prototype Qualification: The prototype Model, T-1B-3, was subjected to a test program designed to simulate operation in environments greater than those expected. The program consisted of electrical "debugging," thermal calibration, vibration environment, spin environment, and (at the Lewis Research Center) thermal-vacuum and transient-vacuum-environment testing.

- Flight Acceptance: The Flight Model, T-3, was subjected to a test program designed to simulate operation in environments similar to those expected in flight. Like the prototype, the program was designed to consist of electrical debugging, thermal calibration, vibration environment, spin environment and (at the Lewis Research Center) thermal-vacuum and transient-vacuum-environment testing. The environmental tests were at a level lower than those of the prototype. The environmental test specifications are detailed in RCA Drawings 1721034 and 1175389.

2. Prototype Model T-1B-3

a. Electrical "Debugging"

The electrical-debugging phase of the qualification tests verified the proper operation of the prototype model under ambient atmospheric conditions. The tests were performed in a "clean room" at AED using the RCA Laboratory Test Station which is described in Section V of this report. A step-by-step procedure of the tests are detailed in Reference VI-32. The flow diagram of Figure VI-3, and the following text briefly describe the test requirements:

- (1) **Command Subsystem Integration and Test:** The integration and test of the equipment as a subsystem included mating of the command subsystem, the antenna coupling network, and the base ring. It was performed to assure the proper operation of this equipment before its installation into the spacecraft column.

The integration process was initiated with a test to verify the correct assembly of the rf cabling to the antenna-coupling network.

The antenna-coupling network was then integrated with the command subsystem for a receiver sensitivity test, an AGC calibration, and check-out of the decoder operation. The assembly was activated with the test-station transmitter and the decoder output was checked for the proper relay closures in response to test-station commands.

The separation-squib firing and monitor wires were then checked and properly terminated at the separation-plane connection point. When bolted together, this assembly was ready to be inserted into the spacecraft column.

The detailed test procedure used in this test can be found in RCA document SPO-16 (Reference VI-31).

- (2) **Harness Power Test:** This test was performed on the partially assembled spacecraft to assure the proper operation of the harness, when integrated with the spacecraft command and control subsystem and the external test and launch-control equipment. The tests were conducted in four phases.

First, the test station control equipment was checked out by activating the pushbuttons and checking for the proper electrical response at the spacecraft end of the interconnecting cabling. Signals which originated at the spacecraft were simulated and the control equipment was checked for the proper electrical response.

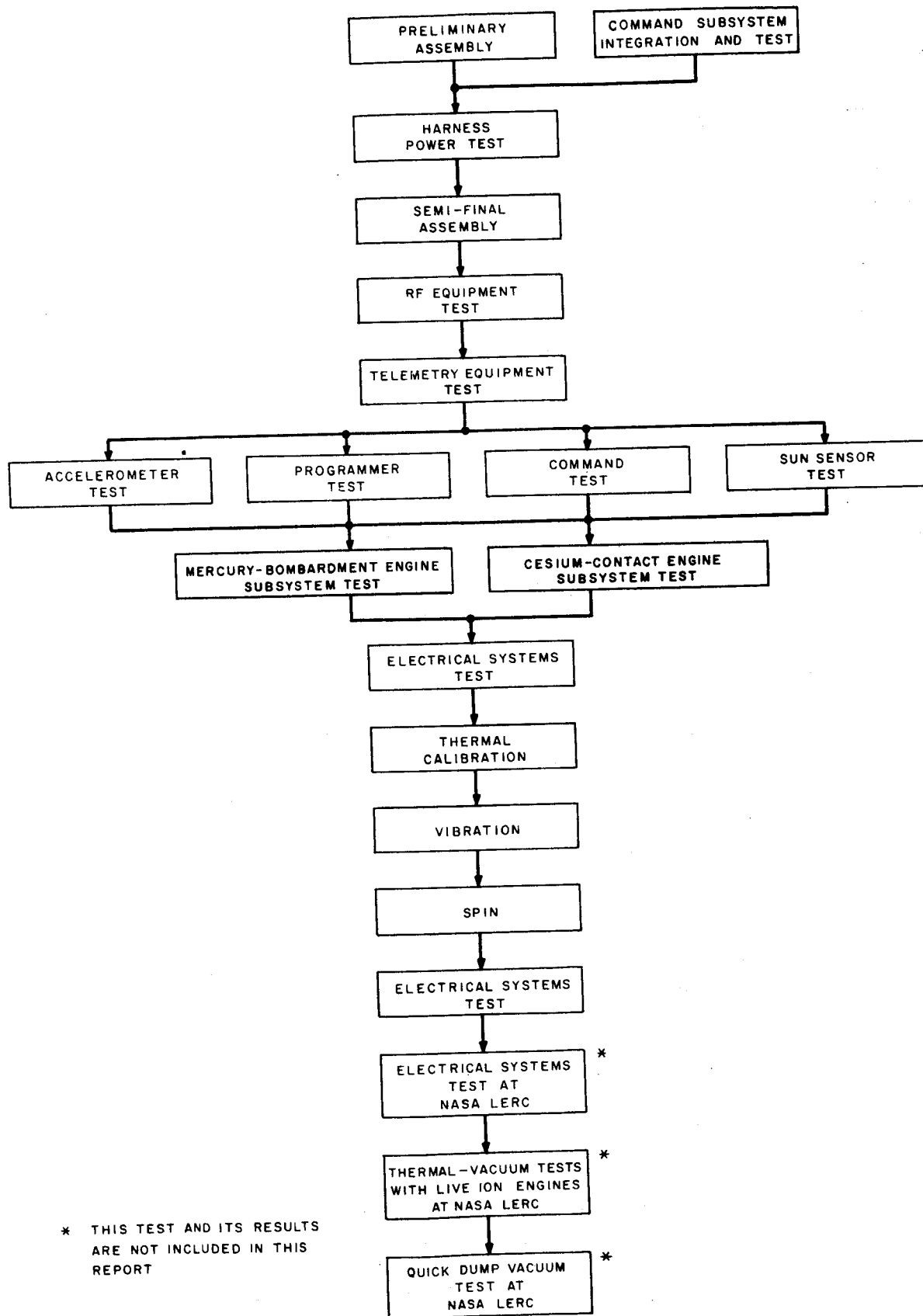


Figure VI-3. Flow Diagram Showing Prototype Testing Sequence

Second, after the control equipment had been checked, the interconnecting cables were connected to the spacecraft for tests of the harness in operation with the power-switching unit. This was accomplished by again activating control panel pushbuttons and monitoring the appropriate harness wire at its load end for the proper response.

Third, after checkout with the power-switching unit, the process was repeated to check out the harness with the programmer (phase 3) and then with the command-backup equipment (phase 4) until all of the command and control equipment was checked for proper operation with the harness and the test control equipment.

Fourth, upon completion of the harness power test, the spacecraft was returned to the assembly area to have the remainder of the components installed.

The detailed test procedure of the harness power testing can be found in RCA document SPO-3 (Reference VI-32).

- (3) **RF Equipment:** This was the first test to be performed on the fully assembled spacecraft. Its purpose was to establish the proper operation of the rf transmission equipment.

The spacecraft was equipped with dummy antennas at each of the four transmission ports. Each dummy antenna consisted of an rf load and a quarter-wavelength matching section to match the 95-ohm port impedance to the 50-ohm test equipment. The rf power at each port was measured to assure agreement with the specification. Port-to-port balance, which had been measured earlier in detail, was rechecked roughly from the individual port rf level measurements. Each transmitter power amplifier output was then tested for a minimum of 10 watts, thus assuring that each transmitter was up to power. The transmitter frequencies were tested for proper operation at the test-station receivers. The detailed test procedure is found in Reference VI-31.

- (4) **Telemetry Equipment Test:** This test followed the checkout of the rf transmission equipment and was intended as the final step in the checkout of the spacecraft telecommunications subsystem. The tests included the adjustment of each transmitter deviation ratio, bandwidth tests of each fm subcarrier oscillator, and a calibration test of the commutated-data signal conditioner. The modulation of each transmitter was adjusted for a carrier-deviation ratio of 1 for the three fm subcarrier oscillators,

and a deviation of 5 for the accelerometer signal. These adjustments were accomplished by adjusting the amplitude of each modulation source for the voltage level corresponding to the source frequency.

The modulation bandwidths of the fm subcarrier oscillators were checked for agreement to the IRIG standard of ± 7.5 percent by applying a three-point modulation signal (corresponding to the two band edges and the center frequency) to each subcarrier, while monitoring the resultant frequency on a counter. The output of the appropriate test-station discriminator input filter served as the frequency monitoring point.

The commutated-data signal conditioner was tested and calibrated at ambient conditions by way of the rf link. For this test, each of the 86 data channels (43 for each transmitter) was activated at the appropriate signal conditioner input using the telemetry signal simulator, which provided a two-point voltage source corresponding to the channel maximum and minimum points. The signals were processed via the commutated telemetry and rf link where each channel was monitored after decommutation at the test station. The detailed test procedure is found in Reference VI-31.

- (5) **Miscellaneous Equipment:** Following the checkout of the telemetry equipment, components such as the radial accelerometer, the programmer, the command backup facilities, and the sun sensors were tested and calibrated through the telemetry link. The test of this equipment was a prelude to the checkout of the ion-engine subsystems.

The radial accelerometer, which at this point was integrated with its signal conditioner, was tested for proper operation by observing the amplitude and the frequency of the output signal relative to the mounting position of the accelerometer at the time of measurement. The measurement was made at the output of the test-station receiver using an oscilloscope.

The programmer and the command functions had been previously tested in detail in the harness power test. At this point, a calibration run of their telemetry-confirmation profiles was made, using the telemetry link. These profiles formed the basis for comparison in later tests.

The operation of the sun sensors was then checked. This was accomplished by activating the solar cells with a Strobotac set at approximately 2 pps and observing the meter which was monitoring the output of the 7.35-kc-telemetry data discriminator at the test station. This test was simply a "go/no-go" operation test.

Upon the successful completion of the miscellaneous tests, the spacecraft was ready for the checkout of the ion-engine subsystems. Since the subsystems are independent of each other, either could be tested first.

- (6) Mercury-Bombardment Engine Subsystem: For test purposes, the mercury-bombardment engine subsystem comprised the ion engine and its associated power supplies (the magnetic field and neutralizer filament batteries), the neutralizer voltage control unit, the ion-beam probe mechanism, the ion-beam probe signal conditioner, and the ion-beam probe power supply. All of these equipments were tested at this point for proper operation and for calibration of their telemetry at ambient room conditions. This subsystem test was conducted in two phases. In phase one, measurement was made of the subsystem telemetry outputs through the use of the dummy signal conditioner. Upon the successful completion of the first phase, the subsystem was tested (second phase) via the telemetry link to obtain a tape recording of its telemetry during a simulation of a flight sequence. The recorded telemetry data was later reduced to confirm the proper operation of the subsystem.

The neutralizer voltage control unit was tested in the first phase for proper operation and telemetry output. The unit was activated by a 150-milliampere simulated beam current, which was derived from a 5000-volt power supply applied through a series current-regulating resistor. The control unit was then stepped in accordance with the flight sequence, while its telemetry was monitored for proper operation into the dummy signal conditioner.

The ion-beam probe mechanism and its signal conditioner were tested in the first phase for proper operation and telemetry readout. The test of the mechanism operation and probe-sweep telemetry indication was accomplished by activating the sweep from the programmer (similar to the flight sequence). The probe sensors were replaced by one-percent resistors to test the five amplifiers of the signal conditioner. The resistors were selected to provide a two-point test of the amplifiers. Performance confirmation was obtained via the telemetry link.

During all engine subsystem testing, the ion engine was replaced by an electrical dummy engine. The dummy engine simulated all of the parameters of the ion engine, including high-current heater loads and high-voltage loads. The phase-one test was conducted by simply applying power to the power supplies in the normal manner and observing each telemetry output at the dummy signal conditioner.

The second phase of testing was conducted with a completely integrated subsystem. The setup included the neutralization-beam simulation equipment for the neutralizer voltage control unit, the resistors in place of the

probe sensors, and the electrical dummy in lieu of the ion engine. The subsystem telemetry was connected to the spacecraft telemetry signal conditioner.

The test was initiated by advancing the programmer using "External Oscillator" at the test-station control panel. At "Mercury-Bombardment Engine on" in the programmer sequence, the stepping rate was reduced to approximately one pps and the mercury-bombardment engine sequence was allowed to run in its normal manner to its completion. The real-time performance observations were supplemented by a playback of the tape-recorded telemetry. In this way, the proper operation of the integrated subsystem was confirmed in detail.

The step-by-step procedure is detailed in RCA document SPO-43 (Reference VI-33).

- (7) Cesium-Contact Engine Subsystem: This subsystem was tested in essentially the same manner as the mercury-bombardment engine subsystem. It was tested for proper operation and for calibration of the telemetry at ambient room conditions in two phases. In phase one, the subsystem was tested with its telemetry driving a dummy signal conditioner. In phase two, the subsystem was tested and the telemetry was tape recorded for later analysis during a simulation of flight sequence.

The step-by-step procedure is detailed in RCA document SPO-44 (Reference VI-34).

- (8) Integrated Systems Test: The integrated systems test was the final electrical debugging test conducted on the spacecraft. Upon the successful completion of this test, the components were "torqued" down to mechanically secure the spacecraft, and it was deemed ready in all respects for the environmental qualification testing.

The integrated systems test was conducted at ambient atmospheric conditions to demonstrate that the spacecraft would perform electrically as intended in flight.

The test actually consisted of three tests conducted in sequence. The first, a full flight sequence, was conducted with external power and external program-timing control. The use of external power, rather than battery power, provided emergency control over the prototype model during the first full systems test. In addition, the use of external power conserved the batteries until it had been proven that the spacecraft was operating correctly. The use of external programming control also permitted speed, stop, and restart control over the test program.

The second and third tests were true simulated-flight tests. They were conducted on internal (battery) power, internal program, and with the spacecraft fully isolated from ground except for the rf link. The second test was a full flight sequence at the normal program rate. This was immediately followed by a command backup flight sequence, wherein the spacecraft was controlled by rf commands.

The test setup utilized most of the special equipment which had been used to conduct the individual subsystem tests. The electrical loads were substituted for the cesium-contact and mercury-bombardment engines. The high-voltage power supply and series-resistance setup simulated neutralization current for the neutralizer voltage control unit. RF dummy loads were used in lieu of antennas, and fuses were used in lieu of squibs.

The real-time observations and recordings which were made during the tests were supported by a tape recording of all of the telemetry data. This was later reduced and analyzed to confirm in detail the proper performance of the spacecraft.

The step-by-step procedure is detailed in an RCA document SPO-24 (Reference VI-35).

b. Thermal Calibration

A temperature calibration of the telecommunications subsystem was performed at atmospheric pressure over the range of temperatures anticipated during test and flight. This measurement was intended to verify the capability of the subsystem to provide the required accuracy (± 5 percent) over the expected temperature range and, in addition, to provide greater accuracy if needed.

The spacecraft was subjected to a thermal-exposure sequence of four steps (25°C, 50°C, 0°C, and 25°C). The return to 25°C confirmed that all data sources had returned to their initial conditions. The spacecraft was allowed to "soak" at each temperature until all of the components had stabilized within two degrees centigrade before any electrical tests were conducted.

The calibration was performed by applying accurately known signals to the telemetry equipment, utilizing the telemetry signal simulator, and then monitoring the output on calibrated test-station telemetry-display equipment. Thus, with a standard source and display, the changes in data over the temperature range were due to the spacecraft telemetry equipment.

The noncommutated telemetry was calibrated by feeding test voltages of 0, 2.5, and 5.0 (± 0.1 -volt) to the 1.7-kc and 7.35-kc fm subcarrier oscillators. The resultant frequencies were read on a counter at the output of the input filter to the appropriate test station discriminators.

The commutated telemetry was calibrated by feeding zero and full-scale signals to each of the 86 data channels (less the thermistor channels) and monitoring the resultant test-station decommutated display. Thus, a two-point calibration of all but the thermistor channels was obtained.

Instead of test voltages, the spacecraft on-board thermistors were applied to the appropriate commutated telemetry channels. Thus, with decommutation, both the thermistor and the appropriate channel were thermally calibrated.

The procedures are detailed in RCA documents SPO-27 (Reference VI-36) and SPO-36 (Reference VI-37).

c. Vibration Testing

(1) General

The SERT I Prototype Vibration Test was designed to represent a simulated vibration environment, the stresses of which were greater than those expected to be encountered by the spacecraft during launch and flight operations. This qualification test program is detailed in Table VI-3.

(2) Mechanical Set-Up

A special test fixture was used, providing a non-resonant interface between the vibration table and the spacecraft. The spacecraft was attached to the fixture at the separation mechanism.

The stress levels were controlled by accelerometers, which measured the vibration outputs at the base of the separation mechanism, and any spurious resonances within the frequencies of interest were damped out. Additional monitoring accelerometers were located at selected points throughout the spacecraft. A stroboscopic light was used for aid in the visual observation of particular structural sections of the spacecraft during the test.

A photograph of the T-1B-3 spacecraft on the 28,000-pound vibration table is presented in Figure VI-4.

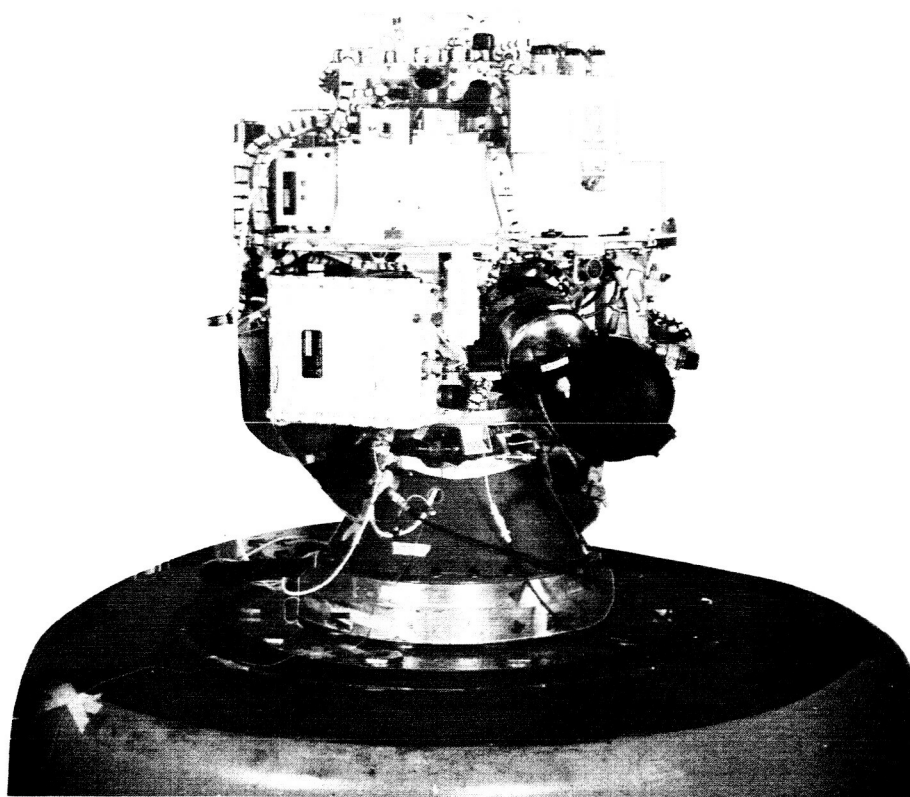


Figure VI-4. Spacecraft T-1B-3 Mounted on 28,000-Pound Vibration Table

(3) Electrical Set-Up

The control panel from the AED Laboratory Test Station was transferred to the environmental area for the performance of the test. Cabling was installed between the environmental area, the laboratory test station, and the environmental recording facility for monitoring and recording of all electrical test parameters. The flyaway umbilical and the rf lines were the only connections external to the spacecraft during the test. The rf lines and dummy loads were installed in place of the spacecraft antennas in order to monitor rf power output.

All spacecraft squib lines were disconnected and their harness ends were monitored by high speed recording equipment for detection of relay closures.

The spacecraft batteries supplied the spacecraft power throughout the test.

Preliminary test preparation included the securing of all spacecraft umbilical connectors and equalization of the vibration table.

(4) Test Description

The prototype vibration test was a series of seven tests in which the spacecraft was exposed to sinusoidal and random vibration loads in each of three axes (Z-thrust, X-lateral, Y-lateral). Throughout the vibration exposures, all electrical and mechanical components of the spacecraft were operated as they would operate during the launch vibration period of the flight and during the prelaunch warmup time. A detailed description of the vibration sequence, stress levels, etc. is given in Table VI-3.

Each vibration test run was initiated by a checkout of the ground station. This was followed by the activation of the spacecraft into its prelaunch warmup condition. Following warmup, the on-board programmer was allowed to count to about 340 to prevent the turn-on of the cesium-contact engine high voltages, at which time it was reset to zero and a recount was started. This count sequence continued throughout the duration of the vibration stresses.

Upon the termination of the vibration stresses, the programmer was allowed to count beyond 1500, and an abbreviated electrical checkout of the spacecraft was made. At the end of each vibration run, a complete visual inspection was made of all structures, parts, and connectors.

An electrical system test was performed at the conclusion of all vibration testing to verify spacecraft operation and to detect any damages due to the stress exposures.

d. Spin Test

(1) General

This test was designed to verify the proper operation of the spacecraft-engine-unfold and precession-damper mechanisms.

After vibration testing, the spacecraft was mounted to a special test fixture and attached to a spin table as shown in Figure II-12. A set of slip rings was utilized to directly connect an external power source to the appropriate set of squibs. The power source for this test was provided by the spacecraft main battery.

At the conclusion of the spin tests, a complete examination of the hydraulic and damper mechanism was performed.

(2) Engine-Unfold Mechanism

The test was performed by activating the spin table and firing the squibs when the spacecraft had reached the desired rotational speed (170 rpm). After the arms unfolded, the spin table was deenergized and the spacecraft allowed to come to rest.

The hydraulic system and arm extension mechanism were visually inspected throughout the test for proper operation, including locking of the arms in the extended position.

(3) Precession Dampers

This test was conducted in much the same manner as that for the engine-unfold mechanism. The precession damper squibs were energized by the main battery. After the spin test, the dampers were removed and the timing verified.

e. Pre-Delivery Acceptance Test

(1) General

This test was conducted to verify spacecraft operation before shipment. The test consisted of a simulated flight sequence at ambient atmospheric conditions.

(2) Test Description

The AED laboratory test station was used for the performance of this test. Control of the prototype model, T-1B-3, was monitored via the rf link and the model was isolated from ground.

The test was performed in two major operational phases. Phase one of the test was initiated with the cesium-contact-engine subsystem warm-up cycle. Upon completion of the warm-up cycle, the on-board programmer was activated and its counting initiated. At the count of 30, launch umbilical separation occurred, and the flyaway cable and building ground were released. The spacecraft was allowed to proceed in the normal flight sequence with monitor and control functions through the rf link. When the programmer reached the count of 3000 (approximately), the second phase of the test was initiated by resetting the programmer through the command back-up system. The spacecraft was then operated through the command back-up system with the spacecraft on-board programmer in parallel to check out all of the command functions.

(3) Thermal-Vacuum Test

In compliance with NASA directions, RCA delivered the SERT I prototype spacecraft to NASA Lewis Research Center in Cleveland, Ohio, for the thermal-vacuum testing with operating engines. The tests were performed by NASA with support from RCA personnel.

The thermal-vacuum testing consisted of two major operational tests. The first test was essentially the flight-sequence operation of the spacecraft during exposure to the thermal-vacuum environments as determined by the mission profile. The flight sequence was not started until after the chamber had been stabilized. The second test was a transient vacuum test, consisting of the flight sequence operation of the spacecraft in a thermal-vacuum environment designed to represent the sudden pressure transition encountered during the launch operation.

3. Flight Acceptance Testing, Flight Model T-3

a. General

The flight acceptance test phase of the SERT I system test program demonstrated that the SERT I flight vehicle had been fabricated and assembled in accordance with the design specifications. The spacecraft was subjected to tests similar to those performed on the prototype spacecraft and included electrical debugging, thermal calibration, and vibration environment testing.

b. Electrical Debugging

The spacecraft requirements during this test were the same as those for the prototype vehicle; the test therefore was conducted in the same manner.

c. Thermal Calibration

The spacecraft requirements during this test were the same as those for the prototype vehicle.

d. Vibration Testing

The SERT I flight acceptance vibration test was designed to certify that flight model T-3 was fabricated and assembled in conformance with all of the design specifications, without subjecting the spacecraft to unnecessary fatigue.

All of the test preparations and the test procedure were identical with those used during prototype testing.

A detailed description of vibration sequence, stress levels, etc. is given in Table VI-4.

e. Spin Test

The spin flight acceptance test performed on the flight model T-3 was designed to test the engine-unfold mechanism. The precession dampers were not uncaged during the spin test because of potential damage in the 1-g environment, as well as to avoid the removal, recaging, and reinstallation process. The test was conducted in the same manner as the prototype test except that the rotational speed was reduced to 130 rpm.

TABLE VI-4. FLIGHT-MODEL VIBRATION TEST SEQUENCE

Run No.	Axis	Excitation Mode	Frequency Range (cps)	PSD* g^2/cps	Acceleration $g-0$ to peak (inches D.A.)	Acceleration $g-RMS$ (approx.)	Duration Minutes
1	Thrust (Z-Z)	Sinusoidal	5 - 10		0.3		0.25
			10 - 50		1.5		0.38
			50 - 500		4.0		0.83
			500 - 2000		12.0		0.50
2	Thrust (Z-Z)	Combustion Resonance Dwell	525 - 625		45.0		0.25
3	Thrust (Z-Z)	Random	20 - 2000	0.03		7.7	2.0
4	Lateral (X-X)	Sinusoidal	5 - 10		0.15		0.25
			10 - 40		0.8		0.50
			40 - 500		1.3		0.91
			500 - 2000		2.7		0.50
5	Lateral (X-X)	Random	20 - 2000	0.01		4.4	2.0
6	Lateral (Y-Y)	Sinusoidal		Same as Run 4			
7	Lateral (Y-Y)	Random		Same as Run 5			

Notes:

- Sinusoidal vibration was applied at a constant-octave sweep rate of 4 octaves per minute.
- The random noise equalization was within ± 3 db.
- * PSD: Power Spectral Density

f. Pre-Delivery Acceptance Test

This test was identical in purpose and procedure as that performed on the prototype model T-1B-3.

4. **Performance, Prototype Model and Flight Model**

The system test program of the SERT I spacecraft demonstrated the design adequacy of all components and subsystems. The test program further demonstrated the flexibility of the spacecraft and the ground station to adapt to the various changes and modifications which were instituted during the course of the program.

The tests were performed in the orderly sequence specified by the components, subsystems and system test procedures. In the initial phases of the test program, minor interface and system problems were detected and corrected. During the environmental phase of the test program the spacecraft performed in accordance with requirements.

REFERENCES

- VI-1 RCA Document SPO-8, "Neutralizer Voltage Control Unit Test Specification," Contract NAS 8-2449, Aug 30, 1965.
- VI-2 RCA Document SPO-66, "Signal Conditioner Qualification Test Procedure," Contract NAS 8-2449, Mar 13, 1964.
- VI-3 RCA Document SPO-67, "Signal Conditioner Acceptance Test Procedure," Contract NAS 8-2449, Mar 17, 1964.
- VI-4 RCA Document SPO-55, "Test Procedure for Sonex DC Amplifiers," Contract NAS 8-2449, Jan 13, 1964.
- VI-5 RCA Document SPO-77, "SERT Lewis Probe Amplifier Test Procedure," Contract NAS 8-2449, May 6, 1964.
- VI-6 RCA Document SPO-46, "Mechanical Commutator Qualification Electrical Test Procedure," Contract NAS 8-2449, Sept 12, 1963.
- VI-7 RCA Document SPO-47, "Mechanical Commutator Acceptance Test Procedure," Contract NAS 8-2449, Dec 4, 1963.
- VI-8 RCA Document SPO-71, "Test Specification for the SCO Package," Contract NAS 8-2449, Feb 25, 1964.
- VI-9 RCA Document SPO-56, "Test Procedure for 10.5-kc SCO," Contract NAS 8-2449, Jan 13, 1964.

- VI-10 SERT Logbooks SL-12, -13, -14, -15, -18, -19, "Log Book Transmitter System" and SL-134, "Log Book RF Subsystem TR-16 S/N 507."
- VI-11 RCA Document SPO-91, "Acceptance Test Procedure for Antenna Complex Assembly," Contract NAS 8-2449, Dec 6, 1963.
- VI-12 RCA Document SPO-92, "Transmitter Coupler and Balun Qualification Test Procedure for Critical Pressure Voltage Breakdown," Contract NAS 8-2449, Dec 12, 1963.
- VI-13 RCA Document SPO-90, "SERT rf Diplexer Ballast Load Qualification Specification and Acceptance Specification," Contract NAS 8-2449, Dec 23, 1963.
- VI-14 "SERT Command Subsystem Test Procedure," May 29, 1962.
- VI-15 RCA Document SPO-52, "SERT Qualification Procedure for Auxiliary Command Unit," Contract NAS 8-2449, Dec 23, 1963.
- VI-16 RCA Document SPO-2, "Qualification Procedure for Power-Switching Unit," Contract NAS 8-2449, Jun 8, 1962.
- VI-17 RCA Document SPO-93, "SERT Sun Sensor Electrical Test Specification," Contract NAS 8-2449, Jan 8, 1964.
- VI-18 RCA Document SPO-48, "SERT Test Specification of the LeRC-Probe Mechanism," Contract NAS 8-2449, Oct 24, 1963.
- VI-19 RCA Document SPO-68, "Acceptance Electrical Test Procedure for Payload Fuse Block," Contract NAS 8-2449, Mar 25, 1964.
- VI-20 RCA Document SPO-70, "Qualification Electrical Test Procedure for Payload Fuse Block," Contract NAS 8-2449, Mar 25, 1964.
- VI-21 RCA Document SPO-88, "Flight Test Specification of the Hydraulic Damper System," NAS 8-2449, Aug 23, 1964.
- VI-22 SERT Logbook SL-36.
- VI-23 SERT Logbook SL-150.
- VI-24 SERT Logbook SL-168.
- VI-25 RCA Document SPO-89 "SERT Flight Test Specification of the Ring and Ground Plane Assembly," Contract NAS 8-2449, Aug 27, 1964.
- VI-26 SERT Logbooks SL-48 and SL-165.

- VI-27 SERT Logbooks SL-145, SL-163, and SL-164.
- VI-28 AED Report, "T-1B-1 Prototype-Level Vibration Test Data," Mar 8, 1963.
- VI-29 AED Report R-1894-2, "SERT T-1B-1 Capsule Qualification Vibration Test Report," Mar 14, 1963.
- VI-30 RCA Document SPO-31, "Results of Prototype Vibration Testing of the SERT T-1B Capsule," Contract NAS 8-2449, Feb 18, 1963.
- VI-31 RCA Document SPO-16, "SERT Telemetry System Accuracy Check Using the Suitcase Simulator," Contract NAS-8-2449, Jan 23, 1963.
- VI-32 RCA Document SPO-3, "Checkout Procedure for Electrical Integration of the SERT Capsule," Contract NAS-8-2449, Jun 8, 1962.
- VI-33 RCA Document SPO-43, "SERT Electrical Test Procedure for the LeRC Ion Engine Subsystem," Contract NAS-8-2449, Sep 11, 1963.
- VI-34 RCA Document SPO-44, "SERT Electrical Test Procedure for the Hughes Ion Engine Subsystem," Contract NAS-8-2449, Sep 11, 1963.
- VI-35 RCA Document SPO-24, "SERT Overall Electrical Systems Test Procedure," Contract NAS-8-2449, Feb 14, 1963.
- VI-36 RCA Document SPO-27, "Flight Thermal Electrical Test Procedure," Contract NAS-8-2449, Feb 21, 1963.
- VI-37 RCA Document SPO-36, "Thermo-Humidity Test Procedure for T-1B-2," Contract NAS-8-2449, Apr 8, 1963.

SECTION VII

RELIABILITY ANALYSIS

A. INTRODUCTION

This section contains a description of a reliability study performed by RCA of the RCA portions of the SERT system. The purposes of the analysis were (1) to accumulate data required to perform trade-off evaluations of possible system configurations; (2) to provide a basis for recommending methods of improving reliability; and (3) to determine the survival probability of the RCA subsystems and equipments.

To accomplish these goals, mathematical reliability models of the functional subsystems were prepared, the survival probabilities of all equipment were calculated, failure modes and effects were investigated, and the results were integrated into over-all reliability predictions. The reliability evaluation was performed about half-way through the program, at the time when the design was fairly well established (thus providing a firmer basis for the evaluation), but at a time when any necessary modifications could still be incorporated.

The reliability analysis consisted of three major phases: a Failure Mode and Effects Analysis of the SERT I Spacecraft, a Failure Mode and Effects Analysis of the SERT I Ground Support Equipment, and a Reliability Estimate and Parts Application Review.

This section of the report contains a summary of the evaluations performed, the recommendations made during the analysis, the corrective actions taken, and the modifications made.

B. FAILURE MODE AND EFFECTS ANALYSIS OF SERT I

The Failure Mode and Effects Analysis performed on the SERT I spacecraft by AED included the following:

1. Preparation of appropriate system and/or subsystem block or logic diagrams;
2. Assumption of part- or circuit-failure modes;

3. Determination of possible causes for the particular assumed failure mode;
4. Determination of symptoms and local effects;
5. Listing of compensating provisions, if any;
6. Determination of the ultimate effect upon system performance;
7. Assignment of part- or circuit-failure probabilities; and
8. Assignment of part- or circuit-failure class factors.

A qualitative ranking was used for the failure class and failure probability factors; these factors were ranked into the following four categories of importance.

<u>RANK</u>	<u>SIGNIFICANCE</u>
A	Catastrophic data or system loss
B	Major data or system loss
C	Moderate data or system loss
D	Minor data or system loss

The failure-probability factors used were estimates of the relative probability of occurrence for the particular failure mode. The range was divided into five arbitrary levels of 1 to 5, with 1 denoting a relatively high probability of occurrence and with 5 denoting a relatively low probability of occurrence.

The relative importance of each telemetry data point was assigned by NASA, and AED then indicated the failure class factors for each assumed failure. The details of the analysis, the components analyzed, and the subsystem results were previously presented (Reference VII-1).

When the Failure Mode and Effects Analysis of SERT I was completed, the results were reviewed with the responsible AED Design Skill and the Systems Groups, the NASA Resident Representative, and, subsequently, the NASA Lewis Research Center. Certain of the recommendations arising out of the study were then implemented at the request of the Lewis Research Center. Table VII-1 is a compilation of the recommendations and the subsequent action taken or modifications made and the spacecraft affected.

TABLE VII-1. SUMMARY OF RESULTS FROM RELIABILITY ANALYSIS OF SERT I

Component/Item	Subsystem	Recommendation	Reason for Recommendation	Action/Modification	Spacecraft Affected
Power Switching Unit	Main Power Distribution and Control	Application of run-in procedure to relays after Class A and Class B testing per Military Spec. MIL-R-5757	Sort out defects to which the run-in testing is not sensitive	Run-in testing procedure was instituted, but not to be implemented until after T-3 model	None
Telemetry Power Supply	Main	(1) Provide an OR-gate arrangement between the 28-volt telemetry battery and the main 28-volt battery for one of the two telemetry subsystems	Provide redundant source of power for both telemetry and the command channels	Not incorporated	None
		(2) Fuse both telemetry subsystems and the command subsystem	Protection against catastrophic short circuits	Not incorporated	None
Telemetry Calibration	Telemetry	Eliminate 2.5-volt calibration channel on each telemetry subsystem	Use of that position to cross-feed the 5-volt calibration from each of the two subsystems to the other	Not incorporated	None
Zero Suppress Bias Source for Signal Conditioner	Data Collection, Conditioning, and Transmission	(1) Add redundant minus 23.7-volt supply to each commutated channel	Loss of a single minus 23.7-volt supply does not cause a loss of any data	Redundant channel added	T-1B-3, T-3
		(2) Provide an OR gate between the two minus 23.7-volt zero-suppress bias sources	Maintain data-collection capability of both commutated channels	Not incorporated	None

TABLE VII-1. SUMMARY OF RESULTS FROM RELIABILITY ANALYSIS OF SERT I (Continued)

Component/Item	Subsystem	Recommendation	Reason for Recommendation	Action/Modification	Spacecraft Affected
Ion-Beam-Probe Drive Mechanism	Mechanical	Fuse the probe-drive motor for the condition where the motor becomes stalled	A stalled motor could discharge the 28-volt main battery	Not Incorporated	None
Programmer (GFE)	Main Power Distribution and Control	(1) Provide "backup" for the mercury-bombardment engine system through the use of a timer to disable the output of the space decoder channel until the programmer is scheduled to generate the cesium-contact engine "Off" command at which time a ground command can be transmitted through the Command Subsystem to gate the mercury-bombardment engine "On" through the now-open window of the spare channel.	No command "backup" was available to program "On" the mercury-bombardment engine; "backup" was provided for commanding the cesium-contact engine "On".	Ground command "backup" capability added for the mercury-bombardment engine; however, no "open-window" capability of the spare channel was added. This modification was effected through addition of auxiliary command unit.	T-1B-3, T-3
		(2) Use of a direct-operating timer in place of the recommendation to use ground command.	Provide "backup" command capability for programming "On" the mercury-bombardment engine	Not Incorporated	None
Commutators (2)	Data Collection, conditioning, and Transmission	Study the effects of induced pulses and of any variation or "noise" reflected back to the momentary high-current overloads, particularly test, and analyze operation of the complete system under vacuum conditions	Prevent damage from transients and provide protection in the Signal Conditioner to prevent over-voltage noise from being propagated through the Signal Conditioner and to other electronic components.	Per NASA direction, mechanical commutators were substituted for the original electronic commutators.	T-1B-3, T-3

C. FAILURE MODE AND EFFECTS ANALYSIS OF SERT I GROUND SUPPORT EQUIPMENT

The Failure Mode and Effects Analysis performed on the SERT I Ground Support Equipment by AED included the following steps:

1. Preparation of appropriate system and/or subsystem block or logic diagrams;
2. Assumption of part- or circuit-failure modes;
3. Determination of possible causes for the particular assumed failure mode;
4. Determination of symptoms and local effects;
5. Listing of compensating provisions if any;
6. Determination of the ultimate effect upon system performance;
7. Assignment of part- or circuit-failure probabilities; and
8. Assignment of part- or circuit-failure class factors.

A qualitative ranking was used for the failure class and failure probability factors; these factors were ranked into the following four categories of importance.

<u>RANK</u>	<u>SIGNIFICANCE</u>
A	Catastrophic data or system loss
B	Major data or system loss
C	Moderate data or system loss
D	Minor data or system loss

The failure-probability factors used were estimates of the relative probability of occurrence for the particular failure mode. The range was divided into five arbitrary levels of 1 to 5, with 1 denoting a relatively high probability of occurrence and with 5 denoting a relatively low probability of occurrence.

The relative importance of each telemetry data point was assigned by NASA, and AED then indicated the failure class factors for each assumed failure. The details of the analysis, the components analyzed, and the subsystem results were previously presented (Reference VII-2).

When the Failure Mode and Effects Analysis of SERT I Ground Support Equipment was completed, the results were reviewed with the responsible AED Design Skill and the Systems Groups, and subsequently with the NASA Lewis Research Center.

Table VII-2 is a compilation only of the recommendations made by RCA, and the subsequent action taken or modifications made and the spacecraft affected.

D. RELIABILITY STRESS ANALYSIS

The reliability stress analysis performed on the SERT I system was a systematic procedure of determining the reliability of the component, circuit, or device, which is a prime contributor to the reliability of the subsystem or system. The electrical operating stresses were derived from a combination of the parts rating, the actual electrical usage, and the thermal and environmental factors. The steps in performing the reliability stress analysis were as follows.

- (1) Identification of the part and determination of its rating.
- (2) Determination of the electrical stresses imposed by the circuitry in which the part is used.
- (3) Determination of part ambient or hot-spot temperature from the electrical stress and thermal environment.
- (4) Calculation of the percent of rated stress derived from (1), (2), and (3) above.
- (5) Assignment of the applicable part generic failure rate from acceptable Parts Reliability Factors handbooks.
- (6) Application of the appropriate environmental failure-rate acceleration factor.
- (7) Summation of all parts failure rates in an appropriate manner.

The summation of the failure rates of all parts in a component results in a total failure rate for that component. This failure rate is the component reliability estimate and, from it, the probability of failure is determined. Such a probability of failure was determined for the selected components summarized in Table VII-3; the details were previously presented. (Reference VII-3)

TABLE VII-2. SUMMARY OF RESULTS FROM RELIABILITY ANALYSIS OF SERT I GROUND SUPPORT EQUIPMENT

Component/Item	Subsystem	Recommendation	Reason for Recommendation	Action/Modification	Spacecraft Affected
Relay Box and Power Supplies, 28-volt and 56-volt	Launch Tower, Terminal Building Equipment	Voltage limiting of the power supplies should be installed in the relay box and the terminal building for the error-sensing and remote regulation lines.	Unsafe operational condition which could expose the spacecraft to excessive over-voltages	Voltage and current "overloads" were set, at the power supplies, to the operating limits of the spacecraft prior to operation	T-1B-3, T-3

TABLE VII-3. SUMMARY OF RESULTS FROM RELIABILITY ANALYSIS OF RELIABILITY ESTIMATE AND PARTS APPLICATION REVIEW

Component/Item	Subsystem	Recommendation	Reason for Recommendation	Action/Modification	Spacecraft Affected
Command Decoder	Command	(1) Replace resistor RCA 8977933 with equivalent parts purchased from Corning or Electra.	Improved reliability	Not incorporated; unit had already been qualified and accepted, and no operational failures due to these parts had occurred.	None
		(2) Replace transistor type 2N2303 with type USN2N1132	Improved reliability		
		(3) Purchase CR1 (1N914) as JAN1N914, 1N3018B as USN1N3018B, and CR85 (1N754) as USN 1N754.	Improved reliability		
Neutralizer Voltage Control	Data Collection, Conditioning, and Transmission	(1) Purchase R1 and R2 (RH50) as RHM50 (Mil version)	Improved reliability	Not incorporated; unit had already been qualified and accepted, and no operational failures due to these parts had occurred.	None
		(2) Purchase the 1N540 as a JAN1N540, or as a type USN 1N3189.	Improved reliability		
Ion-Beam-Probe Signal Conditioner and Probe Mechanism	Data Collection, Conditioning, and Transmission	(1) Purchase the 1N969B diode as a type USN1N969B from either Dickson or Motorola, and replace the 1N457 diode with the type JAN1N645	Improved reliability	Not incorporated; unit had already been qualified and accepted, and no operational failures due to these parts had occurred.	None
		(2) Replace relay type Astro KX 4H4D-24 from Kurman with GE type 3SAH, or with Branson type AR4C	Improved reliability		
		(3) Replace Helipot type TSP potentiometer with Type 5200	Improved reliability		

TABLE VII-3. SUMMARY OF RESULTS FROM RELIABILITY ANALYSIS OF RELIABILITY ESTIMATE AND PARTS APPLICATION REVIEW (Continued)

Component/Item	Subsystem	Recommendation	Reason for Recommendation	Action/Modification	Spacecraft Affected
Sun Sensor and Associated Voltage Regulator	Data Collection, Conditioning, and Transmission	(1) Increase the value of resistor R1 to 270 ohms.	Reduce dissipation in Zener diodes 1N3022B and increase reliability	Not incorporated	None
		(2) Purchase the 1N3023B diodes as USN1N3023B, and replace the 1N457 diode with the JAN1N645.	Increase reliability	MIL. parts purchased;	After T-3
		(3) Purchase the 2N329A transistors as JAN2N329 and the 2N335 as USN 2N335	Increase reliability	MIL. parts purchased;	After T-3
Accelerometer Signal Conditioner	Data Collection, Conditioning, and Transmission	Replace the Bourns wire-wound 100-kilohm trimmer potentiometers (RCA 1700820-4) with the Bourns Type 3011.	Increase reliability	Change incorporated	T-1B-3 and T-3
SERT Signal Conditioner	Data Collection, Conditioning, and Transmission	(1) Replace diodes 1N457, 1N643, 1N3029, 1N752, 1N033, and 1N751, with diodes JAN1N645, USA1N643, USN1N3029B, USN1N752A, USN1N3033B and USN1N751A respectively.	Increase reliability	JAN1N645 incorporated but it was not expedient to incorporate the others.	T-1B-3 and T-3
		(2) Consider replacing transistor DEP03A (2N338) with type 2N1893 from either Fairchild or Texas Instruments, and purchase type 2N328A as JAN2N528-AM	Increase reliability	Not incorporated; unit had already been qualified and accepted, and no operational failures due to these parts had occurred.	None
		(3) Modify RCA Dwg. No. 1700850 to require Group A and Group B testing per MIL-R-5757, and follow by RCA run-in testing developed by RCA Central Engineering	Increase reliability and sort out defects to which the run-in testing is not sensitive	Not incorporated; parts had already been preconditioned per RCA, AED specifications. Run-in procedure was instituted.	None

The stress analysis served a twofold purpose:

- (1) It ensured that the parts selected had a proven capability of operating over the intended environment (i.e., shock, vibration, and thermal-vacuum).
- (2) It ensured that the electrical stresses imposed on the part by the associated circuitry in combination with environmental conditions were such that the part did not present an unusual reliability risk.

The components analyzed were those developed by AED. Details were not available on the RF subsystem components or subcarrier oscillator packages (SCO's); analysis of these purchased components did not form a part of the effort.

The reliability estimate for the system components was the probability that the components would survive the launch environment and the succeeding mission interval. For SERT, the launch environment had a time duration of 0.083 hour, with 0.80 hour following for the remainder of the mission. The individual probabilities of component survival were as follows:

<u>Component</u>	<u>P_s</u>
Power Switching Unit (exclusive of squib-resistors)	0.999958
SERT Signal Conditioner	0.999955
Command Subsystem	0.9994
Neutralizer Voltage Control Unit	0.99924
LeRC Probe and Amplifier	0.99987
Sun-Sensor Assembly, Regulator, and Revolution Counter	0.999983
Accelerometer Signal Conditioner	0.9985
Mechanical Subsystem	0.997
Precession Dampers	
Engine Unfold	
Antenna Ground Plane	
Squib Current-Limiting Resistors	0.975

E. SUMMARY OF RELIABILITY ANALYSIS

A reliability estimate of the RCA-developed portions of the SERT I Spacecraft was 0.969. This probability was based upon a launch interval of 0.083 hour followed by a mission lasting 0.80 hour; this estimate was a product of the probabilities of the components listed in paragraph VII-D and was based upon an all-MIL-parts system. A review of the parts distribution in the SERT Spacecraft revealed that approximately two-thirds of the parts used were either military standard types or those purchased to RCA drawings or specifications calling for military standards types of testing, qualification, and approval. Those failure rates appearing in MIL-Handbook 217 then apply to these parts, so long as their usage falls within the limits as specified by the handbook. The remaining one-third of the parts used were of commercial grade. Since the analysis and failure-rate assignment was based upon usage of Military parts throughout, the following procedure was utilized to estimate the reliability of the system as it existed with one-third commercial parts.

- (1) The total failure rate of the present system was estimated, exclusive of special parts, unusual applications, and mechanical operations.
- (2) One-third of this total, assuming a uniform distribution of part types and failure rates, was increased by a factor of ten. This was the assumed higher failure rate of commercial parts.
- (3) The resulting rate was added to the system, along with the failure rates applicable to the unusual parts or unusual part applications.
- (4) From this total, a probability of survival was estimated and the product of this and the probabilities of the one-shot devices gave an over-all reliability estimate.

REFERENCES

-
- VII-1 RCA Report AED R-2096, "Failure Mode and Effect Analysis of SERT I," Contract NAS-8-2449, Sep 10, 1963.
- VII-2 RCA Report AED R-2139, "Failure Mode and Effect Analysis of SERT I Ground Support Equipment," Contract NAS-8-2449, Oct 10, 1963.
- VII-3 RCA Report AED R-2140, "SERT I Spacecraft Reliability Estimate and Parts Application Review," Contract NAS-8-2449, Oct 21, 1963.

APPENDIX A

ANALYTICAL DETERMINATION OF SERT BALANCE AND MOMENTS OF INERTIA (Configuration C)

1. General

This appendix describes the analytical determination of the balance (static and dynamic) and the moments of inertia for the SERT spacecraft. The final configuration (C) is considered.

2. Analytical Relationships

The expression for the static unbalance of the SERT spacecraft, whose reference axes are described in Figure A-1 are:

$$\bar{x}_o \sum_{n=1}^k W_n = \sum_{n=1}^k W_n x_n \quad (\text{A-1})$$

and

$$\bar{y}_o \sum_{n=1}^k W_n = \sum_{n=1}^k W_n y_n \quad (\text{A-2})$$

where

W_n is the weight of the n^{th} discrete weight element (in this case, spacecraft component),

x_n, y_n are the X- and Y-components of distance from the center of the axis system to the center of mass of the n^{th} component, and

\bar{x}_o, \bar{y}_o define the location of the composite center of mass with respect to the reference axes.

Similarly, the location of the total center of mass along the Z-axis is given by:

$$\bar{z}_o = \frac{\sum_{n=1}^k (W_n z_n)}{\sum_{n=1}^k (W_n)} \quad (\text{A-3})$$

where z_n is the Z-component of distance from the center of the axis system to the center of mass of the n^{th} component.

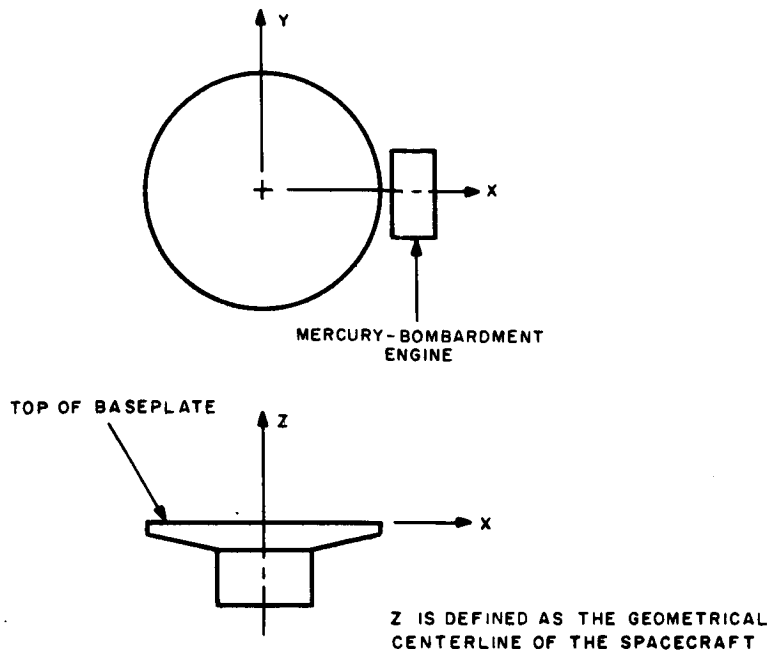


Figure A-1. SERT Reference Axes

In the engines-folded condition, SERT must be statically balanced to 50 ounce-inches; i. e., the right-hand summations of equations (A-1) and (A-2) must be within this value. The only requirement on the engines-extended condition is that the center of mass be known.

The relationships for the dynamic unbalance about the X-, Y-, and Z-axes passing through the center of mass are:

$$g J_{x_0 z_0} = \sum_{n=1}^k W_n x_n z_n + \sum_{n=1}^k (g J_{xz})_n - \bar{x}_0 \bar{z}_0 \sum_{n=1}^k W_n \quad (A-4)$$

$$g J_{y_0 z_0} = \sum_{n=1}^k W_n y_n z_n + \sum_{n=1}^k (g J_{yz})_n - \bar{y}_0 \bar{z}_0 \sum_{n=1}^k W_n \quad (A-5)$$

where

g is the acceleration due to gravity,

$J_{x_0 z_0}$, $J_{y_0 z_0}$ are products of inertia with respect to the reference axes, and

J_{xz} , J_{yz} are the products of inertias of the individual components, about axes parallel to the reference axes and passing through the individual center of mass. The remaining symbols have been defined for equations (A-1) and (A-2).

The dynamic unbalances, $g J_{x_0 z_0}$ and $g J_{y_0 z_0}$, cannot exceed 200 ounce-inches in the engines-folded condition, and must be known in the engines-extended condition.

The X- and Y-principal axes may be located using Mohr's circle and the relationship:

$$g J_{x_0 y_0} = \sum_{n=1}^k W_n x_n y_n + \sum_{n=1}^k (g J_{xy})_n - \bar{x}_o \bar{y}_o \sum_{n=1}^k W_n \quad (A-6)$$

The moment of inertias are expressed as follows:

$$g I_{x_0 y_0} = \sum_{n=1}^k W_n y_n^2 + \sum_{n=1}^k W_n z_n^2 + \sum_{n=1}^k (g I_{xx})_n - \bar{y}_o^2 \sum_{n=1}^k W_n - \bar{z}_o^2 \sum_{n=1}^k W_n \quad (A-7)$$

$$g I_{y_0 y_0} = \sum_{n=1}^k W_n x_n^2 + \sum_{n=1}^k W_n z_n^2 + \sum_{n=1}^k (g I_{yy})_n - \bar{x}_o^2 \sum_{n=1}^k W_n - \bar{z}_o^2 \sum_{n=1}^k W_n \quad (A-8)$$

$$g I_{z_0 z_0} = \sum_{n=1}^k W_n x_n^2 + \sum_{n=1}^k W_n y_n^2 + \sum_{n=1}^k (g I_{zz})_n - \bar{x}_o^2 \sum_{n=1}^k W_n - \bar{y}_o^2 \sum_{n=1}^k W_n \quad (A-9)$$

where

$I_{x_0 x_0}$, $I_{y_0 y_0}$, $I_{z_0 z_0}$ are mass moments of inertia about the reference X-, Y-, and Z-axes.

3. Calculations

Table A-1 summarizes the tabulations of the balance and moment of inertia contributions of the various components, and, in addition, important summations for engines-folded balance (with balance weights) and engines-extended unbalance.

a. Static and Dynamic Balance

The tabulations for static and dynamic balance are given in columns 1 through 7 and 11, 12, and 13 of Table A-1. Subtotal A (fixed components) and subtotal B (moving components in folded condition) are summed with balance weights (C) selected such as to give $\sum Wx = 0$, $\sum Wy = 0$, $\sum Wxz = 0$, and $\sum Wyz = 0$. Note that the second and third terms in equations (A-4), (A-5) and (A-6) are not considered; the individual products of inertia were found to be negligible for the purposes of the analytical investigation, and the third item is zero in each case since the balance weights provide for $\bar{x}_o = \bar{y}_o = 0$. The Z-axis location of the center of mass as given by equation (A-3) is

$$\bar{z}_o = \frac{-267.20}{362.10^*} = -0.74 \text{ inches (below top of baseplate).}$$

*Note that the final computed weights are approximately ten pounds less than the equivalent empirical weight of the T-3 spacecraft. This 3-percent difference is due to a combination of (1) a special umbilical and circuit for cooling the cesium-contact-engine inverter added at NASA request, (2) harness tacking and potting added after assembly, (3) a different final balance-weight configuration, (4) additional miscellaneous hardware, and (5) uncertainties in actual T-3 hardware weights.

COMPONENT	Component No.	W (lbs)	X (in)	Y (in)	Z (in)	WX	WY
Mercury-Bombardment-Engine DC Power Supply	1A	30.43	3.92	9.16	-6.25	119.29	278.74
Mercury-Bombardment-Engine AC Power Supply	1B	30.18	-2.90	-10.66	-6.55	-87.52	-321.72
Cesium-Contact-Engine Inverter	2A	7.89	12.62	0.00	1.10	99.57	0.0
Cesium-Contact-Engine AC Power Supply	2B	16.29	7.60	-8.77	2.81	123.80	-142.86
Cesium-Contact-Engine DC Power Supply	2C	9.82	-8.14	8.00	2.12	-79.93	78.56
Cesium-Contact-Engine Control Box	2D	6.75	-8.35	9.75	7.28	-56.36	65.81
Telemetry Converter	3A	3.30	7.37	7.10	1.60	24.32	23.43
Telemetry Converter	3B	3.26	-7.40	-7.10	1.60	-24.12	-23.15
Baseplate	4A	10.72	0.0	0.00	-0.40	0.0	0.0
Upper Column	4B	3.16	0.0	0.00	-5.70	0.0	0.0
Lower Column		6.98	0.0	0.0	-11.28	0.0	0.0
Ground Plane, Clamp, & Squib	43	0.50	0.0	0.0	-11.50	0.0	0.0
Pallet Spacer		0.27	0.0	0.0	-8.40	0.0	0.0
Mercury-Bombardment-Engine Neutralizer Power Supply & Transformer	5A, 5C	9.79	-7.15	0.10	2.45	-70.00	0.98
Mercury-Bombardment-Engine NVCU	5B	3.12	0.42	-2.50	13.00	1.31	-7.80
Main Battery	6A	27.98	0.50	9.46	2.60	13.99	264.69
Main Battery	6B	27.98	-0.80	-9.46	2.60	-22.38	-264.69
Telemetry Battery	7	10.71	-11.70	0.17	2.00	-125.31	1.82
Programmer	8	11.55	1.55	-2.50	5.85	17.90	-28.88
Mercury-Bombardment-Engine Magnetic Field Supply & Voltage Transducer	9A, 9B	9.79	9.30	-0.08	2.45	91.05	-0.78
Signal Conditioner (& commutators)	10, 19A & 19B	7.76	2.87	2.23	6.38	22.27	17.30
Telemetry SCO	11A	1.15	-1.30	10.14	6.40	-1.50	11.66
Telemetry SCO	11B	1.15	1.00	-11.64	6.40	1.00	-13.39
Telemetry Power Amp	12A	1.43	2.52	10.14	6.70	3.60	14.50
Telemetry Pwr Ampl	12B	1.43	-2.74	-11.64	6.70	-3.92	-16.65
Command Subsystem	13A, 13B	5.10	0.0	0.0	-5.92	0.0	0.0
Power Switching Unit	14A	6.29	-2.30	2.55	4.65	-14.47	16.04
Distributor Frame Assy.	14B	4.87	0.40	0.58	5.42	1.95	2.83
Transmitter Mount	15A	1.41	7.50	11.60	2.50	10.58	16.36
Transmitter Mount	15B	1.41	-8.65	-11.65	2.50	-12.20	-16.43
Ion-Beam Probe Signal Cond.	16B	3.00	7.44	-9.05	-4.40	22.32	-27.15
Squib for release of engines	A	0.15	-5.50	1.50	-7.50	-0.83	0.23
	B	0.15	4.70	3.50	-8.00	0.71	0.53

A-5

TABLE A-1. SERT BALANCE AND
MOMENT OF INERTIA COMPUTATION -
T-3 SPACECRAFT

WZ	WX ²	WY ²	WZ ²	WXZ	WYZ	WZY	g lxx	g lyy	g lzz
-190.19	467.6	2553.3	1188.7	-745.6	-1742.1	1092.7	326	386	370
-197.68	253.8	3429.5	1294.8	573.3	2107.3	933.0	324	385	366
8.68	1256.6	0.0	9.6	109.5	0.0	0.0	110	7	109
45.77	940.9	1252.9	128.6	347.9	-401.4	-1085.7	102	120	120
20.82	651.0	629.0	44.0	-170.0	167.0	-640.0	45	45	49
49.14	471.0	642.0	358.0	-410.3	479.1	-550.0	31	31	34
5.28	179.2	166.4	8.5	38.9	37.5	172.7	11	5	9
5.22	178.5	164.4	8.4	-38.6	-37.0	171.3	11	5	9
-4.29	0.0	0.0	2.0	0.0	0.0	0.0	563	56.3	1127
-18.01	0.0	0.0	102.7	0.0	0.0	0.0	41	41	61
-78.73	0.0	0.0	888.1	0.0	0.0	0.0	66	66	126
-5.75	0.0	0.0	66.0	0.0	0.0	0.0	-	-	-
-2.27	0.0	0.0	19.0	0.0	0.0	0.0	-	-	-
23.99	501.0	0.0	59.0	-172.0	2.0	-7.0	58	28	50
40.56	1.0	20.0	527.0	17.0	-101.0	-3.0	5	38	38
72.75	7.0	2504.0	189.2	36.4	688.2	132.4	260	260	379
72.75	17.9	2504.0	189.2	-58.2	-688.2	217.8	260	260	379
21.42	1466.0	0.0	43.0	-251.0	4.0	-21.0	74	37	70
67.57	28.0	72.0	395.0	105.0	-169.0	-45.0	116	174	97
23.99	847.0	0.0	59.0	223.0	-2.0	-7.0	58	28	50
49.51	64.0	39.0	316.0	142.0	110.0	50.0	1	2	2
7.36	2.0	118.2	47.0	-9.6	74.6	-15.2	1	2	2
7.36	1.0	115.9	47.0	6.4	-85.7	-11.6	2	2	2
9.58	9.1	147.0	64.0	24.1	97.2	36.5	2	2	2
9.58	10.7	193.8	64.0	-26.3	-111.5	45.6	2	2	2
-30.19	0.0	0.0	179.0	0.0	0.0	0.0	75	75	125
29.25	33.0	41.0	136.0	-67.0	75.0	-37.0	68	71	19
26.40	0.8	1.6	143.1	10.6	15.3	1.1	126	161	181
3.53	79.4	189.8	8.8	26.5	40.9	122.7	4	5	4
1.52	34.0	99.0	3.0	10.0	17.0	58.0	-	-	-
3.53	105.5	191.4	8.8	-30.5	-41.1	142.1	4	5	4
1.52	57.0	100.0	3.0	-13.0	-17.0	76.0	-	-	-
-13.20	166.1	245.7	58.1	-98.2	119.5	-202.0	9	9	9
-1.13	4.6	0.3	8.5	6.2	-1.7	-1.3	-	-	-
-1.20	3.3	1.9	9.6	-5.7	-4.2	2.5	-	-	-

Form No. E515

A-6

COMPONENT	Component No.	W (lbs)	X (in)	Y (in)	Z (in)	WX	WY
Mercury-Bombardment-Engine Arm Brackets (2)		0.81	10.00	0.0	-2.10	8.10	0.0
Cesium-Contact-Engine Center Arm							
Bracket (1)		0.79	-9.60	0.0	-2.32	-7.58	0.0
Cesium-Contact-Engine Side Arm							
Brackets (2)	17	0.56	-9.35	0.0	-1.82	-5.24	0.0
Mercury-Bombardment-Engine Damper (1)		1.93	8.70	0.0	-3.30	16.79	0.0
Cesium-Contact-Engine Dampers (2)		3.86	-7.50	0.0	-4.10	-28.95	0.0
Coupling Network	20A	2.33	0.0	0.0	-10.40	0.0	0.0
A-R Diplexer	20B	1.20	4.93	-8.44	-2.90	5.92	-10.13
Sun Sensor	21A	0.78	-2.60	13.00	-3.25	-2.03	10.14
Sun Sensor	21B	0.78	5.34	-13.00	-3.25	4.17	-10.14
Precession Damper	27A	1.24	10.40	7.10	0.0	12.90	8.80
Precession Damper	27B	1.24	-10.40	-7.10	0.0	-12.90	-8.80
Antenna & Cabling	29	0.56	0.0	0.0	-12.50	0.0	0.0
Harness (Cabling, Conn, etc.)	30	15.50	0.0	0.0	5.50	0.0	0.0
Misc. Hardware		1.77	0.0	0.0	0.0	0.0	0.0
Underside Mounting							
Blocks	32A	0.43	-4.70	-4.57	-1.30	-2.02	-1.97
	B	0.43	-8.38	-5.80	-1.30	-3.60	-2.49
	C	0.43	-7.20	-10.82	-1.30	-3.10	-4.65
	D	0.43	2.50	-12.72	-1.30	1.08	-5.47
	E	0.43	2.10	-10.55	-1.30	0.90	-4.54
	F	0.43	2.60	-6.08	-1.30	1.12	-2.61
	G	0.43	5.93	4.00	-1.30	2.55	1.72
	H	0.43	8.69	5.75	-1.30	3.74	2.47
	I	0.43	9.10	9.20	-1.30	3.91	3.96
	J	0.43	0.09	13.27	-1.30	0.04	5.71
	K	0.43	-3.87	9.95	-1.30	-1.66	4.28
	L	0.43	-1.45	6.82	-1.30	-0.62	2.93
	M	0.43	6.77	-6.75	-1.30	2.91	-2.90
	N	0.43	7.45	-11.05	-1.30	3.20	-4.75
	O	0.30	3.78	-6.44	-1.30	1.13	-1.93
	P	0.30	3.90	-10.95	-1.30	1.17	-3.29
	Q	0.30	6.08	-10.54	-1.30	1.82	-3.16
	R	0.30	5.48	-5.98	-1.30	1.64	-1.79
	S	0.30	5.98	-4.20	-1.30	1.79	-1.26
	T	0.30	6.09	-2.75	-1.30	1.83	-0.83
Underside Mounting	U	0.30	9.07	-4.28	-1.30	2.72	-1.28
Blocks	32V	0.30	9.00	-2.80	-1.30	-0.70	-0.84

A-7

TABLE A-1. SERT BALANCE AND
MOMENT OF INERTIA COMPUTATION -
T-3 SPACECRAFT (Continued)

WZ	WX ²	WY ²	WZ ²	WXZ	WYZ	WXY	gIxx	gIyy	gIzz
-1.70	81.0	0.0	3.6	-17.0	0.0	0.0	3	2	3
-1.83	72.8	0.0	4.3	17.6	0.0	0.0	1	1	1
-1.02	49.0	0.0	1.9	9.5	0.0	0.0	9	2	9
-6.37	146.1	0.0	21.0	-55.4	0.0	0.0	2	5	5
-15.83	217.1	0.0	64.9	118.7	0.0	0.0	19	10	25
-24.23	0.0	0.0	252.0	0.0	0.0	0.0			
-3.48	29.2	85.5	10.1	-17.2	29.4	-50.0	4	1	4
-2.54	5.3	131.8	8.3	6.6	-33.0	-26.4	2	2	0
-2.54	22.3	131.8	8.3	-13.6	33.0	-54.2	2	2	0
0.0	134.2	62.5	0.0	0.0	0.0	91.6	26	26	0
0.0	134.2	62.5	0.0	0.0	0.0	91.6	26	26	0
-7.00	0.0	0.0	88.0	0.0	0.0	0.0			
85.25	0.0	0.0	468.9	0.0	0.0	0.0	821	821	1423
0.0	0.0	0.0	0.0	0.0	0.0	0.0	210	210	420
-0.56	9.5	9.0	0.7	2.6	2.56	9.23			
-0.56	30.2	14.4	0.7	4.7	3.24	20.88			
-0.56	22.3	50.3	0.7	4.0	6.05	33.54			
-0.56	2.7	69.6	0.7	-1.4	7.11	-13.74			
-0.56	1.9	47.9	0.7	-1.2	5.90	-9.50			
-0.56	2.9	15.9	0.7	-1.5	3.39	-6.81			
-0.56	15.1	6.9	0.7	-3.3	-2.24	10.20			
-0.56	32.5	14.2	0.7	-4.9	-3.21	21.51			
-0.56	35.6	36.4	0.7	-5.1	-5.15	35.97			
-0.56	0.00	75.8	0.7	-0.1	-7.42	0.53			
-0.56	6.4	42.6	0.7	2.2	-5.56	-16.52			
-0.56	0.9	20.0	0.7	0.8	-3.81	-4.23			
-0.56	19.7	19.6	0.7	-3.8	3.77	-19.64			
-0.56	23.8	52.5	0.7	-4.2	6.18	-35.36			
-0.39	4.3	12.4	0.5	-1.5	2.51	-7.28			
-0.39	4.6	36.0	0.5	-1.5	4.28	-12.81			
-0.39	11.1	33.3	0.5	-2.4	4.11	-19.18			
-0.39	9.0	10.7	0.5	-2.1	2.33	-9.81			
-0.39	10.7	5.3	0.5	-2.3	1.64	-7.52			
-0.39	11.1	2.3	0.5	-2.4	1.08	-5.03			
-0.39	24.7	5.5	0.5	-3.5	1.66	-11.64			
-0.39	24.3	2.4	0.5	-3.5	1.09	-7.56			

Form No. E515

A-8

COMPONENT	Component No.	W (lbs)	X (in)	Y (in)	Z (in)	WX	WY
Radial Accelerometer & Mounting Bracket	36	5.00	-6.35	9.40	-5.45	-31.75	47.00
		2.34	-4.20	6.25	-5.00	-9.83	14.63
Ion-Beam Probe SPS	38	1.71	7.50	-4.20	-4.40	12.83	-7.18
Sun Sensor Volt. Reg.	40	0.20	-1.30	-11.53	-2.20	-0.26	-2.31
D. C. Amplifier	41A	0.40	5.50	2.00	13.00	2.20	0.80
D. C. Amplifier	41B	0.40	1.20	2.00	13.00	0.48	0.80
Duplexer Ballast Load	42	0.82	2.20	11.00	-0.45	1.80	9.02
Flyaway Mounting Block		0.15					
Fuse Block	44	0.79	0.50	7.30	6.40	0.40	5.77
Auxiliary Command Unit	37	1.39	-0.80	-7.10	6.70	-1.11	-9.87
SUBTOTAL A		322.34				42.75	-44.22
Ion-Beam Probe Ass'y	16A	3.10	10.95	-4.75	-3.90	33.95	-14.73
Cesium-Contact Ion Engine	18	14.00	-10.20	0.0	-10.40	-142.80	0.00
Mercury-Bombardment-Engine Mounting Arm	22	1.41	11.75	0.0	-3.65	16.57	0.00
Cesium-Contact-Engine Mounting Arm	23	0.91	-12.00	0.0	-3.10	-10.92	0.00
Mercury-Bombardment Ion Engine	28	11.60	10.20	0.0	-10.50	118.32	0.00
Detuning Wing	31A	0.20	0.0	12.80	-9.00	0.0	2.56
Detuning Wing	31B	0.20	0.0	-12.80	-9.00	0.0	-2.56
SUBTOTAL B		31.42				15.12	-14.73
Balance Weights							
C	K ₁	4.13	-14.00	0.00	1.26	-57.87	0.00
		3.33	0.0	14.00	-9.30	0.00	46.62
		0.88	0.0	14.00	0.00	0.00	12.32
TOTAL (Engines Folded) (A + B + C)		362.10				0.00	0.00
Ion-Beam Probe Ass'y	16A	3.10	15.40	-4.75	-2.20	47.74	-14.73
Cesium-Contact Engine	18	13.15	-21.75	0.30	-3.35	-286.01	3.94
Mercury-Bombardment-Engine Mounting Arm	22	1.41	14.95	0.00	-1.40	21.08	0.00
Cesium-Contact-Engine Mounting Arm	23	0.91	-14.30	0.00	-1.70	-13.01	0.00
Mercury-Bombardment Ion Engine	28	11.60	20.25	0.00	-1.35	224.90	0.00
Detuning Wing	31A	0.20	0.0	21.80	1.00	0.00	4.36
Detuning Wing	31B	0.20	0.0	-21.80	1.00	0.00	-4.36
SUBTOTAL D		30.57				4.70	-10.79
TOTAL (Engines Extended) (A + C + D)		361.25				-10.42	+3.93

TABLE A-1. SERT BALANCE AND
MOMENT OF INERTIA COMPUTATION -
T-3 SPACECRAFT (Continued)

WZ	WX ²	WY ²	WZ ²	WXZ	WYZ	WXY	g Ixx	g Iyy	g Izz
-27.25	201.6	441.8	148.5	173.0	-256.2	-298.5	24	24	24
-11.70	41.3	91.4	58.5	49.2	-73.2	-61.4			
-7.52	96.2	30.2	33.1	-56.5	31.6	-53.9	1	3.	3.
-0.44	0.3	26.6	1.0	0.6	5.1	3.0	-	-	-
5.20	12.1	1.6	67.6	28.6	10.4	4.40	-	-	-
5.20	0.6	1.6	67.6	6.2	10.4	1.0	-	-	-
-0.37	4.0	99.2	0.2	-0.8	-4.1	19.8	-	-	-
5.06	0.2	42.1	32.4	2.6	36.9	2.9	-	-	-
9.31	0.9	70.1	62.4	-7.4	-66.1	7.9	3	4	5
49.63	9388.7	17,323.8	8092.1	-204.9	386.41	251.63	3908	3954	5717
-12.09	372.0	70.0	47.0	-132.0	57.0	-161.0	14	6	12
-145.60	1457.0	0.0	1514.0	1485.1	0.0	0.0	224.0	112	224
-5.15	194.7	0.0	18.8	-60.5	0.0	0.0	-	-	-
-2.82	131.0	0.0	8.7	33.9	0.0	0.0	-	-	-
-121.80	1206.9	0.0	1278.9	-1242.4	0.0	0.0	79	64	79
-1.80	0.0	32.8	16.2	0.0	-23.0	0.0	-	-	-
-1.80	0.0	32.8	16.2	0.0	23.0	0.0	-	-	-
-291.06	3361.6	135.6	2899.8	84.1	57.0	-	317	182	315
5.20	810.2	0.0	6.6	-72.8	0.0	0.0	-	-	-
-30.97	0.0	652.7	288.0	0.0	-433.6	0.0	-	-	-
0.0	0.0	172.5	0.0	0.0	0.0	0.0	-	-	-
-267.20	13560.23	18284.6	11350.9	0.0	0.0	181.26	4225	4136	6032
-6.82	735.0	70.0	15.0	-105.0	32.0	-227.0	14.	6.	12.
-44.05	6221.0	1.0	148.0	958.1	-13.2	-86.0	224.	112	224
-1.97	315.1	0.0	2.8	-29.5	0.0	0.0	-	-	-
-1.55	186.0	0.0	2.6	22.1	0.0	0.0	-	-	-
-15.66	4756.7	0.0	21.1	-317.1	0.0	0.0	79	64	79
0.20	0.0	95.1	0.2	0.0	4.36	0.0	-	-	-
0.20	0.0	95.1	0.2	0.0	-4.36	0.0	-	-	-
-69.65	12213.8	261.2	189.9	528.6	18.8	-313.0	317	182	315
-45.79	22412.7	18410.2	8576.6	250.9	-28.39	29.26	4225	4136	6032

Form No. E515

A-10

The engine-extended relationships may be derived from subtotal D and equations (A-1) through (A-6), as follows:

$$\bar{x}_o = \frac{-10.42}{361.25} = -0.029 \text{ inches.}$$

$$\bar{y}_o = \frac{+3.93}{361.25} = -0.011 \text{ inches.}$$

$$\bar{z}_o = \frac{-45.79}{361.25} = -0.127 \text{ inches.}$$

About axes parallel to X, Y, and Z and passing through the center of mass:

$$g J_{x_o z_o} = 250.9 - (-0.029)(-0.127)(361.25) = 249.6 \text{ lb-in}^2$$

$$g J_{y_o z_o} = 28.39 - (0.011)(-0.127)(361.25) = 27.88 \text{ lb-in}^2$$

$$g J_{x_o y_o} = 29.26 - (-0.029)(0.011)(361.25) = 29.37 \text{ lb-in}^2$$

b. Moments of Inertia

The tabulations for the moment-of-inertia calculations are presented in columns 8, 9, 10, 14, 15, and 16 of Table A-1. For the engines-folded conditions, equations (A-7), (A-8), and (A-9) yield the following (for axes parallel to X, Y, and Z and passing through the center of mass):

$$g I_{x_o x_o} = 18,284.6 + 11,350.9 + 4225 - (-0.74)^2 (362.10) = 33,662.2 \text{ lb-in}^2$$

$$g I_{y_o y_o} = 13,560.2 + 11,350.9 + 4136 - (-0.74)^2 (362.10) = 28,848.8 \text{ lb-in}^2$$

$$g I_{z_o z_o} = 13,560.2 + 18,284.6 + 6032 = 37,876.8 \text{ lb-in}^2$$

For the engines-extended conditions, the moments of inertia about axes parallel to X, Y, and Z and passing through the center of mass are:

$$\begin{aligned} g I_{x_o x_o} &= 18,410.2 + 8,576.6 + 4225 - (0.011)^2 (361.25) - (-0.127)^2 (361.25) \\ &= 31,206.0 \text{ lb.-in}^2 \end{aligned}$$

$$\begin{aligned}
 g I_{y_0 y_0} &= 22,412.7 + 8,576.6 + 4136 - (-0.029)^2 (361.25) - (-0.127)^2 (361.25) \\
 &= 35,119.2 \text{ lb-in}^2
 \end{aligned}$$

$$\begin{aligned}
 g I_{z_0 z_0} &= 22,412.7 + 18,410.2 + 6032 - (-0.029)^2 (361.25) - (0.011)^2 (361.25) \\
 &= 46,854.6 \text{ lb-in}^2
 \end{aligned}$$

The location of the principal axes and values of principal moments of inertias for the engines-extended case are given by the characteristic equations:

$$\begin{aligned}
 (I_{x_0 x_0} - \lambda) \alpha - J_{x_0 y_0} \beta - J_{x_0 z_0} \gamma &= 0 \\
 -J_{x_0 y_0} \alpha + (I_{y_0 y_0} - \lambda) \beta - J_{y_0 z_0} \gamma &= 0 \\
 -J_{x_0 z_0} \alpha - J_{y_0 z_0} \beta + (I_{z_0 z_0} - \lambda) \gamma &= 0
 \end{aligned}$$

where α , β , and γ are the direction cosines to the principal axes.

Solution of these equations will show that the principal axes are within several degrees of the geometric axes and the inertia values are essentially equivalent to those for the geometric axes.

APPENDIX B

SIGNAL-CONDITIONING DATA

This appendix lists the signal-conditioner characteristics for each telemetered parameter; also given are the channel assignments for each parameter. Note that redundancy is provided in twelve of the major signals; these major parameters are assigned to two channels.

LEWIS ENGINE SUBSYSTEM DATA

TELEMETERED PARAMETER ASSIGNMENT		SIGNAL CHARACTERISTICS			SIGNAL CONDITIONER CHARACTERISTICS				REMARKS
SYMBOL		MEASURED RANGE	REFERENCE TO GROUND	ACCURACY, PERCENT OF FULL SCALE	CONDITIONING NETWORK	INPUT IMPEDANCE	OUTPUT IMPEDANCE	CHANNEL ASSIGNMENT	
L-1	Mercury Heater Temperature	0 to 10 v p-p	gnd	2	Rectifier	≈ 1 K	< 18 K	I-17, II-17	-
L-2	Mercury Heater Current	0 to 6 v	gnd	2	Linear	61.1 K ± 1%	8.35 K ± 1%	I-4	-
L-3	Cathode Heater Current	0 to 5 v	gnd	2	Linear	61.1 K ± 1%	8.35 K ± 1%	I-35	-
L-4	Anode-Cathode Voltage	0 to 5 v	gnd	2	Linear	86 K *	22 K	I-36	+ 25 v nominal signal level
L-5	Anode-Cathode Current	0 to 5 v	gnd	2	Linear	61.1 K ± 1%	8.35 K ± 1%	I-18, II-18	-
L-6	Anode-Package Voltage	0 to 5 v	gnd	2	Linear	86 K *	22 K	I-5, II-5**	+ 25 v nominal signal level
L-7	Anode-Package Current	0 to 5 v	gnd	2	Linear	61.1 K ± 1%	8.35 K ± 1%	I-19, II-19	-
L-8	Accelerator-Package Voltage	0 to (-5 v)	gnd	2	Linear	86 K *	22 K	I-37	+ 25 v nominal signal level
L-9	Accelerator-Package Current	0 to 5 v	gnd	2	Linear	61.1 K ± 1%	8.35 K ± 1%	II-20	-
L-10	Neutralizer-Package Current	0 to 6 v	gnd	< 5	Linear	61.1 K ± 1%	8.35 K ± 1%	I-6, II-6	-
L-11	Probe Voltage	50 to 100 mv	+ 2500 v	-	-	-	-	II-21	-
L-12	Probe Voltage	50 to 100 mv	+ 2500 v	-	-	-	-	II-22	-
L-13	Probe Voltage	50 to 100 mv	+ 2500 v	-	-	-	-	II-23	-
L-14	Probe Voltage	50 to 100 mv	+ 2500 v	-	-	-	-	II-24	-
L-15	Probe Voltage	50 to 100 mv	+ 2500 v	-	-	-	-	II-25	-
L-16	Lewis Probe Position	0-5 v	gnd	< 5	Linear	-	-	II-26	-
L-17	Magnetic Field Battery Current	0-5 v	gnd	1	Linear	100 K ± 5%	-	I-29	-
L-18	Neutralizer Battery Current	0-5 v	gnd	1	Linear	100 K ± 5%	-	I-30	-
L-19	Neutralizer Potential	0 to +2500 v	gnd	< 5	Linear	> 5 Megohm	< 10 K	II-27	-

NOTE: All input impedance marked with an asterisk (*) are nominal impedance values. The actual impedance will be adjusted so that the sum of the signal conditioning impedance plus the source impedance is brought to a predetermined impedance level.

HOUSEKEEPING DATA

TELEMETERED PARAMETER		SIGNAL CHARACTERISTICS			SIGNAL CONDITIONER CHARACTERISTICS					REMARKS
SYMBOL	ASSIGNMENT	MEASURED RANGE	REFERENCE TO GROUND	ACCURACY PERCENT OF FULL SCALE	CONDITIONING NETWORK	INPUT IMPEDANCE	OUTPUT IMPEDANCE	CHANNEL ASSIGNMENT		
N-1	Command Receiver AGC.	-0.3 to -1 v	+ 28 v	-	D-C Amp.	-	-	I-25	-	-
N-2A	Main Battery Voltage	0 to 67 v	gnd	2	Linear	129 K *	22.5 K	I-26	56 v nominal	
N-2B	Main Battery Voltage	0 to 67 v	gnd	2	Linear	68.5 K ± 1%	4.75 K ± 1%	II-30	-	
N-3	Main Battery Current	50 mv	gnd	<5	D-C Amp.	-	<5 K	II-39	-	
N-4	Main Battery Pressure	0 to 5 v	gnd	1	Linear	100 K ± 5%	-	II-32	2 K Pair* 5 v supplied by RCA	
N-5	Main Battery Temperature	0 to 5 v	gnd	2	Linear	-	<35 K	II-4	10°C - 80°C	
N-6	Telemetry Battery Voltage	0 to 34 v	gnd	2	Linear	97.6 K *	29.2 K	I-28	28 v nominal	
N-7	Telemetry Battery Current	50 mv	gnd	<5	D-C Amp.	-	<5 K	II-33	-	
N-8	Telemetry Battery Temperature	0 to 5 v	gnd	2	Linear	-	<35 K	II-34	10°C - 80°C	
N-9	Main Battery Temperature	0 to 5 v	gnd	2	Linear	-	<35 K	II-35	10°C - 80°C	
N-10	Power Supply #1A Temperature	0 to 5 v	gnd	2	Linear	-	<35 K	I-31	10°C - 80°C	
N-11	Power Supply #1B Temperature	0 to 5 v	gnd	2	Linear	-	<35 K	II-31	10°C - 80°C	
N-12	Power Supply #1A Pressure	0 to 5 v	gnd	2	Linear	-	<35 K	I-27	10°C - 80°C	
N-13	Power Supply #1B Pressure	0 to 5 v	gnd	2.	Linear	-	<35 K	II-40	10°C - 80°C	
N-14	0 v Calibration	-	gnd			Not Conditioned		I-1, II-1		
N-15	2.5 v Calibration	-	gnd			Not Conditioned		II-3		
N-16	5.0 v Calibration	-	gnd			Not Conditioned		I-2, II-2		
N-17	AYU Mode Indication	0 to 5 v	gnd			Not Conditioned		I-3		Coded Channel **

* In GFE pressure transducer

** Code is as follows:

Mode	Voltage
I	2.0 v
II	4.0 v

HOUSEKEEPING DATA

SYMBOL	TELEMETRED PARAMETER ASSIGNMENT	SIGNAL CHARACTERISTICS		SIGNAL CONDITIONER CHARACTERISTICS					REMARKS
		MEASURED RANGE	REFERENCE TO GROUND	ACCURACY, PERCENT OF FULL SCALE	CONDITIONING NETWORK	INPUT IMPEDANCE	OUTPUT IMPEDANCE	CHANNEL ASSIGNMENT	
R-1	Confirm Unfold - Separate	0 to 28 v	gnd	2	Linear	-	<35 K	I-20	Coded Signal †
R-2	Hughes Inverter #2A Temperature	0 to 5 v	gnd	2	Linear	-	<35 K	I-21	10° - 80° C
R-3	Telemetry P. A. # 12A Temperature	0 to 5 v	gnd	2	Linear	-	<35 K	I-22	10° - 80° C
R-4	Neut. Voltage Control Unit Temp.	0 to 5 v	gnd	2	Linear	-	<35 K	II-28	10° - 80° C
R-5	Telemetry D-C Converter #3B Temp.	0 to 5 v	gnd	2	Linear	-	<35 K	II-29	10° - 80° C
R-6	F. M. Transmitter #15B Temp.	0 to 5 v	gnd	2	Linear	-	<35 K	I-23	10° - 80° C
R-8	Command Receiver Temperature	0 to 5 v	gnd	2	Linear	-	<35 K	I-24	10° - 80° C

† Code is as follows:

Lewis Engine	Hughes Engine	Separate	Voltage
Unfolded	Unfolded	Yes	0
Folded	Unfolded	No	1.0
Unfolded	Folded	Yes	1.35
Folded	Folded	No	2.0
Unfolded	Unfolded	Yes	2.25
Folded	Unfolded	No	2.85
Unfolded	Folded	Yes	3.15
Folded	Folded	No	3.95

HUGHES ENGINE SUBSYSTEM DATA

TELEMETERED PARAMETER ASSIGNMENT		SIGNAL CHARACTERISTICS		SIGNAL CONDITIONER CHARACTERISTICS					REMARKS
SYMBOL	ASSIGNMENT	MEASURED RANGE	REFERENCE TO GROUND	ACCURACY, PERCENT OF FULL SCALE	CONDITIONING NETWORK	INPUT IMPEDANCE	OUTPUT IMPEDANCE	CHANNEL ASSIGNMENT	REMARKS
H-1	Boiler Heater Voltage	0 to 30 v	gnd	2	Linear	61.1 K ± 1%	8.35 K ± 1%	I-32	-
H-2	Boiler Heater Current	0 to 30 v	gnd	2	Linear	61.1 K ± 1%	8.35 K ± 1%	II-36	-
H-3	Stinger Current	0 to 30 v	gnd	2	Linear	61.1 K ± 1%	8.35 K ± 1%	II-37	-
H-4	Valve Heater Current	0 to 30 v	gnd	2	Linear	61.1 K ± 1%	8.35 K ± 1%	I-33	-
H-5 A	Ionizer Heater Voltage	0 to 30 v	gnd	2	Linear	61.1 K ± 1%	8.35 K ± 1%	I-34	-
H-5 B	Ionizer Heater Voltage	0 to 30 v	gnd	2	Linear	100 K *	23.2 K	II-38	22 v nominal
H-6 B	Ionizer Heater Current	0 to 30 v	gnd	2	Linear	86 K *	22 K	I-7, II-7	25 v nominal
H-7 B	Main Drive Voltage	0 to 25 v	gnd	2	Linear	66.4 K *	16.2 K	I-8, II-8	20 v nominal
H-8 A	Main Drive Current	0 to 30 v	gnd	2	Linear	61.1 K ± 1%	8.35 K ± 1%	I-9	-
H-8 B	Main Drive Current	0 to 30 v	gnd	2	Linear	86 K *	22 K	II-9	25 v nominal
H-9	Open	0 to 5 v	gnd	3	Linear	-	-	-	-
H-10	Accelerator Electrode Current	0 to 30 v	gnd	2	Linear	61.1 K ± 1%	8.35 K ± 1%	I-41, II-41	-
H-11	Accelerator Electrode Voltage	0 to 5 v	gnd	1	Linear	100 K ± 5%	-	I-38	-
H-12	Neutralizer Bias Current	0 to 30 v	gnd	2	Linear	61.1 K ± 1%	8.35 K ± 1%	II-42	-
H-13	Neutralizer Voltage	0 to 5 v	gnd	1	Linear	100 K ± 5%	-	I-10, II-10	-
H-14	Neutralizer Current	0 to 30 v	gnd	2	Linear	61.1 K ± 1%	8.35 K ± 1%	I-11, II-11	-
H-15	Neutralizer Heater Voltage	0 to 30 v	gnd	2	Linear	61.1 K ± 1%	8.35 K ± 1%	I-39	-
H-16	Neutralizer Heater Current	0 to 30 v	gnd	2	Linear	61.1 K ± 1%	8.35 K ± 1%	II-43	-

NOTE: All input impedance marked with an asterisk (*) are nominal impedance values. The actual impedance will be adjusted so that the sum of the signal conditioning impedance plus the source impedance is brought to a predetermined impedance level.

DATA (Cont.)

SYMBOL	TELEMETERED PARAMETER ASSIGNMENT	SIGNAL CHARACTERISTICS		SIGNAL CONDITIONER CHARACTERISTICS					REMARKS
		MEASURED RANGE	REFERENCE TO GROUND	ACCURACY, PERCENT OF FULL SCALE	CONDITIONING NETWORK	INPUT IMPEDANCE	OUTPUT IMPEDANCE	CHANNEL ASSIGNMENT	
H-17	Neutralizer Bias Voltage	0 to 5 v	gnd	1	Linear	100 K ± 5%	-	1-12, 11-12	± 10% Accuracy Required
H-18	Beam Probe Current, Outer	0 to 1 microamp	gnd	3	Amplifier	-	<40 K	1-13	± 10% Accuracy Required
H-20	Beam Probe Current, Inner	0 to 1 microamp	gnd	3	Amplifier	-	<40 K	11-13	-
H-21	Electric Field, Low	0 to 5 v	gnd	1	Linear	100 K ± 5%	-	1-40	-
H-22	Electric Field, High	0 to 5 v	gnd	1	Linear	100 K ± 5%	-	1-14, 11-14	-
H-23	Spare	0 to 5 v	gnd	1	Linear	100 K ± 5%	-	1-42	-
H-24	Thermocouple Vacuum Gauge Pod Return Current	0 to 5 v	gnd	1	Linear	100 K ± 5%	-	1-43	Switched *
H-25	Pod Door Open Alternate Neutralizer ON Auto Program	0 to 5 v	gnd	-	Linear	< 100 K	-	1-15, 11-15	Coded Channel **
H-26	Override Received	0 to 5 v	gnd	-	Linear	< 100 K	-	1-16, 11-16	-

* Channel H-24 is switched from "Thermocouple Vacuum Gauge" to "Pod Return Current" during flight by the Hughes Control Box.

** Code is as follows:

Pod Door	Alternate Neutralizer	Auto Program	Voltage
closed	off	off	5.0 v
open	on	reverse	4.8 v
open	off	reverse	3.6 v
open	on	forward	3.0 v

APPENDIX C

TELECOMMUNICATIONS ANALYSIS

1. General

The majority of the following material is drawn from RCA Report SERT TM-1101, Telemetry Subsystem Design Report, dated July 30, 1962. In spite of some minor system changes since the report, such as the addition of the radial accelerometer and the changing of the subcarrier-deviation ratios, the basic design remained conservative and in keeping with mission requirements.

The function of the SERT telecommunications subsystem was to retrieve data during the flight of the SERT spacecraft. This data should, wherever possible, be in a format which lends itself to reception and reduction by standard telemetry ground stations. During the program, particular attention was paid to the capability existing at Wallops Island to insure a maximum degree of compatibility with that telemetry station.

2. Data Requirements

Data to be transmitted from the spacecraft falls into one of the following three categories:

a. Engine and Spacecraft Parameters

This data consists of a total of 80 parameters to be measured during flight. The specified maximum frequency response requirement for any one channel is 1 cps. Parameters include voltages, currents, and other measurements, pertinent to engine performance, which have been converted into voltages and currents acceptable to the telecommunications subsystem.

b. Engine Thrust

The engine thrust is measured by observing the change in spacecraft spin rate produced by each of the engines, in turn; the thrust of the engine is used to provide a torque which either increases or decreases the spin rate of the spacecraft.

c. Spacecraft States

The spacecraft is programmed to go through a definitive operation cycle during flight. The possible states of the spacecraft, at any time during the flight, are confirmed via the telecommunications subsystem. Receipt of commands by the spacecraft are also confirmed via this subsystem.

3. System Design

a. General

To ensure some measure of reliability, two almost identical communications links were selected. Critical telemetered parameters are divided between the two links to insure that some pertinent data from each system will be telemetered even if a malfunction occurs in one of the links.

For compatibility with existing equipment at Wallops Island, and to utilize proven "off-the-shelf" equipment, a standard fm-fm telemetry was chosen as best satisfying the requirements of the SERT spacecraft. A multi-subcarrier approach with PAM (pulse amplitude modulation) commutation was selected in favor of other techniques (e.g., digital) because of its simplicity and compatibility with existing ground facilities. The three separate subcarriers were selected based on the differences in the data response requirements, as well as need to separate the individual types of data. The 10.5-kc channels of both communications links were used to transmit basic engine-performance data with complete redundancy. Similarly, because of its importance, completely redundant active links were specified for the spin-rate data on the 7.35-kc channels. The lesser importance of the programmer and command-status information, which in many cases may be inferred from the engine-performance data, dictated the assignment of non-redundant channels to each of these.

b. RF Bandwidth Considerations

To conserve transmitter-power, the telecommunications subsystem rf bandwidth was kept to a minimum, consistent with the data and stability requirements for bandwidth.

(1) Data Bandwidth Requirements

The maximum subcarrier frequency required for each of the two systems is that necessary to accommodate the 40 channels of data which are time-division multiplexed. Adding two channels for frame synchronization and another three for zero, full scale, and mid range calibration, a 45-channel commutator is required. A two sample-per-second rate is sufficient to accommodate 1 cps for each channel, so that the resulting PAM train is at 90 pps. A baseband of 330 cps (a standard IRIG lowpass filter value) is more than sufficient to provide good pulse reproduction. Similarly, IRIG standards dictate a minimum subcarrier frequency of 10.5 kc to accommodate this wave train. Thus, the maximum baseband frequency for the rf portion of the subsystem is the upper band edge for the 10.5 kc SCO or 11,288 cps.

$$\therefore (f_{sc})_{\text{maximum}} = 11,288 \text{ cps} = \text{maximum rf baseband requirement.}$$

(2) Doppler Shift

The maximum doppler carrier shift will occur when the rocket has reached burnout and, thus, has maximum velocity in a direction away from the observer. Re-entry will not be a problem, since spacecraft motion will be nearly tangential to the observer. Assuming a 200-mile altitude at burnout:

$$V_{\text{max}} = 7.55 \times 10^3 \text{ meters/second;}$$

$$\text{Doppler shift} \approx \frac{V_{\text{max}}}{C} \times f_c \approx \frac{V_{\text{max}}}{C} \times 245 \times 10^6 \approx 6.2 \text{ kc;}$$

$$\text{Where } C = \text{velocity of light} = 3 \times 10^8 \text{ meters/second.}$$

Since spacecraft motion is away from the observer at this point in flight, the doppler shift will be negative. Since effects at re-entry may be neglected, the following figure represents the total doppler frequency shift which may be anticipated.

$$\therefore (BW)_D = 6.2 \text{ kc} = \text{Required r-f doppler bandwidth.}$$

(3) Frequency Stability Requirements

State-of-the-art spacecraft transmitter specifications show that a reasonable transmitter frequency stability is $\pm 0.01\%$. The i.f. bandwidth required for this factor is

$$2 \times 0.01 \times 10^{-2} \times 245 \times 10^6 = 49 \text{ kc};$$

$\therefore (BW)_S = 49 \text{ kc} =$ Bandwidth required to accommodate frequency instability.

(4) Frequency-Deviation Allotment

In keeping with the preceding numbers, the permissible deviation is found as follows:

$$F_d = \frac{(BW)_{IF} - BW}{2},$$

Where $(BW)_{IF}$ is the system i. f. bandwidth and BW is the bandwidth required due to all of the previous considerations.

$$BW = (BW)_D + (BW)_S + 2 (f_{sc}) \text{ maximum} = 77.7 \text{ kc.}$$

If an i. f. bandwidth of 100 kc is used,

$$F_d = 11.15 \text{ kc.}$$

(5) Transmitter Power Requirements

The spacecraft transmitter requirements may be established through the use of the free-space propagation relationship:

$$P_r = P_t - L_{FS} + G_R + G_r - L_D - 0,$$

where

P_r is the received power in db relative to one watt,

P_t is the spacecraft transmitter power in db relative to one watt,

$$L_{FS} \text{ is the } 10 \log \left[\frac{\lambda^2}{(4\pi R)^2} \right],$$

G_R is the gain of the receiving antenna in db,

L_D is the spacecraft diplexer loss in db, and

θ is the polarization loss in db.

The following parameters are known:

L_{FS} (4000 miles maximum range at a transmitter frequency of 245 mc)
= 158.9 db,

G_R (Antenna at Wallops) = 29 db,

G_T (Isotropic radiation on payload) = 0 db,

L_D = 0.5 db,

θ (Power divided between horizontal and vertically polarized receiving antennas) = 3 db,

and

$$P_r = P_n + 12 \text{ db} + P_M.$$

where

P_n is the noise power in the receiver (100 kc i.f. bandwidth),

P_M is the added margin above threshold in the fm receiver (12 db threshold is assumed),

P_n may be found from

$$P_n = K T_S B,$$

where

K is Boltzmann's constant = 1.37×10^{-23} ,

T_S is system temperature, and

B is system i.f. bandwidth = 100 kc.

$$T_S = T_r + T_a,$$

where

T_r is the receiver noise temperature, and

T_a is the antenna temperature (sky temperature).

$$T_r = 290 (NF-1),$$

where NF is the noise factor in absolute units. Assuming a system noise figure of 4 db, $NF = 2.5$, and $T_r = 290 (2.5-1) = 435^\circ$ Kelvin.

T_a at 250 mc may be taken at 620° K, a conservative number if the hottest one percent of the sky area is excluded. Then $T_S = 435 + 620 = 1055^\circ$ K, and $P_n = -148.4$ dbw.

From these figures, and using the free-space propagation relationship, the transmitter power with respect to the system margin may be computed:

$$-148.4 + 12 + P_M = P_t - 157 + 29 + 0 - 0.5 - 3;$$

$$P_t = -5.1 \text{ dbw} + P_M.$$

If a transmitter with a power of 10 watts is used, the resulting system margin above fm threshold is 15 db. In actuality, with the use of phase-locked receivers, the system margin is increased by approximately 5 db from this figure. Since phase-locked receivers are installed at Wallops Island, the above numbers are conservative. The margin computed for a 12-db threshold is necessary, however, due to the aforementioned uncertainty regarding the environment seen by the transmitting antennas during flight.

Thus, a 10-watt transmitter in the spacecraft will provide sufficient received signal strength to insure that ground receiver inputs will not fall below the fm threshold.

(6) Signal-to-Noise Computation for Commutated Channels

The signal-to-noise ratio at the output of each decommutated channel, as indicated in the section on rf bandwidth considerations, will be the same as that computed for the wideband PAM train. The rms signal-to-noise ratio for the PAM train is

$$\frac{S}{N} = \frac{C}{N_{IF}} D_1 D_2 \sqrt{\frac{3}{2}} \sqrt{\frac{(BW)_{IF}}{2 f_m}},$$

where

$\frac{S}{N}$ is the channel or PAM rms signal-to-noise ratio,

C is the rms carrier in the i.f.;

N_{IF} is the rms noise in the i.f.;

D_1 is the deviation ratio of the subcarrier on the carrier;

D_2 is the deviation ratio of the PAM signal on the subcarrier;

$(BW)_{IF}$ is the receiver i.f. bandwidth; and

f_m is the low-pass filter required to pass the PAM waveshape.

The system parameters are

$$\frac{C}{N} = 12 \text{ db} + \text{system margin} = 27 \text{ db};$$

$$D_1 = 1 \text{ or } 0 \text{ db (unity deviation ratio is assumed for the subcarrier);}$$

$$D_2 = 0.8 \times \frac{788}{330} = 1.9 \text{ or } 5.6 \text{ db (where 788 cycles is the maximum allowable deviation on a 10.5 KC subcarrier, and a factor of 0.8 is included due to the pedestal);}$$

$$(BW)_{IF} = 100 \text{ kc};$$

$$f_m = 330 \text{ cycles;}$$

$$\begin{aligned} \frac{S}{N} &= \left(\frac{C}{N}\right)_{\text{db}} + (D_1)_{\text{db}} + (D_2)_{\text{db}} + \left(\sqrt{\frac{3}{2}}\right)_{\text{db}} + \left(\sqrt{\frac{(BW)_{\text{IF}}}{2 f_m}}\right)_{\text{db}} \\ &= 27 + 0 + 5.6 + 2 + 21.8 \\ &= 56.4 \text{ db.} \end{aligned}$$

This figure includes the margin previously computed. At receiver threshold, S/N is 41.4 db.

Perhaps of more interest is the rms error in full-scale output from each of the channels. This may be determined by multiplying rms signal-to-noise by a factor of $2\sqrt{2}$ (the ratio of peak-to-peak to rms value for a sine wave). Under these circumstances, S/N peak is 50.4 db at the receiver threshold, or the rms error due to the transmission path is 0.33%.

Thus the rf transmission link does not limit system resolution under the most adverse conditions.

(7) Signal-to-Noise Computation for Spin-Rate Data

The spacecraft spin rate is determined by accurately measuring the time between successive pulses originating in the spacecraft and produced by one of two sun sensors mounted on the spacecraft rim. These pulses frequency-modulate the 7.35-kc subcarrier oscillators. Baseband frequency response of the telemetry is not of prime importance in this instance, since the parameter of interest (time between pulses) requires only that the waveshape of the pulse arriving at the ground station be consistent from one pulse to the next, as shown in Figure C-1.

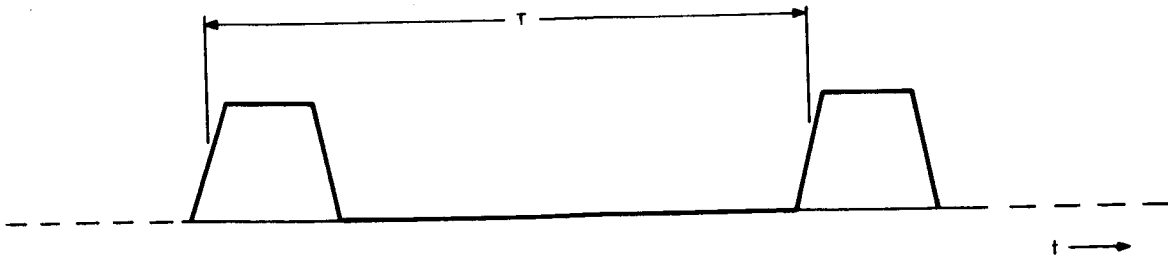


Figure C-1. Typical Sun-Sensor Pulses

If the same point on the slope of the rise time is used each time to measure the interval, resolution in time is not predicated upon a pulse with a short rise time. This method of interval measurement depends on the short-term consistency of circuit operation both in the spacecraft and on the ground. Consistency sufficient to achieve system performance in accord with measurement accuracy requirements is easily obtained through the use of standard circuits.

Of interest in this instance is the amount of rms jitter appearing on the leading edge of the pulse arriving at the ground station. This jitter will result in an indeterminacy in actual spin-period measurement and may be computed as follows:

$$\text{rms jitter} = N \times \frac{T_r}{S_p},$$

where

N is the rms noise at the system low-pass output filter,

T_r is the output-pulse rise time, and

S_p is the peak-to-peak output signal

A first look at the above expression would seem to indicate that a shorter rise time will produce less jitter. It must be remembered, however, that in an fm system a shorter rise time (which results in a correspondingly greater baseband requirement) results in larger noise output. To be more precise

$$N \propto (b)^{3/2}, \text{ and}$$

$$T_r \propto \frac{1}{b}.$$

Where b is the system baseband, $\text{rms jitter} \propto b^{3/2} \times 1/b = b^{1/2}$, and a shorter rise time will increase the rms jitter appearing on the leading edge of the pulse. For this reason, a relatively large deviation ratio is used on the subcarrier despite the resulting rise-time degradation.

The rms jitter = $\frac{N}{S} T_r \frac{1}{2.82}$, where N/S is the rms noise-to-signal ratio at the system output. The rms signal-to-noise ratio at the subcarrier discriminator output may be computed from the same relationship used previously.

$$\frac{S}{N} = \frac{C}{N_{IF}} D_1 D_2 \sqrt{\frac{3}{2}} \sqrt{\frac{(BW)_{IF}}{2 f_m}};$$

In this instance,

$$\frac{C}{N} = 12 \text{ db} + \text{system margin} = 27 \text{ db},$$

$$D_1 = 1 \text{ or } 0 \text{ db},$$

$$D_2 = 5 \text{ or } 14 \text{ db (IRIG Std deviation ratio in this case)},$$

$$f_m = 110 \text{ cycles (standard for a 7.35 KC subcarrier)},$$

$$(BW)_{IF} = 100 \text{ kc.}$$

Then,

$$\frac{S}{N} = 27 + 0 + 14 + 2 + 26.6 = 69.6 \text{ db.}$$

If a pessimistic attitude is adopted and the margin eliminated, $\frac{S}{N}$ will be 54.6 db. (at threshold). The rms jitter in microseconds is found by the previous expression:

$$T_r = \frac{0.35}{b} = \frac{0.35}{110} = 3.15 \text{ milliseconds};$$

rms jitter = $\frac{1}{535} \times 3.15 \times \frac{1}{2.82} \times 10^{-3} = 2.2 \mu\text{sec}$, and the rms jitter due to the transmission path will be negligible compared to other factors in the system.

(8) Signal-to-Noise Ratio for Command and Programmer Channels

These channels, one on each of the two systems aboard the spacecraft, are assigned a subcarrier frequency of 1.7 kc. With unity deviation ratio on the carrier and a deviation ratio of five on the subcarrier, the output signal-to-noise ratio will be at least as good as that obtained in the other channels.

APPENDIX D

TELECOMMUNICATION ACCURACY DETERMINATION

The purpose of the SERT telecommunication subsystem is to provide an information link between the spacecraft and the controlling ground station equipment. The subsystem will monitor various critical physical parameters of interest and provide an indication of the performance of the various subsystem functions.

To achieve these purposes, six telemetry channels are provided with the following information assignments:

- | | |
|---------------------|---------------------------|
| (1) 10.5-kc channel | commutated information |
| (2) 10.5-kc channel | commutated information |
| (3) 7.35-kc channel | sun sensor 1 |
| (4) 7.35-kc channel | sun sensor 2 |
| (5) 1.7-kc channel | programmer telemetry |
| (6) 1.7-kc channel | command decoder telemetry |

The two 10.5-kc commutated channels provide a total of 90 monitored data points. Each of these two channels operates at 90 pps and provides two complete frames of information per second. The overall accuracy requirement for the commutated channels is 5.0 percent from the input to the signal conditioner unit to any of the readout devices in the ground station.

The actual accuracy capability of the spacecraft and ground-station telemetry equipment for the commutated channels will be considerably better than 5.0 percent. Zero and full-scale reference voltages are applied to the commutated channels once per frame and have an accuracy tolerance of 0.25 percent of full scale (5.0 volts). As a result of these reference voltages the end points of the readout voltage range are known to 0.25 percent, and the accuracy of intermediate points is only affected by the linearity tolerances of the various components in the telemetry channels. The total error will be equal to the square root of the sum of the squares of the errors introduced by the signal conditioner, linearity errors of the various telemetry components, and the linearity accuracy of the readout devices.

The following is a list of the tolerances of the components in the commutated telemetry channels:

<u>Components</u>	<u>Worst case accuracy (\pm percent)</u>
Signal conditioner	2.0 (worst channel)
Commutator	0.1 linearity
SCO (10.5kc oscillator)	0.5 linearity
Transmitter	1.0 linearity for 100 kc deviation
Receiver	1.0 linearity for 150 kc deviation
Discriminator	0.1 linearity taken for best straight line for bandwidth
Control translator	0.5 linearity
Output converter	0.5 linearity
MMU meters	2.0
Path Loss	0.33

Total calculated error $E = \pm 3.029$ percent (root square sum)

This calculation has been made using a 2.0 percent tolerance for the signal conditioner; actually, all channels with the exception of the AGC circuit exhibit tolerances in the range of 0.5 percent. If the 14-channel oscillograph is used as the readout device instead of the MMU meters, the readout device accuracy will actually be 1.68 percent instead of 2.0 percent. Using these figures for the overall error calculation, E is found to be 2.43 percent.

The information received on the sun-sensor channels will provide the basis for determining the acceleration imparted to the spacecraft by the cesium-contact and mercury-bombardment-ion engines. The accuracy requirement for this information is that the time interval between succeeding sun pulses be read to 0.1 percent of the spacecraft spin rate.

The two remaining channels (command decoder telemetry and command programmer telemetry) have a 5.0 percent accuracy specification. The actual error which can be expected on these two channels may be calculated from the following list of component tolerances.

<u>Channel Component</u>	<u>Overall Accuracy (\pm percent)</u>
Signal source	1.0 over environmental range
SCO (1.7kc channel)	2.0 over environmental range
Transmitter	1.4 distortion and linearity for 100 kc deviation
Receiver	1.0 linearity 150 kc deviation
Discriminator	0.5 overall error
Chart Recorder	2.0 overall error

Total calculated error, $E = 3.5$ percent

This calculation is based on the telemetry signals being known to a 1.0 percent tolerance. This tolerance can be achieved by measuring these signals to such tolerances during component environmental tests and using this measured data in interpreting the received telemetry data.

APPENDIX E

SPIN RATE CHANGE DUE TO ION ENGINE THRUST

This appendix shows the method used to calculate changes in spin rate which result from thrust generated during operation of the ion engines.

Operation of the ion engines on board the SERT spacecraft will be initiated approximately two minutes after the engines have been deployed (following 4th stage separation). The spin rate of the spacecraft at this time will be approximately 100 rpm. The cesium-contact engine will be operated first and will decrease the spacecraft spin rate; then the mercury-bombardment engine will be operated to increase the spin rate.

If the moment of inertia of the spacecraft spin axis, the initial spin rate, the engine thrust level, and the engine lever arm are known, then the change in spin rate during engine operation can be calculated.

The following symbols are applicable throughout these calculations:

M is the torque about spacecraft spin axis due to engine thrust;

Y_{eng} is the engine lever arm;

F is the engine thrust;

I is the moment of inertia about the spacecraft spin axis;

ω is the spacecraft angular velocity in radians per second;

N is the spacecraft spin rate in revolutions per minute;

$\dot{\omega}$ is the angular acceleration;

T is the spin period;

ΔT is the change in spin period in microseconds; and

Δt is the time increment in seconds.

The torque about the spin axis can be expressed as

$$M = I \dot{\omega}. \quad (\text{E-1})$$

Also the spin period can be expressed as

$$T = \frac{2\pi}{\omega}. \quad (\text{E-2})$$

Differentiating equation (E-2) with respect to time

$$\dot{T} = - \frac{2\pi \dot{\omega}}{\omega^2}. \quad (\text{E-3})$$

Rearranging equation (E-1) and substituting it into equation (E-3),

$$\dot{T} = - \frac{2\pi}{\omega^2} \frac{M}{I}. \quad (\text{E-4})$$

Torque can also be expressed as

$$M = F Y_{\text{eng}}, \quad (\text{E-5})$$

and the relation between ω and N is

$$N = \frac{30}{\pi} \omega. \quad (\text{E-6})$$

Substituting equations (E-5) and (E-6) into equation (E-4)

$$\dot{T} = \frac{-2\pi}{\left(\frac{\pi}{30}\right)^2 N^2} \frac{F Y_{\text{eng}}}{I} = - \frac{1800}{\pi} \frac{F Y_{\text{eng}}}{I N^2}. \quad (\text{E-7})$$

If consistent units are used throughout, we may use the following approximation of equation (E-7) for small changes in N:

$$\frac{\Delta T}{\Delta t} = - \frac{1800}{\pi} \frac{F Y_{\text{eng}}}{I N^2} \quad (\text{E-8})$$

Since the ion engines used in SERT are very low-thrust devices, the change in spin rate due to their operation will be very small; therefore, small units of measure for changes in spin period and thrust, microseconds per second and millipounds, respectively, would be most readily useable. The final relationship for thrust is

$$F = \frac{\pi I N^2}{1.8 \times 10^6 Y_{\text{eng}}} \left| \frac{\Delta T}{\Delta t} \right| \quad (\text{E-9})$$

using the following units:

F in millipounds,

Y_{eng} in feet,

I in slug-ft²,

N in revolutions per minute,

ΔT in microseconds, and

Δt in seconds.

APPENDIX F

SPIN RATE ELECTRONICS AND COMMUNICATION DETECTION ERROR

This appendix describes an experiment that was performed to determine the spin-period-detection error introduced by the telecommunications, spacecraft, and ground system. The data was in the form of the measurements between the rise slopes of the n and the $n + 10$ pulse. The errors could be introduced by jitter in rise time, by distortion in frequencies, or by nonlinearities, etc. inherent in the ground readout equipment. These errors and their corresponding sources are discussed in this appendix.

1. Sun Sensor

The information regarding the error in the sun sensor was provided by the Lewis Research Center. An experiment was performed in which the input to the pre-amp was a ramp function instead of a response from the solar cell. The results show a jitter of nine microseconds in the rise time of the output waveform over temperature range of 100°F.

2. Subcarrier Oscillator, Communication Link, and Subcarrier Discriminator

These stages were considered together for practical reasons. According to theoretical calculations* the jitter due to communication link is in the order of a microsecond. Since the input to the subcarrier discriminator (SCD) is identical to the output of the subcarrier oscillator (SCO) with negligible error due to communication, the communication link can be neglected in studying the SCO-SCD detection error. Therefore, the experimental test was performed with the equipment set-up as shown in Figure F-1.

In the experiment, the sun sensor was triggered by a strobe light at a rate of 100 ppm. The output of the sun sensor triggered the VCO and the "start" count. From the oscillator to the discriminator, the signal was 1-volt peak-to-peak. The output of the discriminator triggered the "stop" count. The counter reads the delay and jitter of the system to 0.1 microseconds while the recorder printed out the data.

*"RCA Technical Memorandum TM 1101, Telemetry System Design Report" issued July 30, 1962

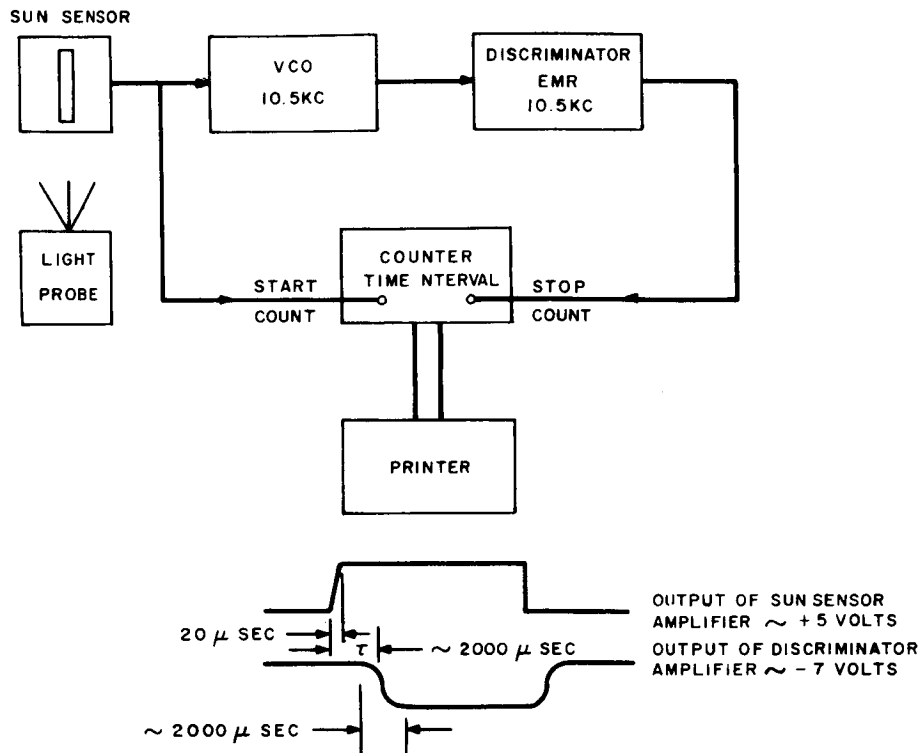


Figure F-1. Block Diagram Showing Test Set-up for Determining Subcarrier-Oscillator/Subcarrier-Discriminator Error

The accumulated data was analyzed by plotting the number of occurrences of a time delay (τ) versus the time delay. Then the amount of jitter was the variation in the time delay about a peak which was the most probable value of the time delay. A graph of data taken over a period of 7 hours on July 30, 1962 is shown in Figure F-2.

The data included three definite curves each of which corresponds to data taken over a specified period of time. Also, four peaks are displayed each with a jitter of ± 2.5 microseconds. If we consider the overall data, the total variation is about 14 microseconds. A closer investigation of the data shows that a large majority of the variations from one reading to the next are in the order of 1-3 microseconds and that only a very few variations are in the order of 5 to 7 microseconds. Thus, for the worst probable case, the jitter should be ± 7 microseconds, while in a majority of cases the jitter should be ± 2.5 microseconds.

The cause of the shifting of peaks was not firmly established. A possible source was a slight variation of the threshold in the triggering level of the start count and stop count; the latter would explain a change in the most probable delay time.

Analysis of the experimental test data, the sun-sensor jitter of 5 microseconds, and the fact that a 7.35-kc VCO would give a larger jitter than a 10.5-kc VCO indicated that a value for jitter to be used in accuracy calculations should be estimated at about ± 7 microseconds.

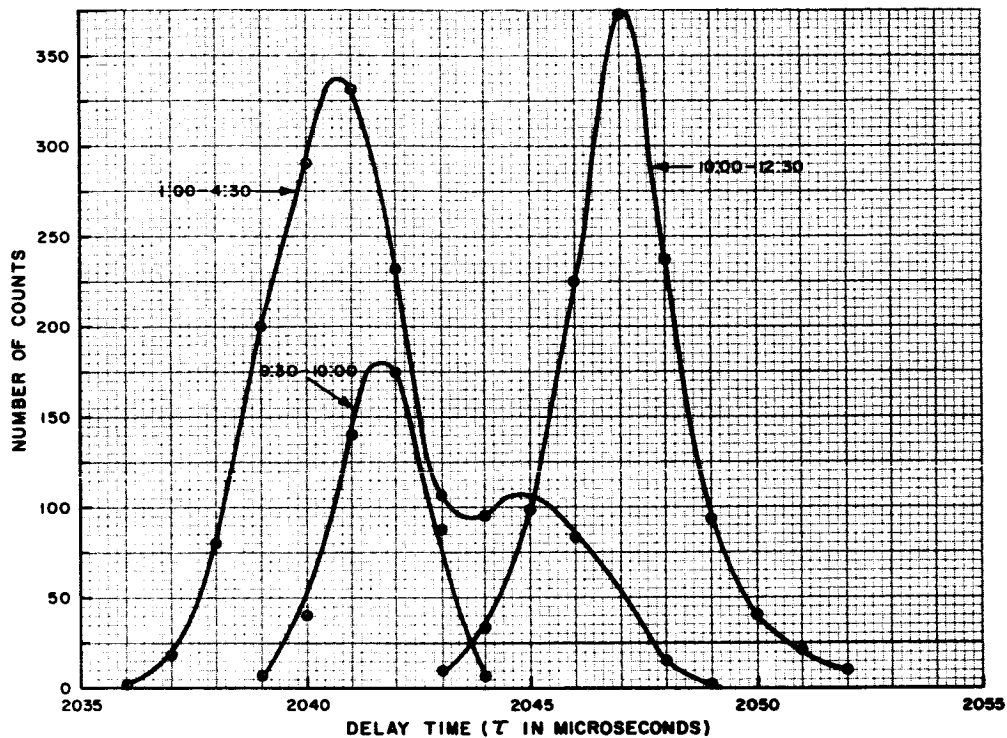


Figure F-2. Number of Counts Versus Delay Time (Plus or Minus) Jitter

3. Spin-Rate Detection Rack

The jitter in the electronic detection board was measured and found to be negligible (± 5 microsecond). A considerable error was found due to the counter; a plus or minus one count error introduces ± 10 microsecond error while a pessimistic figure supplied by the manufacturer for the time-base stability accounts for ± 10 microsecond error. Thus an overall of ± 20 microsecond is accountable to the Spin-Rate Detection Rack.

4. Summary

The accuracy of the system therefore, can be represented as having three major sources of error:

- (1) The sun sensor which introduces jitter of ± 9 microseconds;
- (2) The SCO-SCD which introduces jitter of ± 7 microseconds; and
- (3) The Spin Rate Rack which has an inherent error of ± 20 microseconds.

Since these errors are random, the total error of the system was obtained by taking square root of the sum of the squares of each individual error. The total system error was found to be ± 23.5 microseconds. The system error will be present in each ten-cycle time interval which will be recorded.

APPENDIX G

THRUST MEASUREMENT ERRORS

1. General

This appendix describes some of the important sources of error which can result when measuring the thrust of the ion engines as a function of changes in spin rate; errors in spin-rate measurement, however, are not covered in this appendix. It is shown that none of the errors investigated are very significant with the possible exception of the one arising during nutation damping. This error also becomes negligible several minutes after ion-engine extension.

2. Thrust-Axis Misalignment Error

An error in thrust measurement will result if the thrust vector is angularly misaligned from its proper orientation; that is, if the thrust vector is not normal to both the moment-arm vector and the spin axis. It can be shown that this thrust error $\epsilon(F)$ is

$$\epsilon(F) = F(1 - \cos \delta),$$

where

F is the thrust, and

δ is the misalignment error angle.

$\cos \delta$ may be expanded in a power series to give

$$\frac{\epsilon(F)}{F} = \frac{\delta^2}{2} - \dots,$$

from which it can be seen that a 1-degree misalignment results in an error of less than 0.02 percent. Errors in the assumed spin-axis location (i. e., due to "dynamic unbalance") are similarly small.

3. Thrust-Axis Offset Error

The engine thrust axes for the SERT are offset from the spin-axis plane containing the c.m. (center of mass) as shown in Figure G-2.

This offset results in a moment about the vehicle X-axis, rotating at the spin rate. To estimate the effect of this torque on spin-axis motion, we may write the Euler equations in simplified form, as follows:

$$M_x \cong (I_z - I_y) (-\dot{\theta} \sin \psi + \dot{\phi} \theta \cos \psi) \omega_z, \quad (G-1)$$

$$M_y = (I_x - I_z) (\dot{\theta} \cos \psi + \dot{\phi} \theta \sin \psi) \omega_z, \text{ and} \quad (G-2)$$

$$M_z = I_z \dot{\omega}_z + \dots \quad (G-3)$$

where

M_x , M_y , and M_z are the torques about the principal X, Y, and Z axes of the spacecraft respectively (these axes are defined in Figure G-1);

I_x , I_y , and I_z are the moments of inertia about the principal X, Y, and Z axes of spacecraft, respectively; and

ϕ , θ , and ψ are the Euler angles defined in Figure G-2.

Equations (G-1) and (G-2) above, which do not include the terms $I_x \dot{\omega}_x$ and $I_y \dot{\omega}_y$ respectively, will provide solutions to the precessional but not the nutational motion. Since, as will be seen later, precessional motion is extremely small, nutational motion can be expected, likewise, to be negligible.

For simplicity, the principal X axis shall be assumed coincident with the geometric X axis; then

$$M_x = F Z_{\text{eng}}, \quad (G-4)$$

and

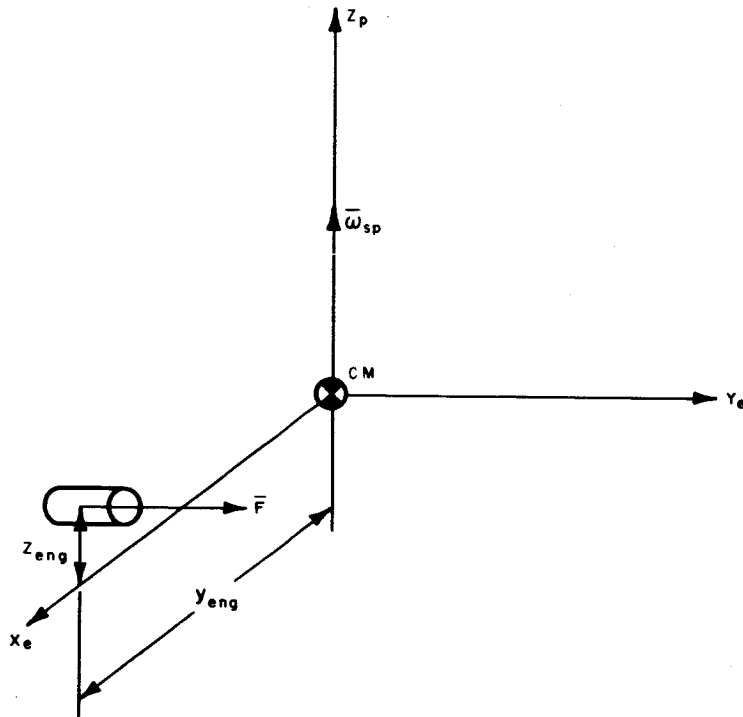
$$M_y = 0. \quad (G-5)$$

Substituting the result of equation (G-5) in equation (G-2),

$$\dot{\theta} = \dot{\phi} \theta \tan \psi. \quad (G-6)$$

Substituting equations (G-6) and (G-4) in equation (G-1),

$$M_x = F Z_{\text{eng}} = \frac{(I_z - I_y)}{\cos \psi} \dot{\phi} \theta \omega_z. \quad (G-7)$$



X_e is the engine reference axis (\perp to \bar{F});

Y_e is the engine reference axis (\parallel to \bar{F});

Z_p is the spin axis (principal axis);

$\bar{\omega}_{sp}$ is the spin vector;

\bar{F} is the engine thrust vector; and

Y_{eng}, Z_{eng} are coordinates of the engine force vector.

Figure G-1. Spin-Rate and Engine-Thrust Geometry

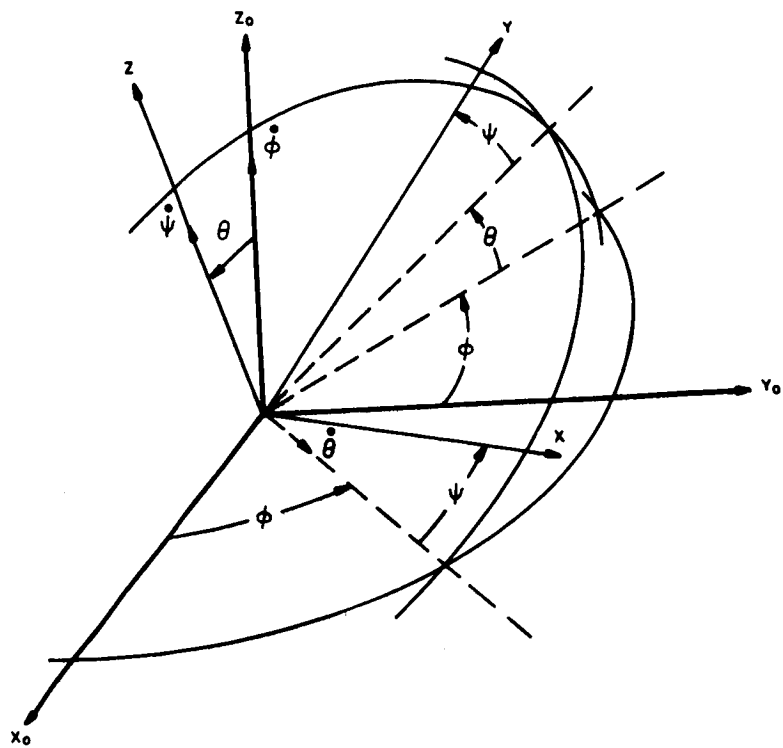


Figure G-2. The Euler Coordinate System

The precession rate is given by

$$\dot{\phi} \approx \frac{I_z}{I_z - I_y} \omega_z \approx \frac{I_z}{I_z - I_y} \omega_{sp} \quad (G-8)$$

where ω_{sp} is the spacecraft spin rate.

Using equations (G-7) and (G-8), the precession angle can be determined as follows:

$$\dot{\theta} \approx \frac{F_z \cos(\psi t)}{I_z \omega_{sp}^2} \quad (G-9)$$

As anticipated for the rotating torque vector, the precession angle is cyclic at rate $\dot{\psi}$. The maximum nutation angle for the 1.6-millipound cesium-contact engine, offset approximately 3 inches from the X-Y plane, is 4.3×10^{-7} radians at a spin rate of 90 rpm. This nutation angle is extremely small and results in a negligible error either as an apparent angular misalignment or due to a rate effect.

4. Nutation Error

Nutation may be present during ion-engine operation because of spin-axis disturbances arising from spacecraft separation and engine extension. As will be shown, nutation results in errors in spin rate.

In order to simplify the following solution, a cylindrical inertia distribution is assumed. The results should be generally applicable to the SERT spacecraft. Because the effect of engine torque is small, it is disregarded.

Figure G-3 shows the relationships between the axial, transverse, and total components of angular momentum and angular velocity for a nutating body of revolution. The vector average of the total angular velocity, representative of the average sensed spin rate ω_{av} of the spacecraft, is

$$\omega_{av} = \omega_z \cos \theta + \omega_p \sin \theta, \quad (G-10)$$

which is the projection of the angular velocity $\bar{\omega}$ on the total angular momentum \bar{H} .

Since, from Figure G-3, $\omega_z = \frac{H \cos \theta}{I_z}$ and $\omega_p = \frac{H \sin \theta}{I_p}$, we may obtain from equation (10) the expression

$$\omega_{av} = \frac{H}{I_z} \left[1 + \left(\frac{I_z}{I_p} \right) - 1 \sin^2 \theta \right]. \quad (G-11)$$

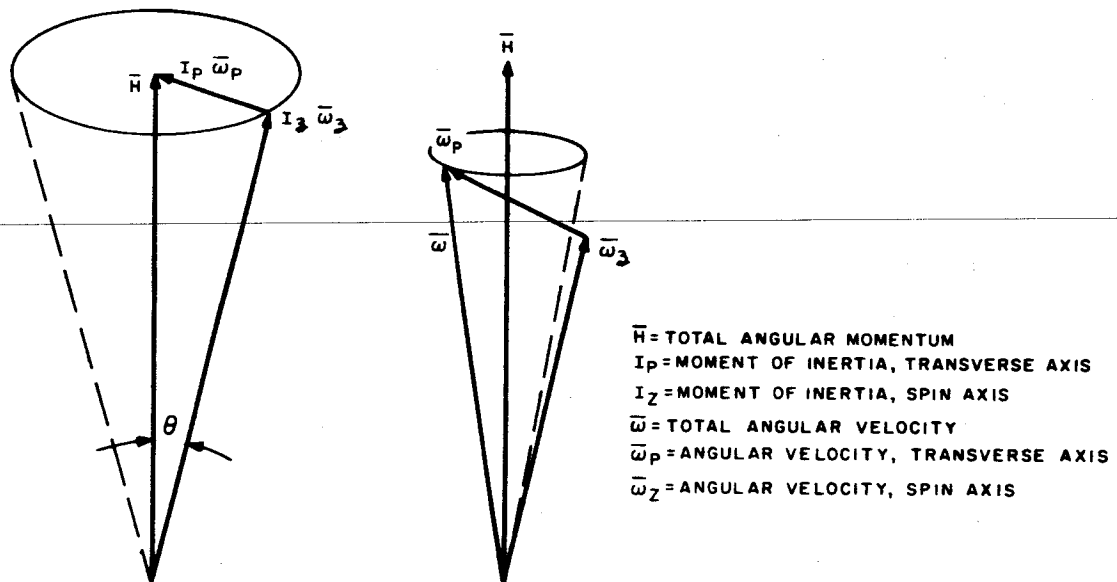


Figure G-3. Angular Momentum and Velocity for a Nutating Body of Revolution

If we define the no-nutation spin rate as $\omega_{\text{nom}} = \frac{H}{I_z}$, then, after expansion of $\sin^2 \theta$ in a power series, equation (G-11) becomes

$$\frac{\Delta \omega_{\text{av}}}{\omega_{\text{nom}}} = \frac{\omega_{\text{av}} - \omega_{\text{nom}}}{\omega_{\text{nom}}} = \left(\frac{I_z}{I_p} - 1 \right) \theta^2 + \dots, \quad (\text{G-12})$$

or

$$\frac{\Delta T_{\text{av}}}{T_{\text{nom}}} \cong - \left(\frac{I_z}{I_p} - 1 \right) \theta^2; \quad (\text{G-13})$$

where

ΔT_{av} is the period error, and

T_{nom} is the no-nutation period.

From equation (G-13), we can develop the following expression for the rate of change of period as a function of nutation angle rate of change

$$\frac{d T_{\text{av}}}{dt} = - \frac{4 \pi}{\omega_{\text{nom}}} \left(\frac{I_z}{I_p} - 1 \right) \theta \frac{d \theta}{dt}. \quad (\text{G-14})$$

Since the measure of thrust is angular acceleration, or rate of change of spin period, we can observe from equations (G-13) and (G-14) that a constant nutation angle has no net effect upon thrust measurement, whereas a change in nutation angle appears as an apparent thrust error.

It is shown in Appendix J that the quantity $\theta \frac{d \theta}{dt}$ is proportional to both the spin rate and to the effective coefficient of friction (μ) of the precession dampers. Figure G-4 illustrates the damping behavior for SERT for various effective coefficients of friction and an initial nutation of two degrees. It is reasonable to assume that the effective friction coefficient will only decrease as the nutation angle decreases because, as this occurs, end-bumper impacts will decrease. Since the slope of the damping curve in Figure G-4 is proportional to $\frac{d T_{\text{av}}}{dt}$, it may readily be shown that errors due to nutation damping will decrease below 10 percent of the cesium-contact engine thrust within 3 minutes.

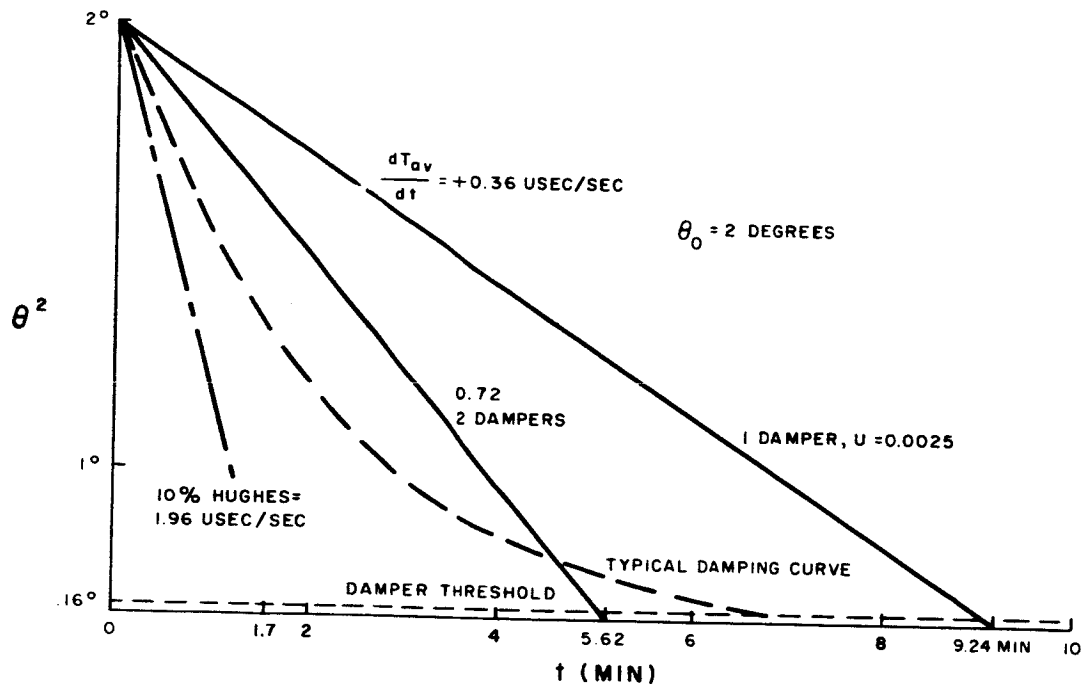


Figure G-4. Nutation Damping Behavior

APPENDIX H

EFFECT OF THERMAL EXPANSION ON MOMENT OF INERTIA AND SPIN RATE

1. Purpose

The following analysis has been conducted to obtain an order-of-magnitude value for the spin-deceleration error resulting from thermal expansion (which changes moment of inertia) of the SERT spacecraft during flight.

2. Summary and Conclusions

For simplicity, the analysis assumes isothermal distribution over the surface of the spacecraft. Using this approach, a solution is obtained which shows the spin-acceleration error to be only several percent of the acceleration resulting from operation of the cesium-contact engine.

3. Technical Description

(a) Baseplate Expansion

The assumptions of equal mass and temperature distribution over the surface of the spacecraft permits use of the simple equation

$$\Delta r = \alpha r \Delta T, \quad (H-1)$$

where

Δr is the change in radius,

r is the radius,

α is the coefficient of linear expansion, and

ΔT is the temperature rise.

The moment of inertia can be expressed as

$$I = K R^2, \quad (\text{H-2})$$

where

R is the spacecraft radius,

and for small changes,

$$\frac{\Delta I}{I} = \frac{2 \Delta R}{R} = 2\alpha \Delta T. \quad (\text{H-3})$$

Now

$$M = \frac{d}{dt}(I\omega) = \omega \dot{I} + I \dot{\omega} \quad (\text{H-4})$$

where

M is the torque,

ω is the spin rate, and

I is the spin-axis moment of inertia.

Therefore,

$$\dot{\omega} = \frac{M}{I} - \frac{\omega}{I} \frac{dI}{dT} \dot{T}. \quad (\text{H-5})$$

Using equation (H-3), the rate change due to inertia change is

$$\dot{\omega}_T = - \frac{\omega}{I} \frac{dI}{dT} \dot{T} = - \frac{\omega}{I} (2\alpha I) \dot{T} = - 2\alpha \omega \dot{T}. \quad (\text{H-6})$$

For magnesium, $\alpha = 27 \times 10^{-6}$ (length per °C). For a nominal spin rate (ω) of 10 radians per second, and a constant rate temperature rise of 50° C in one hour,

$$\dot{\omega}_T = - 2 (27 \times 10^{-6}) (10) \frac{50}{3600} = - 7.5 \times 10^{-6} \text{ rad/sec}^2.$$

The deceleration from the cesium-contact engine, for 1.6 millipounds of thrust, is

$$\dot{\omega}_M = \frac{M}{I} = \frac{F}{I} = \frac{(1.6 \times 10^{-3}) (2)}{10.5} = 0.3 \times 10^{-3} \text{ rad/sec}^2.$$

Therefore, the percentage error is

$$\left| \frac{\dot{\omega}_T}{\dot{\omega}_M} \right| = \frac{7.5 \times 10^{-6}}{3 \times 10^{-4}} = 2.25\% \text{ error.}$$

From equation (H-3), the total change in moment of inertia over a one-hour period is

$$\begin{aligned} \frac{\Delta I}{I} &= 2\alpha\Delta T = 2(27 \times 10^{-6})(50) = 27 \times 10^{-4} \\ &= 0.27\%. \end{aligned}$$

(b) Engine-Arm Expansion

A more detailed analysis should include a possibly large effect due to expansion of the cesium-contact-engine arm. If we pessimistically assume that the complete arm increases in temperature as does the engine, the increase in arm length can be expressed as

$$\frac{\Delta l}{\Delta T} = \alpha L, \tag{H-7}$$

where

Δl is the increase in arm length,

α is the coefficient of thermal expansion,

L is the arm length, and

ΔT is the temperature rise.

The inertia can be expressed as

$$I = I_b + I_e, \tag{H-8}$$

where

I is the total spin axis inertia,

I_b is the "baseplate" inertia, and

I_e is the engine inertia.

Therefore,

$$\dot{I} = \dot{I}_b + \dot{I}_e. \quad (\text{H-9})$$

Since

$$I_e \approx (R_p + L)^2 + I_{e_o}, \quad (\text{H-10})$$

where

m is the engine mass,

R_p is the radius to arm pivot, and

I_{e_o} is the engine moment of inertia about its own axis;

then

$$\dot{I}_e = 2m(R_p + L) \dot{l} = 2m(R_p + L) \times (\alpha L) \dot{T}. \quad (\text{H-11})$$

The R_p term has been neglected since this has, in essence, already been considered in Paragraph 3(a) above.

A numerical solution to equation (H-11) may be obtained using the following values:

$$mg = 14 \text{ lbs.}$$

$$(R_p + L) = 22 \text{ inches}$$

$$\alpha = 24 \times 10^{-6} \text{ (length per } ^\circ\text{C) (aluminum)}$$

$$L = 9.5 \text{ inches (to center of Hughes engine)}$$

$$\dot{T} = 133^\circ\text{C in 32 minutes (assumed linear).}$$

These numbers yield

$$\dot{I}_e = 2.09 \times 10^{-6} \text{ slug-ft}^2/\text{sec.}$$

Using equation (H-4), we may express the apparent torque error as

$$\frac{\dot{\omega}_{T_e}}{\dot{\omega}} = \frac{\omega \frac{dI_e}{dt}}{M} = \frac{\omega \frac{dI_e}{dt}}{F (R + L)}$$

Using a thrust of 1.6×10^{-3} pounds (for the cesium-contact engine),

$$\frac{\dot{\omega}_{T_e}}{\dot{\omega}_M} = 0.73 \text{ percent;}$$

which is a pessimistic value.

NOTE: The above analysis neglects a number of second-order effects which would yield errors considerably smaller than those indicated.

APPENDIX J

MODULATION OF SPIN-PERIOD MEASUREMENTS DUE TO NUTATION

1. Purpose

In this appendix, the modulation of spin period due to the nutation of a spin-stabilized spacecraft of arbitrary inertia distribution is determined (when the spin period is measured by the sun-sensor technique). The following investigation was performed to determine theoretically the small variation about the mean period between consecutive sun-line crossings, due to small nutations of the spin axis, as registered by a sun sensor mounted on a spin-stabilized spacecraft having three distinct principal inertias and no external torques.

2. Summary

The period deviation was determined as a function of time and found to be cyclic with variable periods. The discarding of products of small order terms in the derivation represents the only approximation involved. A numerical example that closely approximates the properties of the SERT spacecraft is given, and the magnitude of the period deviation is found to be on the order of less than 1/2 percent of the mean period.

3. Technical Description

The derivation given herein is based on following the sun line as it moves in the vehicle, thereby taking the point of view of an observer fixed in the spacecraft as he watches the sun line rotate about him.

Let O denote the mass center of the vehicle; OX, OY, and OZ the principal axes of inertia at O; and I_x , I_y , and I_z the corresponding inertias. For preciseness, let values of OX, OY, and OZ be assigned so that $I_z > I_x > I_y$, and OXYZ is a right-handed system. Since this investigation is concerned with a spin-stabilized spacecraft, this choice of body-fixed axes predicates that OZ is the spin axis and, since the nutation is small, that the Z component of the angular velocity is much greater than the X and Y components. Then, in the OXYZ system, the angular-velocity vector can be expressed as

$$\bar{\omega} = \omega_x \bar{i} + \omega_y \bar{j} + \omega_z \bar{k}, \quad (\text{J-1})$$

where $\omega_z \gg$ both ω_x and ω_y , and \bar{i} , \bar{j} , and \bar{k} are unit vectors along the positive X, Y, and Z axes, respectively.

Let \bar{s} be the unit vector in the direction of the sun line. From Figure J-1, \bar{s} is determined by the declination, σ , and the azimuth, η , in OXYZ to be

$$\bar{s} = \sin \sigma \cos \eta \bar{i} + \sin \sigma \sin \eta \bar{j} + \cos \sigma \bar{k}. \quad (\text{J-2})$$

Now, the sun sensor can be imagined as a pair of adjacent, parallel, plane segments, forming a sandwich, and so mounted on the spacecraft that the spin axis would lie wholly between the planes if they were extended far enough. Light rays cannot pierce these planes; the only rays which can enter the device are those passing through the slit-shaped aperture from outside the spacecraft, and which are directed toward the spin axis, parallel to and between the planes. It is evident that the location of the sensor is specified by its azimuth, ranging from 0° to 360° . The sun sensor is designed and mounted on the spacecraft so that it responds to the sun line, \bar{s} , whenever the azimuth of \bar{s} corresponds to the location of that sensor for a large range of declinations not too near 0° or 180° .

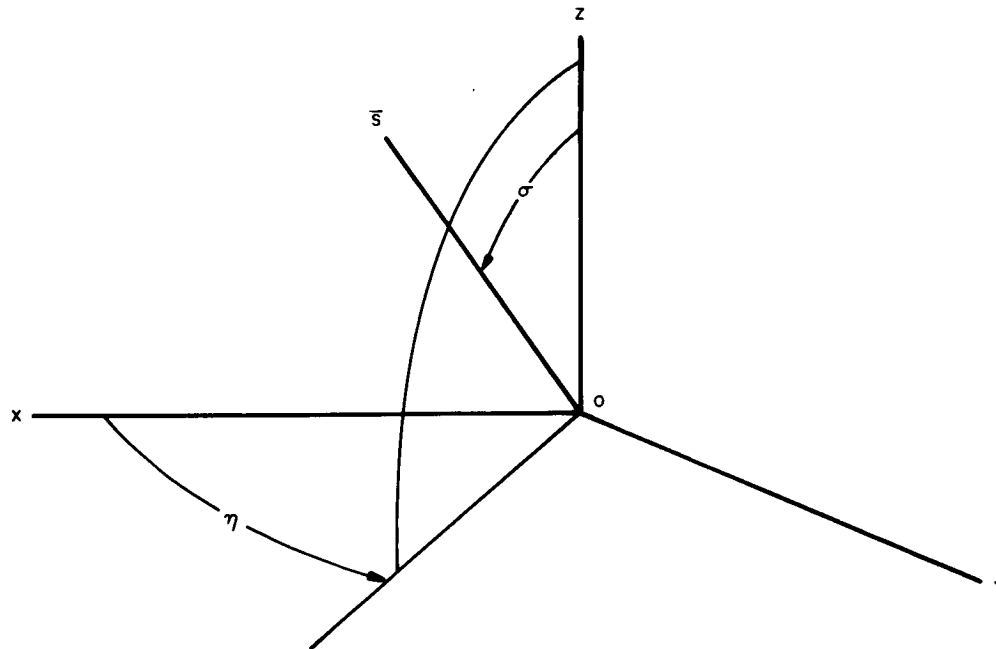


Figure J-1. Position of Sun Line in the Vehicle

Suppose that the vehicle is equipped with an infinite number of sun sensors placed around its periphery. Basically, what follows is the determination of the sun-line azimuth in OXYZ as a function of time. Indeed, this function defines the vertical plane instantaneously containing the sun line and, hence, the particular sensor being activated at each instant.

The first step in determining η as a function of time is to compute $\dot{\bar{s}}$ from equations (J-2) and (J-1), set it equal to zero (since \bar{s} is fixed in space), and solve for $\dot{\eta}$. Thus:

$$\begin{aligned} \dot{\bar{s}} = 0 = \bar{\omega} \times \bar{s} + (\dot{\sigma} \cos \sigma \cos \eta - \dot{\eta} \sin \eta \sin \sigma) \bar{i} \\ + (\dot{\sigma} \cos \sigma \sin \eta + \dot{\eta} \cos \eta \sin \sigma) \bar{j} - \dot{\sigma} \sin \sigma \bar{k}. \end{aligned} \quad (J-3)$$

Expanding $\bar{\omega} \times \bar{s}$ and setting the coefficients of \bar{i} , \bar{j} , and \bar{k} equal to zero, we get:

$$(\dot{\sigma} \cos \sigma \cos \eta - \dot{\eta} \sin \sigma \sin \eta) + (\omega_y \cos \sigma - \omega_z \sin \sigma \sin \eta) = 0 \quad (J-3-a)$$

$$(\dot{\sigma} \cos \sigma \sin \eta + \dot{\eta} \sin \sigma \cos \eta) + (\omega_z \sin \sigma \cos \eta - \omega_x \cos \sigma) = 0 \quad (J-3-b)$$

$$-\dot{\sigma} \sin \sigma + (\omega_x \sin \sigma \sin \eta - \omega_y \sin \sigma \cos \eta) = 0. \quad (J-3-c)$$

Equations (J-3-a) and (J-3-b) may be combined and expressed as

$$\dot{\eta} = -\omega_z + \frac{\omega_y \sin \eta + \omega_x \cos \eta}{\tan \sigma}. \quad (J-4)$$

Once the right-hand side is determined explicitly in terms of time, equation (J-4) will be integrated to give η as a function of time. This will be accomplished by neglecting all products of small terms, since a closed form integration of equation (J-4) is a difficult task.

We begin by determining the first-order solution to Euler's equations for the angular-velocity components under no (or negligible) external torques. Neglecting the product $\omega_x \omega_y$, Euler's equations for zero couple may be expressed as

$$\dot{\omega}_z = 0 \quad (J-5-a)$$

$$I_x \dot{\omega}_x - (I_y - I_z) \omega_y \omega_z = 0 \quad (J-5-b)$$

$$I_y \dot{\omega}_y - (I_z - I_x) \omega_z \omega_x = 0. \quad (J-5-c)$$

Integration of equation (J-5-a) yields

$$\omega_z = \omega_{sp}, \text{ a constant spin rate.} \quad (\text{J-6-a})$$

Substituting equation (J-6-2) into equations (J-5-b) and (J-5-c) and solving simultaneously

$$\omega_x = P \alpha \cos (K \omega_{sp} t + \beta) \quad (\text{J-6-b})$$

$$\omega_y = \alpha \sin (K \omega_{sp} t + \beta) \quad (\text{J-6-c})$$

where

$$\frac{(I_z - I_y) I_y}{(I_z - I_x) I_x} = P^2, \quad (\text{J-6-d})$$

and

$$\frac{(I_z - I_x) (I_z - I_y)}{I_x I_y} = K^2, \quad (\text{J-6-e})$$

and where α and β are determined from initial conditions.

No approximations were made in equations (J-5-b) and (J-5-c). Therefore, by eliminating ω_z and integrating, the following exact expression is obtained:

$$\frac{\omega_x^2}{(\alpha_1 P)^2} + \frac{\omega_y^2}{\alpha_1^2} = 1, \quad (\text{J-6-f})$$

where α_1 is a constant of integration (even if a torque acts about the spin axis). Of course, equation (J-6-f) is not valid if there is any couple normal to the spin axis. Since ω_x and ω_y always remain small, P can be considered a measure of the ellipticity of ω_x and ω_y .

It is appropriate at this point to introduce a spatially fixed coordinate system, and the Euler angles specifying the orientation of the vehicle in this system. In the case of zero external moment, the vehicle's angular momentum vector \bar{h} will remain unchanged. Let the Z_0 axis lie in the direction of \bar{h} . Construct the X_0 axis perpendicular

to the Z_0 axis in the plane formed by Z_0 and the sun line. Let δ_s be the angle from Z_0 to the sun line. The orientation of the vehicle is then specified by the ordered set of Euler angles ϕ , θ , and ψ as shown in Figure J-2. It can be shown that

$$\sin \sigma \cos \eta = \sin \delta_s \left(\cos \phi \cos \psi - \cos \theta \sin \psi + \frac{\sin \theta \sin \psi}{\tan \delta_s} \right) \quad (\text{J-7-a})$$

$$\sin \sigma \sin \eta = \sin \delta_s \left(-\cos \phi \sin \psi - \cos \theta \cos \psi \sin \phi + \frac{\sin \theta \cos \psi}{\tan \delta_s} \right) \quad (\text{J-7-b})$$

These are reduced to first order terms since θ remains small throughout the motion.

Thus, with the aid of Figure J-2, the components of \bar{h} along the X, Y, and Z axes are found to be

$$\begin{aligned} I_x \omega_x &= h \sin \theta \sin \psi \\ I_y \omega_y &= h \sin \theta \cos \psi \\ I_z \omega_z &= h \cos \theta. \end{aligned} \quad (\text{J-8})$$

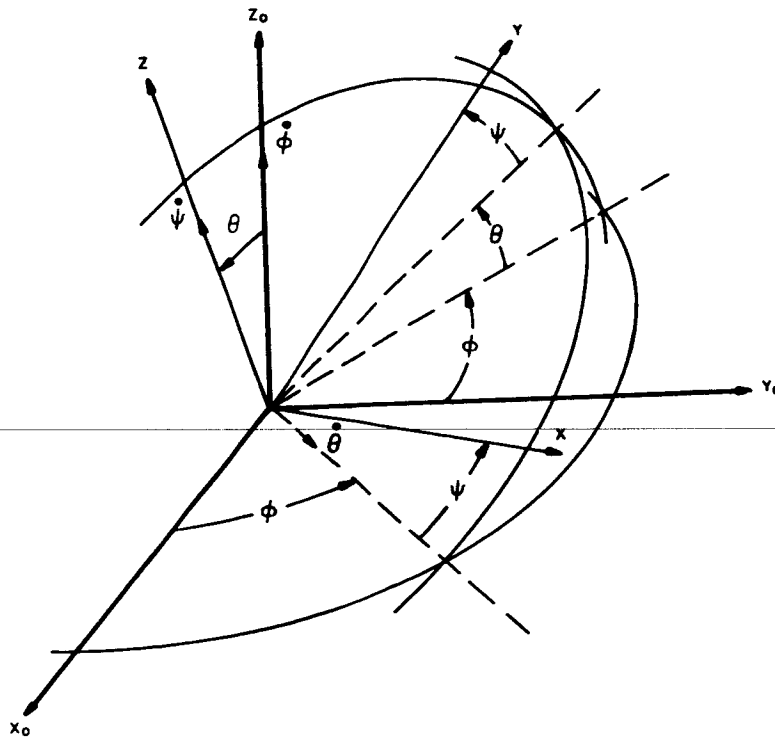


Figure J-2. The Euler Coordinate System

Assuming small perturbations in θ and substituting equation (J-8) into equations (J-7-a) and (J-7-b), we have the first order approximation to $\sin \eta$, and $\cos \eta$:

$$\begin{aligned}\cos \eta &= \frac{\sin \delta_s}{\sin \sigma} \left[\cos (\varphi + \psi) + \frac{I_x \omega_x}{h \tan \delta_s} \right] \\ \sin \eta &= \frac{\sin \delta_s}{\sin \sigma} \left[-\sin (\varphi + \psi) + \frac{I_y \omega_y}{h \tan \delta_s} \right].\end{aligned}\tag{J-9}$$

It is seen from Figure J-2 that

$$\omega_z = \dot{\psi} + \cos \theta \dot{\varphi}.$$

Hence, to first order:

$$\psi + \varphi = \omega_{sp} t + \xi_0,\tag{J-10}$$

where

$$\xi_0 = \psi + \varphi \text{ (at } t = 0\text{)}.$$

Substituting equation (J-10) into equation (J-9) and the result into equation (J-4)

$$\dot{\eta} = \omega_z + \frac{\omega_x \cos (\omega_{sp} t + \xi_0) - \omega_y \sin (\omega_{sp} t + \xi_0) + (I_x \omega_x^2 + I_y \omega_y^2) / h \tan \delta_s}{\left(\frac{\sin \sigma}{\sin \delta_s} \right) \tan \sigma}$$

Finally, by dropping the second order terms in the numerator (noting that $\sigma = \delta_s$), and by substituting equation (J-6) into this expression and simplifying, we obtain the first order approximation for $\dot{\eta}$:

$$\dot{\eta} = -\omega_{sp} + \frac{\alpha}{2 \tan \delta_s} \left\{ (p+1) \cos \left[(1+k) \omega_{sp} t + \beta_1 \right] + (p-1) \cos \left[(1-k) \omega_{sp} t + \beta_2 \right] \right\}\tag{J-11}$$

where

$$\begin{aligned}\beta_1 &= \beta + \xi_0, \text{ and} \\ \beta_2 &= -\beta + \xi_0.\end{aligned}\tag{J-12}$$

At a particular instant, η , α , β_1 , and β_2 have the values η_0 , α_0 , β_{10} and β_{20} . By choosing $t = 0$ at this instant, and letting $\Delta \eta(t) = \eta(t) - \eta_0$ be the increase in η from $t = 0$ to $t = t$, we obtain the following by the integration and simplification of equation (J-11):

$$\begin{aligned}\Delta \eta(t) &= -\omega_{sp} t + \frac{\alpha}{\omega_{sp} \tan \delta_s} \left\{ \frac{(p+1)}{(1+k)} \sin \frac{(1+k)}{2} \omega_{sp} t \cos \left[\frac{(1+k)}{2} \omega_{sp} t + \beta_{10} \right] \right. \\ &\quad \left. + \frac{(p-1)}{(1-k)} \sin \frac{(1-k)}{2} \omega_{sp} t \cos \left[\frac{(1-k)}{2} \omega_{sp} t + \beta_{20} \right] \right\}\end{aligned}\tag{J-13}$$

Now, T , the period for consecutive sun crossings of a particular sensor, is such that

$$\Delta \eta(T) = -2\pi\tag{J-14}$$

since η is retrogressive with respect to ω_{sp} .

Define ΔT , a small variation about the mean period, T_0 , by

$$T = T_0 + \Delta T = \frac{2\pi}{\omega_{sp}} + \Delta T,\tag{J-15}$$

and call it the period deviation. Then, by substituting equations (J-14) and (J-15) into equation (J-13), and by neglecting second order terms and simplifying

$$\Delta T = \frac{\alpha \sin \pi k}{\omega_{sp}^2 \tan \delta_s} \left\{ \frac{(p+1)}{(1+k)} \cos(\beta_{10} + \pi k) - \frac{(p-1)}{(1-k)} \cos(\beta_{20} - \pi k) \right\}\tag{J-16}$$

Equation (J-16) gives the first period deviation recorded by a sensor encountering the sun at $t = 0$. Suppose we were to wait for t seconds and then compute the period deviation which would be registered by the sensor encountering the sun at time t . By this time, $\varphi + \psi$ would have progressed to $\omega_{sp} t + \xi_0$, from equation (J-10), and ω_x and ω_y would have progressed to $P\alpha \cos(k\omega_{sp} t + \beta_0)$ and $\alpha \sin(k\omega_{sp} t + \beta_0)$, respectively, from equation (J-6). Then, from equation (J-12), the values of β_1 and β_2

computed at this latter time would be expressed as $(k \omega_{sp} t + \beta_0) + (\omega_{sp} t + \xi_0)$ and $-(k \omega_{sp} t + \beta_0) + (\omega_{sp} t + \xi_0)$, respectively. Hence, the ΔT corresponding to this latter time, t , would be computed by equation (J-16) again except

$$\left. \begin{array}{l} (1+k) \omega_{sp} t + \beta_{10} \text{ substituted for } \beta_{10} \\ (1-k) \omega_{sp} t + \beta_{20} \text{ substituted for } \beta_{20} \end{array} \right\} \text{and} \quad (J-17)$$

Substituting equation (J-17) into equation (J-16), we obtain the period deviation as a function of time:

$$\Delta T(t) = \frac{\alpha \sin \pi k}{\omega_{sp}^2 \tan \delta_s} \left\{ \begin{array}{l} \frac{(p+1)}{(1+k)} \cos [(1+k) \omega_{sp} t + \gamma_1] \\ - \frac{(1+k)}{(p+1)} \frac{(p-1)}{(1-k)} \cos [(1-k) \omega_{sp} t + \gamma_2] \end{array} \right\} \quad (J-18)$$

where we have set

$$\gamma_1 = \xi_0 + \beta_0 + \pi k, \text{ and} \quad (J-18-a)$$

$$\gamma_2 = \xi_0 - \beta_0 - \pi k. \quad (J-18-b)$$

Equation (J-18) is the primary desired result of this investigation. The predominant characteristic resulting from the existence of three distinct principal inertias in a spin-stabilized spacecraft is exhibited in this first-order solution by the parameter P_0 . Since $I_z > I_x > I_y$ in this general case, it can be seen from equation (J-6-d) that P is not unity, and from equation (J-6-f) that P is a direct measure of the elliptic behavior of the transverse angular-velocity components ω_x and ω_y . It is for this reason that the second cosine term is present in equation (J-18); thereby making $\Delta T(t)$ the superposition of two different frequency components. In general, the ratio of the two frequencies, $(1+k)/(1-k)$, is not a rational number. Therefore, the waveform traced out over any time interval will never be repeated; hence, $\Delta T(t)$ is not a periodic function of time.

For a Body of Revolution:

However, if the vehicle is a spin-stabilized body of revolution, which is characterized by $I_z > I_x = I_y$, then P is unity and the above difficulties disappear.

Thus,

$$I_z = I_{\text{spin}}$$

$$I_x = I_y = I_{\text{pitch}}$$

$$P = 1$$

$$K = I_s / I_p - 1$$

$$\omega_z = \omega_{\text{sp}}, \quad \omega_x = \alpha \cos(k \omega_{\text{sp}} t + \beta), \quad \omega_y = \alpha \sin(k \omega_{\text{sp}} t + \beta)$$

$$\theta = \text{const.}$$

$$I_s \omega_{\text{sp}} \tan \theta = I_p \sqrt{\omega_x^2 + \omega_y^2}$$

for small θ then,

$$\alpha = \frac{I_s}{I_p} \omega_{\text{sp}} \theta.$$

Then for a body of revolution, the delta time reduces from equation (J-18) to

$$\Delta T(t)_{\text{rev.}} = \frac{2 \theta \sin \pi k}{\omega_{\text{sp}} \tan \delta_s} \cos \left[\frac{I_s}{I_p} \omega_{\text{sp}} t + \gamma_o \right]; \quad (\text{J-19})$$

γ_o is a phase angle.

Equation (J-19) gives us justification for calling the first cosine term in equation (J-18) the body-of-revolution term, and the second term in equation (J-18) the modulation term.

A Numerical Example:

Assume that $I_z = 8$, $I_x = 6$, and $I_y = 5$ (lb. - sec.² - ft.);

Nutation $\dot{\delta} = 0.9$ degrees;

$T_o = 0.5$ seconds; and

$\delta_s = 45^\circ$.

Then

$K \dot{=} 0.45$,

$p \dot{=} 1.12$

and the delta period is given by

$$\Delta T(t) = (0.003) T_0 \left\{ \cos(18.25t + \gamma_1) - 0.15 \cos(5.67t + \gamma_2) \right\}.$$

The quantity $\Delta T(t)/(0.003) T_0$ has been plotted in Figure J-3 over two cycles for $\gamma_1 = \gamma_2 = 0^\circ$ and $\gamma_1 = \gamma_2 = 45^\circ$. For comparison purposes, the body-of-revolution term has been plotted (the dotted curve).

It can be seen that the modulation does not have very much effect. The times of zero crossings and extremes are not very much different from the body-of-revolution curve. However, there are two prominent features caused by the modulation. In the plot for $\gamma_1 = \gamma_2 = 0$, the fourth zero crossing illustrates the "S-shaped" zero crossing resulting in a region where the body-of-revolution term and the modulating term are 90 degrees out of phase; and the plot for $\gamma_1 = \gamma_2 = 45^\circ$ illustrates the accentuation of extremes resulting from "beating phase shifting" of the modulation. In any case, the complete time record of $\Delta T(t)$ would display both of these phenomena, regardless of initial conditions.

This example closely approximates the properties of the SERT spacecraft. Since P is close to unity, the low-frequency modulation term amounts to only 15 percent of the body-of-revolution term. In addition, the entire period deviation is in the neighborhood of less than 1/2 percent of the mean period.

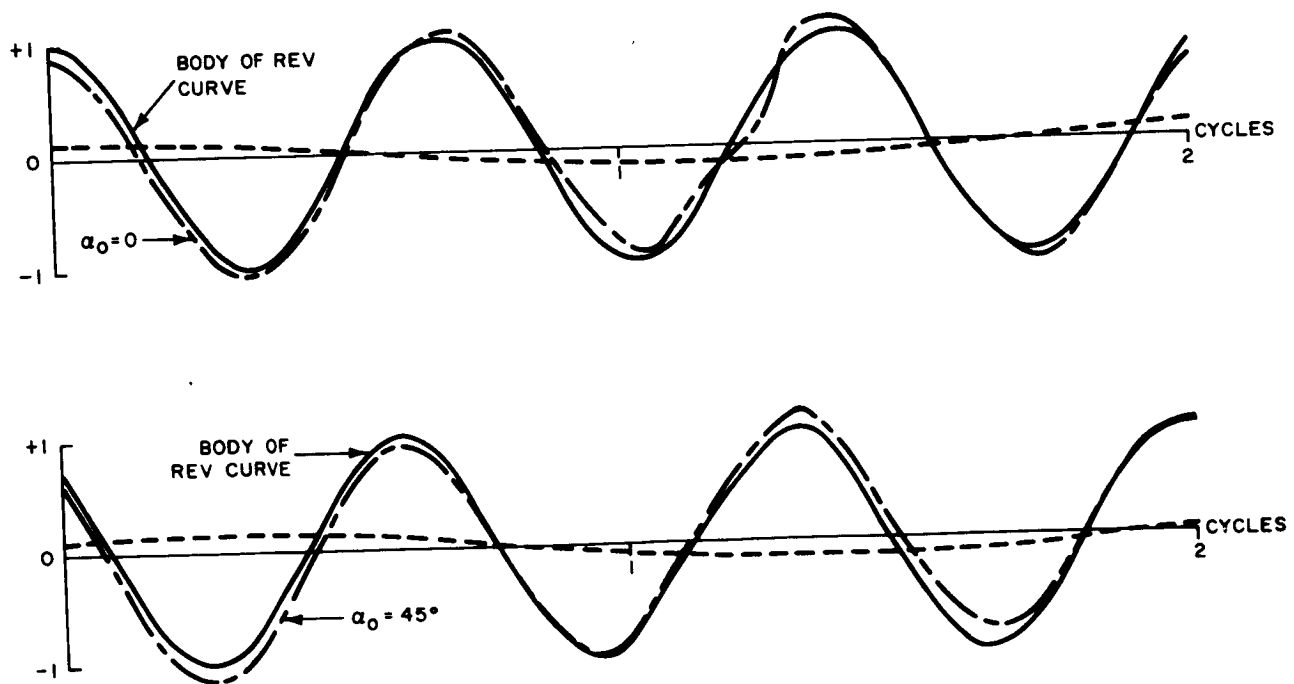


Figure J-3. Normalized Period Deviation

4. Flight Data Analysis

It should be noted that the SERT spacecraft, having only two sun sensors (only one of which provides signals to the spin-rate counters at any one time), will generate ΔT only once each revolution. Therefore, the sampling rate will be lower than that required for discrete reconstruction of the modulation. However, by utilizing prior knowledge of the spacecraft inertias, the two characteristic frequencies can be stipulated and, by a study of the flight data, it should be possible to identify maximum and minimum modulations, certainly of the body-of-revolution term if not the second-order modulation. A degree of reconstruction, and removal of the nutation effect from the data, may thus be achieved.

The extensive flight data analysis needed to remove nutation errors would be required, in the practical case, only if the engine thrust levels were much lower than anticipated or if the operating times were restricted to several minutes. Ordinarily, however, a mean-square fit of the period data over several minutes should suffice to provide acceptable (less than one percent) accuracy. A discussion of statistical techniques for the handling of spin-period data is presented in Appendix K.

APPENDIX K

THE TREATMENT OF SPIN-PERIOD DATA

1. Purpose

This appendix discusses the treatment and analysis of spin-period data required to extract the rate of change of period as required for thrust determination. An analysis of errors in the treatment is also presented.

2. Basic Equations

The data provided by the spin-rate instrumentation (sun sensors) during the SERT flight will be found in the form shown in Figure K-1, with n , the number of cycles of rotation, as the independent variable, and t , the time, as the dependent variable.

A parabola can now be fitted to the above curve by a least squares fit* using the following equation:

$$t = a + Pn + cn^2, \quad (K-1)$$

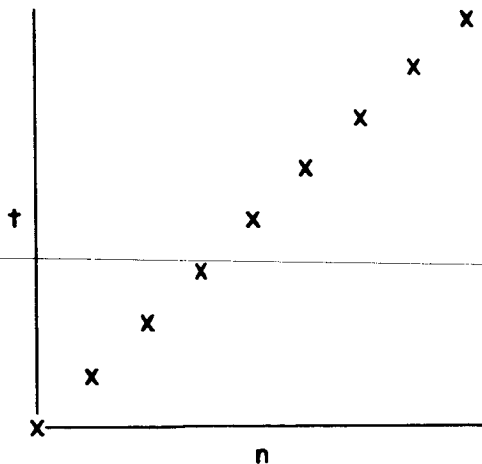


Figure K-1. Spin-Rate Instrumentation Data

*Statistical treatment of the data should certainly be acceptable in consideration of all errors except those due to nutation. Nutation errors are discussed in the latter part of this appendix.

where

a is a measure of the initial time (and of no particular interest to us),

P is the average period of rotation during the time of measurement, and

e is a measure of the change in time of the period, and is therefore a measure of the angular acceleration.

It can be shown that

$$P = \frac{2\pi}{\omega}, \quad \dot{\omega} = \frac{2\pi}{P}, \quad C = \frac{1}{2} \dot{P}P, \quad \text{and} \quad \dot{\omega} = -\frac{\omega^3 C}{2\pi}. \quad (\text{K-2})$$

For simplicity, it will be assumed that $a = 0$. The least squares fit is then given by the expression

$$P = \left(\sum_i n_i t_i \right) / \sum_i n_i^2, \quad C = \frac{N \sum_i n_i^2 t_i - \sum_i n_i^2 \sum_i t_i}{N \sum_i n_i^4 - \left(\sum_i n_i^2 \right)^2}. \quad (\text{K-3})$$

If a time measurement is made regularly after a specific number n_0 of cycles, and the total number of measurements made is N , then

$$P = \frac{12}{n_0^2 (N^3 - N)} \sum_{i=1}^N n_i t_i; \quad \text{and} \quad (\text{K-4})$$

and

$$C = \frac{180}{n_0^4 (N^3 - N) (N^2 - 4)} \sum_{i=1}^N \left(n_i^2 - \bar{n}^2 \right) t_i. \quad (\text{K-5})$$

The principal reason for having the equation in this form is that C is a linear function of the time measurements and will be useful in an error analysis. For illustration, a specific case for $N = 3$ can be used; this is the least number of measurements that will still determine C . The equations will resolve into

$$P = \frac{1}{2\eta_0} t_3 - \frac{1}{2\eta_0} t_1; \quad (\text{K-6})$$

and

$$C = \frac{1}{2\eta_0} t_3 - \frac{1}{\eta_0} t_2 + \frac{1}{2\eta_0} t_1. \quad (\text{K-7})$$

The first equation is easily understood: the average period is simply the total time ($t_3 - t_1$) divided by the total number of cycles ($2n_0$).

3. Random Errors

The errors in the determination of P and C will now be obtained. It will be assumed, for the present, that errors in successive time measurements are uncorrelated, and the errors in each are equal. The quantities of interest are in the form:

$$C = f_1 t_1 + f_2 t_2 + f_3 t_3 + f_4 t_4 + \dots \quad (\text{K-8})$$

Where f_1 is a weighting function.

The variance of C will then be

$$\sigma_C^2 = f_1^2 \sigma_t^2 + f_2^2 \sigma_t^2 + f_3^2 \sigma_t^2 + f_4^2 \sigma_t^2 + \dots \quad (\text{K-9})$$

where σ_t is the standard deviation in the time measurement; this has been estimated to be 8 microseconds for SERT. The indicated operations can be performed on equations (K-4) and (K-5), and the results are as follows:

$$\sigma_P = \frac{2\sqrt{3}}{n_0 \sqrt{N^2 - 1} \sqrt{N}} \frac{\sigma_t}{\sqrt{N}}; \quad (\text{K-10})$$

and

$$\sigma_C = \frac{6\sqrt{5}}{n_0^2 \sqrt{N^2 - 1} \sqrt{N^2 - 4} \sqrt{N}} \frac{\sigma_t}{\sqrt{N}}. \quad (\text{K-11})$$

Of perhaps more physical interest are the errors in the average angular frequency and the angular acceleration, which are expressed as

$$\sigma_\omega = \frac{2\sqrt{3}}{T} \left(\frac{N}{\sqrt{N^2 - 1}} \right) \frac{\omega \sigma_t}{\sqrt{N}}; \quad (\text{K-12})$$

and

$$\sigma_{\dot{\omega}} = \frac{12\sqrt{5}}{T^2} \left(\frac{N^2}{\sqrt{N^2-1} \sqrt{N^2-4}} \right) \frac{\omega \sigma_t}{\sqrt{N}} \quad (\text{K-13})$$

where T is the total time of measurement; that is, $T = PNn_0$. Note that the expressions in parentheses approach unity for large values of N, and need only be considered for small samples.

For illustration, we shall calculate the error in angular acceleration for a time measurement lasting 1 minute. If the period of revolution is 0.5 second, and if measurements are made every ten cycles, the error is

$$\begin{aligned} 3\sigma_{\dot{\omega}} &= \frac{12\sqrt{5}}{(60 \text{ sec})^2} \left(\frac{13^2}{\sqrt{168} \sqrt{165}} \right) \frac{(12.5 \text{ rad/sec}) (20 \mu\text{sec})}{\sqrt{13}} \quad (\text{K-14}) \\ &= 0.53 \times 10^{-6} \text{ rad/sec}^2. \end{aligned}$$

Since an angular acceleration of $280 \times 10^{-6} \text{ rad/sec}^2$ is expected for the cesium-contact-ion engine, this corresponds to an accuracy of two-tenths of one percent.

A plot of measurement accuracy as a function of time and frequency of measurement is presented in Figure K-2 for a thrust rate of $400 \times 10^{-6} \text{ rad/sec}^2$.

4. Nutation Errors

Superimposed on the variations already discussed will be a sinusoidal variation due to the nutation. The time measurements (t) as a function of the number of spacecraft rotations (n) will presumably be in the form:

$$t = a + Pn + cn^2 + b \sin n\dot{\phi}P + d \cos n\dot{\phi}P. \quad (\text{K-15})$$

where the two constants, b and d, define the phase and amplitude of the nutation.

For a simplified body of revolution, $\dot{\phi}$ is the angular frequency of nutation, and P is the period of rotation so that

$$\dot{\phi}P = \frac{I_z}{\sqrt{I_x I_y}} \omega P = \frac{2\pi I_z}{\sqrt{I_x I_y}}. \quad (\text{K-16})$$

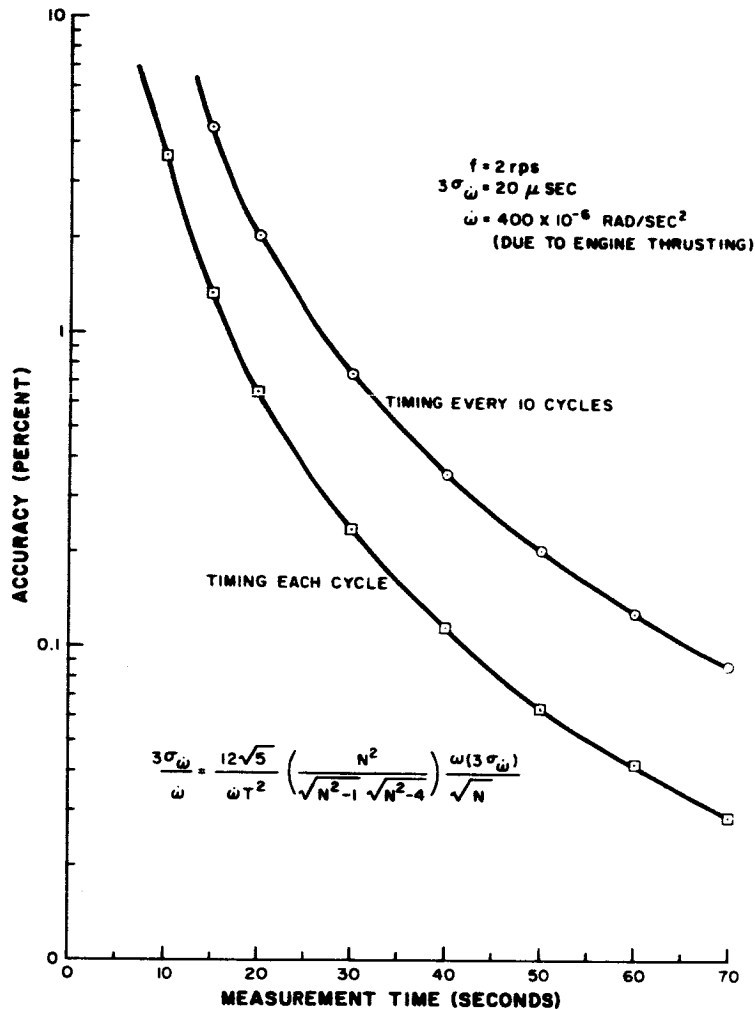


Figure K-2. Acceleration Measurement Accuracy

The simplest way of minimizing the error in a small number of cycles is to count such a number that $\dot{\phi}P_i$ is a multiple of 2π . The error is thereby canceled. The difficulty with this method is that it cannot be done exactly, and a small error will result.

To estimate this error, assume i cycles are counted each time, and

$$i \frac{I_z}{\sqrt{I_x I_y}} = m + \epsilon, \tag{K-17}$$

where m is an integer and ϵ is a small fractional residual. It then follows that

$$Cn^2 + d \cos n \dot{\phi}P = Cn^2 + d \cos 2\pi n(m + \epsilon) \approx d + \left(C - 2\pi^2 \epsilon^2 d \right) n^2, \tag{K-18}$$

where the expansion of the cosine is valid if our total measurements are over a small enough range so that the sum of ϵ does not build up to a full cycle. The fractional error in c is therefore

$$\text{Error} = \frac{d 2\pi \epsilon^2}{C} = \frac{(400 \mu\text{sec}) 2\pi \epsilon^2}{(4 \mu\text{sec})} \approx 2000 \epsilon^2, \quad (\text{K-19})$$

where C is obtained from equation (K-1) for an angular acceleration of 400×10^{-6} rad/sec². It therefore follows that for the error to be less than 1 percent, ϵ must be less than 0.002; in other words, if the ratio of moment of inertias is approximately 1.3 and we count ten cycles, then

$$1.2998 < \sqrt{\frac{I_2}{I_x I_y}} < 1.3002. \quad (\text{K-20})$$

Another method that can be used, if the constraint of equation (K-20) is impractical, is to actually determine the coefficient d . This cannot be done if ϵ is very small, because then it is difficult to distinguish curvature due to thrust from curvature due to nutation. However, if we choose i in equation (K-17) so that ϵ is close to one half, then we maximize the fluctuations due to nutations and can determine d . A least squares fit can then be made to Equation (K-15). If we assume, as before, that measurements are made at equal intervals (after i cycles every time) and that $n = 0$, then the odd functions are uncoupled from the even functions and the least squares equations for the determination of C are

$$\sum_i t_i = a N + c \sum_i n_i^2 + d \sum_i \cos n_i \dot{\phi} P;$$

$$\sum_i n_i^2 t_i = a \sum_i n_i^2 + C \sum_i n_i^4 + d \sum_i n_i^2 \cos n_i \dot{\phi} P \quad (\text{K-21})$$

$$\sum_i t_i \cos n_i \dot{\phi} P = a \sum_i \cos n_i \dot{\phi} P + C \sum_i n_i^2 \cos n_i \dot{\phi} P + d \sum_i \cos^2 n_i \dot{\phi} P.$$

These three equations can be solved for a , C , and d , and can be used regardless of the value of ϵ ; however, it is important to choose a value of ϵ that is not too close to zero, or the error discussed previously will appear. By choosing a value of ϵ close to one half, there is the advantage that, for preliminary analysis, we can add consecutive periods, thereby eliminating most of the error, and for later analysis we still have the information to determine d .

Further analysis would be required for a quantitative determination of the errors, but it would appear that such a least-squares analysis would decrease the errors to where they are limited by the time measurements (and thereby comparable to the errors presented at the front of this appendix). The effect of the error in nutation frequency could also be investigated.

ABSTRACT

The purpose of the SERT program is to test, in the space environment, the behavior of ion-beam neutralization in ion engines. The engines, mounted on hinged arms at the periphery of the circular baseplate, extend after Scout fourth-stage separation and vary the spacecraft spin rate during thrusting, thus providing a simple method of measuring engine thrust. The electrical systems provide conditioned power for engine operation and telemeter performance data throughout the 1-hour ballistic flight. The ground equipment was developed to test the spacecraft before launch as well as to monitor flight performance.

**DISTRIBUTION LIST FOR SUMMARY REPORT
CONTRACT NAS8-2449**

NASA-Lewis Research Center (1)
Spacecraft Technology Procurement Section
21000 Brookpark Road
Cleveland, Ohio 44135
Attention: J. H. DeFord

NASA-Lewis Research Center (1)
Technology Utilization Office
21000 Brookpark Road
Cleveland, Ohio 44135

NASA Headquarters (2)
FOB-10B
600 Independence Avenue, NW
Washington, D. C. 20546
Attention: RNT/J. Lazar

NASA-Lewis Research Center (2)
Spacecraft Technology Division (MS54-3)
21000 Brookpark Road
Cleveland, Ohio 44135
Attention: J. H. Childs

NASA-Lewis Research Center (1)
Electric Propulsion Laboratory
21000 Brookpark Road
Cleveland, Ohio 44135
Attention: W. R. Mickelsen

NASA Marshall Space Flight Center (1)
R-RP-DIR
Huntsville, Alabama 35812
Attention: Dr. E. Stuhlinger

Commander
Aeronautical Systems Division (1)
Wright-Patterson AFB, Ohio 45433
Attention: AFAPL (APIE), R. Supp

NASA-Lewis Research Center (2)
21000 Brookpark Road
Cleveland, Ohio 44135
Attention: Library

NASA-Lewis Research Center (1)
21000 Brookpark Road
Cleveland, Ohio 44135
Attention: Reports Control Office

NASA Scientific and Technical
Information Facility (6)
P.O. Box 5700
Bethesda, Maryland
Attn: NASA Representative RQT-2448

Jet Propulsion Laboratory (1)
Institute of Technology
Pasadena, California
Attention: J. J. Paulson

Aerospace Corporation (1)
P.O. Box 95085
Los Angeles 45, California
Attention: Library Technical
Documents Group

AFWL (1)
Kirtland AFB, New Mexico
Attention: WLPC/Capt. C. F. Ellis

NASA-Lewis Research Center (1)
21000 Brookpark Road
Cleveland, Ohio 44135
Attention: W. Moeckel

Hughes Research Laboratories (1)
3011 Malibu Canyon Road
Malibu, California
Attention: Dr. George R. Brewer

NASA-Lewis Research Center (15)
Spacecraft Technology Division
21000 Brookpark Road
Cleveland, Ohio 44135
Attention: R. J. Rulis

Thompson Ramo Wooldridge Inc. (1)
Electromechanical Division
7209 Platt Avenue
Cleveland, Ohio 44104
Attention: David Powell